



HAL
open science

The role of riverbed on suspended sediment transport dynamics in Alpine Catchments

Clément Misset

► **To cite this version:**

Clément Misset. The role of riverbed on suspended sediment transport dynamics in Alpine Catchments. Hydrology. Université Grenoble Alpes, 2019. English. NNT: 2019GREAU020 . tel-02436785

HAL Id: tel-02436785

<https://theses.hal.science/tel-02436785>

Submitted on 13 Jan 2020

HAL is a multi-disciplinary open access archive for the deposit and dissemination of scientific research documents, whether they are published or not. The documents may come from teaching and research institutions in France or abroad, or from public or private research centers.

L'archive ouverte pluridisciplinaire **HAL**, est destinée au dépôt et à la diffusion de documents scientifiques de niveau recherche, publiés ou non, émanant des établissements d'enseignement et de recherche français ou étrangers, des laboratoires publics ou privés.

THÈSE

Pour obtenir le grade de

DOCTEUR DE LA COMMUNAUTE UNIVERSITE GRENOBLE ALPES

Spécialité : **Ocean, Atmosphère, Hydrologie**

Arrêté ministériel : 25 mai 2016

Présentée par

Clément Misset

Thèse dirigée par **Alain Recking**
Et codirigée par **Cédric Legout**

Préparée au sein d'**IRSTEA Grenoble**, équipe **Erosion Torrentielle,
Neige et Avalanches** dans l'École Doctorale **Terre Univers
Environnement**

The role of riverbed on suspended sediment transport dynamics in Alpine catchments

Thèse soutenue publiquement le **18/10/2019**, devant le jury composé
de :

Hélène, ROUX

Maître de conférences, INPT-IMFT, Toulouse, *Rapporteuse*

Eric, LAJEUNESSE

Physicien CNAP, IPGP, Paris, *Rapporteur*

Eric, BARTHELEMY

Professeur, Université Grenoble Alpes, INPG-LEGI, Grenoble, *Président*

Ramon J, BATALLA

Professor, Catalan Institute for Water Research, Lleida, *Examineur*

Alain, POIREL

Ingénieur EDF-DTG, Grenoble, *invité*

Cédric, LEGOUT

Maître de conférences, Université Grenoble Alpes, IGE, Grenoble,
Codirecteur de thèse

Alain, RECKING

Chercheur, Université Grenoble Alpes (IRSTEA-ETNA), Grenoble,
Directeur de thèse



Remerciements

Cette thèse est indéniablement le résultat d'un travail collaboratif que je souhaite rappeler ici. En premier lieu je souhaite remercier Alain Recking et Cédric Legout, mes deux directeurs grâce à qui cette thèse a été une réussite. Ils m'ont permis de travailler dans les meilleures conditions, ont tous deux été très présents durant ces trois années faisant d'eux des contributeurs majeurs de ces travaux. Je souhaite ensuite remercier les personnes d'EDF-DTG qui ont contribué de manière significative en apportant leur expertise, un accès à de très nombreuses données et leur confiance pour utiliser les moyens d'EDF lors de campagnes de mesures. Merci à Alain Poirel, Marine Cazihlac, Sébastien Zanker, François Lauters, Ludovic Michel et Guy Cellier. J'aimerais remercier mes deux rapporteurs de thèse, Eric Lajeunesse et Hélène Roux, qui ont effectué une relecture très détaillée du manuscrit et ont montré un intérêt pour ces travaux. Merci également aux autres membres du jury, Eric Barthelemy qui a accepté d'être président et Ramon J. Batalla venu spécialement d'Espagne malgré des blocages dans les transports en Catalogne. Merci à tous pour la qualité des échanges durant la soutenance de cette thèse. Je tiens à remercier Alain Crave, Magali Jodeau, Oldrich Navratil, Frédéric Liebault et Benoit Camenen d'avoir durant trois ans été membres du comité de pilotage de la thèse et d'avoir apporté un regard extérieur et objectif sur l'avancée de ces travaux. Ce travail a également bénéficié de collaborations scientifiques très riches. Merci à Mélanie Bertrand pour les analyses spatialisées dans les Alpes, à Michel Estèves pour avoir partagé des données sur la Bléone et à Oldrich Navratil pour les analyses sur la relation suspension/charriage. Merci à Laurent Borgniet pour les nombreux vols drones réalisés, à Hervé Piegay et Mathieu Cassel pour les traçages RFID, à Thomas Geay, Florent Gimbert et Maarten Bakker pour l'utilisation des hydrophones et capteurs sismiques. Merci à Daniel Vazquez Tarrio pour son aide sur la Séveraisse et à Guillaume Brousse pour son aide sur le Drac. La réalisation des nombreuses mesures de terrain n'aurait également pas été possible sans l'enthousiasme de nombreux stagiaires que je tiens à rappeler. Merci à Brenno Viana Bandeira, Laura Blanc, Mélanie Brachet, Nathan Bodereau, Nathan Valsangkar, Federico Bonazzi, Jack Paloucek, Lucas Montabonnet, Sara Posi, Francesco Tanganelli et Maxence Regazzoni. Merci aux habitants du Valgaudemar, les employés du parc des Ecrins et Bertrand Breuil pour leur accueil chaleureux dans la vallée.

Au-delà des collaborations scientifiques, je tiens à rappeler la qualité de l'environnement dans lequel j'ai évolué durant ces trois années. Merci aux nombreux doctorants, CDD, stagiaires, chercheurs d'IRSTEA et de l'IGE avec qui j'ai partagé mon quotidien. Je tiens en particulier à remercier Guillaume Piton mon co-bureau pour ses conseils et nos nombreuses discussions. Merci également à mes amis et ma famille pour leur soutien. Enfin, merci à Eloïse qui durant ces trois années m'a supporté, encouragé et m'a même aidé à faire des mesures, et bien plus encore.

Résumé

Les grandes quantités de sédiments transportés en suspension dans les rivières alpines sont associées à des problématiques socio-économiques et environnementales telles que le transport de polluants, la dégradation des milieux aquatiques ou l'envasement des retenues hydroélectriques. Pour faire face à ces enjeux, il est important de mieux comprendre le rôle joué par le lit des rivières alpines sur la dynamique de ce transport.

Dans ce but, la première partie de cette thèse rapporte une étude à l'échelle régionale. A partir de larges bases de données issues de la littérature et de nouvelles mesures de terrain, elle étudie i) l'influence de la configuration des sources sédimentaires sur la variabilité du transport solide par suspension (via l'analyse des hystérésis entre débits et concentrations), ii) l'estimation de la quantité et de la disponibilité des particules fines stockées dans le lit des rivières Alpines et iii) l'analyse de la relation entre transport solide par suspension et mobilité du lit de ces rivières. Ces analyses montrent que la configuration du bassin versant en amont du point d'observation, i.e. la capacité à produire des flux versus la capacité à stocker temporairement ces flux, contrôle significativement la dynamique du transport solide par suspension observée en aval. Ce travail montre également que de grandes quantités de sédiments fins sont stockées dans le lit de certaines rivières Alpines. Pour ces rivières et pour des gammes de débits élevées, il est possible de prédire une partie significative des flux en suspension à partir d'une modélisation de la mobilité du lit.

La seconde partie de la thèse teste ces résultats à une échelle locale. Pour cela, une campagne de mesures a été réalisée durant une saison complète de fonte sur un cours d'eau alpin, la Séveraisse. Un large panel de mesures directes (échantillonnage des flux, relevés topographiques et granulométriques, traçage sédimentaire, mesure de concentration en particules fines dans la matrice graveleuse) et indirectes (capteurs sismiques, turbidimètres, imagerie aérienne et au sol) a été mis en œuvre pour mesurer la suspension, le charriage et les évolutions topographiques sur un tronçon de 3.5 km. Ces mesures confirment que les particules fines transportées par suspension interagissent fortement avec le lit dans ce type de tronçon morphodynamiquement actif. Ce dernier peut être perçu comme une zone tampon intermédiaire contrôlée par le forçage amont sédiments-débit liquide ainsi que par la mobilité du lit et sa morphologie. Nous montrons également dans cette partie l'intérêt de combiner des mesures continues indirectes des flux en suspension (turbidimètre) et de la mobilité du lit (capteur sismique) pour détecter les interactions entre sédiments fins et grossiers et identifier la source des particules en suspension.

ABSTRACT

The large quantities of sediment transported as suspension in Alpine rivers are associated with important socio-economic and environmental issues such as pollutant transfer, aquatic habitat degradation or dam siltation. To address these issues, it is required to better understand the role of Alpine river beds on the dynamics of this transport.

To this end, the first part of the manuscript reports a regional study in which large datasets from the literature and new field measurements are used to investigate i) the influence of sediment sources configuration on suspended load variability (through the analysis of hysteresis between flow rate and suspended sediment concentration), ii) the quantity and availability of fine particles stored in Alpine river beds and iii) the relation between suspended load and river bed mobility. These analyses show that the catchment configuration upstream the observation point, i.e. the capacity to produce upstream suspended sediment versus the capacity to buffer these fluxes can significantly control the suspended load dynamics observed downstream. This first part also shows that large quantities of fine particles can be stored in certain Alpine rivers. For these rivers and for high flow rates ranges, it was possible to predict a significant part of suspended load by using riverbed mobility modeling.

The second part of the thesis tests these results at a local scale. To do so, an important field campaign was performed during the entire melting season of a typical Alpine river, the Séveraisse. A large panel of direct (fluxes samplers, topographic and grain size surveys, particle tracking, gravel matrix fine particle concentration sampling) and indirect measurements (seismic and turbidity sensors, aerial and ground based imagery) was used to measure suspended load, bedload and topographic changes on a 3.5-km reach. These measurements confirm that suspended particles strongly interact with the river bed of that kind of morphodynamically active streams. The latter can be considered as an intermediate buffer controlled by the upstream hydro-sedimentary forcing (suspended sediment concentration and water discharge) and by the river bed mobility and morphology. We also show in this part the interest to combine continuous indirect measurements of suspended load (turbidity sensor) and bed mobility (seismic sensor) to detect fine-coarse sediment interactions and unravel suspended load sources.

Table of content

Résumé.....	3
Abstract.....	5
Table of content.....	6
Introduction.....	12
0.1 Motivations.....	12
0.2 Scientific context.....	15
0.2.1 Suspended load partitioning.....	15
0.2.2 Modelling strategies.....	18
0.2.3 Field measurement techniques.....	22
0.2.4 State of the art of field observations.....	24
0.3 Scientific questions.....	29
Chapter 1. An attempt to link suspended load hysteresis patterns and sediment sources configuration in alpine catchments.....	32
1.1. Abstract.....	33
1.2. Introduction.....	33
1.3. Material and methods.....	36
1.3.1. Hydro-Geomorphological characteristics of the catchments.....	36
1.3.1.1. Spatial information used.....	36
1.3.1.2. Hydrological regimes.....	37
1.3.1.3. Geomorphological characteristics.....	38
1.3.2. Suspended load time series.....	39
1.3.3. Hysteresis analysis tools.....	40
1.3.4. Sediment sources characterization.....	42
1.4. Results.....	45
1.4.1. Runoff event characteristics.....	45
1.4.2. Variability of discharge-concentration hysteresis in alpine catchments.....	46
1.4.3. Sediment sources analysis.....	48
1.4.4. Relation between sediment sources configuration and dominant hysteresis patterns.....	51
1.5. Discussion.....	53
1.5.1. dominant hysteresis patterns and transport efficiency.....	53

1.5.2.	Influence of catchment geomorphological characteristics	55
1.5.3.	Limitations and implications	56
1.6.	Conclusions	57
1.7.	Notations	58
1.8.	Acknowledgements	59
1.9.	Appendix	60
1.9.1.	Source configuration index.....	60
1.9.2.	Eroded area index.....	60
1.9.3.	Bed area index.....	61
Chapter 2.	Assessment of fine sediment river bed stocks in seven alpine catchments.....	62
2.1.	Abstract	63
2.2.	Introduction.....	63
2.3.	Material and Methods	64
2.3.1.	Studied area.....	64
2.3.2.	Sampling protocol	65
2.3.3.	Local stocks integration over the catchment	67
2.3.4.	Estimate of available stocks.....	69
2.3.5.	Suspended sediment yield measurements	72
2.4.	Results	73
2.4.1.	General overview of the measurements	73
2.4.2.	Local stocks	74
2.4.3.	Aerial photo analysis.....	78
2.4.4.	Total stocks and comparison with annual fluxes	80
2.4.5.	Assessment of available stocks	82
2.5.	Discussion	83
2.5.1.	Spatial variability of the river bed stocks	83
2.5.2.	Temporal variability of the river bed stocks	85
2.5.3.	Available river bed stocks significance.....	86
2.6.	Conclusion.....	87
2.7.	Notations	88
2.8.	Appendix	90
2.8.1.	Parameters used for river bed stock estimate.....	90
2.8.2.	Settling velocity and flocculation properties of riverbed stocks	91

Chapter 3. Quantifying bed-related suspended load in gravel bed rivers through an analysis of the bedload-suspended load relationship 93

- 3.1. Abstract 94
- 3.2. Introduction..... 94
- 3.3. Material and methods 97
 - 3.3.1. Data sets..... 97
 - 3.3.2. Data analysis 99
- 3.4. Results 100
 - 3.4.1. Correlation analysis 100
 - 3.4.2. Calibration of a relation explaining the SSC..... 102
 - 3.4.3. SSC prediction for the alpine data set..... 104
- 3.5. Discussion 108
 - 3.5.1. Sediment transport variability 108
 - 3.5.2. Sediment sources in alpine rivers 108
 - 3.5.3. River bed mobility 111
 - 3.5.4. On the origin of fine sediments 112
- 3.6. Conclusion..... 113
- 3.7. Appendix 114
 - 3.7.1. Bed load calculation..... 114
 - 3.7.2. Prediction in alpine rivers using proxies derived from the flow rate..... 115
- 3.8. Notations 118

Chapter 4. Combining multi-physical measurements to quantify bedload transport and morphodynamics interactions in an Alpine braiding river reach..... 121

- 4.1. Abstract 122
- 4.2. Introduction..... 122
- 4.3. Study area 125
- 4.4. Material and Methods 126
 - 4.4.1. Direct bedload transport sampling 126
 - 4.4.2. Indirect bedload transport measurements..... 127
 - 4.4.3. Coarse particles displacement 128
 - 4.4.4. Quantifying morphological changes 129
 - 4.4.5. Hydraulic calculations 130
- 4.5. Results 131
 - 4.5.1. Overview 131
 - 4.5.2. Bedload dynamic 132

4.5.3. Seismic observations	134
4.5.4. Bedload particle mobility	136
4.5.5. Morphological changes	138
4.5.6. Hydraulic changes	141
4.6. Discussion	142
4.6.1. on the interest to combine multiple field techniques.....	142
4.6.2. Interaction of braided river bed morphology with bedload fluxes	145
4.6.3. Implications for reach-averaged bedload modeling.....	147
4.7. Conclusion.....	148
4.8. Acknowledgments and data	149
4.9. Notations	149
4.10. Appendix A	150
4.10.1. Hydraulics calculation	150
4.10.2. Bed load calculation.....	151
4.10.3. Resampling technique to detect temporal trend on bedload sampling.....	151
4.11. Appendix B	152
4.11.1. Ground-based camera observations.....	152
4.12. Appendix C.....	156
4.12.1. Bed load measurement.....	156
4.12.2. Bed grain size distribution.....	158
Chapter 5. Quantifying erosion and deposition of fine sediments in a typical alpine river.....	160
5.1. Abstract	161
5.2. Introduction.....	161
5.3. Area studied	163
5.4. Material and Methods	164
5.4.1. Fine sediment budget framework.....	164
5.4.2. Suspended load measurement	165
5.4.3. Uncertainty analysis for suspended fluxes	166
5.4.4. Fine sediment stock estimate.....	168
5.4.5. Bedload transport measurement.....	169
5.5. Results	169
5.5.1. Rating curves	169
5.5.2. Hydrosedimentary dynamics.....	170
5.5.3. Sediment budget.....	172

5.5.4. Temporal changes	174
5.5.5. Factors controlling erosion and deposition processes	176
5.6. Discussion	177
5.6.1. Importance of erosion and deposition processes	177
5.6.2. Conceptual description of the processes involved	178
5.6.3. Implication for suspended load modeling	179
5.7. Conclusion.....	180
5.8. Notations	181
5.9. Appendix	182
5.9.1. Error quantification for suspended load measurements.....	182
5.9.2. Fine sediment stock estimate.....	188
5.9.1. Fine particle grain size distribution.....	189
5.9.2. Ferguson equation	189
5.9.3. Main event characteristics.....	190
Chapter 6. Identifying bed-related suspended load by using continuous turbidity and seismic measurements in a gravel bedded alpine stream	192
6.1. Introduction.....	193
6.2. Field site and Methods	194
6.3. Results	197
6.4. Discussion	199
6.4.1. Evolution of the origin of suspended particles during a 4 month period ...	199
6.4.2. Interest of the combined use of turbidity and seismic measurements	201
6.5. Conclusions.....	201
6.6. Appendix	202
Conclusion and perspectives	205
Synthesis	205
Consistency between observations made at the catchment and at the reach scale.....	205
Main conclusions concerning the processes observed.....	207
Perspectives	209
Practical application.....	209
Future challenges.....	213
Appendix.....	216
Conceptual modelling.....	216
References.....	221

Introduction

0.1 MOTIVATIONS

Rivers transport sediments from the mountains to the oceans. The coarser fraction of sediments (from boulder to sand size) is transported at the bottom of the river bed when forces exerted by the water flow are sufficient to initiate sliding, rolling or saltating of these particles. This mode of transport is called bedload. The finer fraction of sediments (from sand to clay size) is transported in the water column when the flow turbulence is high enough to keep these particles in suspension. This mode of transport is called suspended load. In most rivers, suspended load represents a significant part if not the majority of sediment fluxes (Figure 0.1). Thus suspended load is an important component of river system functioning. This is particularly true in Alpine rivers on which this manuscript is focused. Indeed, mountainous environments have been shown to generate high suspended fluxes [*Mano et al.*, 2009; *Meybeck et al.*, 2003; *Navratil et al.*, 2012; *Sadaoui et al.*, 2016; *Vanmaercke et al.*, 2011].

While the finest fraction of particles transported as suspension are a vector of nutrients essential for estuarine ecosystems [*Le Pape et al.*, 2013; *Ludwig and Probst*, 1998], river managers and practitioners often have to deal with issues associated with this fine particle transport. Water resources can be affected by pollutant such as PCB or heavy metal carried by fines and stored in the river bed or in flood plains [*Estrany et al.*, 2011; *Karickhoff et al.*, 1979; *Owens et al.*, 2005; *Walling et al.*, 2003]. In Alpine rivers, hydropower plants reservoirs are commonly flushed to prevent siltation [*Camenen et al.*, 2013; *Legout et al.*, 2018]. Other anthropogenic activities (construction work in the river bed or mining activities) and natural functioning of Alpine watersheds (floods, debris flows and landslides) can also release important quantities of fine particles in the river system. These suspended load pulses can lead to river bed clogging (Figure 0.2) which often generate a subsequent degradation of aquatic habitats [*Armstrong et al.*, 2003; *Mathers et al.*, 2017; *Owens et al.*, 2005; *Sear*, 1993; *Waters*, 1995].

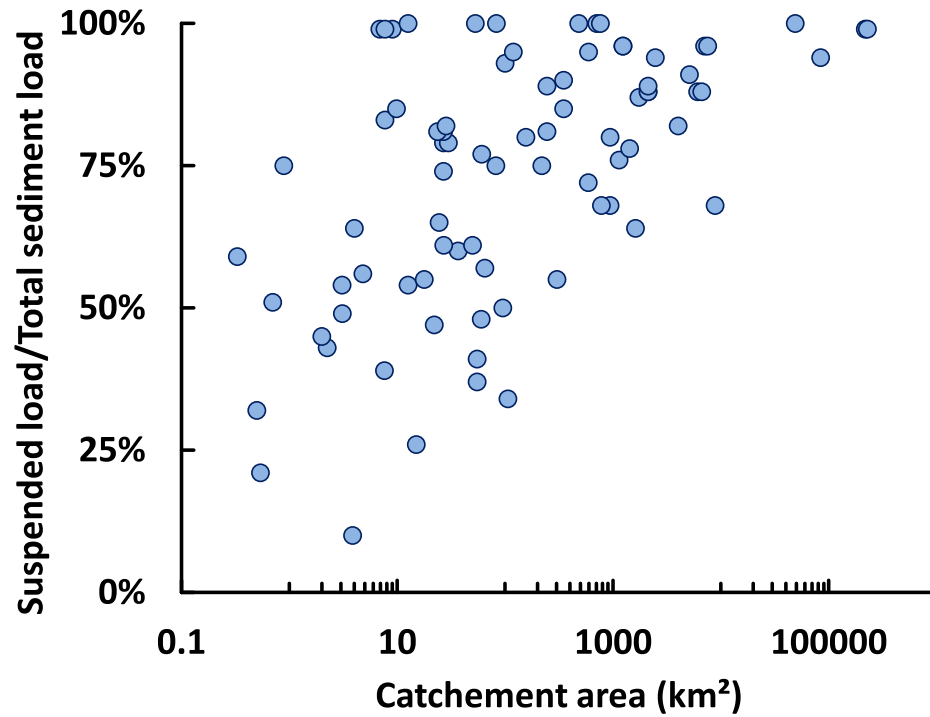


Figure 0.1: Long term measurements of suspended load fraction (suspended load versus total sediment load) in 82 gravel bed rivers worldwide using the dataset collected by Turowski et al. (2010).



Figure 0.2: Example of clogged river bed in the Arc River (French Alps).

Fine particles delivered to the river system can also impact the long term riverbed morphology. Observations in the field and in flume experiments have for instance shown that increasing the presence of cohesive material mainly in the clay-silt range ($<63\mu\text{m}$) leads to an increase in the flow conditions needed to initiate river bed mobilization in gravel bedded streams [Barzilai et al., 2013; Perret et al., 2018] leading to gravel bar stabilization. Perret et al. (2018) reported a 12% increase of the critical shear stress in their flume experiment while Barzilai et al. (2013) reported a critical value twice larger in the presence of cohesive material in the Nahal Eshtemoa River. On the other way around, it has been observed that adding fine particles in the sand size range can lead to an increase of riverbed mobility [Dudill et al., 2017; Hill et al., 2017; Perret et al., 2018]. Fine particles deposits can also enhance vegetation growth in the active corridor of rivers. This can lead to safety issues due to gravel bars fixation, channel narrowing or increase of river bed roughness [Asaeda and Rashid, 2012]. Such long term morphology stabilization is a particular important issue in Alpine rivers that have recalibrated beds, impacted hydrological regimes and high fine sediment supply [Claude et al., 2018; Jourdain, 2017].

Finally, the transport of fine particles is often associated with the siltation of dams and reservoirs. Siltation worldwide has been estimated in 2004 to be equivalent of 0.5% of storage capacity lost per year which suggests that half the total storage capacity will be lost in 2100 ignoring new dams created after 2004 [Kondolf et al., 2014; Sumi et al., 2004]. Annandale (2013) estimated that despite new dams are built every year, the effective storage capacity is decreasing since 1995. A typical example of dam siltation problem in the French Alps is shown in Figure 0.3.



Figure 0.3: Example of siltation on the Escale Dam on the Durance river in the south of France ($44^{\circ} 05' 08'' \text{ N}$, $6^{\circ} 00' 42'' \text{ E}$) built between 1959 and 1963. Aerial photograph were obtained from the IGN website (<http://remonterletemps.ign.fr/>).

The above mentioned issues show that studying the transport of fine particles is crucial for an environmentally friendly, economically viable and safe river management. Practitioners typically need to estimate the flux of fine particles from instantaneous to annual time scales in watersheds for which suspended load measurements are not necessarily available. As mentioned previously, this is particularly true for Alpine catchments characterized by high suspended loads associated with important socio-economic and environmental issues. These basins generally have large alluvial streams and highly active hillslopes sources [Navratil et al., 2012]. It is consequently often

difficult in that context to identify the origin of fine sediments and their interactions with the river bed. This information is however fundamental for suspended load modeling and consequently for long term catchments and rivers management in the Alps. In the following manuscript we investigate the role of riverbed on suspended sediment transport dynamics in Alpine catchments.

0.2 SCIENTIFIC CONTEXT

0.2.1 SUSPENDED LOAD PARTITIONING

As introduced previously, sediment transport was conceptually partitioned into bedload and suspended load. However, Einstein et al. (1940) observed in the Enoree river that the finer fraction of suspended load was independent from the water discharge and could not be found in appreciable quantities (<10%) at the surface of the riverbed. On the contrary, the coarser fraction of suspended load co-varied with the flow rate and could be found at the riverbed surface. They consequently proposed that the finer fraction of suspension not found in appreciable quantities on the river bed surface was produced from an upstream source and was washed through the system without interacting with the river bed. This suspended load fraction was called wash load. Following this concept, Partheniade (1977) proposed that a part of suspended load called suspended-bed material load could have a bedload function (being a function of flow capacity) while wash load (being a function of sediment supply) couldn't. Partheniade proposed a critical sediment size of 0.06mm for this partition. A third distinction between the two suspended fractions was based on the concentration profile in the cross section that can be described by the Rouse number (R_o) [Rouse, 1937] which balances the settling velocity and the turbulence suspending fine particles:

$$R_o = \frac{w_s}{\kappa u^*} \quad (0.1)$$

in which, w_s (m s^{-1}) is the settling velocity for suspended particles considered, κ (-) is the Von Karman constant equal to 0.4 and u^* (m s^{-1}) the friction velocity at the bottom of the river bed. For instance, Belperio (1979) observed on the Burdekin River that clay and silt particles (low Rouse numbers) were homogeneously distributed in the cross section while sand particles (higher Rouse numbers) were more concentrated near the bottom of the bed. A critical Rouse number of 0.06 was proposed by Wang and Dittrich (1992) for this partition. More recently, Hill et al. (2017) investigated the criteria defining wash load using flume experiments. They used a flume at equilibrium fed with coarse particles in which they added a second equivalent load composed of a finer material. They changed the size ratio between initial and added load from 1/1 to 1/150. For size ratio close to one, the river bed slope increased because higher shear stresses were needed

to transport the additional load. For intermediate a size ratio when the fine load could not freely percolate in the gravel matrix and strongly interact with coarsest particles at the bed surface, the river bed slope decreased. They considered it as a lubrication regime. When an even finer load was added, the river bed slope did not significantly changed and the load added, deeply infiltrated in the subsurface of the gravel matrix was considered as wash load. Hill et al. (2017) observed that the transition between lubrication and wash load occurred for sediment size ratios (D^* , Eq.0.2) between bed particles (D_{bed} , m) and suspended particles ($D_{suspension}$, m) larger than 30, Rouse numbers for suspended material (Ro , Eq.0.1) lower than 0.8 and supply ($q_{Ssupply}$, $m^2 s^{-1}$) versus transport capacity ($q_{Scapacity}$, $m^2 s^{-1}$) ratios for suspended material (qs^* , Eq.0.3) lower than 0.05.

$$D^* = \frac{D_{bed}}{D_{suspension}} \quad (0.2)$$

$$qs^* = \frac{q_{Ssupply}}{q_{Scapacity}} \quad (0.3)$$

All these observations and concepts led to the general idea that the finest fraction of sediment is transported efficiently with limited interactions with the river bed in natural rivers. However, in the past few decades, several studies questioned about the relevance of the wash load concept and its definition. In Alpine rivers having large alluvial streams [Navratil et al., 2010] and shallow turbulent flows strongly interacting with the river bed [Legout et al., 2018] the relevance of this concept was questioned by several field observations [Navratil et al., 2012]. Indeed, while fine particles are sometimes absent from the river bed surface, flume and field observations show that large quantities of this finest material can be stored in the subsurface of gravel bedded streams especially when pore spaces are initially empty [Camenen et al., 2015; Diplas, 1994; Frostick et al., 1984; Gibson et al., 2009]. Such subsurface storage of fines can be observed in most Alpine gravel bedded rivers (Figure 0.4):

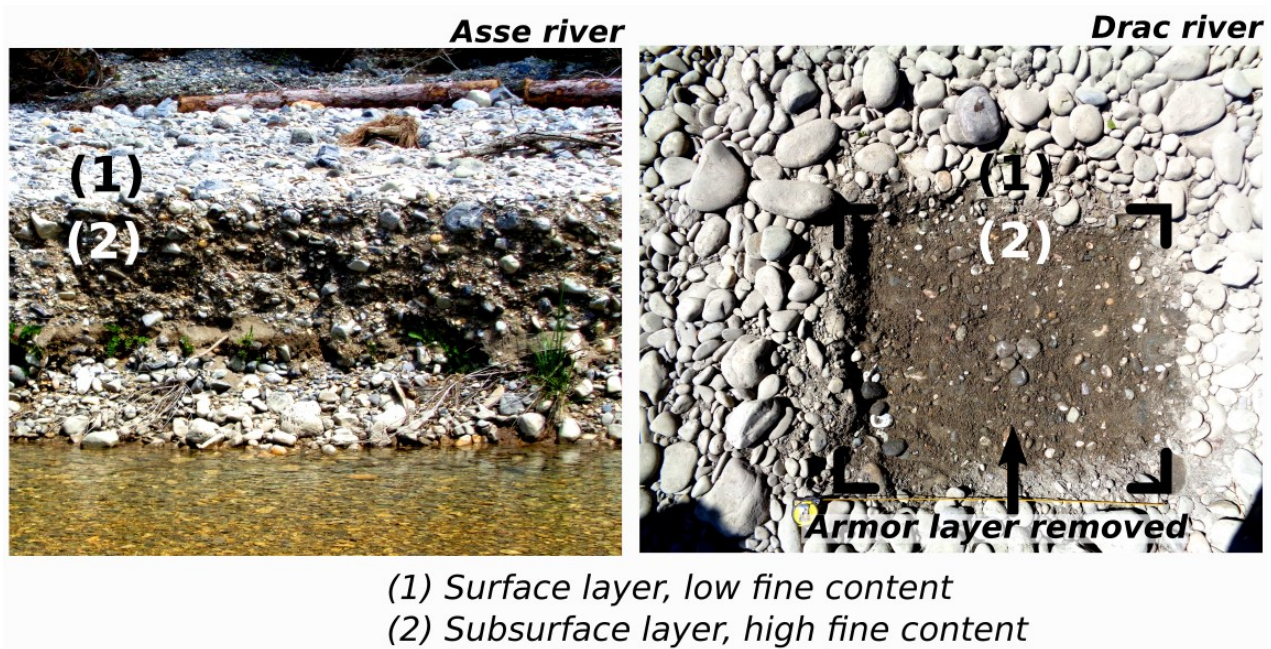


Figure 0.4: Fine particles stored in subsurface under a poorly mobile armor layer in the Asse and Drac Rivers.

At the catchment scale, several studies in various contexts have shown that the quantity of these fine particles stored in the river bed can be equivalent to the annual fluxes [Collins and Walling, 2007a; Estrany et al., 2011; H. Marttila and Kløve, 2014; Navratil et al., 2010]. The infiltration and capture of fines into the gravel matrix was found to occur even for conditions attributed to wash load considering all the above mentioned criteria [Mooneyham and Strom, 2018]. Several studies have also shown by using sediment budget approach [Guillon et al., 2018; Marteau et al., 2018; Navratil et al., 2012; Orwin and Smart, 2004b] or by measuring simultaneously suspended load and bedload transport [Meunier et al., 2006; Turowski et al., 2010] that even the finest fraction of suspension interacts with the river bed. All of the mentioned studies show that suspended load is a complex process. Alpine catchments are often characterized by large active riverbeds composed of poorly sorted gravel bedded streams connected to highly active primary hillslope sources (Figure 0.5). Consequently, in that context, the degree to which suspended load interact with the riverbed is uncertain which makes it difficult to be understood and modelled.

Badland area few km upstream



Large alluvial gravel bed river

Figure 0.5: Typical Alpine catchment configuration with highly active hillslope sources connected to large alluvial gravel bed river (Asse catchment, Southern French Alps).

0.2.2 MODELLING STRATEGIES

A large variety of modeling approaches have been developed for suspended load in the last decades. This diversity of approaches resulted from the range of application, the variety of conceptual descriptions, the complexity and the availability of suspended load data.

Physically based approaches

Similarly to bedload, bed-material suspended load has been modeled by semi-theoretical laws based on flume or field data [Bagnold, 1966; Camenen and Larson, 2008; Celik and Rodi, 1991; Engelund and Hansen, 1967; Van Rijn, 1984]. These equations generally relate local flow conditions such as flow velocity (U), Shield number (τ^* , Eq.0.4) or stream power (P , Eq.0.5) with a capacity to transport a certain flux of suspended material (q_s , $\text{m}^2 \text{s}^{-1}$).

$$\tau^* = \frac{\tau}{(\rho_s - \rho)gD} \quad (0.4)$$

$$P = \rho gQS \quad (0.5)$$

In these equations, τ (Pa) is the shear stress at the bottom of the river bed, ρ_s (kg m^{-3}) the sediment density, ρ (kg m^{-3}) the water density, g (m s^{-2}) the gravity acceleration, D (m) the sediment diameter considered, Q ($\text{m}^3 \text{s}^{-1}$) the water discharge and S (-) the river bed slope. The energetic approach initially proposed by Bagnold (1966, Eq.0.6) considers that the river dissipates a certain quantity of energy to transport some particles as bedload and to maintain others in suspension:

$$q_s = e_s(1 - e_b) \frac{P}{(\rho_s - \rho)gW} \times \frac{U}{w_s} \quad (0.6)$$

in which W (m) is the width of the river, e_b (-) and e_s (-) are respectively the bedload and suspended load transport efficiency. These efficiency coefficients are ratios between the bedload work rate or suspended load work rate and the stream power. Mechanistic approaches such as the ones of Van Rijn (1984) or Camenen and Larson (2008) rely on a detailed description of flow velocity (U) and suspended sediment concentration (SSC) profiles. Suspended load is then derived by integrating the product of these two profiles over the water depth, between the water surface ($z = d$) and the top of the bedload layer ($z = a$):

$$q_s = \int_{z=a}^d SSC(z)U(z)dz \quad (0.7)$$

One of the main difficulties of such approach is to define the bedload layer height a and the bottom concentration $SSC(a)$ which is often considered a function of bedload transport.

These physically based approaches were mainly built using flume or field measurements in lowland sandy rivers. They implicitly consider that the availability of fine particles is infinite at the riverbed surface and that particles are progressively extracted from the bedload layer when forces exerted by the flow are increasing. These models provide a good understanding of the local physical processes and can be used with limited data. However, their reliability is usually limited and their applications should be restricted to cases for which the equations were built. In particular, these approaches exclude the transport of suspended particles over a coarse and poorly mobile armor layer typically found in Alpine gravel bedded rivers (Figure 0.4). In these armored river beds, fine particles are generally absent at the bed surface. Consequently, their availability is likely to be finite and could depend on the armor layer mobility.

For the finest suspended load fraction that cannot be modeled by capacity functions, an approach widely used in numerical models is to solve advection-dispersion equations with source terms representing erosion and deposition [Guertault *et al.*, 2018; Launay *et al.*, 2019]. Deposition fluxes (D , Eq.0.8) are represented by the Krone (1962) equation for shear stresses lower than a critical value for deposition ($\tau_{c,deposition}$, Pa).

$$D = w_s \times SSC \times (1 - \tau / \tau_{c,deposition}) \quad (0.8)$$

Erosion fluxes (E , Eq.0.9) are resented by the Partheniade (1977) equation for shear stresses higher than a critical value for erosion ($\tau_{c,erosion}$, Pa):

$$E = K \times (\tau / \tau_{c,erosion} - 1) \quad (0.9)$$

These erosion and deposition relations were both derived from flume experiments with fine material alone. Consequently, one can expect they are relevant in case of transport over a riverbed mainly composed of uniform fine particles that can be considered more or less impervious. However, in case of a permeable river bed typically found in gravel bedded Alpine streams these relations might be dramatically different as was observed by Mooneyham and Strom (2018) or by Krishnappan and Engel (2006). Also in Alpine rivers, fine particles can have cohesive properties which are difficult to quantify [Legout *et al.*, 2018]. This generates aggregation-disaggregation processes [Grangeon *et al.*, 2014] so that suspension deviates substantially from the non-cohesive laws previously mentioned [Wendling *et al.*, 2015] which makes it even more complex to model in that context.

Data driven approaches

Due to the complexity and variety of process to consider, other types of modeling approach have been proposed based on a large availability of suspended load measurements. This data driven approach includes empirical, statistical and conceptual models that were used for both suspended-bed material load and wash load.

Empirical models based on hydro-meteorological and land use data have for instance been proposed to estimate annual suspended load [Ludwig and Probst, 1998; Wischmeier and Smith, 1978] or suspended yield at the event scale [Duvert et al., 2012]. These approaches can be useful and provide information on the main drivers of suspended load for large spatial analysis. They however remain limited for detailed local studies or for shorter time scales analysis. Several conceptual models having conceptual reservoirs and functions to produce, store and transfer fine sediments have been proposed to reproduce and predict suspended load on a daily basis or at the event scale [Asselman, 1999; Doomen et al., 2008; Mano, 2008; Picouet et al., 2009]. In recent works, Park and Hunt (2018) and Park et al. (2019) developed a conceptual model to reproduce storage and release of fine particles depending on the river bed mobility in gravel bed rivers. Based on observations made in 38 rivers and a literature review, their model considers that fine particles infiltrate in the gravel river bed during low flow conditions until there is no more available space in the river bed. Then, when a critical flow rate corresponding to gravel mobilization is exceeded, their conceptual model considers that fine particles stored in the river bed are resuspended.

Purely statistical models have also been widely used to predict suspended load. The simplest one is a power law regression between suspended sediment concentration (SSC) and the water discharge (Q). It is often used to predict suspended load using continuous Q measurements (rating curve technique):

$$SSC = k_1 Q^{k_2} \quad (0.10)$$

While widely used such approach usually leads to low accuracy as the relation between SSC and Q is often highly variable through time [Walling and Webb, 1988] and particularly in Alpine catchments [Mano et al., 2009]. More complex statistical models using multiple regression techniques [Mano et al., 2009], stepwise regression [Gellis, 2013] or data mining models and artificial neuronal network [Boukhrissa et al., 2013; Chen and Chau, 2016; Khosravi et al., 2018] were also used to increase significantly the accuracy of predictions for practical studies. While these conceptual and statistical models can give reliable predictions even at short time scales, it is difficult to use them to better understand the physical processes involved, especially when purely statistical models are used. Also these approaches intrinsically need long term measurements as they need to be calibrated for each site.

This wide variety of modeling approach developed in the last past decades show the large range of possible applications and the variety of physical processes considered as suspended load. Consequently, one key question for practical studies is to determine which processes control the dynamic of suspended load and what are the main sources of fine particles. Also for all modeling strategies, including those based on a detailed physical description, measurements are the base of any model development. Some of the commonly used field measurement techniques are presented in the following section.

0.2.3 FIELD MEASUREMENT TECHNIQUES

a) Fluxes measurements

Suspended load fluxes are usually measured in the field by direct water sampling to determine the suspended sediment concentration. Automatic pumping samplers are often used when the SSC concentration can be considered homogeneous in the cross section. Because suspended load can be highly variable in time, especially in mountainous and mediterranean catchments [Mano *et al.*, 2009; Williams, 1989] these direct sampling are often coupled with continuous water turbidity measurement (Figure 0.6) to allow interpolation through time [Guillon *et al.*, 2018; McDonald and Lamoureux, 2009; Navratil *et al.*, 2011; Smith and Dragovich, 2009]. Turbidity sensors generally have a detector aligned with a certain angle to a beam and record the scattered light which is function of the concentration of fine particles in the flow.

By assuming a homogeneous concentration over the cross section and by measuring the water discharge (through continuous water pressure sensor and gauging) at the same station, suspended sediment load (SSL, g s^{-1}) can be calculated by multiplying SSC (g l^{-1}) and Q ($\text{m}^3 \text{s}^{-1}$):

$$SSL = SSC \times Q \quad (0.11)$$

While turbidity is a function of SSC, it is also influenced by several other parameters and particularly by the suspended sediment size [Landers and Sturm, 2013]. Consequently, turbidity cannot be used alone to accurately estimate SSL. It can however be used as a proxy to capture the temporal dynamic of both SSC and suspended sediment size changes. When the SSC cannot be considered homogeneous over the cross section, which can for instance be the case for sand suspension in large rivers having not well mixed flows, isokinetic depth integrating samplers can be used [Thomas, 1985]. These measurements are however time consuming and do not provide a continuous measurement though time. Indirect techniques using for instance the intensity of backscattered sound of acoustic Doppler current profilers (ADCP) to measure the cross

section distribution of SSC are consequently under development [Baranya and Józsa, 2013].

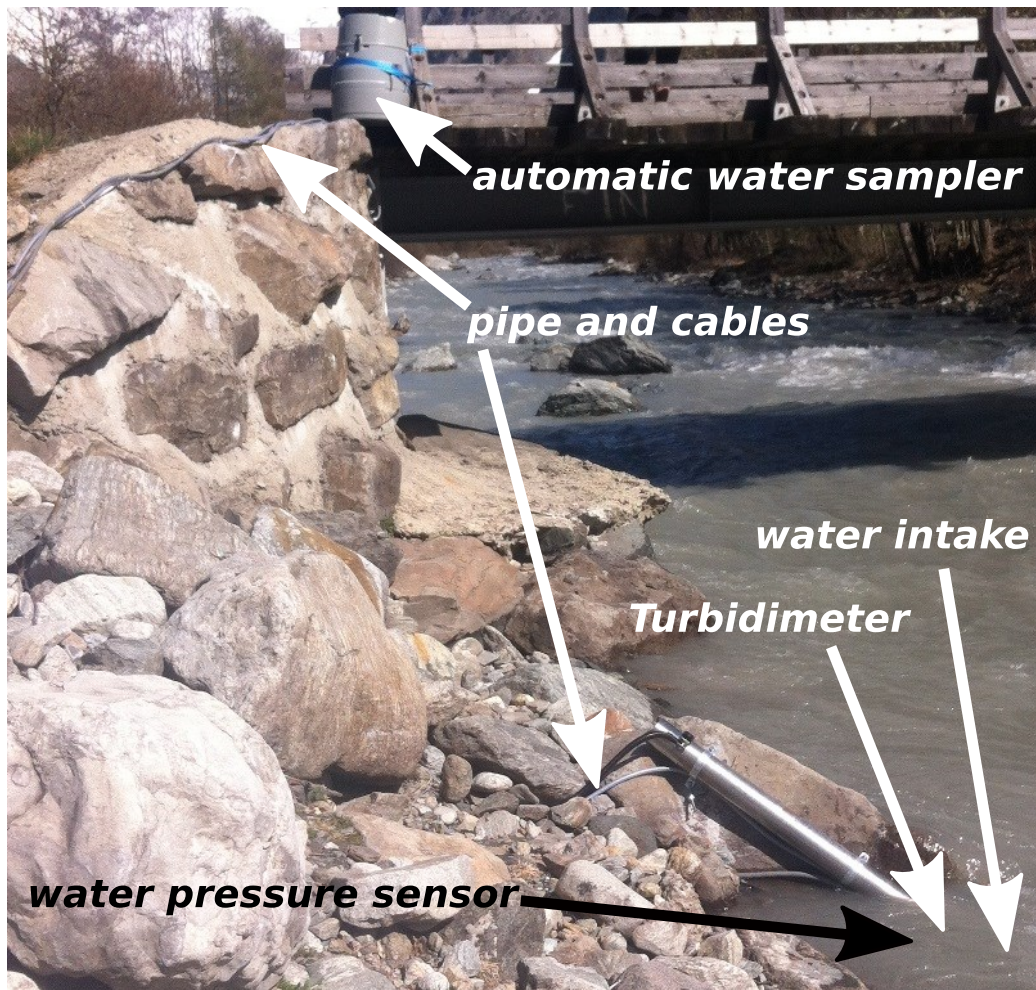


Figure 0.6: Typical monitoring station used to measure suspended sediment load by coupling direct automatic samples, continuous turbidity measurements and water pressure sensor.

b) Stocks measurements

In addition to measuring the fluxes of fine particles, it is often of interest to estimate their stocks in the river bed. Lambert and Walling (1988) were the first to apply a simple field protocol to estimate the concentration of fine particles in the Exe riverbed, a gravel bedded river in the UK. This technique is based on a resuspension of fine sediment stored under water in a cylinder. Several degrees of bed disturbance are used to make a difference between surface deposits and subsurface storage. While associated with large uncertainties [Duerdoth *et al.*, 2015] this method has been widely used in various environments to quantify temporal changes in bed storage and to perform sediment budget approach at the catchment scale [Buendia *et al.*, 2016; Collins and Walling,

2007a; Marteau *et al.*, 2018; Naden *et al.*, 2016; Piqué *et al.*, 2014]. Compare to frozen cores which can be considered a reference, the Lambert and Walling protocol is much faster and less expensive which permits to perform many measurements and cover the large spatial variability [Duerdoth *et al.*, 2015]. However, this protocol can only be used for underwater storage. For mountainous rivers having large active width and large potential stocks stored in dry areas, the protocol was adapted by Navratil *et al.* (2010).

0.2.4 STATE OF THE ART OF FIELD OBSERVATIONS

The way we conceptualize and understand suspended load should necessary be compared with available field observations to test and validate hypothesis. Some of these field observations are reported in the following section.

a) Variability and hysteresis of the SSC-Q relation

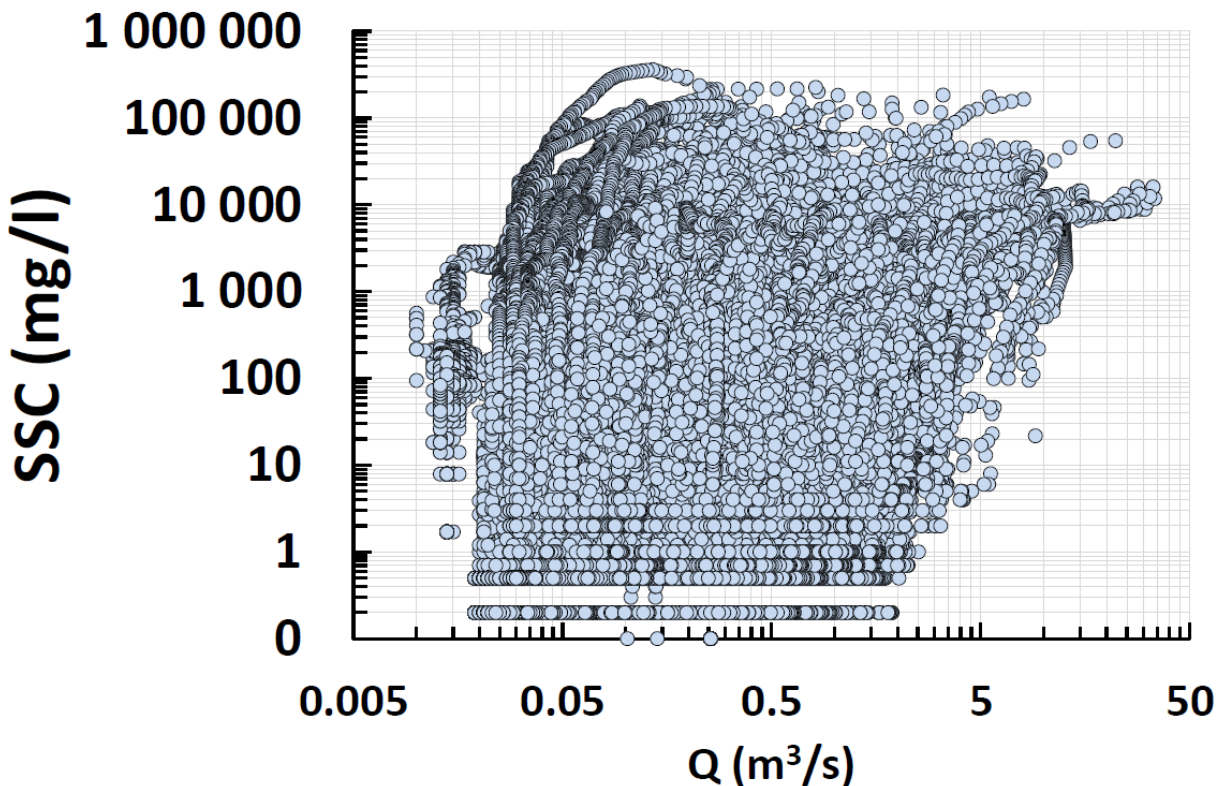


Figure 0.7: Relation between suspended sediment concentration (SSC) and the water discharge (Q) in the Galabre Catchment (22km²) in the southern French Alps (2007-2013, 10-min time step).

In many field studies, the relation between flow rate (Q) and suspended sediment concentration (SSC) has been analyzed using high frequency measurement techniques. This SSC-Q relation was found to be highly variable between catchments. Vaughan *et al.* (2017) have observed that this variability was controlled by the near channel environments for moderate to high flow rates while SSC dynamic during low to moderate

flow rates was controlled by the catchment land use. This SSC-Q relation is also highly variable though time in a given catchment which makes it difficult to predict suspended load [Walling and Webb, 1988]. An example of the temporal variability of the SSC-Q relation observed on the Galabre catchment in the Alps [Esteves et al., 2018; Legout et al., 2013; Navratil et al., 2012] is shown in Figure 0.7.

This temporal variability is often characterized by hysteresis phenomena that are observed at various time scales [Aguilera and Melack, 2018; Andermann et al., 2012; Mao and Carrillo, 2016; Sun et al., 2016]. At the event scale, these hysteresis loops have been first classified by Williams (1989). A simplified classification based on the one of Williams is shown in Figure 0.8.

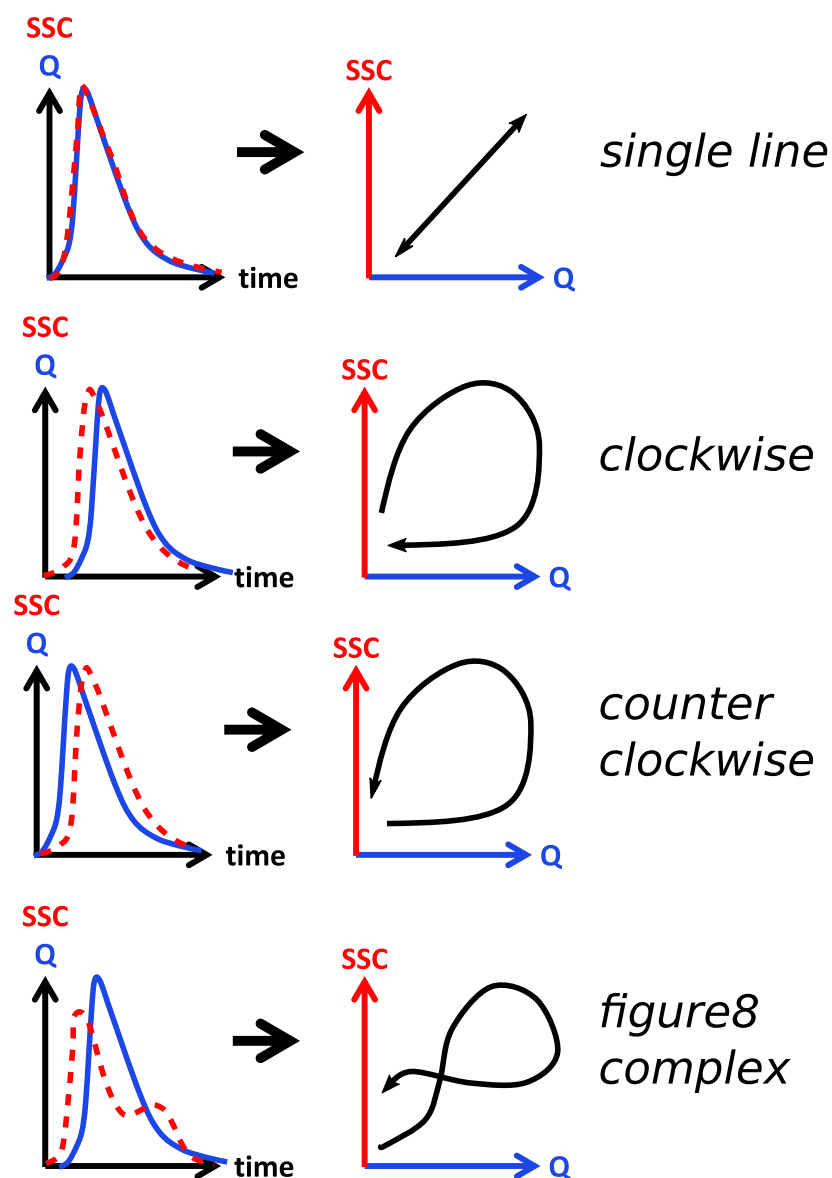


Figure 0.8: Simplified SSC-Q hysteresis classification proposed by Williams (1989).

Many explanations have been proposed to qualitatively interpret these phenomena [Gellis, 2013]. Amongst the large variety of interpretations proposed, the contribution of various sediment sources is often considered as the main explanation of these loops. Clockwise hysteresis are often considered as the result of close source contribution (riverbed network) while counterclockwise loops are considered as the result of more distant sources (hillslopes) [Baca, 2010; Klein, 1984; Hannu Marttila and Kløve, 2010; Navratil et al., 2012; Park and Hunt, 2017; Williams, 1989]. No-hysteresis is often interpreted as an unlimited sediment supply [Nistor and Church, 2005; Williams, 1989]. Complex loops such as “figure 8” hysteresis being the result of several processes combination can also be observed. While having information on the origin of fine particles is useful to understand suspended load, a direct link between sources and SSC-Q hysteresis has not yet been confirmed with a quantitative analysis.

b) Fine particles storage in the river network: relative contribution to total fluxes, temporal variability and control parameters

To better understand the way fine particles transit in catchments or because of aquatic habitat quality issues, many studies have focused on fine particles stored in the riverbed. They were mainly based on the Lambert and Walling technique. Depending on the study site, local in-channel fine particle storage was found to be controlled to various degrees by land use [Naden et al., 2016]. The later report recently that stream power (P) calculated for the bankfull discharge significantly explains these local stocks in 230 agricultural streams in the UK. Studying a reservoir release, Petticrew et al. (2007) observed that local storage of fine particles in a trap was controlled by the local Froude number ($Fr = U/\sqrt{gd}$). Similar observation was made by Marteau et al. (2018) observing that pools stored much more fines than riffles or plane beds. In an Alpine environment, Navratil et al. (2010) observed that the quantity of fine particles stored in a braided river reach depends mainly on the facies considered. They observed low local stocks in the main channel and in naked gravel bars while secondary channels and vegetated bars contained high quantities. These studies suggest that in addition to particle size criteria [Frostick et al., 1984], local hydraulic conditions seem to significantly control the quantity of fine particles found in the river bed. Using that kind of local stock measurements integrated over the entire river network, several authors have estimated the fraction of annual load stored in river beds (Table 0.1).

Study	River	Location	Riverbed storage vs annual load (%)
Collins et al. (2007)	Frome	UK	11-39
Collins et al. (2007)	Piddle	UK	29-97
Owens et al. (1999)	Tweed	UK	4+40 ^(a)
Walling et al. (1998)	Ouse	UK	10+39 ^(a)
Walling et al. (1998)	Warfe	UK	9+49 ^(a)
Lambert and Walling (1988)	Exe	UK	40-70 ^(b) , 60-100 ^(c) , 110-160 ^(d)
Piqué et al. (2014)	Isábena	Spain	10
Estrany et al. (2011)	Borges	Mallorca	87
Marttila and Kløve (2014)	Sanginjoki	Finland	13-116
Navratil et al. (2010)	Bès	France	80 ^(e)

Table 0.1: Ratios of riverbed stocks versus annual suspended load obtained in several studies. Two values separated with a dash indicate time variability. ^(a) Includes the floodplain storage. ^(b) ^(c) ^(d) correspond to different degree of riverbed disturbance: water agitation, water and bed surface agitation, water and subsurface riverbed material agitation. ^(e) Includes in-channel dry facies storage.

Table 0.1 indicates that the ratio between riverbed storage and annual suspended load is highly variable between catchments as it ranges from nearly 0 to more than 100 %. It can also vary in time as riverbed stocks can dramatically change [Buendia et al., 2016; Collins and Walling, 2007b; Marteau et al., 2018; Piqué et al., 2014; Walling et al., 2003].

This temporal variability is for instance highlighted by the repeated measurements of river bed stocks performed before and after flood events by Buendia et al. (2016) in the Isábena River (Figure 0.9). Storage values were found to increase after the flood event for peak discharges lower than 10m³/s while they decrease for larger peak flow rates suggesting a control of fine particle storage and release by this variable. Most of these studies were performed in lowland or agricultural catchments or focused mainly on under-water storage. Except the study of Navratil et al. (2010) few data are available for Alpine rivers concerning that specific topic. This raises questions about the potential contribution of Alpine riverbed stocks to total load and the way fine particles are stored to better understand their transfer.

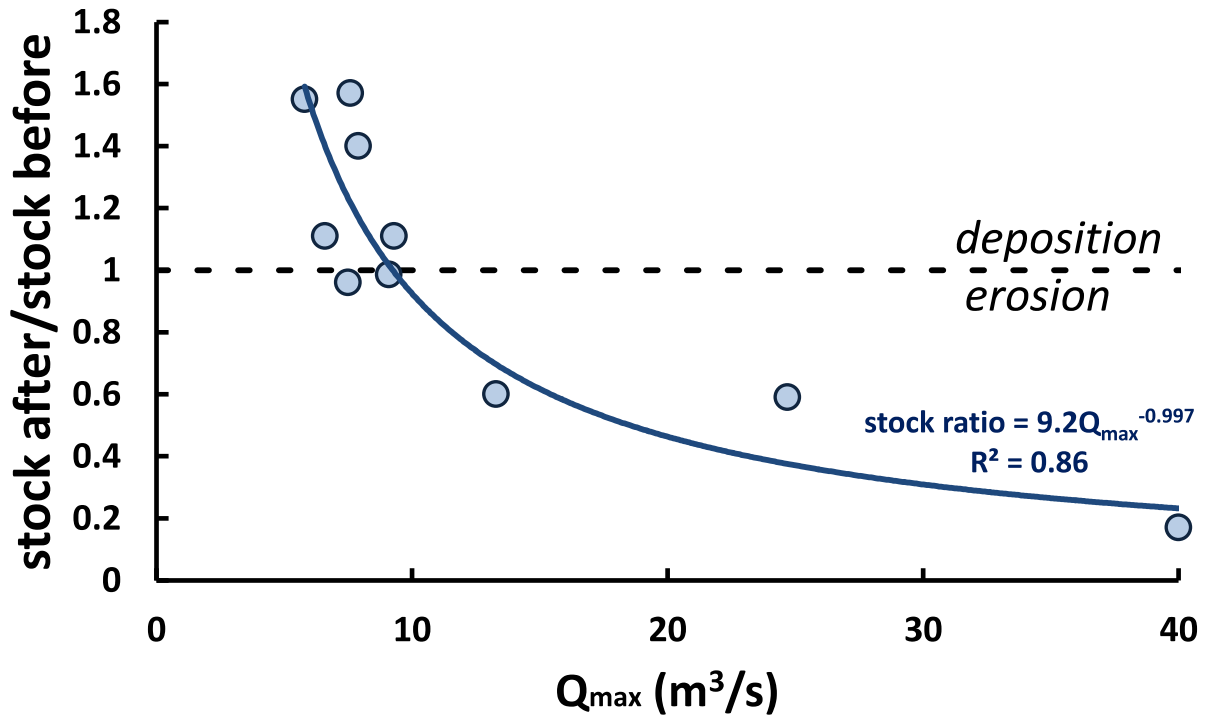


Figure 0.9: Ratio between in-channel stock after and before of flood event as a function of the peak discharge observed in the Isábena river using the data of Buendia et al. (2016).

c) Current observation of the relation between suspended load and river bed mobility

The previously detailed field observations suggest that the interactions between fine particles and the river bed can be significant in mountainous rivers. It is obvious that these interactions are difficult to capture in the field. Consequently, only few studies managed to report some interesting observations. By measuring input and output suspended load in proglacial streams, Orwin et al. (2004) and Guillon et al. (2018) observed significant buffering effects in the river reach at the season and at the event scale. The latter conclude that the buffering property was controlled by variations of transport capacity, a function of the river bed slope, water discharge and upstream suspended sediment concentration. By measuring simultaneously bedload and suspended load transport in an alpine braided reach, Meunier et al. (2006) were able to observe a relation between both variables which they attributed to a release of fine particles due to riverbed mobilization. Later Turowski et al. (2010) collected simultaneous bedload and suspended measurements in the literature and also observed such relation between both fluxes. These observations suggest that in armored alpine rivers, the riverbed mobility and bedload fluxes could be a good proxy of suspended load in case of a significant riverbed release of fine particles.

0.3 SCIENTIFIC QUESTIONS

Based on the previous description of our current observations and knowledge the present manuscript focuses on the following specific questions concerning the transport of fine particles in Alpines Rivers:

- How fine particles eroded on hillslopes are transferred downstream?
- When are erosion and deposition of fine particles in the river bed significant?
- How do fine particles interact with the coarse ones and the riverbed mobility?

Two simplified hypothesis can be formulated to answer these questions (Figure 0.10). Assuming first an efficient and direct transfer from the hillslopes to a given target with limited riverbed interactions, the suspended load dynamics would be mainly driven by erosion processes on hillslopes. An alternative hypothesis is to consider that significant deposition and remobilization could occur in the river bed. In that second case, a significant part of the suspended load dynamic would be controlled by the interactions between suspended fine particles and the riverbed. We hypothesized that the riverbed mobility could be a good proxy of these interactions in Alpine rivers.

To investigate these questions, the approaches synthetized in Figure 0.10 have been used. We first performed a macroscale study using catchment scale analysis (chapters 1, 2 and 3). In the first chapter, we analyzed long term measurements of suspended load in a dozen of contrasted alpine catchments to assess to which extent SSC-Q hysteresis could be linked to the catchment geomorphological characteristics. We then completed this first analysis by an estimation of river bed stocks of fine particles in 7 of these catchments in chapter 2. This was used to quantify whether alpine river beds contained significant stocks of fine particles. To estimate the conditions and the quantity of fine particles that could be released when these river bed stocks were mobilized, we gathered in chapter 3 simultaneous bedload and suspended load measurements performed in 56 gravel bedded rivers worldwide. We used these data to investigate the impact of riverbed mobility on suspension.

The second part of this manuscript reports detailed observations of suspended load-river bed interactions at the reach scale (chapters 4, 5 and 6). It allowed us to study the mechanisms associated to the assumptions of riverbed-suspension interactions derived from the broader scale approaches presented in the first part of the manuscript. The fourth chapter reports observations of bedload transport and its interactions with the reach morphodynamics using multi-physical measurements. Then, these observations were used in chapter 5 to interpret the sediment budget and erosion/deposition of fine particles in the reach. Finally, we showed in the sixth chapter how indirect and

continuous suspended load and bed mobility measurements could evidence suspension-river bed interactions.

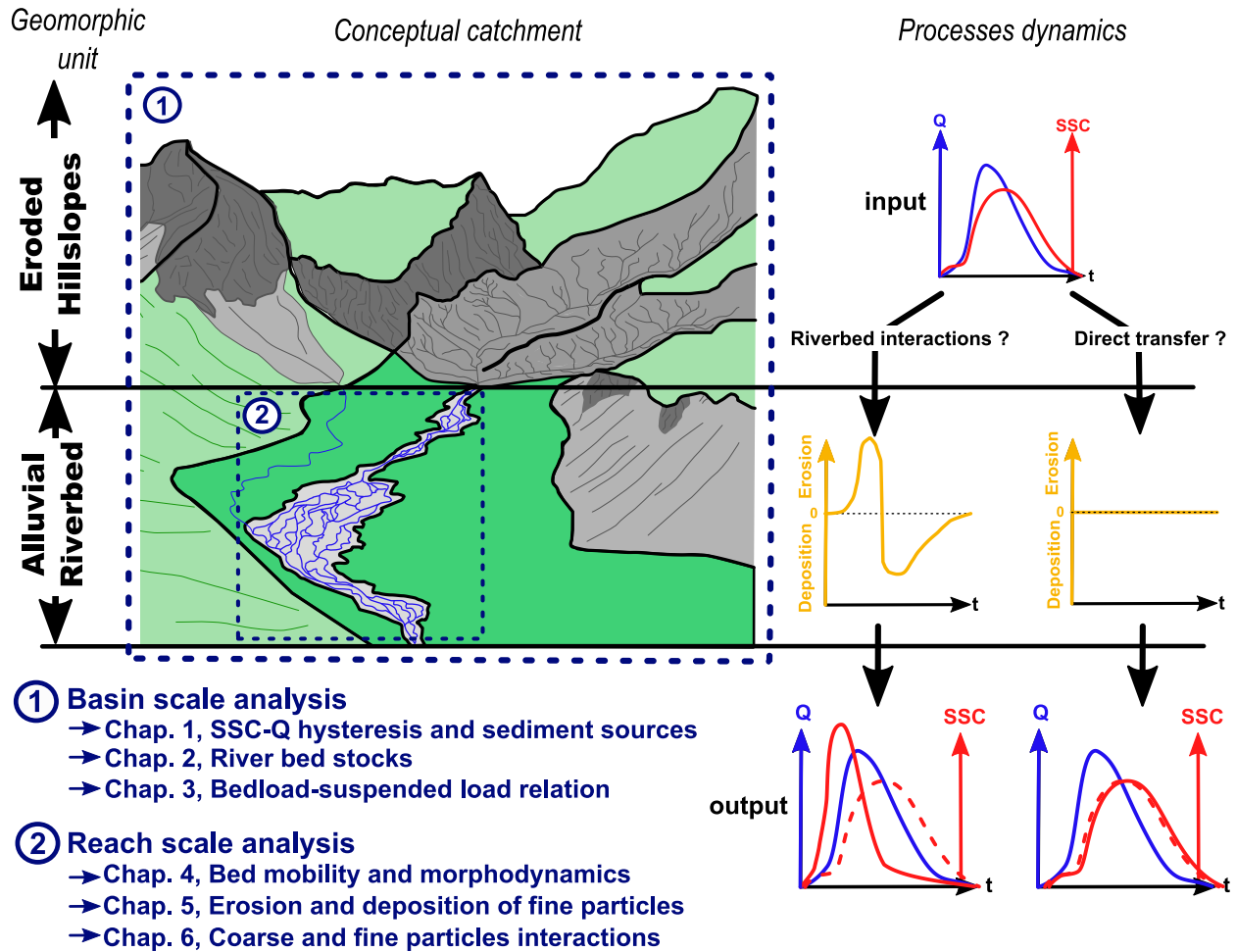


Figure 0.10: Schematic description of the manuscript content and the main questions addressed. Q, SSC and t denote respectively the water discharge, the suspended sediment concentration and the time.

PART 1

Chapter 1

An attempt to link suspended load hysteresis patterns and sediment sources configuration in alpine catchments

This first chapter presents an analysis of hysteresis phenomena between suspended load and flow rate which are often considered the result of various sediment sources contributions. These phenomena are widely used to interpret fine particles transport dynamic in catchments while a direct link with sediment source has not been yet demonstrated. Such relation is investigated in the following article accepted in Journal of Hydrology, by Misset C., Recking A., Legout C., Poirel A., Cazihlac M., Esteves M., and Bertrand M. (doi: 10.1016/j.jhydrol.2019.06.039).

Ce premier chapitre présente une analyse des phénomènes d'hystérésis entre transport solide par suspension et débit liquide, très souvent considérés comme le résultat de la contribution de différentes sources sédimentaires. Ces phénomènes sont largement utilisés pour interpréter la dynamique de transport de sédiments fins dans les bassins versants. Un lien direct entre hystérésis et contribution de sources sédimentaires n'a cependant pas été démontré. Cette relation est étudiée dans l'article suivant accepté dans journal of Hydrology par Misset C., Recking A., Legout C., Poirel A., Cazihlac M., Esteves M., and Bertrand M. (doi: 10.1016/j.jhydrol.2019.06.039).

1.1. ABSTRACT

A large part of total solid flux is transported as suspension in mountainous rivers. It is crucial for water resource management and for environmental issues to be able to model and to understand these fluxes. However, suspended load is known to be highly variable in time and space, as fine sediments can originate from various erosion processes and from various sources. Among the different methodologies available for analyzing the suspended sediment flux dynamics, hysteretic loops in discharge and suspended load signals are commonly used to assess sediment sources and production processes. However, the shape of these loops is often analyzed qualitatively for a single or a small number of catchments. Hence it is still unclear how the geomorphological catchment properties influence the variability of the flow rate - suspended sediment concentration relationship through the hysteresis effects. This is particularly true in mountainous catchments where important sources of fine sediments may originate from the river bed in addition to hillslopes.

In this study we analyzed quantitatively ten long-term series of high-frequency observations of suspended sediment load measured in contrasted alpine catchments. Hysteresis effects were analyzed in a high number of automated sampled events and the dominant response for each catchment was sought. This was done by using a normalized hysteresis index developed by Lloyd et al. (2016), which we weighted by the mass transported during each event. The various catchments were characterized with a normalized geomorphological index expressing the relative importance of sediment sources originating from the river bed or from eroded areas as a function of the distance to the outlet of the catchment.

The dominant hysteresis response of the ten alpine catchments studied was found to be greatly linked to their geomorphological index. These results suggest that the sediment source configuration upstream of a measuring station drive hysteresis effects and thus the variability of the flow rate-suspended sediment concentration relationship.

1.2. INTRODUCTION

Suspended sediment load (SSL) assessment is essential for water resource management and for many environmental issues. Whereas fine sediments transported by rivers are a vector of nutrients that are essential for estuarine ecosystems [Le Pape et al., 2013; Ludwig and Probst, 1998], they are also associated with socio-economic issues due to reservoir siltation or contaminant transport [Vercruyssen et al., 2017; Walling et al., 2003].

SSL is known to be highly variable in time and space especially in mountainous areas given that fine sediments can originate either from the main fluvial system or from external sources in similar proportions [Guillon et al., 2018; Navratil et al., 2010; Orwin

and Smart, 2004b]. According to the concept proposed by Bogen (1980) and the conceptual models used by Picouet (2009) or Park and Hunt (2017), the first type of production consists of sediment resuspension from the river bed. This part of suspension is believed to be related to flow rate, shear stress, or stream power [Park and Hunt, 2017]. In this case, fine sediments are produced by resuspension of deposited fine particles on bars, in secondary channels, when the armor layer is mobilized [Navratil et al., 2010] or when bank erosion occurs [Lefrançois et al., 2007]. The second type concerns erosion processes that take place in the catchment and that may not be directly related to the flow rate measured in the main channel. Fine particles are produced by rainfall or runoff detachment on eroded areas, in first-order tributaries or by mass movement.

The coexistence of these two kinds of fine sediment production processes often generates a huge variability in the flow rate (Q)–suspended sediment concentration (SSC) relationship. As observed in many field studies at the event, inter-event, or seasonal time scale, the same flow solicitation does not lead to the same sediment response of the watershed [Aich et al., 2014; Andermann et al., 2012; Mao and Carrillo, 2016; Sun et al., 2016]. This non-unique relation between Q and SSC is often highlighted through hysteresis loop observations. These phenomena have been widely analyzed in the past few decades and in various environments [Aguilera and Melack, 2018; Baca, 2010; Bogen, 1980; Gharari and Razavi, 2018; Klein, 1984; Smith and Dragovich, 2009; Tananaev, 2015; Zuecco et al., 2016]. The first classification of hysteresis loops was proposed by Williams (1989). Five classes were distinguished: single-valued line, clockwise loops, counterclockwise loops, single line plus a loop, and figure-of-eight loop. This classification was then re-used and completed with more complex figures by various authors such as Nistor and Church (2005), Tananaev (2015), Duvert et al. (2010) or Hamshaw et al. (2018). In a literature review, Gellis (2013) highlights that a given hysteresis effect observed at a measuring station can be explained by various erosion and physical processes.

However, at the event scale, distant sediment sources were found to generate mainly counterclockwise loops [Baca, 2010; Klein, 1984; Williams, 1989]. Suspended sediments are transported more or less at the mean flow velocity, which is lower than the flood wave celerity. This means that if the travelling distance and the relative difference between the celerity of the two waves is high enough, a time delay will be observed between the two signals generating a counterclockwise loop [Klein, 1984; Nistor and Church, 2005; Williams, 1989]. By contrast, depletion in the SSC during the falling limb of the flood or an SSC peak prior to a Q peak will generate a clockwise loop. This is usually attributed to a mobilization of relatively close and supply limited sources [Marttila and Kløve, 2010; Park and Hunt, 2017], dilution due to base flow increase during the falling limb [Baca, 2010], or rainfall close to the catchment outlet [Jansson,

2002]. Many other processes could generate hysteresis between SSC and Q such as the contribution of upstream tributaries [Asselman, 1999], bank erosion [Smith and Dragovich, 2009], or hysteresis effects in the SSC–turbidity calibration curve [Landers and Sturm, 2013]. In some cases, the SSC and Q curve are synchronized, leading to no hysteresis pattern. Such situations were often interpreted as an unlimited sediment supply [Nistor and Church, 2005; Williams, 1989]. Finally, complex patterns can be observed for multi-peak events or when several processes described previously occur at the same time in the catchment.

Given the high number of processes leading to Q–SSC hysteresis, it is doubtful to infer even qualitatively the major erosion processes acting in a unique catchment with this single information especially when measurements are conducted for short time periods [Esteves *et al.*, 2018]. On the other hand, using measurements made on several contrasted watersheds at regional scale could help to assess to which extent the sediment sources configuration may control the shape of these hysteresis and thus to better understand the spatial variability in the Q–SSC relation. During the last decades, there has been a growing interest in sediment sources characterization [Parsons *et al.*, 2015; Wohl, 2017] as sediment contributing areas have been shown to control sediment yield in alpine catchments [de Vente *et al.*, 2006; Haas *et al.*, 2011]. Despite the respective contribution of each sediment sources are often highly variable in time and space [Legout *et al.*, 2013], several methods have been proposed to quantify sediment connectivity in catchments [Borselli *et al.*, 2008; Heckmann *et al.*, 2018; Heckmann and Schwanghart, 2013]. Most of these methods conceptually consider an upslope (contributing area) and a downslope (source to sink) component to spatially describe the capacity of the catchment to export sediments [Borselli *et al.*, 2008; Cavalli *et al.*, 2013; Heckmann and Schwanghart, 2013]. While this separation in two components in connectivity indexes (i.e. upslope and downslope) is similar to the conceptual distinction in two sediment sources (hillslope vs riverbed production) often depicted as the main controlling factor of discharge-suspended sediment concentration hysteresis, no study reported any attempt to quantify the potential links between hysteresis and conceptual description of sediment sources.

This study attempts to fill this gap by analyzing long-term series with high-frequency observations of SSL made in ten contrasted mountainous catchments in the French Alps. The main objectives were (i) to describe the dominant hysteresis patterns, (ii) to propose a method describing fine sediment source configuration at the catchment scale, and (iii) to analyze the link between dominant hysteresis patterns and sediment source configuration.

1.3. MATERIAL AND METHODS

1.3.1. HYDRO-GEOMORPHOLOGICAL CHARACTERISTICS OF THE CATCHMENTS

Four of the ten catchments studied (Asse, Bléone, Galabre, and Bès) are located in the southern part of the French Alps, and four others (Romanche, Arvan, Glandon, and Arc) are in the northern part (Figure 1.1). Two basins (Drac and Buëch) have intermediate positions. The ten catchments belong to the long-term observatory networks of two French research infrastructures (OZCAR and RZA) or from the monitoring network of Electricité de France Company (EDF).

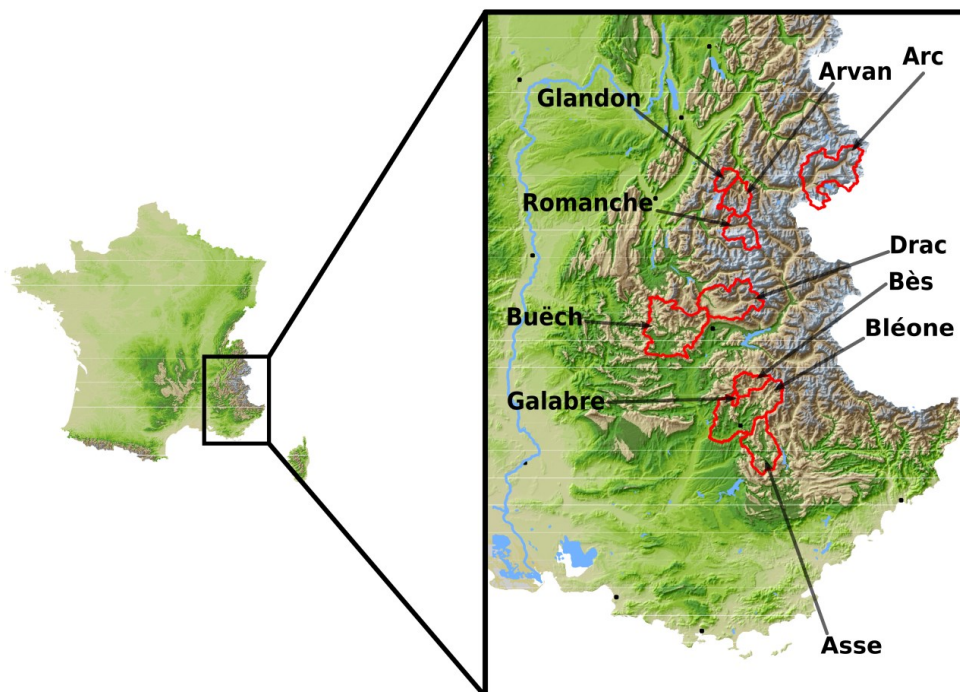


Figure 1.1: Catchment locations

1.3.1.1. Spatial information used

Data were collected for several characteristics of the basins (Table 1.1). Monthly average specific discharges were obtained from the French hydrometric agency (Banque Hydro: <http://www.hydro.eaufrance.fr/>) whereas spatial catchment properties were obtained thanks to a GIS analysis of several spatial databases (BD ORTHO®, BD ALTI®, Corine Land Cover®, GeoFLA®, IGN©). Active channel widths were digitalized manually on aerial orthophotographies and the fluvial corridor tool box [Roux *et al.*, 2015] was used in ARCGIS 10.3 to extract the active channel width at a regular step of 20 m. The median active river bed width calculated over the first 10 km upstream the

station (W_{10}). The mean riverbed slope was obtained from the French National Institute of Geography website (<https://geodesie.ign.fr/fiches/>) for approximately 10 km upstream of each measuring station (S_{10}). A georeferenced dataset of polygonal features with the location of eroded areas in the Alps (<https://journals.openedition.org/rga/3543#tocto2n6>) was used for the Bléone, Asse, Bès, Galabre, Buëch, Drac, and Romanche catchments [Bertrand, 2014; Bertrand et al., 2017]. These areas can be easily recognized in alpine catchments on high-resolution orthophotos and manually digitized using classic GIS toolkits or using automatic extraction procedure as it have been done in several previous studies [Marden et al., 2005; Trustrum and Stephens, 1981; Vrieling, 2006]. Bertrand et al. (2017) obtained the eroded patches map used in this study by combining object-based supervised classification models on infrared aerial orthophotographies (831 tiles, 0.5 m resolution) and a pixel-based supervised classification model on Landsat 7 ETM+ images (three images, with 30 m resolution and offering a wider spectral range than aerial orthophotographies) to extract eroded areas in the southern part of the Alps. The training and validation datasets used are each constituted of 30 infrared aerial orthophotographies tiles (randomly sampled in the 831 tiles) automatically segmented into objects having homogeneous textures and manually classified into two categories: eroded areas and non-eroded areas. The final classification model is a weighted sum of these calibrated models (both object-based and pixel-based). They obtained a model sensitivity, specificity and overall classification score of respectively 0.81, 0.94 and 0.9. They also performed an expert classification on 500 randomly distributed points in the Bléone catchment and obtained similar results (0.74, 0.99 and 0.96 respectively) confirming the reliability of this method. For the Glandon, Arvan, and Arc basins, this map was not available and eroded areas were digitalized manually using 50-cm resolution aerial orthophotographies. In both cases, eroded patches are considered through the image analysis as exposed and unvegetated areas exhibiting erosion patterns or gullies. This eroded areas description is consistent with the fact that increasing bare soils cover increases suspended sediment yield [Douglas, 1967; Duvert et al., 2012].

1.3.1.2. Hydrological regimes

Table 1.1 shows the contrasting characteristics of the ten catchments. Their areas range from 22 km² to nearly 900 km². The hydrology of the catchments located in the Southern Alps, including the Buëch basin, exhibits a high-flow period in winter and late autumn, separated by a low-flow period in summer (Figure 1.2). The northern catchments have higher specific water discharges. They are characterized by the presence of snow cover and glaciers resulting in a melting season generating high flows from late spring to mid-summer and low-flow periods the rest of the time. The Drac catchment exhibits an intermediate discharge regime with a melting season in late spring followed by low-flow period in summer and another high-flow period in autumn due to widespread rainfall events. The northern catchments are higher in altitude (61% of mean area above 2,000

m) than southern ones (98% of mean area under 2,000 m), with the Drac exhibiting an intermediate situation (35% of catchment area above 2,000 m).

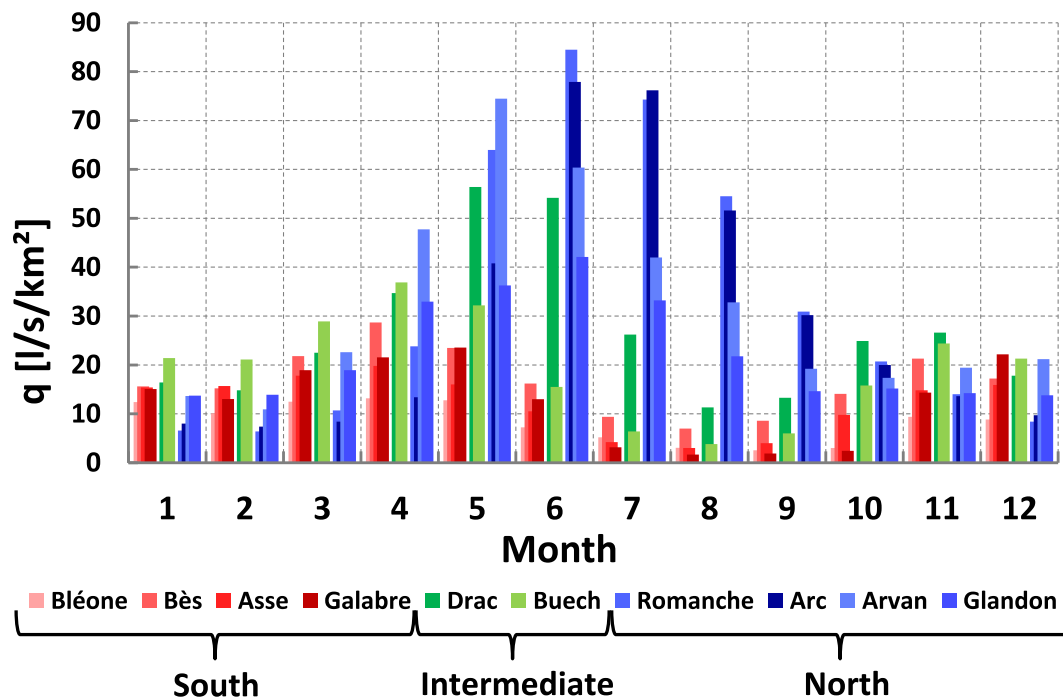


Figure 1.2: Monthly average specific discharge for the ten Alpine catchments. Sources: <http://www.hydro.eaufrance.fr/>

1.3.1.3. Geomorphological characteristics

Various land cover and lithologies are present on these catchments. Northern catchments, including the Drac basin, have large areas prone to erosion with zones having no or low vegetation cover ranging from 24% to 51% of their total area and rocks considered as non-resistant covering between 57% and 99% of their area. The Arvan, Glandon and Romanche catchments comprise mainly narrow mountain valleys with laterally constrained streams. Few alluvial reaches are included in the dominant step-pool sections with mean river bed slopes on the first 10 km upstream the station (S_{10}) comprised between 4% and 5.9% and median river bed active widths on the first 10 km upstream the station (W_{10}) ranging between 8m and 22m. Having a larger catchment area, the Arc has a gentler river bed slope ($S_{10}=1.12\%$) and a wider river bed active width ($W_{10}=33m$). It exhibits mainly plan bed sections with few gavel bars downstream active tributaries punctuated with narrow gorge sections. The Drac basin has poorly laterally constrained streams in its downstream part and a gentle slope ($S_{10}=1.01\%$) enabling the development of braiding sections on dozen of kilometers ($W_{10}=60m$). Southern catchments, including the Buëch basin are also prone to erosion with a fraction

of their basin that has low or no vegetation cover ranging between 10% and 19% and non-resistant rocks cover ranging between 79% and 100%. Their valleys are wider than the northern catchments except for the Galabre catchment which is a small headwater stream ($A=22\text{km}^2$) with constrained gorges and step-pool sections ($W_{10}=8\text{m}$, $S_{10}=8.8\%$). The Bléone and Buëch exhibit braiding morphologies (W_{10} of respectively 162m and 118m) with gentle slopes (S_{10} of respectively 0.82% and 0.81%). The Asse and Bès catchments also exhibit long alluvial and gentle sections which are punctuated with narrower sections in gorges or more constrained valleys (W_{10} of respectively 28m and 20m, S_{10} of respectively 0.87% and 2.57%). Mano *et al.* (2009) reported specific suspended sediment fluxes around $500 \text{ t km}^{-2} \text{ year}^{-1}$ for the Asse, Bléone and Romanche catchment while Navratil *et al.* (2012) reported specific suspended sediment fluxes of respectively 330, 690, and $680 \text{ t km}^{-2} \text{ year}^{-1}$ for the Bléone, Bès and Galabre basins which can be classified as high according to the classification proposed by Meybec *et al.* (2003). These studies suggest that the studied catchments have highly active fine sediment sources. Also, all of these catchments have been chosen for their limited human impact, i.e. with limited presence of embankments or weirs in the rivers, limited urbanized areas and absence of large dams. Few small water intakes with limited storage capacity are however present (Glandon, Arvan, Drac, Romanche and Arc basins) but can be considered to have a negligible effect on the downstream suspended load transfer during the studied flood events.

Basins names	A [km ²]	No [%]	Fo [%]	Gl [%]	SCR [%]	HR [%]	RR [%]	W ₁₀ [m]	S ₁₀ [%]	q [l/s/km ²]	Period
Arc	635	49	11	9	0	64	36	33	1.12	30	2012 - 2016
Arvan	220	24	18	2	38	61	1	22	5.92	32	2011 - 2015
Asse	375	10	41	0	9	70	21	28	0.87	12	2011 - 2016
Bès	165	14	43	0	42	46	11	20	2.57	17	2007 - 2013
Bléone	896	14	41	0	19	68	11	162	0.82	8	2007 - 2009
Buech	723	12	47	0	83	1	12	118	0.81	19	2015 - 2017
Drac	510	35	20	0	32	34	18	60	1.01	27	2007 - 2016
Galabre	22	19	11	0	39	61	0	8	8.86	13	2007 - 2013
Glandon	110	31	28	2	0	57	43	8	5.80	23	2011 - 2016
Romanche	230	51	4	12	25	33	42	14	4.17	33	2007 - 2016

Table 1.1: Main catchment characteristics. Catchment size (A), no/low vegetation cover (No), forest cover (Fo), glacier cover (Gl), soft coherent rocks (SCR), heterogeneous rocks (HR), resistant rocks (RR), mean annual specific discharge (q), median active channel width calculated for the first 10 km (W_{10}), mean slope of the river bed calculated for approximately the first 10 km (S_{10}).

1.3.2. SUSPENDED LOAD TIME SERIES

The available SSL time series range from 3 to 10 years (Table 1.1). For each catchment, the water discharges Q were calculated from automated measurements of the water

levels with a frequency of 1 h. Stage-discharge rating curves were obtained thanks to numerous technics (Acoustic Doppler Current Profiler, salt-dilution, current meters or Large Scale Particle Image Velocimetry techniques), regularly performed during the study period. The surrogate technique for SSC estimation (i.e., turbidity-meter), coupled with direct sampling of SSC for calibration was used as commonly done for such field monitoring [Mano *et al.*, 2009; Navratil *et al.*, 2011]. SSC was assumed to be uniform over the cross section owing to the high levels of turbulence in these rivers, generating well-mixed flows. SSL was computed by multiplying SSC and Q at a 1-h frequency.

1.3.3. HYSTERESIS ANALYSIS TOOLS

In order to determine the dominant hysteresis pattern for the ten alpine catchments, a database of runoff events was created. Individual events were selected considering both SSL and SSC. In a first step, the events having a maximum SSL below a given threshold were not considered. A SSL threshold value ($SSL_{1\%}$) was used, corresponding to the value below which 1% of the cumulated suspended sediment fluxes were transported (Figure 1.3). A similar approach was adopted to remove events exhibiting SSC values below a threshold corresponding to 1% of the cumulated suspended sediment fluxes ($SSC_{1\%}$).

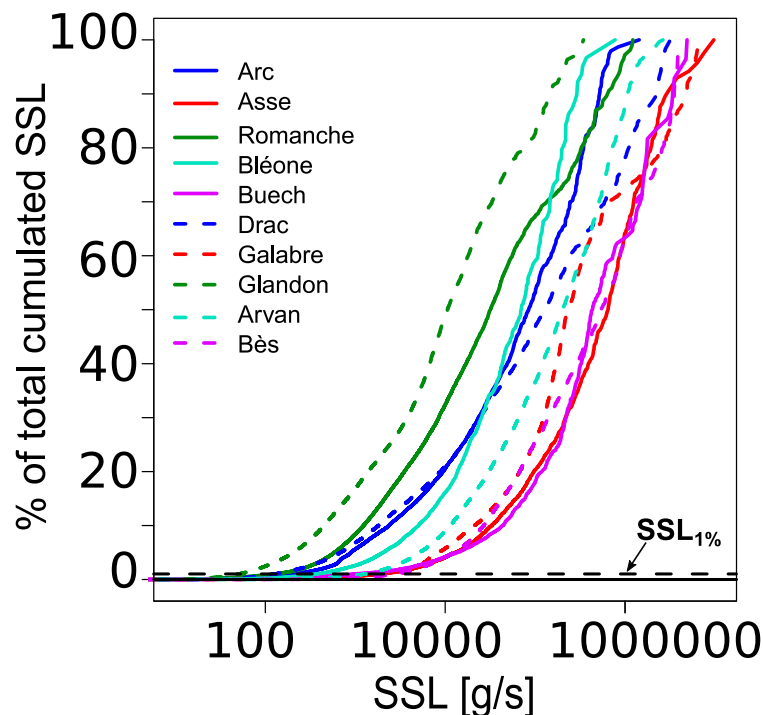


Figure 1.3: Definition of SSL threshold ($SSL_{1\%}$) as SSL below which 1% of cumulated suspended fluxes are transported.

The normalized index (HI_{Lloyd}) proposed by Lloyd et al. (2016) was used (Eq.1.3). This non-dimensional index is non-sensitive to the absolute value of SSC and Q, which makes it possible to do inter-event and inter-catchment comparison of hysteresis strength and direction. This index tends towards +1 for clockwise loops and towards -1 for counterclockwise loops.

To compute HI_{Lloyd} for a given event, SSC and Q were normalized using their minimum and maximum values (Eq.1.1 and Eq.1.2) to obtain SSC^* and Q^* . The differences between SSC^* monitored during the rising and the falling limb were then computed for each of the 100 values of Q^* ranging between 0.01 and 1 (Figure 1.4). Finally, HI_{Lloyd} corresponds to the mean of these differences (Eq.1.3).

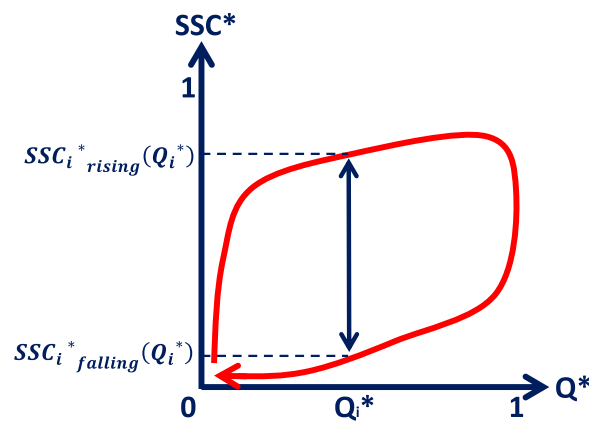


Figure 1.4: Calculation of the hysteresis index proposed by Lloyd et al. (2016).

$$SSC_i^* = \frac{SSC_i - SSC_{min}}{SSC_{max} - SSC_{min}} \quad (1.1)$$

$$Q_i^* = \frac{Q_i - Q_{min}}{Q_{max} - Q_{min}} \quad (1.2)$$

$$HI_{Lloyd} = \text{mean} \left[SSC_i^* \text{ rising}(Q_i^*) - SSC_i^* \text{ falling}(Q_i^*) \right] \quad (1.3)$$

$$i \in [0.01, 1]$$

For each catchment and each selected events, a HI_{Lloyd} value was calculated. The median value was considered representative of the dominant hysteresis patterns ($\text{median}(HI_{Lloyd})$). However, the most frequent hysteresis patterns might not necessarily be those that transport most of the fine sediments. Thus, a new index (HI_{Ms}) was introduced to investigate the “transport efficiency” associated to hysteresis. This was achieved by weighting each event by the transported mass (Ms_i):

$$HI_{Ms} = \frac{\sum(HI_{Lloyd_i} \times Ms_i)}{\sum Ms_i} \quad (1.4)$$

Whereas several HI_{Lloyd} index are calculated (one for each event), only one HI_{Ms} index is calculated (for the series of events) and inform which HI_{Lloyd} index is associated with the maximum transport.

These two continuous indexes were completed with classic pattern classifications [Gellis, 2013; Williams, 1989]. Hysteresis patterns were arbitrarily considered as clockwise when at least 80% of positive differences were observed between SSC^* during the rising and falling limb (Nb_{cl}). Counterclockwise loops were considered when at least 80% of negative differences were obtained (Nb_{ccl}). Otherwise, the flood was considered to have a complex hysteresis patterns or no hysteresis ($Nb_{complex}$). Finally, the percentages of the mass transported as clockwise hysteresis (Ms_{cl}), as counterclockwise hysteresis (Ms_{ccl}), and as complex or no hysteresis ($Ms_{complex}$) were calculated for each catchment. This classification permits a direct comparison between the number of events having a certain shape and the mass exported within this shape.

1.3.4. SEDIMENT SOURCES CHARACTERIZATION

An analysis of each catchment was performed following the conceptual sediment sources description (river bed vs hillslopes) proposed by Bogen (1980) and often considered for qualitative hysteresis interpretations at the catchment scale [Buendia et al., 2016; Guillon et al., 2018; Mao and Carrillo, 2016; Smith and Dragovich, 2009]. According to connectivity concepts developed by Borselli et al. (2008) and Cavalli et al. (2013), the area of eroded patches and the traveling distance needed to reach the outlet from these zones are important factors controlling the catchment connectivity. Also, according to numerous studies on fine sediments storage in the river network, the river width and the river bed area are parameters that have a strong control on the quantity of fine particles that can be stored in the river bed [Collins and Walling, 2007b; Lambert and Walling, 1988; Navratil et al., 2010; Piqué et al., 2014]. These latter parameters may also be good proxies of the buffering capacity of the river bed and of its influence on fine sediments connectivity. Indeed, the exchanging surface between the flow and the river bed may have important control on fine particles infiltration in the gravel matrix [Frostick et al., 1984; Mooneyham and Strom, 2018]. Following these evidences, a simplified sediment sources characterization was developed. The surface occupied by the active river channel width was considered as the first type of sediment source, whereas eroded areas were considered as the second type (Figure 1.5). The erosion maps described in section 1.3.1 were used for eroded areas identification.

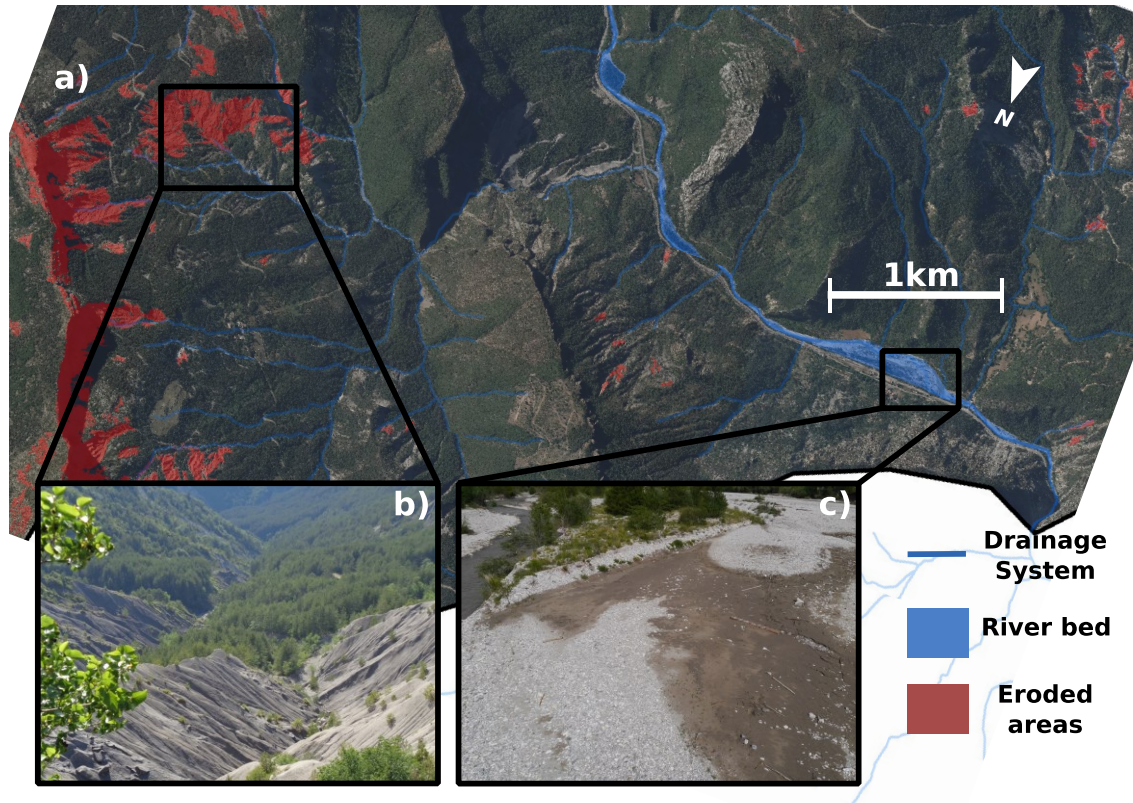


Figure 1.5: Example of sediment sources classification on the Asse River. (a) Orthophotograph classification of eroded area (red) and river bed area (blue). Pictures of typical eroded areas (b) and river bed (c) sediment sources.

The distance needed by the water to reach the measuring station for each of these eroded area was estimated by using a digital elevation model with 25-m horizontal resolution and various algorithms of the Spatial Analyst toolbox of ARCGIS 10.3 (Fill, FlowLength, and FlowDirection). This water path from eroded areas to the outlet of the basin was calculated by considering the maximum slope for each grid of the digital elevation model. For a given location in the watershed, and considering the total area between this point and the measuring station downstream, we defined the cumulative eroded area as the sum of the eroded patches area ($A_{eroded\ cum}$) and the cumulative area of the river bed as the sum of the active channel area ($A_{bed\ cum}$), which was extracted using the active channel width digitalization. These two cumulative areas as well as their ratio ($A_{eroded\ cum}/A_{bed\ cum}$) were calculated for each distance x from the monitoring station, with an incremental spatial step of 20 m, from downstream to upstream. For each catchment, the most upstream point was arbitrarily defined by a drainage area threshold of 1 km². This point was located at a flow distance L from the outlet. Finally, the Sources Configuration Index (SCI_x) was defined as the mean of the ratios ($A_{eroded\ cum}/A_{bed\ cum}$) calculated for the first x percent of the distance L :

$$SCI_x = \text{mean} \left(\frac{A_{eroded\ cum}(i)}{A_{bed\ cum}(i)} \right), i \in [0; x] \quad (1.5)$$

This geomorphological index gives information on the relative importance of each type of sediment source depending on the distance from the measuring station. It is a simplified description developed to test the reliability of usual qualitative interpretation made for hysteresis patterns (hillslopes vs river bed). The slope is not explicitly taken into account even if it is often negatively correlated with the active river width. Likewise, local weighting factors (roughness or land use in Borselli *et al.* (2008) and Cavalli *et al.* (2013)) that could better describe the capacity to produce, transfer or store fine sediments were not considered as they were difficult to estimate “a posteriori” and more questionable for suspended load than for bedload or debris flow processes.

This simple index permits to compare different spatial sources configuration (Figure 1.6). For instance, simplified conceptual cases (a) and (b) could probably lead to different hysteresis patterns at the outlet of the basin even if they have similar total cumulated bed and eroded area at the catchment scale. In case (a), eroded areas are located in the upper part of the basin whereas large storage zones of the river bed are located in the downstream part close to the monitoring station. Case (b) has the same bed configuration but eroded areas are located much closer to the outlet of the catchment ($d_1 \gg d_2$). In that case, the ratio ($A_{eroded\ cum}/A_{bed\ cum}$) increases much closer to the outlet than in case (a). Calculating the mean value of this ratio on a given distance permits to discriminate between these two cases. They have the same $A_{eroded\ cum}/A_{bed\ cum}$ ratio considering the total length ($x=100\%$), but the mean of these ratios calculated for x between 0% and 100% (SCI_{100} , average of the red curve in Figure 1.6) is much lower in case (a) than in case (b). Comparing conceptual cases (a) and (c) highlights the capacity of the index to compare different buffering effect played by the river bed. These cases have similar eroded areas located at the same distance from outlet (d_1) but the cumulative bed area is much lower in case (c). Eroded areas could be less buffered in case (c) than in case (a). The mean value of the $A_{eroded\ cum}/A_{bed\ cum}$ ratio calculated for x between 0% and 100% (SCI_{100}) will be smaller in case (a) than in case (c). In order to discriminate the relative influence of hillslope sources and river bed on the hysteresis variability, an Eroded Area Index (EAI_x) and a Bed Area Index (BAI_x) were also defined and calculated for the ten catchments (Eq.1.6 and Eq.1.7).

$$EAI_x = \frac{\text{mean}(A_{eroded\ cum}(i))}{\max(A_{eroded\ cum})}, i \in [0; x] \quad (1.6)$$

$$BAI_x = \frac{\text{mean}(A_{bed\ cum}(i))}{\max(A_{bed\ cum})}, i \in [0; x] \quad (1.7)$$

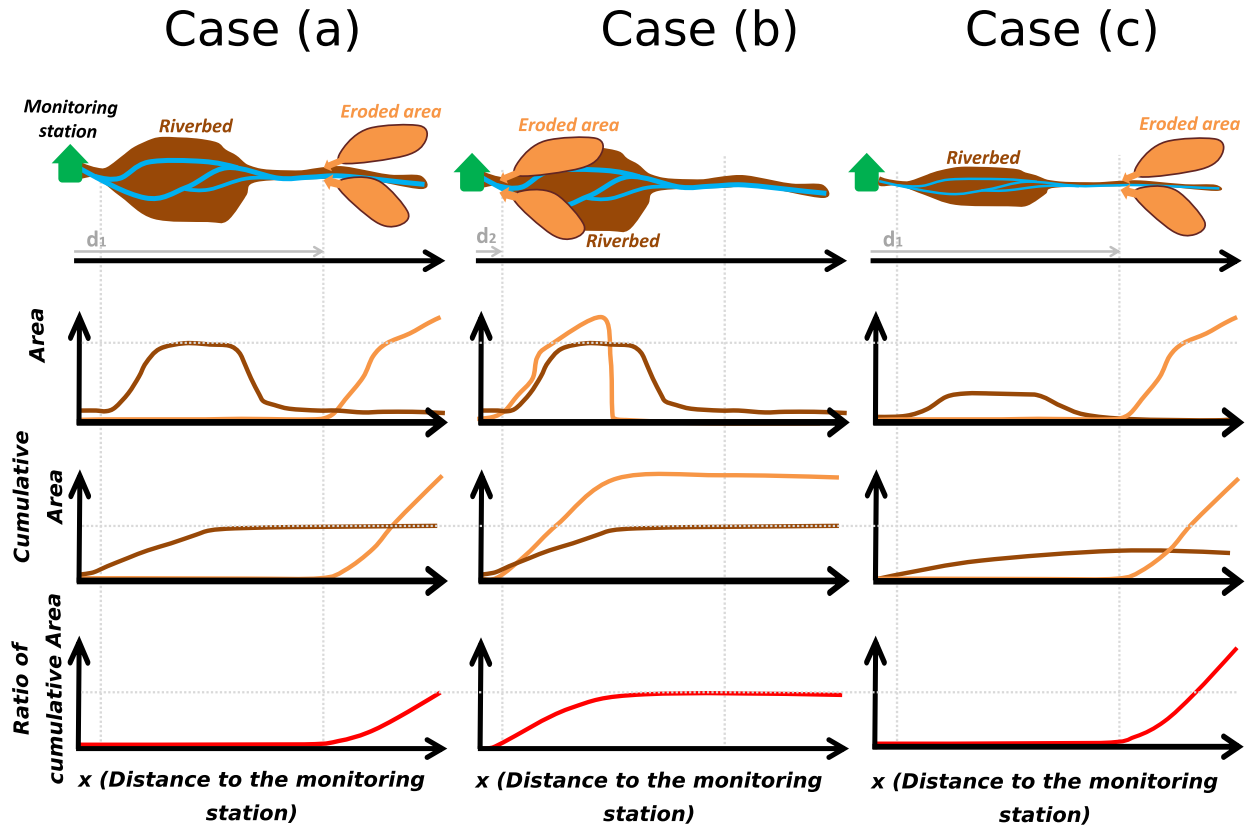


Figure 1.6: Three different conceptual sediment source configurations; case (a) is the reference case with large active width close to the measuring station and eroded areas located far upstream, case (b) is similar to the reference case but has eroded areas much closer to the monitoring station ($d_2 \ll d_1$), and case (c) is similar to case (a) but the active width is twice as narrow. For each case, the area, cumulated area, and ratio of cumulated area of the riverbed and eroded areas as a function of the distance from the outlet of the catchment are plotted. Brown curves correspond to the riverbed, orange curves correspond to eroded areas, red curves correspond to the ratio of cumulative eroded area over cumulative riverbed area, and gray dotted curves correspond to previous case for a better comparison.

1.4. RESULTS

1.4.1. RUNOFF EVENT CHARACTERISTICS

Following the event selection procedure (see Figure 1.3), the thresholds for SSL and SSC were calculated, and a dataset of events was created for each river (Table 1.2). More events were selected for northern catchments exhibiting daily floods during the melting season. While the observation periods were similar for the Glandon and the Asse, there were twice more selected events for the Glandon. Large differences were

also observed in $SSL_{1\%}$ and $SSC_{1\%}$ values, e.g., the Galabre and the Bès rivers have suspended fluxes transported for higher values of SSC in comparison with other rivers.

River	$SSL_{1\%}$ [g/s]	$SSC_{1\%}$ [mg/l]	t_{exceed} [h]	number of event
Arc	199	23	8	758
Arvan	1252	330	8	1048
Asse	1877	311	8	217
Bès	2677	868	8	155
Bleone	2000	181	12	104
Buech	960	104	8	94
Drac	125	14	12	1076
Galabre	360	1215	4	179
Glandon	50	21	8	561
Romanche	125	26	6	1656

Table 1.2: Runoff event characteristics. ($SSL_{1\%}$) corresponds to the threshold of SSL below which 1% of the cumulated suspended sediment fluxes were transported, ($SSC_{1\%}$) corresponds to the threshold of SSC below which 1% of the cumulated suspended sediment fluxes were transported, t_{exceed} corresponds to the minimum time step for which a valid SSL peak should exceed all following and preceding values.

1.4.2. VARIABILITY OF DISCHARGE-CONCENTRATION HYSTERESIS IN ALPINE CATCHMENTS

While the standard deviations of the HI_{Lloyd} were rather high for all catchments, some consistent observations can be made on the basis of the median HI_{Lloyd} (Table 1.3, Figure 1.7).

River	Mass transported			Number of events			Indexes		
	Ms_{cl} [%]	Ms_{ccl} [%]	$Ms_{no/complex}$ [%]	Nb_{cl} [%]	Nb_{ccl} [%]	$Nb_{no/complex}$ [%]	median(HI_{Lloyd})	Sd(HI_{Lloyd})	HI_{Ms}
Arc	26	32	42	30	32	37	0.01	0.27	0.02
Arvan	34	28	38	34	30	36	0.02	0.28	0.04
Asse	58	11	31	23	31	47	-0.04	0.25	0.12
Bès	58	4	38	38	15	47	0.02	0.26	0.19
Bleone	84	2	14	60	11	30	0.15	0.24	0.22
Buech	41	31	28	62	19	19	0.18	0.31	0.05
Drac	41	24	35	43	16	41	0.12	0.26	0.10
Galabre	53	21	26	37	41	22	-0.02	0.33	0.15
Glandon	44	22	34	38	28	34	0.04	0.25	0.06
Romanche	25	28	47	28	28	43	0.01	0.25	0.01

Table 1.3: Results of hysteresis analysis between SSC and Q. The percentage of the mass transported with a given hysteresis shape (Ms), the percentage of events with a given shape (Nb), and the mean, standard deviation (sd) of the Lloyd hysteresis index (HI_{Lloyd}) were calculated as well as the average mass weighted hysteresis index (HI_{Ms}). cl : clockwise hysteresis, ccl : counterclockwise hysteresis, no/complex : no or complex hysteresis.

Most rivers exhibited median values of HI_{Lloyd} around zero, because this value was often the most frequent and also because high positive or negative values had similar frequencies. This suggests an absence of a dominant hysteresis trend (clockwise or counterclockwise) in terms of the frequency of events having a certain shape. However, mainly clockwise loops ($\text{median}(HI_{Lloyd}) \gg 0$) were observed for the Buech, Drac, and Bléone catchments that have dominant braided bed morphology close to the monitoring stations, suggesting a more frequent contribution of the river bed sediment sources than in other catchments.

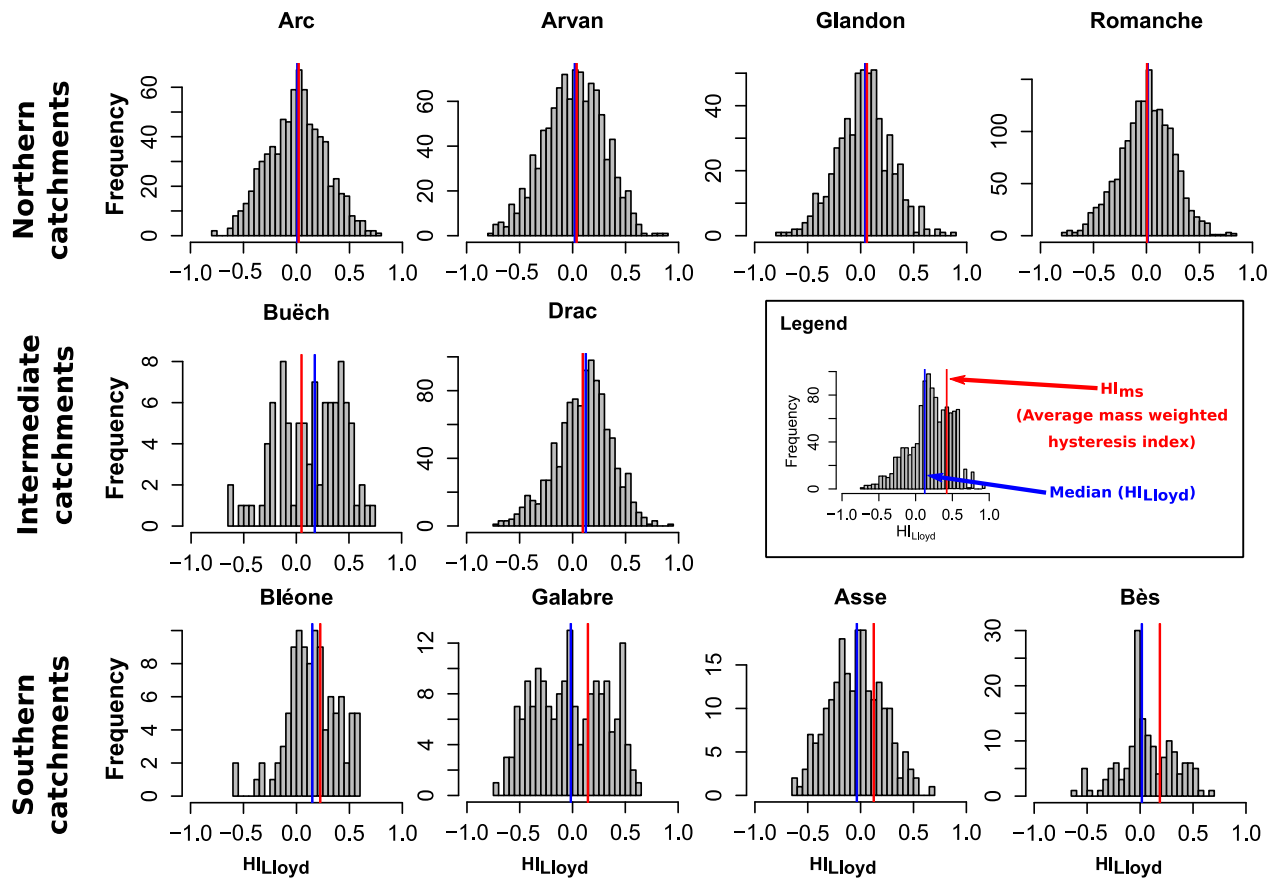


Figure 1.7: Distributions of Lloyd hysteresis index on the ten alpine catchments. The median value of the Lloyd hysteresis index is indicated by a vertical blue line while the average mass weighted hysteresis index is indicated by a vertical red line. A difference in position of these two lines indicates a difference in transport efficiency depending on the type of hysteresis.

Different conclusions can be drawn when comparing the HI_{MS} index (most transporting) with the median (most frequent) HI_{Lloyd} index for each catchment (Table 1.3 and Figure 1.7). In northern catchments, median HI_{Lloyd} and HI_{MS} values were similar (maximum

index difference of 0.02). However in the southern catchments, larger differences were observed between the two hysteresis indexes with differences ($\text{median}(HI_{\text{Lloyd}}) - HI_{\text{Ms}}$) ranging between -0.13 and +0.16. Thus, the most frequent hysteresis shape was often not the most transport efficient one. For instance, 23% of events were classified as clockwise in the Asse and they contribute to 58% of the total SSL while 31% of events were classified as counterclockwise and contribute to only 11% of the total SSL. This suggests a higher transport efficiency of clockwise hysteresis patterns than counterclockwise ones.

1.4.3. SEDIMENT SOURCES ANALYSIS

Large differences in the relative location of river bed and eroded area sediment sources were observed between catchments. As shown in Figure 1.8-b, the Arvan exhibited large eroded areas close to the measuring station with a limited bed area leading to a ratio of $A_{\text{eroded cum}}/A_{\text{bed cum}}$ equal to one at a distance of roughly 7 km. By contrast, for the Bléone, the bed area is larger than the eroded areas in the first 50 km close to the monitoring station (Figure 1.8-a). The cumulative eroded areas exceeded the cumulative bed areas only after 55 km.

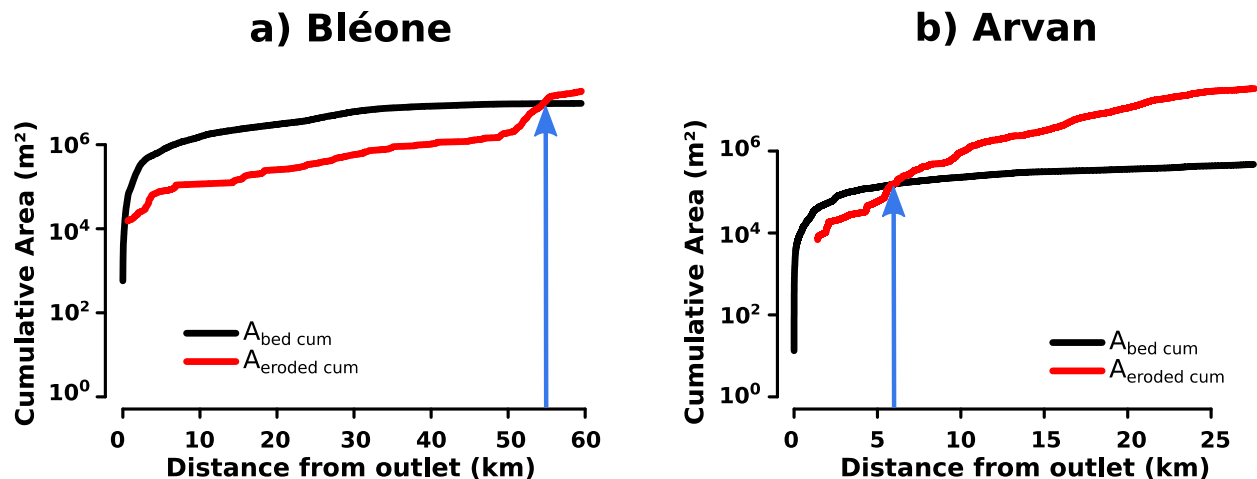
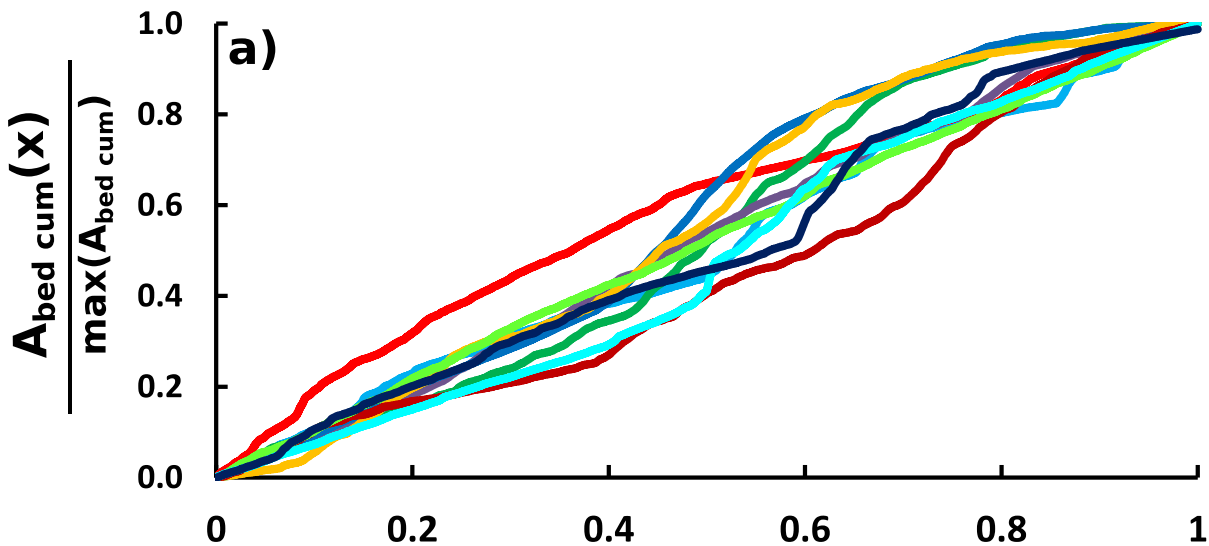


Figure 1.8: Cumulated values of bed area and eroded area as a function of the distance from the outlet for a) the Bléone river and b) the Arvan river. The vertical blue arrow indicates equality between cumulative eroded and bed areas.

To quantitatively compare these differences between the ten basins we plot in Figure 1.9:

- $\frac{A_{eroded\ cum}(x)}{\max(A_{eroded\ cum})}$: the fraction of the total cumulative eroded area as a function of the distance from the outlet,
- $\frac{A_{bed\ cum}(x)}{\max(A_{bed\ cum})}$: the fraction of the total cumulative bed area as a function of the distance from the outlet,
- SCI_x : the average values of the ratios $A_{eroded\ cum}/A_{bed\ cum}$ calculated on a given distance upstream the outlet (0% to x%).

For the ten catchments, the cumulative bed area exhibited a relative constant increase with increasing distance to the outlet (Figure 1.9-a). This suggests that bed areas were, as a first approximation, homogeneously distributed along the x distance. In comparison, the cumulative eroded area showed a more sudden increase with the increasing distance to the outlet (Figure 1.9-b). A small fraction of eroded area was located close to the monitoring stations as less than 50% of eroded areas are located for x distance smaller than 0.5 and less than 10% for x smaller than 0.2. Also, much more variability between the ten catchments was observed. For instance, the normalized cumulative eroded area of the Romanche basin starts to increase significantly for x around 0.5 while the Bléone basin showed a sudden increase for x larger than 0.8. This suggests that eroded areas were located more in the upstream part of the Bléone watershed than for the Romanche. Some catchments as the Arc basin exhibited a more smooth increase indicating a more homogeneous eroded patches distribution along the x distance.



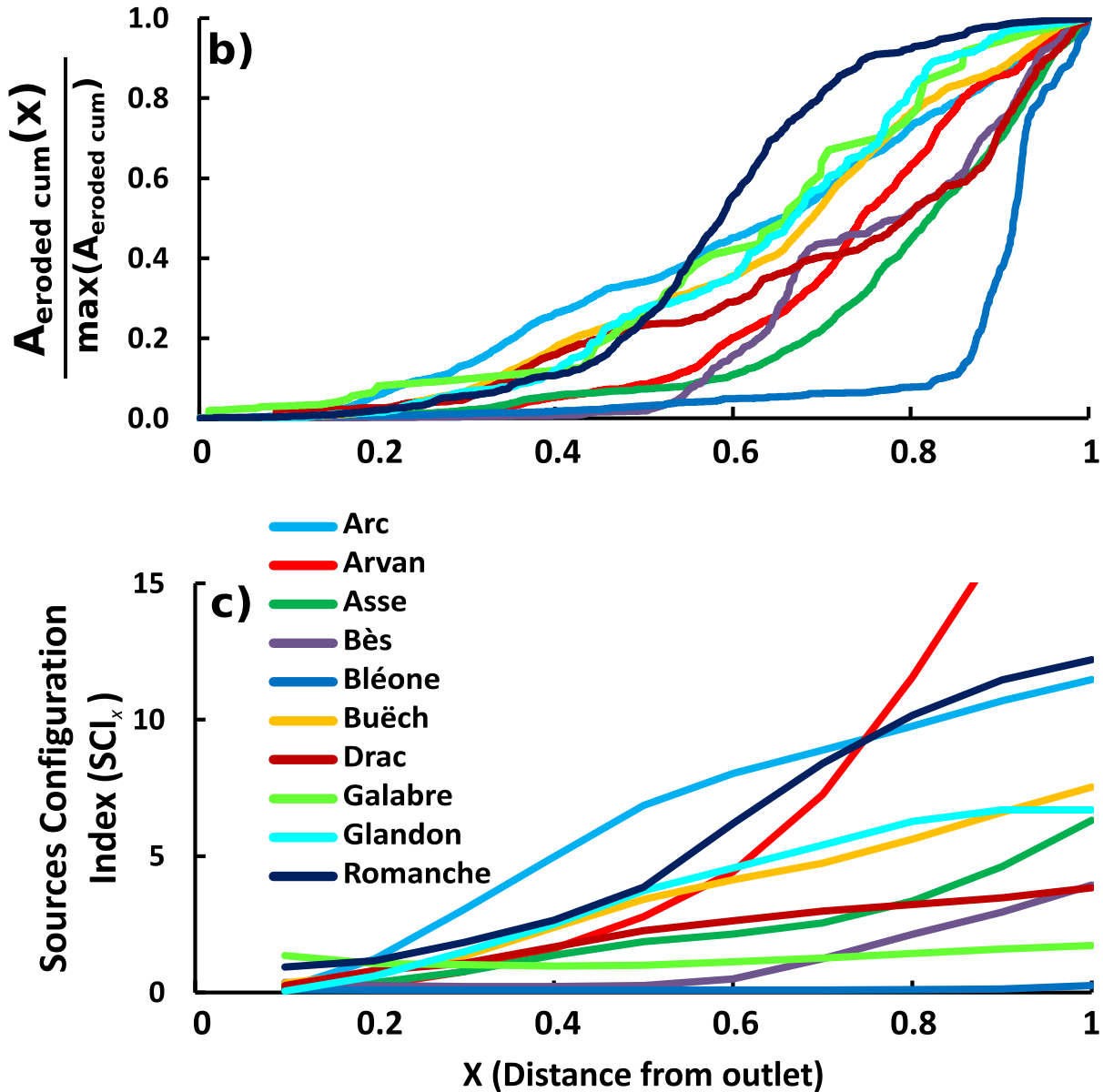


Figure 1.9: (a) Normalized cumulative bed area ($\frac{A_{bed\ cum}(x)}{\max(A_{bed\ cum})}$) as a function of the distance from outlet. (b) Normalized cumulative eroded area ($\frac{A_{eroded\ cum}(x)}{\max(A_{eroded\ cum})}$) as a function of the distance from outlet. (c) Source configuration index (SCI_x) as a function of the distance from outlet calculated with a x step of 0.1 for the 10 catchments.

Finally, the source configuration index SCI_x (Eq.1.5) shows for all rivers an increase in the relative importance of eroded areas as compared with bed areas when moving in the upstream direction (Figure 1.9-c). This confirms that river bed sources were closer to the measuring station than eroded areas sources. However, some small eroded tributaries could locally generate a high value of SCI_x near the observation station, as was the case

for the Galabre River. SCI_x were highly variable from one catchment to another. The shortest distance considered ($x=10\%$) to compute this index led to small differences between catchments whereas longer distances led to large differences. For instance, the two extreme cases, the Bléone and Arvan rivers, had the same SCI_{10} (0.1) but their SCI_{100} values were very different (0.3 and 21.3, respectively). The sources indexes (SCI_x , BAI_x , EAI_x) values calculated for x ranging from 10% to 100% with a x step of 10% are provided as supplementary material for more details.

1.4.4. RELATION BETWEEN SEDIMENT SOURCES CONFIGURATION AND DOMINANT HYSTERESIS PATTERNS

The general catchment characteristics, the index describing the river bed area distribution (BAI_x), the index describing the eroded area distribution (EAI_x) and the index comparing river bed and eroded area distribution (SCI_x) were compared with the dominant hysteresis pattern for each catchment (Table 1.4). While some significant correlations were found between general catchment characteristics and hysteresis indexes, the values remained rather low and did not exceed 0.63. Overall the Lloyd hysteresis index (HI_{Lloyd}) exhibited only limited and small significant correlations with the three sediment sources indexes (SCI_x , BAI_x , EAI_x), in comparison with the mass weighted hysteresis index (HI_{MS}).

	General catchment characteristics		River bed area configuration		Eroded area configuration		River bed and eroded area configuration				
	HI_{MS}	HI_{Lloyd} median	HI_{MS}	HI_{Lloyd} median	HI_{MS}	HI_{Lloyd} median	HI_{MS}	HI_{Lloyd} median			
S10	-0.19	-0.44	BAI_{10}	0.10	-0.45	EAI_{10}	0.32	0.02	SCI_{10}	-0.01	-0.35
W10	0.12	0.56	BAI_{30}	0.13	-0.13	EAI_{30}	-0.26	-0.08	SCI_{30}	-0.78	-0.14
A	-0.05	0.47	BAI_{50}	0.38	-0.04	EAI_{50}	-0.43	-0.14	SCI_{50}	-0.94	-0.07
No	-0.63	-0.08	BAI_{70}	0.37	0.25	EAI_{70}	-0.71	-0.22	SCI_{70}	-0.98	-0.13
Fo	0.54	0.49	BAI_{90}	0.35	0.22	EAI_{90}	-0.71	-0.25	SCI_{90}	-0.93	-0.10

Table 1.4: Spearman correlation coefficients between hysteresis indexes considering the frequency of event with a given hysteresis (median value of the Lloyd index, HI_{Lloyd}) or the mass transported with a given hysteresis (average mass weighted hysteresis index, HI_{MS}) and catchment characteristics: S_{10} is the mean river bed slope calculated for the first 10 km, W_{10} is the median active width calculated for the first 10 km, A is the catchment size, No is the percentage of the catchment having no or low vegetation cover, and Fo is the forest cover, BAI_x is the mean ratio of cumulated river bed area over total cumulated river bed area considering a length x upstream of the station, EAI_x is the mean ratio of cumulated eroded area over total cumulated eroded area considering a length x upstream of the station and SCI_x is the mean ratio of cumulated eroded area over cumulated bed area considering a length x upstream of the station. Bold values are significant with a confidence interval of 95% ($p_{value}<0.01$).

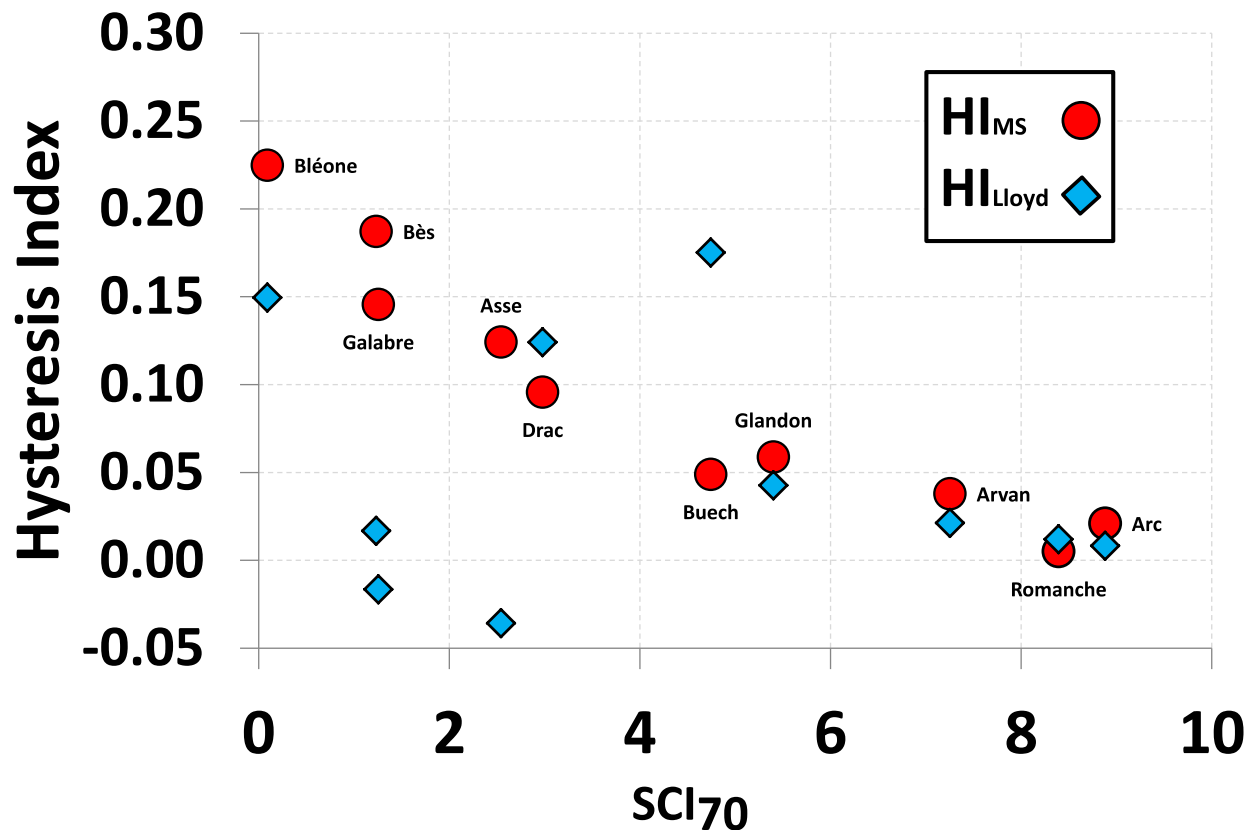


Figure 1.10: Relation between dominant mass weighted hysteresis index (HI_{MS} , red circles), median Lloyd hysteresis index (HI_{Lloyd} , blue diamonds) and source configuration index considering 70% of the upstream the monitoring station for the ten alpine catchments (SCI_{70}).

Significant negative correlations ($\rho < -0.98$, $pvalue < 0.01$) were found between HI_{MS} and the sediment sources index (SCI_x , Figure 1.10 and Table 1.4). This result suggests that the part of the fluxes exported with clockwise loops decreases when the relative importance of the eroded areas relative to the bed areas increases. Lower but also significant negative correlations ($\rho < -0.71$, $pvalue < 0.01$) were obtained between the mass weighted hysteresis index (HI_{MS}) and the eroded area distribution index (EAI_x) while no significant correlations were obtained between HI_{MS} and the bed area distribution index (BAI_x). It indicates that the spatial distribution of eroded areas in the catchment is an important factor for explaining the hysteresis variability while river bed area distribution alone cannot explain this variability. However using both information (i.e. bed area distribution combined with eroded area distribution, SCI_x) permits a much better explanation of the hysteresis variability between catchments than considering eroded area distribution alone.

The correlation between the mass weighted hysteresis index HI_{MS} and the sediment source configuration index SCI_x (in a lesser extent with eroded area distribution index EAI_x) was found to increase when averaging the values over increasing distance (x) from the outlet. Both explanatory variables reached their maximum correlation value at a distance upstream of the monitoring station of approximately 70% (Table 1.4 and Figure 1.10). The closest source configuration indexes were not found to explain the variability of hysteresis patterns between catchments, suggesting that close source configurations alone cannot explain the suspended load dynamics.

1.5. DISCUSSION

1.5.1. DOMINANT HYSTERESIS PATTERNS AND TRANSPORT EFFICIENCY

Hysteresis effects are usually analyzed by counting the number of events having a certain shape [Aguilera and Melack, 2018; Aich et al., 2014; Buendia et al., 2016; Hamshaw et al., 2018; Navratil et al., 2010]. However, the comparison done in this study of ten contrasted alpine catchments highlighted that different results can be obtained by considering the fluxes transported with a given shape (Figure 1.7). From these results, two recommendations can be made, depending on the objective of the study. For those aiming at identifying the dominant sediment production processes for a given catchment, the hysteresis analysis should necessarily consider the intensity of each event, i.e., the average mass weighted hysteresis index. For studies aiming at understanding more in detail the hydro-sedimentary catchment functioning both in terms of occurrence and efficiency of the events transporting fine sediments, the analysis of hysteresis should be done simultaneously for both indexes. In our case, no relation was found between the median value of the Lloyd hysteresis index (HI_{Lloyd}) considering the number of events and any sediment source index (SCI_x , EAI_x , BAI_x) while significant correlations were found with the average mass weighted index. This suggests that the transport efficiency of hysteresis loops should be considered as a proxy of sediment production processes.

Calculating the two indices also allowed us to observe distinct behaviors for the ten alpine catchments. The differences between the fluxes exported and the frequency of events having a certain hysteresis shape were much higher for the southern catchments including the Buëch River than for the northern ones (Figure 1.7). This could be due to differences in hydrological regimes (Figure 1.2). Indeed, the southern catchments exhibited a more pronounced seasonal variability of the hysteresis values than the northern ones (Figure 1.11). Counterclockwise patterns were mainly observed during summer, corresponding to dry periods associated to short and intense convective storms. Clockwise patterns were observed during wet periods characterized by low intensity but rather long precipitation events leading to larger rainfall amounts than

during summer. These results were consistent with those from Navratil *et al.* (2012) reporting that clockwise hysteresis loops exported the bulk of total suspended load during widespread flood events in the Bléone catchment. They observed marked counterclockwise loops during summer rainstorms in upper tributaries which generate suspended fluxes that were not efficiently transferred downstream. This might explain why large differences were observed between the frequency and the fluxes exported with a given hysteresis for these southern basins. Similar trends were observed by Soler *et al.* (2008) or Buendia *et al.* (2016) in Pyrenean catchments having similar hydrological regimes. In comparison, the northern catchments exhibited a much more constant export of fine sediments during the frequent daily flood events of the melting season. Many more flood events were observed for similar monitoring periods in the north than in the south (Table 1.2). Mano *et al.* (2009) reported that 90% of the suspended fluxes were transported in 5% and 7% of the time for the Bléone and Asse Rivers, respectively, while 25% of the time was needed for the Romanche River.

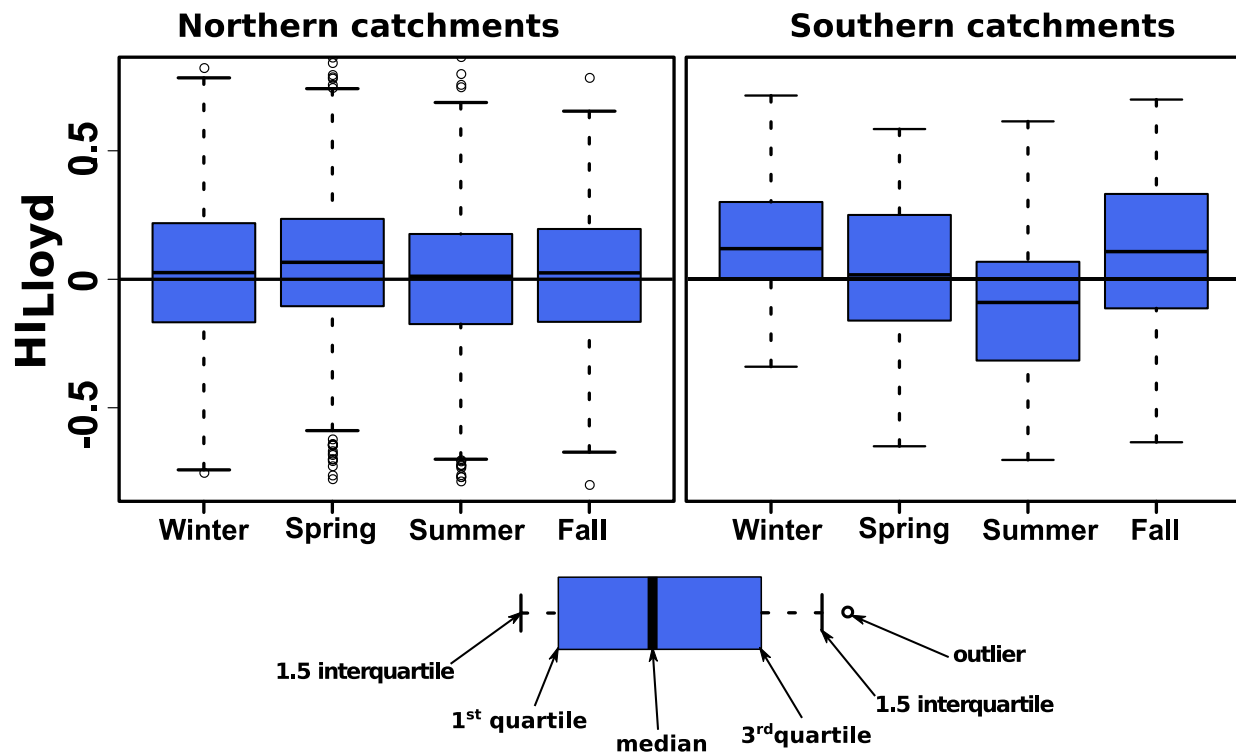


Figure 1.11: Seasonal variability of Lloyd hysteresis index considering all the events for the northern (Arc, Arvan, Drac, Glandon and Romanche) or southern (Asse, Bès, Bléone, Buëch and Galabre) catchments. It should be stressed that catchments with longer time series have more weight in the boxplot.

1.5.2. INFLUENCE OF CATCHMENT GEOMORPHOLOGICAL CHARACTERISTICS

The relation between the mass weighted hysteresis and catchment sources configuration (river bed vs. eroded areas) is consistent with previous findings and typical qualitative analyses of the hysteresis patterns which considers that a counterclockwise loops indicates a distant contribution while a clockwise loop results from a relatively close source mobilization [Bogen, 1980; Gellis, 2013; Guillon et al., 2018; Mao and Carrillo, 2016; Navratil et al., 2012; Navratil et al., 2010; Smith and Dragovich, 2009]. Influence of watershed characteristics on SSL hysteresis patterns was observed by Aguilera et al. (2018) in ten mountainous Californian catchments. Also, using a random forest model on 45 measuring stations, Vaughan et al. (2017) showed that considering near-channel morphological characteristics in addition to land use contributes to a better explanation of the sediment rating curve parameters than using land use only. Their random forest model explained 38% and 43% of the hysteresis variance when considering respectively only watershed metrics or watershed plus near channel metrics. In our analysis, we also observed that both sources need to be considered. However our results show the importance to consider not only global catchments properties but the relative importance of these two types of sources (bed vs eroded areas) as well as their “travelling distance” to the monitoring station to explain hysteresis variability between catchments. Also, as was observed by Vaughan et al. (2017), we should stress that including the bed area information by considering the relative spatial distribution of eroded versus bed area (SCI_x) and not the spatial distribution of eroded area (EAI_x) alone, permits a much better explanation of the hysteresis variability and thus of the suspended load dynamics. This result is also consistent with several studies that reported a significant buffering effect played by the river bed which could be considered as a significant fine sediment source in mountainous catchments having relatively large and active alluvial reaches [Guillon et al., 2018; Navratil et al., 2012; Navratil et al., 2010; Orwin and Smart, 2004b].

The results obtained in this paper and in previous studies bring us to propose the following conceptual description of hysteresis and sediment configuration interactions (Figure 1.12). The dominant hysteresis effect observed at a given location in a catchment could depend on the upstream capacity to produce distant erosion and to buffer these upstream fluxes. If the remobilization of fine sediments from the river bed did not exist, mainly counterclockwise hysteresis should have been observed because of celerity differences between the flow rate and SSC waves [Klein, 1984]. Thus, the hysteresis patterns would depend on the location of the observation point for a given geomorphological scale (point A, B, C or D in Figure 1.12). Following the conceptual configuration in Figure 1.12, the fraction of SSL coming from the river bed and driven by the total flow rate could increase when moving to the downstream part of a catchment,

while SSL coming directly from primary hillslope sources and driven by rainfall or runoff could decrease. Such scale dependencies of hysteresis processes have been already noticed in hydrological studies [Gharari and Razavi, 2018]. For instance, Davies and Beven (2015) have shown by using a synthetic case that hysteresis between streamflow and catchment storage was changing with the catchment size considered.

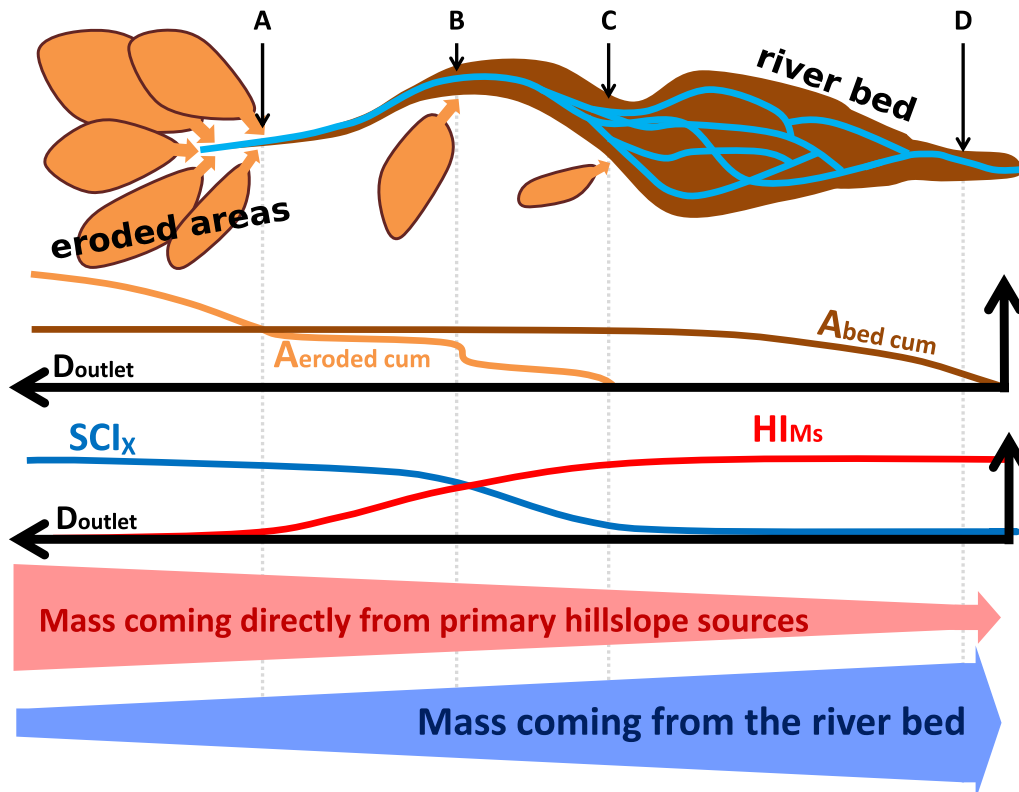


Figure 1.12: Conceptual catchment and evolution of hysteresis effects considering the flux exported (HI_{Ms}), sediment sources configuration (SCI_x), cumulated riverbed area ($A_{bed\ cum}$), cumulated eroded area ($A_{eroded\ cum}$) and fraction of suspended sediment load coming from the bed or from primary hillslope sources. A, B, C and D denote four different observation points.

1.5.3. LIMITATIONS AND IMPLICATIONS

Given the wide range of characteristics of the 10 studied alpine catchments, comprising various sizes, geologies, altitudes, hydrological and sedimentary regimes the proposed approach can be considered as relevant in other mountainous environments. However, its relevance should be tested in other contexts such as low-land, agricultural or arid environments. The analysis of the sediment sources might be improved to get a more detailed description of the catchment sources configuration to investigate its relation with suspended load at shorter spatial and temporal scales. For instance, the mechanical properties of rocks in eroded areas could be taken into account to give more importance

to soft rocks than to more resistant ones for catchments with contrasted lithologies. The local river bed slope could also be explicitly considered in addition to the active river width to get a proxy of the buffering capacity of the bed. This would probably give less importance to steep streams and more importance to gentle ones. These potential improvements might be tested in future work.

However, while the approach used does not represent all the complexity of interactions between suspended load and sediment source configuration a significant part of the variability of SSL hysteresis can be explained by this simplified source description at a regional scale. This confirms the strong link between hysteresis processes and the variable sediment sources activation that have been qualitatively described for decades [Gellis, 2013; Gharari and Razavi, 2018; Williams, 1989]. Our results suggest that even for small catchments, fine sediment dynamics and hysteresis effects could be largely influenced by erosion and deposition processes occurring in the river bed. This might be the case in catchments where eroded areas are located far enough upstream so that the main channel can act as a buffering reservoir of fine sediments. However, larger catchments with well-developed fluvial systems could, conversely, be influenced in a non-negligible way by hillslope process production if some eroded areas are located at a short distance from the monitoring station. Both processes are probably inevitably linked. The fractions of SSL coming from the bed or from the hillslopes seem to change depending on the point considered in the catchment. The simple sediment sources analysis proposed in this study could be performed prior to the installation of a gauging station or prior to modeling effort in order to assess which kind of processes should be considered in a conceptual modeling approach. It could also be helpful to determine the dominant fine sediment production process for river or dam management at the catchment scale.

1.6. CONCLUSIONS

This study aimed at testing the links between Discharge-Suspended Sediment Concentrations (Q-SSC) hysteresis and the spatial configuration of sediment sources which have been qualitatively considered for decades without been quantitatively tested. A quantitative analysis of sediment sources configuration and Q-SSC hysteresis was performed in ten contrasted alpine catchments. Hysteresis indexes were calculated on a high number of automated sampled events to extract the dominant hysteresis pattern for each catchment. Simple indexes were developed to describe the river bed and eroded patches area distribution as well as a “travelling distance to the outlet”. The main findings can be summarized as follows:

- (i) Considering the dominant SSL hysteresis in a given catchment as the most frequent pattern or as the most efficient in terms of transport can lead to different results. Our observations suggest that the transport efficiency of

hysteresis should be considered to infer the dominant sediment production process. This could be particularly true for catchments having most of their fluxes exported during few short events and exhibiting marked seasonal hysteresis variability. Thus an averaged mass weighted hysteresis index was proposed.

- (ii) A strong correlation was found between mass weighted hysteresis index and sediment sources configuration index (river bed vs eroded area) which confirms the qualitative interpretations often made for SSC-Q hysteresis processes. We also observed that the sources configuration should be considered on a long enough fraction of the catchment (at least 50% of the whole principal river network) upstream the observation point to explain the spatial hysteresis variability. This is consistent with the rather long travelled distances of suspended particles.
- (iii) In comparison to previous studies, these results show the importance to consider not only general catchment properties or sediment sources to understand SSL dynamics but their spatial distribution and connectivity. Furthermore, including bed related information increases significantly the explanatory power of the SSC-Q hysteresis variability than using only primary hillslope sources information.

1.7. NOTATIONS

The following symbols are used in this paper.

<i>SSL</i>	Suspended sediment load
<i>SSC</i>	Suspended sediment concentration
<i>Q</i>	Flow rate
<i>A</i>	Catchment area
<i>No</i>	Fraction of catchment with low or no vegetation cover
<i>Fo</i>	Fraction of catchment forest cover
<i>Gl</i>	Fraction of catchment with glacier cover
<i>SCR</i>	Fraction of catchment with soft coherent rock cover
<i>HR</i>	Fraction of catchment with heterogeneous rock cover
<i>RR</i>	Fraction of catchment with resistant rock cover
<i>W₁₀</i>	Median active width extracted on the first 10 km upstream the station
<i>S₁₀</i>	Mean riverbed slope extracted on the first 10 km upstream the station
<i>q</i>	Mean annual specific discharge
<i>HI_{Lloyd}</i>	Lloyd hysteresis index
<i>SSC*</i>	Normalized suspended sediment concentration at the flood scale
<i>Q*</i>	Normalized flow rate at the flood scale
<i>HI_{MS}</i>	Mass weighted average hysteresis index
<i>MS_i</i>	Mass of suspended sediment transported during the event i
<i>Nb_{cl}</i>	Fraction of event having a clockwise hysteresis shape
<i>Nb_{ccl}</i>	Fraction of event having a counterclockwise hysteresis shape

$Nb_{complex}$	Fraction of event having complex or no hysteresis shape
MS_{cl}	Fraction of the mass exported with a clockwise hysteresis shape
MS_{ccl}	Fraction of the mass exported with a counterclockwise hysteresis shape
$MS_{complex}$	Fraction of the mass exported with complex or no hysteresis hysteresis
$A_{eroded\ cum}$	Cumulative eroded area at a given distance from the station
$A_{bed\ cum}$	Cumulative riverbed area at a given distance from the station
SCI_x	Sources Configuration Index (mean ratio of cumulative eroded area over cumulative bed area calculated on the first x% of the main channel length)
EAI_x	Eroded Area Index (mean cumulative eroded area over total eroded area on the first x% of the main channel length)
BAI_x	Bed Area Index (mean cumulative bed area over total bed area on the first x% of the main channel length)
L	Maximum distance used to compute the sediment source configuration index
$SSL_{99\%}$	Threshold on SSL above which 99% of cumulated suspended fluxes are transported
$SSC_{99\%}$	Threshold on SSC above which 99% of cumulated suspended fluxes are transported
t_{exceed}	Minimum time step for which a SSL should exceed all following and preceding values for the event detection

1.8. ACKNOWLEDGEMENTS

This study was funded by IRSTEA (National Research Institute of Science and Technology for the Environment and Agriculture) and EDF (Electricité de France). The field monitoring data provided by IRSTEA, EDF and IGE (Institute for Geosciences and Environmental research) field teams are greatly appreciated. The authors also want to thank three anonymous reviewers who greatly contributed to improve to this paper by providing helpful reviews of an earlier version of this manuscript.

1.9. APPENDIX

1.9.1. SOURCE CONFIGURATION INDEX

River	SCI_{10}	SCI_{20}	SCI_{30}	SCI_{40}	SCI_{50}	SCI_{60}	SCI_{70}	SCI_{80}	SCI_{90}	SCI_{100}
Arc	0.1	1.2	3.0	5.0	6.9	8.0	8.9	9.8	10.7	11.5
Arvan	0.1	0.3	0.8	1.6	2.8	4.4	7.3	11.6	16.6	21.3
Asse	0.2	0.4	0.8	1.4	1.9	2.1	2.5	3.4	4.6	6.3
Bès	0.4	0.3	0.2	0.2	0.2	0.5	1.2	2.1	2.9	3.9
Bleone	0.1	0.1	0.1	0.1	0.1	0.1	0.1	0.1	0.1	0.3
Buech	0.3	0.7	1.3	2.4	3.4	4.1	4.7	5.6	6.6	7.5
Drac	0.3	0.8	1.1	1.7	2.3	2.6	3.0	3.2	3.5	3.8
Galabre	1.3	1.1	1.0	1.0	1.0	1.1	1.3	1.4	1.6	1.7
Glandon	0.0	0.6	1.5	2.5	3.7	4.6	5.4	6.3	6.7	6.7
Romanche	0.9	1.2	1.8	2.7	3.9	6.2	8.4	10.2	11.5	12.2

Table 1.5: SCI_x index calculated for each river for x from 10% to 100% of the total length L. SCI_x is the mean ratio between cumulated eroded area and cumulative bed area calculated on a given distance from the outlet of the catchment.

1.9.2. ERODED AREA INDEX

River	EAI_{10}	EAI_{20}	EAI_{30}	EAI_{40}	EAI_{50}	EAI_{60}	EAI_{70}	EAI_{80}	EAI_{90}	EAI_{100}
Arc	0.00	0.01	0.04	0.08	0.12	0.17	0.22	0.27	0.33	0.39
Arvan	0.00	0.00	0.00	0.01	0.02	0.04	0.07	0.13	0.20	0.27
Asse	0.00	0.00	0.01	0.01	0.02	0.03	0.05	0.09	0.14	0.21
Bès	0.00	0.00	0.00	0.00	0.00	0.02	0.05	0.11	0.16	0.24
Bleone	0.00	0.00	0.01	0.01	0.01	0.02	0.02	0.03	0.04	0.11
Buech	0.00	0.00	0.02	0.04	0.08	0.12	0.16	0.22	0.29	0.36
Drac	0.00	0.01	0.02	0.04	0.07	0.10	0.14	0.18	0.22	0.29
Galabre	0.02	0.03	0.05	0.07	0.09	0.13	0.19	0.25	0.32	0.38
Glandon	0.00	0.00	0.02	0.03	0.07	0.11	0.16	0.22	0.30	0.37
Romanche	0.00	0.01	0.02	0.03	0.06	0.11	0.20	0.28	0.36	0.42

Table 1.6: EAI_x index calculated for each river for x from 10% to 100% of the total length L. EAI_x is the mean ratio between cumulated eroded area and total cumulative eroded area calculated on a given distance from the outlet of the catchment.

1.9.3. BED AREA INDEX

River	BAI_{10}	BAI_{20}	BAI_{30}	BAI_{40}	BAI_{50}	BAI_{60}	BAI_{70}	BAI_{80}	BAI_{90}	BAI_{100}
Arc	0.05	0.11	0.16	0.21	0.25	0.30	0.35	0.41	0.46	0.51
Arvan	0.09	0.17	0.24	0.31	0.36	0.42	0.46	0.50	0.54	0.59
Asse	0.05	0.09	0.13	0.17	0.22	0.28	0.36	0.42	0.49	0.54
Bès	0.05	0.09	0.14	0.19	0.25	0.31	0.37	0.42	0.47	0.52
Bleone	0.04	0.09	0.14	0.19	0.25	0.33	0.40	0.47	0.52	0.57
Buech	0.02	0.07	0.14	0.19	0.25	0.32	0.39	0.46	0.51	0.56
Drac	0.05	0.09	0.12	0.15	0.19	0.23	0.28	0.33	0.39	0.45
Galabre	0.05	0.11	0.16	0.22	0.27	0.32	0.37	0.42	0.47	0.52
Glandon	0.04	0.07	0.11	0.15	0.18	0.22	0.28	0.35	0.41	0.46
Romanche	0.00	0.01	0.02	0.03	0.06	0.13	0.21	0.30	0.38	0.51

Table 1.7: BAI_x index calculated for each river for x from 10% to 100% of the total length L. BAI_x is the mean ratio between cumulated bed area and total cumulative bed area calculated on a given distance from the outlet of the catchment.

Chapter 2

Assessment of fine sediment river bed stocks in seven alpine catchments

In alpine catchments, few data are available concerning the river bed stocks of fine sediments. Such information is however crucial to understand the role of river bed on fine particle transfer in that kind of watersheds. In other type of basins, many studies have shown that significant quantities of this finer material could be stored in the gravel matrix. This second chapter reports a field campaign performed in seven Alpine rivers to quantify their fine particle stocks and will be submitted in autumn 2019 to Hydrological Processes (contributors Misset C., Recking A., Legout C., Viana-Bandeira B., Poirel A. and Cazihlac M.).

Dans les bassins versants alpins, peu de données relatives aux stocks de sédiments fins dans le lit des rivières sont disponibles. Cette information est cependant cruciale pour comprendre le rôle que joue le lit des rivières sur le transfert de particules fines dans ce type de bassin versant. De nombreuses études réalisées dans d'autres contextes ont montrées que d'importantes quantités de particules fines pouvaient être stockées dans des matrices graveleuses. Ce second chapitre rapport une campagne de terrain durant laquelle les stocks de sédiments fins dans le lit de sept rivières alpines ont été quantifiés. Ce chapitre sera soumis à l'automne 2019 dans Hydrological Processes (contributeurs Misset C., Recking A., Legout C., Viana-Bandeira B., Poirel A. and Cazihlac M.).

2.1. ABSTRACT

While the finest fraction has long been considered to have limited interactions with the river bed, several recent studies based on flume and field observations raises questions about this hypothesis which is fundamental for suspended load modeling and river management. In this study, we report a large field campaign in which we quantified the river bed stocks of fine particles in 7 alpine catchments. Using a simple protocol, we performed more than 300 riverbed measurements of the local surface and subsurface stocks. Results indicate that even if the river bed surface contains no fine particles, significant quantities can be found in the subsurface layer which is in most cases the layer having the higher stocks. We also observed that stocks highly depend on the facies considered suggesting that storage processes are driven by local hydraulics and river bed characteristics. By integrating the local stocks existing in the first ten centimeters of the riverbed at the catchment scale we estimated that they could represent more than 50% of the mean annual suspended load in catchments with large braided rivers while they could be as small as 1% in highly eroded head water catchments. This suggests that the bed of large alluvial alpine rivers can be considered as a significant source of fine particles. These observations were confirmed by using a simplified scouring model to estimate conditions for these stocks to be released which however ask questions on the bed reworking processes modeling. Finally, these observations suggest that interactions between gravel beds and fine particles transported as suspension are far from being negligible processes in alpine catchments.

2.2. INTRODUCTION

A better understanding of suspended load dynamics in rivers is crucial as fine particles strongly affect the water quality, aquatic habitats and can also lead to siltation problems in hydropower plans [*Kondolf et al., 2014; Mathers et al., 2017; Owens et al., 2005; Vercauteren et al., 2017; Walling et al., 2003*]. Suspended load is highly variable in time as fine particles can originate from various erosion processes. They can either be eroded on hillslopes or originate from the river bed [*Collins and Walling, 2007b; Legout et al., 2013; Park and Hunt, 2017; Piqué et al., 2014; Walling and Collins, 2008*]. In mountainous watersheds, characterized by high sediment yields [*Vanmaercke et al., 2011*] some studies suggest that the river bed can be considered as a buffer controlling downstream fluxes from the event to the annual time scale [*Guillon et al., 2018; Navratil et al., 2012; Navratil et al., 2010; Orwin and Smart, 2004b*]. It is thus of importance to assess the quantity of fine sediments stored in the river bed of these catchments for instance to design a management plan aiming at reducing the fine sediments delivered. Such assessment is also required to calibrate predictive conceptual models of suspended load at the catchment scale such as the ones proposed by [*Asselman, 1999; Park and Hunt, 2018; Picouet et al., 2009*]. These models consider a conceptual storage reservoir which is often statistically calibrated and poorly documented introducing a

substantial uncertainty in the approach. It could also help to understand the complex interactions between fines particles and the gravel matrix [Hill *et al.*, 2017; Mooneyham and Strom, 2018] and more generally the geomorphological factors and hydrological processes controlling fine sediment storage in mountainous rivers.

Several studies already focused on fine particles stored in the river bed [Buendia *et al.*, 2016; Collins and Walling, 2007b; Duerdoth *et al.*, 2015; Lambert and Walling, 1988; Marteau *et al.*, 2018; Naden *et al.*, 2016; Turley *et al.*, 2017]. The ratios between the stocks of fine particles and the annual suspended sediment load were found to be highly variable depending on the catchment considered (ranging from 0 to 100%). This ratio was also found to vary for a given catchment in time and space [Collins and Walling, 2007b; Piqué *et al.*, 2014]. However, most of these studies were conducted in lowland rivers and considered exclusively underwater storage. In mountainous rivers, fine particles stored in the whole active width, i.e. in dried facies could also contribute significantly to the downstream fluxes as the bed of these rivers is often highly mobile and exhibit large gravel bars during low water stages [Navratil *et al.*, 2010]. Few studies such as the one of Navratil *et al.* (2010) proposed a method to quantify fine sediment stocks in mountainous rivers. Following this approach, this study aims to (i) estimate the local stocks of fine particles in the river beds of various alpine catchments and analyze their spatial variability and (ii) compare these stocks at the catchment scale with the suspended fluxes observed at the outlet to estimate the potential river bed contribution to total suspended load.

2.3. MATERIAL AND METHODS

2.3.1. STUDIED AREA

Seven alpine catchments for which long term suspended load measurements are available were analyzed in this study (Figure 2.1). They ranged from 110 to 635km² and comprise a wide range of river bed morphologies (from steep and narrow step pools to wide braiding streams) and catchment characteristics. The approach developed to assess river bed fine sediment stocks in each of these seven catchments combined measurements of local stocks with aerial photography analysis. The local measurements were performed with two distinct protocols, for dried areas or in channel.

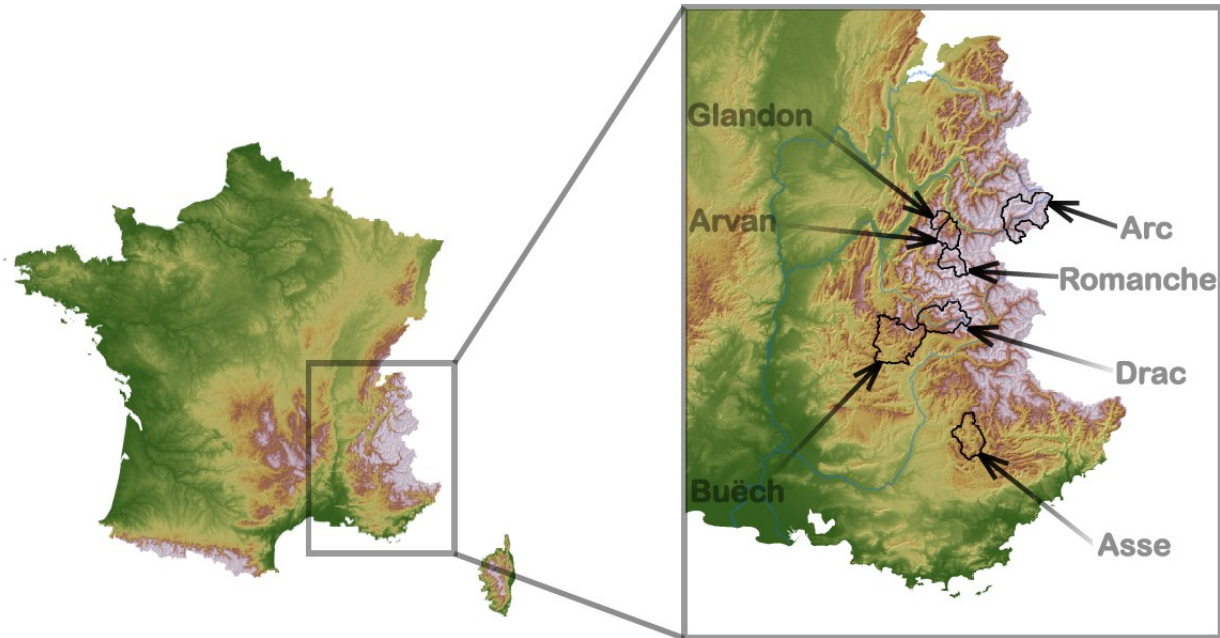


Figure 2.1 : Catchment location.

2.3.2. SAMPLING PROTOCOL

2.3.2.1. Dried areas sampling protocol

A sampling technic adapted from the protocol proposed by Navratil et al. (2010) was used to measure local stocks of fine sediments in dried parts of the active width of the river. Two layers were distinguished. A first layer comprises fine sediments deposited on and into the armor layer denoted h_1 in Figure 2.2. A second layer denoted h_2 in Figure 2.2, under the first one and comprising fine sediments in the subsurface was considered.

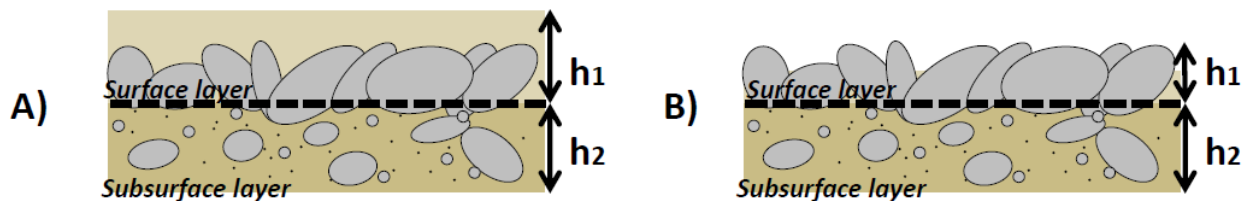


Figure 2.2: Definition of the two layers for dried storage areas. h_1 is the depth of the surface layer; h_2 is the depth of the subsurface layer. Case A): fine sediments deposited on the armor layer. Case B): apparent armor layer and fine sediment deposited in the pore spaces.

The steps of this sampling technic are detailed in Figure 2.3. First, a rectangular area (A , m^2) of 28cm by 34 cm was sampled over the h_1 depth and put in a container with 20

liters of water from the river ($V_{container\ 1}$, L). This area was found to be a good compromise between the time needed and the uncertainty associated to the surface considered. Approximately ten minutes were needed to do one measurement with two operators.

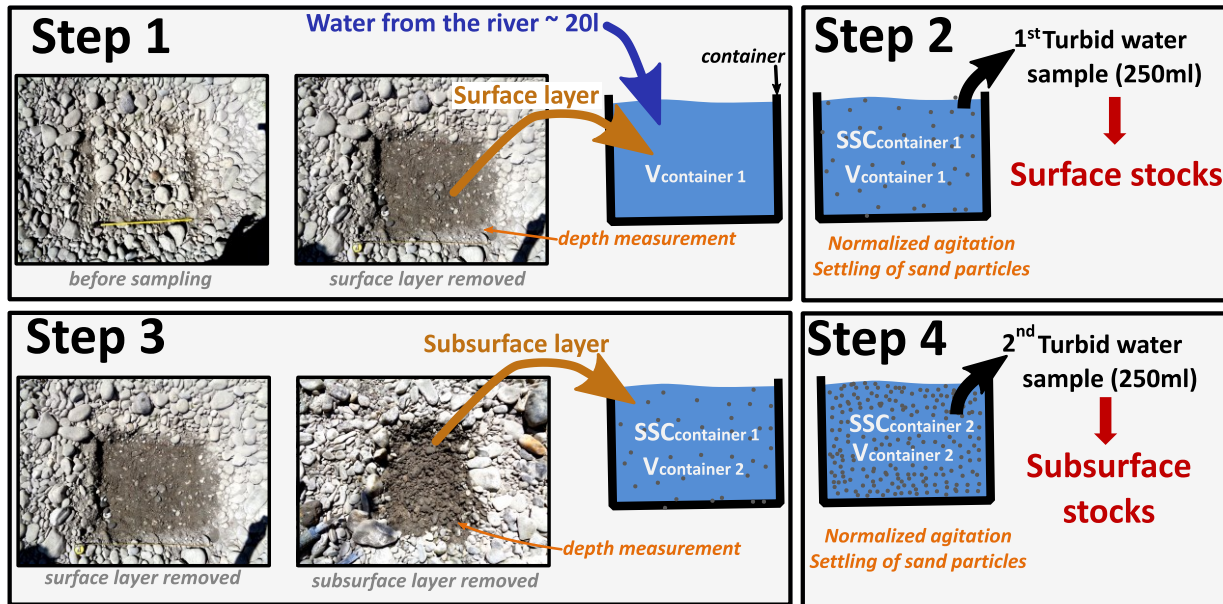


Figure 2.3: Steps of the sampling method used for dried areas. $V_{container\ 1}$ is the volume of clear water in the container taken in the river before any sampling of turbid water, $SSC_{scontainer\ 1}$ is the suspended sediment concentration in the container after adding the surface layer and subtracting suspended concentration of the river, $V_{container\ 2}$ is the volume of water in the container after the first sampling of turbid water, $SSC_{scontainer\ 2}$ is the suspended sediment concentration in the container after the first sampling of turbid water and the adding of the subsurface layer.

A shovel was then used to a shake the mixture and put fine sediments in suspension. This was done in a normalized way by the same operator which turned ten times the shovel in the bottom of the container. Then a 250 ml bottle was used to take a sample of the turbid water after waiting 4 seconds so that the sand particles were settled. This bottle was brought to the laboratory to measure its suspended sediment concentration ($SSC_{scontainer\ 1}$, $g\ L^{-1}$) from which the suspended sediment concentration of the water coming from the river was subtracted. Finally the local stock of fine sediment for the surface layer ($st_{surface}$, $g\ m^{-2}\ dm^{-1}$) could be estimated using Eq.2.1:

$$st_{surface} = \frac{SSC_{contrainer\ 1} \times V_{container\ 1}}{A \times h_1} \quad (2.1)$$

The second step was to add sediments from the subsurface layer in the container without removing the first mixture and to repeat the procedure detailed above. The subsurface stock ($st_{subsurface}$, $g\ m^{-2}\ dm^{-1}$) was estimated using Eq.2.2:

$$st_{subsurface} = \frac{(SSC_{container\ 2} - SSC_{container\ 1}) \times V_{container\ 2}}{A \times h_2} \quad (2.2)$$

2.3.2.2. In channel sampling protocol

The Lambert and Walling (1988) protocol described in many publications was used to estimate in channel storage of fine sediments [Collins and Walling, 2007a; Duerdoth et al., 2015; Piqué et al., 2014; D. E. Walling et al., 1998]. A cylinder with a diameter of 29 centimeters was pushed in the river bed to separate the sampling area from the flow. Then a trowel was used to disturb and agitate the bed before a turbid water sample was taken in a 250 ml bottle to estimate its concentration. No differences were made between surface and subsurface. The depth of bed disturbance ($h_{bed\ disturbance}$, m) was estimated as well as the water depth in the cylinder (h_{water} , m) to finally get the local stocks estimates:

$$st_{water} = \frac{SSC_{cylinder} \times h_{water}}{h_{bed\ disturbance}} \quad (2.3)$$

2.3.3. LOCAL STOCKS INTEGRATION OVER THE CATCHMENT

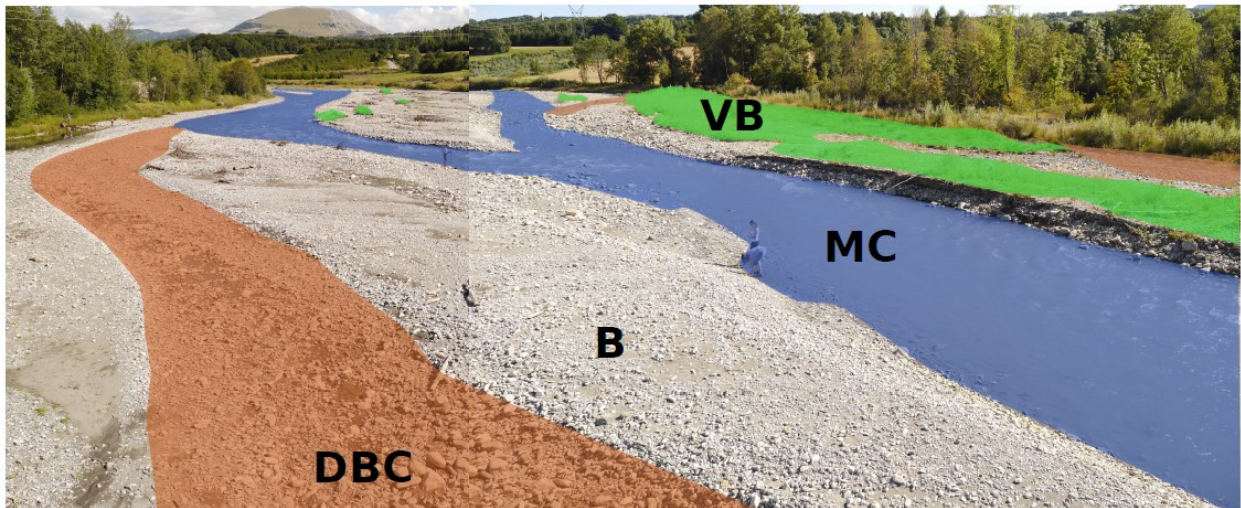


Figure 2.4: Example of the four storage facies on the drac river. MC = main channel, B = bar, DBC = dry braided channel, VB = vegetated bar.

Two strategies were used to integrate the local stocks over all the river system. For large enough rivers (Arc, Asse, Buëch Drac and Romanche Rivers) the four storage facies

proposed by Navratil et al. (2010) were used (Figure 2.4). The main channel (MC) facies was defined as the wetted channel during base flow period. The dry braided channels (DBC) classification was used for secondary channels that flow rapidly when the water level increases. Vegetated bars (VB) and non-vegetated bars (B) were also distinguished. This classification was used because it allows in the field to distinguish these storage zones where physical processes leading to sedimentation could differ. Navratil et al. (2010) observed large differences of storage values on these facies. Sediments were also not mobilized in the same way and with the same frequency. The samples were taken on cross sections distributed along the river. The mean stock obtained for the facies i (\overline{st}_i , $\text{g m}^{-2} \text{ dm}^{-1}$) was then multiplied by the surface of this facies (A_i , m^2). The mass stored in all the river bed for a given depth ($St_{catchment}$, t dm^{-1}) was obtained by adding the integrated stocks for each storage facies:

$$St_{catchment} = \sum_{i=1}^4 \overline{st}_i \times A_i \quad (2.4)$$

Aerial photographs with a 0.5 m resolution were used to estimate the surface occupied by each facies. An automated classification based on radiometry was performed with Arcgis 10.3 (Figure 2.5). The “Maximum Likelihood Classification” function was used after the active width was manually digitalized. As verified by Navratil et al. (2010), the surface occupied by each facies was assumed to be constant in time. Unfortunately for most photographs, it was not possible to distinguish the DBC from the B facies. Thus, the cross sections with facies delimitation (Figure 2.6) were used to roughly estimate the fraction of area detected as B facies while being a DBC facies ($A_{DBC}/(A_{DBC} + A_B)$). According to measurements in all the cross sections, an average value of 25% for this ratio was considered.

For narrower rivers for which aerial photographs could not be used to estimate properly facies surfaces (Arvan and Glandon) the mean stock measured on a cross section i was integrated using Eq.2.5 considering an average storage value for all facies (\overline{st}_i) for a given active river bed area (A_i). This was repeated for the n cross sections where measurements were made. The surface (A_i) was defined as the surface of the active width between the middle of the distance between section $i-1$ and i and the middle of the distance between section $i+1$ and i . This surface was calculated using the active width digitalization with a 1m spatial step.

$$St_{catchment} = \sum_{i=1}^{nb \text{ cross section}} \overline{st}_i \times A_i \quad (2.5)$$

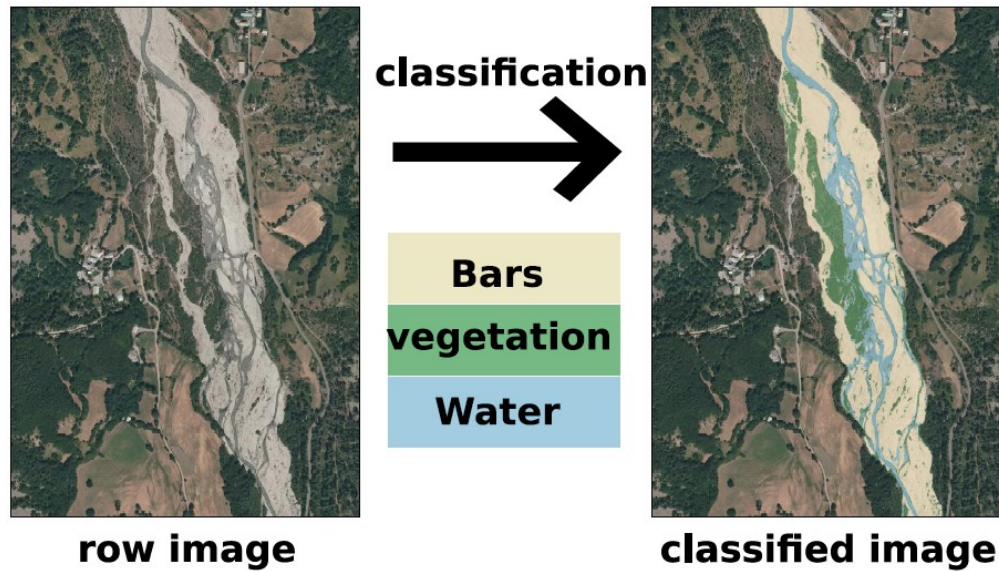


Figure 2.5: Example of automated facies classification for the Drac River.

2.3.4. ESTIMATE OF AVAILABLE STOCKS

Additional measurements were made to roughly assess the flow stage needed to mobilize the fine sediments stored in different zones of the river bed and estimate the available stocks of fines particles for a given flow condition. As samples were taken along cross sections, the topography was measured using a DGPS or a total station having a centimetric precision. Localization of the samples as well as the types of facies were measured (Figure 2.6). We also qualified visually the fraction of fine particles cover at the bed surface for each samples. Those with less than 75% of fine cover was considered as type 1, more than 75% as type 3 and type 2 was considered for intermediate situations.

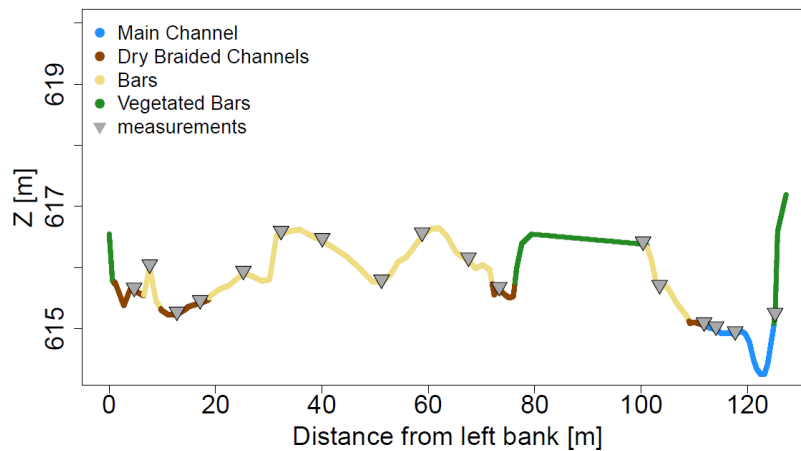


Figure 2.6: Example of a cross section measured in the Asse River. The topography measurement was completed with facies delimitation and sample localization.

The slope of the water surface of each reach was measured as well as the surface grain size distribution using non-truncated Wolman count technic [Wolman, 1954]. These measurements were then used to estimate the mobilized zones for a given flood event. To do so the variable-power law equation for flow resistance proposed by Ferguson (2007) was applied in an iterative way considering several vertical panels to take into account lateral cross section variability. This friction law is well suited for low relative submergence and flow conditions found in the studied alpine rivers [Ferguson, 2010; Rickenmann and Recking, 2011]. The water level corresponding to a given flow rate was calculated using the measured slope (S), the 84% percentile of the grain size distribution (D_{84} , m) and the cross section topography:

$$\frac{U}{\sqrt{gR_hS}} = \frac{2.5 \frac{R_h}{D_{84}}}{\sqrt{1 + 0.15 \left(\frac{R_h}{D_{84}}\right)^{5/3}}} \quad (2.6)$$

in which U (m s^{-1}) is the mean velocity, g the gravitational acceleration (m s^{-2}) and R_h the hydraulic radius (m). It was then possible to estimate a local Shield number (1000 values equally spread over the cross section) with the local water depth (d , m) for coarse sediments over the cross section assuming a constant slope for all the section:

$$\tau_{84}^* = \frac{\rho g d S}{(\rho_s - \rho) g D_{84}} \quad (2.7)$$

in which ρ is the water density (kg m^{-3}) and ρ_s is the sediment density (kg m^{-3}). We estimated the vertical scouring depth when the armor layer was mobilized by using the probability model developed by Haschenburger (1999) based on field measurements in gravel bedded streams. The probability to observe scouring smaller than δ cm ($P(\delta)$) is defined by an exponential distribution with a parameter θ (cm^{-1}):

$$P(\delta) = \begin{cases} 1 - e^{-\theta \times \delta} & \text{for } \delta \geq 0 \\ 0 & \text{otherwise} \end{cases} \quad (2.8)$$

The θ parameter is empirically defined by Haschenburger as a function of the transport stage ($\frac{\tau^*}{\tau_c^*}$):

$$\theta = 3.33e^{-1.52 \frac{\tau^*}{\tau_c^*}} \quad (2.9)$$

which was estimated considering the D_{84} in Eq.2.7 and a critical shield number (τ_{84c}^*) function of the riverbed slope [Recking, 2009]:

$$\tau_{84c}^* = 0.56 * S + 0.021 \quad (2.10)$$

Because riverbed scouring is a stochastic process, we computed several scouring depths (δ) corresponding to non-exceedance probabilities equal to 5%, 50% and 95%:

$$\delta = -\frac{\ln(1 - P(\delta))}{\theta} \quad (2.11)$$

Also, based on DeVries (2002) observations, we considered an upper limit for the possible scouring depth of $2D_{90}$. We considered an average stock per facies and between surface and subsurface for each cross section. Finally, the available river bed stock was computed by integrating the local stock and the local scouring depth over the cross section. This calculation was performed for each cross section where measurements were conducted to obtain a mass of fine particles released ($m_{section}$, $t\ m^{-1}$) as a function of the peak flow rate:

$$m_{section} = \int_{l=0}^W \overline{st_{local\ i}}(l) \times \delta(l) \times dl \quad (2.12)$$

in which $\overline{st_{local\ i}}(l)$ is the local average stock for the facies i ($g\ m^{-2}\ dm^{-1}$), $\delta(l)$ the local scouring depth (dm) and W (m) the total width of the cross section considered. To take into account drainage area differences between the outlet of the basin and the cross section calculation, we used specific peak discharges detrended as a function of the catchment area as is often done in similar studies [Mueller, 2005; Piton and Recking, 2017]. For a given scouring probability (5%, 50% and 95%), an average value of the mass released calculated for all cross sections was considered ($\overline{m_{section}(Q_{peak})}$, $t\ m^{-1}$). It was then multiplied by the stream length considered representative of the storage system ($L_{storage\ system}$, m) based on the active width digitalization to get the total available riverbed stocks ($M_{catchment}$, t) at the catchment scale as a function of the peak discharge:

$$M_{catchment}(Q_{peak}) = \overline{m_{section}(Q_{peak})} \times L_{storage\ system} \quad (2.13)$$

Details about the parameters considered for the calculation can be found in the supplementary material. The calculation procedure is synthetized in Figure 2.7:

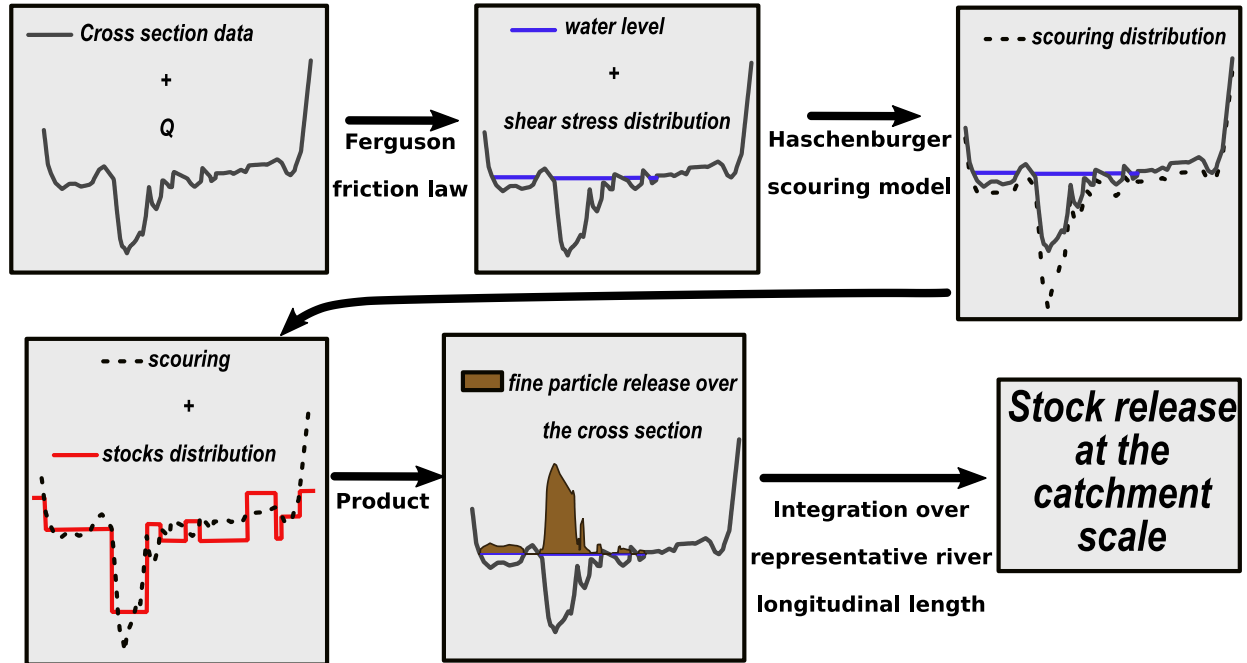


Figure 2.7: Synthesis of the algorithm used to compute the potential river bed stocks released.

2.3.5. SUSPENDED SEDIMENT YIELD MEASUREMENTS

Suspended sediment load (SSL, g s^{-1}) was measured in the seven alpine catchment using high frequency (1h) turbidity and water level measurements as often done in such rivers [Mano *et al.*, 2009; Navratil *et al.*, 2011]. Rating curves between water level and flow rate (Q , $\text{m}^3 \text{s}^{-1}$) or between turbidity and suspended sediment concentration (SSC, g l^{-1}) were built by using repeated flow rate gauging (salt dilution, ADCP, LSPIV and current meters) and SSC sampling (automated ISCO samplers). Suspended load was calculated at each time step by considering a homogeneous concentration over the cross section:

$$SSL = SSC \times Q \quad (2.14)$$

SSL was integrated over each year of measurement and divided by the catchment area to get the specific suspended sediment load ($\text{t km}^{-2} \text{ year}^{-1}$) and mean annual suspended load (t) for each catchment. When turbidity data were missing, a global rating curve fitted for all the available measurements was used to estimate missing SSC [Ferguson, 1986]. Because suspended yield is variable from one year to another, the mean and standard deviation of this value was considered. The stock of fine sediment estimate in the river bed could then be compared to the annual fluxes for each catchment.

2.4. RESULTS

2.4.1. GENERAL OVERVIEW OF THE MEASUREMENTS

In total, 339 measurements were conducted in the seven studied catchments between June and August 2017 (Table 2.1). More samples were performed in large braided rivers as the spatial variability was expected to be higher in these systems (Asse, Buech, Petit Buech and Drac). The sites were located along the main fluvial corridor to be the most representative as possible.

	Arc	Arvan	Asse	Buëch	Petit Buëch	Drac	Glandon	Romanche
Number of sites	4	3	3	5	2	4	3	3
Number of samples	20	9	122	71	29	63	9	16

Table 2.1: Number of sites and measurements conducted in each catchment. Note: the Petit Buech is the main tributary in the Buech catchment.

Because the objective of this approach was to compare stocks and fluxes, we had to estimate the sediment size representative of our measurements. A diameter of 100µm was considered as a first approximation, to be consistent with the upper limit of turbidity technics sensitivity [Lewis, 1996]. Our analysis shows that the two resuspension technics used were representative of the finest fraction of the fine river bed stocks as the fraction larger than 100µm ranged between 10% and 37% (Table 2.2). Similar results were obtained by Lambert and Walling (1988). We also characterized settling properties of surface deposits in five of the catchments (Arc, Drac, Asse, Buëch and Romanche) using an optic device called System Characterizing Aggregates and Floccs (SCAF) [Legout *et al.*, 2018; Wendling *et al.*, 2015]. These measurements are presented in appendix 2.8.2. Observed settling velocities (mean value per river) ranged between 10^{-4} and 10^{-3} (m/s) which corresponds to particle diameters considering the Stokes law of approximately 10-35µm. Also, a significant part of these samples exhibited cohesive properties as aggregation processes were observed during settling.

	Arc	Arvan	Asse	Buëch	Petit Buëch	Drac	Glandon	Romanche
Fraction larger than 100µm	37% ⁽¹⁾	-	10% ⁽²⁾	14% ⁽¹⁾	24% ⁽¹⁾	33% ⁽¹⁾	-	23% ⁽¹⁾

Table 2.2: Fraction of the total mass sampled with a diameter larger than 100µm. ⁽¹⁾ Indicates data obtained by sieving under water the total mass of samples obtained by using the two sampling protocols detailed in material and methods. ⁽²⁾ Indicates data obtained by comparing two masses of sieved samples with the two protocols detailed in material and methods. Note: the Petit Buech is the main tributary of the Buech catchment.

2.4.2. LOCAL STOCKS

2.4.2.1. Stock per facies

Considering average surface and subsurface stocks, several observations can be made. The local stocks were highly variables in a given catchment and between catchments (Figure 2.8, Table 2.3). For instance, the Arvan catchment had much higher local stocks (MC and B) than the other catchments. Also, these stocks covered at least two orders of magnitude considering the four facies and all catchments (Figure 2.8, Table 2.4). Despite this large variability, the four facies (main channel, bars, dry braided channel and vegetated bars) first identified by Navratil *et al.* (2010) exhibited well defined ranges of storage considering measurements in a given catchment or all measurements together (Figure 2.8, Figure 2.9, Table 2.4). It indicates that the storage processes were different in these four zones. The main channel was the facies storing the less fine particles (median stock considering all river of $2 \text{ kg m}^{-2} \text{ dm}^{-1}$) probably because shear stresses were always too high so that large deposition could occur. The naked bars exhibited a bit higher median storage ($2.8 \text{ kg m}^{-2} \text{ dm}^{-1}$) but it was not statistically significant (Mann-Whitney tests positive one-side test gives $p_{\text{value}} > 0.05$). The storage was much important in dry braided channels and in vegetated channels (respectively 5.4 and $20 \text{ kg m}^{-2} \text{ dm}^{-1}$) as confirmed by Mann-Whitney tests ($p_{\text{values}} < 0.001$). Vegetated bars stored significantly more than dry braided channels ($p_{\text{values}} < 0.001$). These storage differences could be due to differences in hydrodynamics and to the frequencies of submersion as discussed in the following sections.

Rivers	MC [kg/m ² /dm]			B [kg/m ² /dm]			DBC [kg/m ² /dm]			VB [kg/m ² /dm]		
	Av.	Surf.	Sub.	Av.	Surf.	Sub.	Av.	Surf.	Sub.	Av.	Surf.	Sub.
Arc	3.6	6.8	10.4	8.6	11.7	9.3	10.5	-	-	-	-	-
Drac	6.0	4.4	6.6	5.5	13.2	21.5	17.4	24.5	82.4	53.4	-	-
Romanche	2.6	3.9	4.5	4.2	8.2	24.9	16.5	15.2	26.1	20.7	-	-
Asse	0.9	1.6	3.5	2.5	4.8	4.9	4.8	10.9	6.2	8.5	-	-
Büech	2.1	1.4	5.2	3.3	22.3	42.4	32.4	35.1	149.8	92.5	-	-
Arvan	7.5	10.8	20.7	15.7	-	-	-	-	-	-	-	-
Glandon	0.7	5.6	8.5	7.1	1.7	3.6	2.6	-	-	-	-	-

Table 2.3: Average stock per storage facies for the seven alpine rivers. “-“ indicates that no measurements were performed in this facies. “Surf.” Indicates surface stocks, “Sub.” Indicates subsurface stocks, “Av.” indicate average stocks between surface and subsurface. MC = main channel, B = bars, DBC = dry braided channel, VB = vegetated channel.

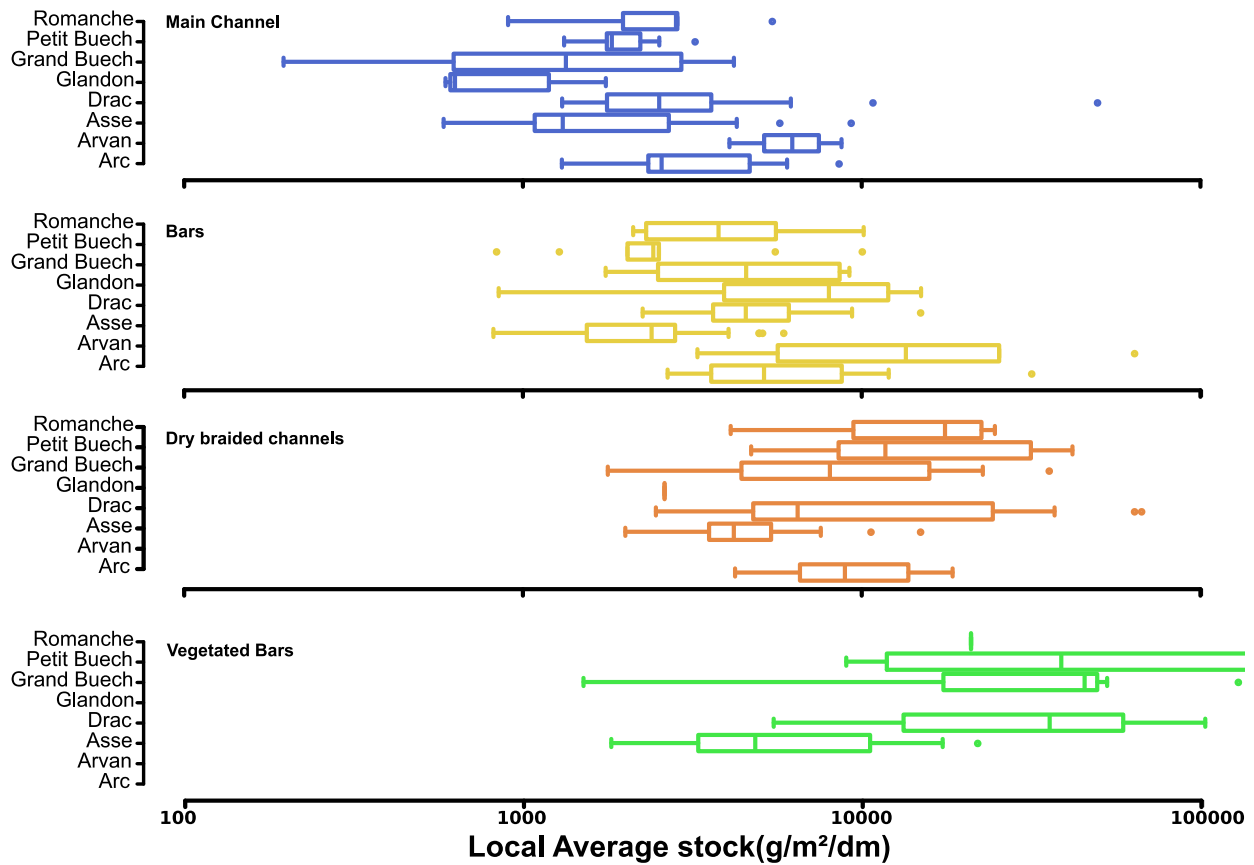


Figure 2.8: Boxplots of average surface and subsurface stock measurements for each river and for each facies storage.

	Average stock MC (kg/m ² /dm)	Average stock B (kg/m ² /dm)	Average stock DBC (kg/m ² /dm)	Average stock VB (kg/m ² /dm)
q5%	0.6	1.1	2.3	2.7
q50%	2.0	2.8	5.4	19.9
q95%	8.6	14.7	36.9	185.5

Table 2.4: Statistical quantiles (5%, 50% and 95%) of the stock measurements distributions depending on the storage facies. All rivers are considered together. MC=main channel, B = bar, DBC = dry braided channel, VB=vegetated bar.

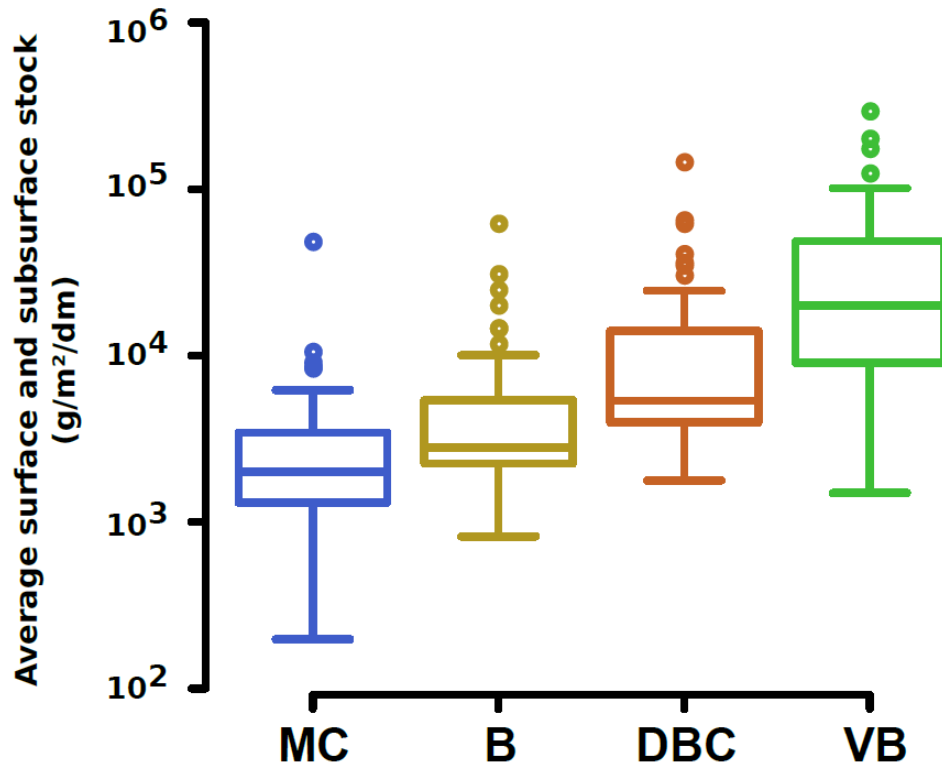


Figure 2.9: Average storage (surface and subsurface) considering all the rivers together as a function of the type of storage facies. MC=main channel, B = bar, DBC = dry braided channel, VB=vegetated bar.

2.4.2.2. Surface versus subsurface

The measurements conducted in dry facies (bars, dry braided channels and vegetated bars, Figure 2.4) allowed us to compare the stocks found in surface and subsurface (Figure 2.10). For the three facies, subsurface stocks were generally larger than surface stocks as confirmed by non-parametric Mann-Whitney tests (positive one-side test): the distribution of subsurface versus surface stocks ratios was statistically larger than 2.23 for bars ($p_{\text{value}} < 0.01$), larger than 1.32 for dry braided channels ($p_{\text{value}} < 0.01$) and larger than 1.35 for vegetated bars ($p_{\text{value}} < 0.01$). This shows that a significant part of the river bed stock is found under a poorly mobile armor layer. The subsurface stocks release might thus be controlled by the armor layer mobility, especially for gravel bars.

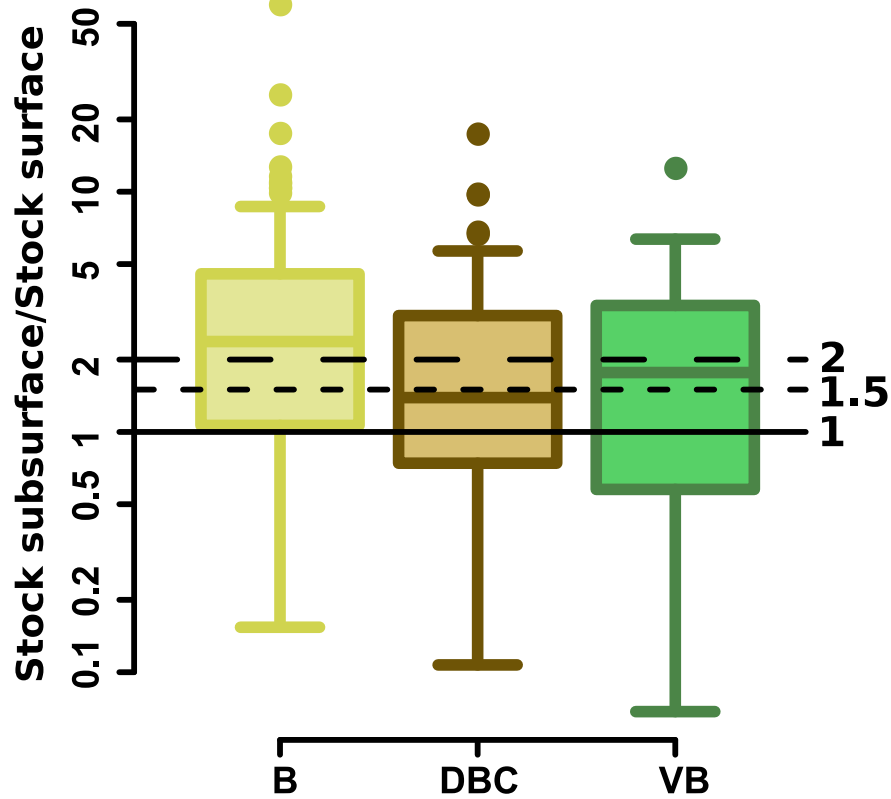


Figure 2.10: Boxplot of the ratios of subsurface stock and surface stocks considering the bar facies (B), the dry braided channel facies (DBC) and the vegetated bar facies (VB).

Considering the relation between surface and subsurface stocks without consideration of the storage facies in the seven alpine gravel bed rivers led to interesting observations (Figure 2.11). While really small surface stocks could be observed, a minimum value of subsurface stock approximately of $1 \text{ kg m}^{-2} \text{ dm}^{-1}$ was measured. Also, only 25% of measurements showed surface stocks higher than subsurface ones. Despite highly variable, the relation between surface and subsurface stocks can be fitted by a 2nd order polynomial relation, considering storage value in $\text{kg m}^{-2} \text{ dm}^{-1}$ (Eq.2.15, $R^2=0.76$):

$$st_{subsurface} = 7.10^{-5}(st_{surface})^2 - 0.023(st_{surface}) + 3000 \quad (2.15)$$

This best fit shows that for surface stocks below 3 or 4 $\text{kg m}^{-2} \text{ dm}^{-1}$ the subsurface stocks were quite constant around $3 \text{ kg m}^{-2} \text{ dm}^{-1}$. Beyond this threshold, subsurface stocks increased when increasing the surface storage. This suggests that below a value of 3 to 4 $\text{kg m}^{-2} \text{ dm}^{-1}$ in the surface, surface and subsurface storage are not dependent while above this threshold, surface and subsurface stock co-evolved.

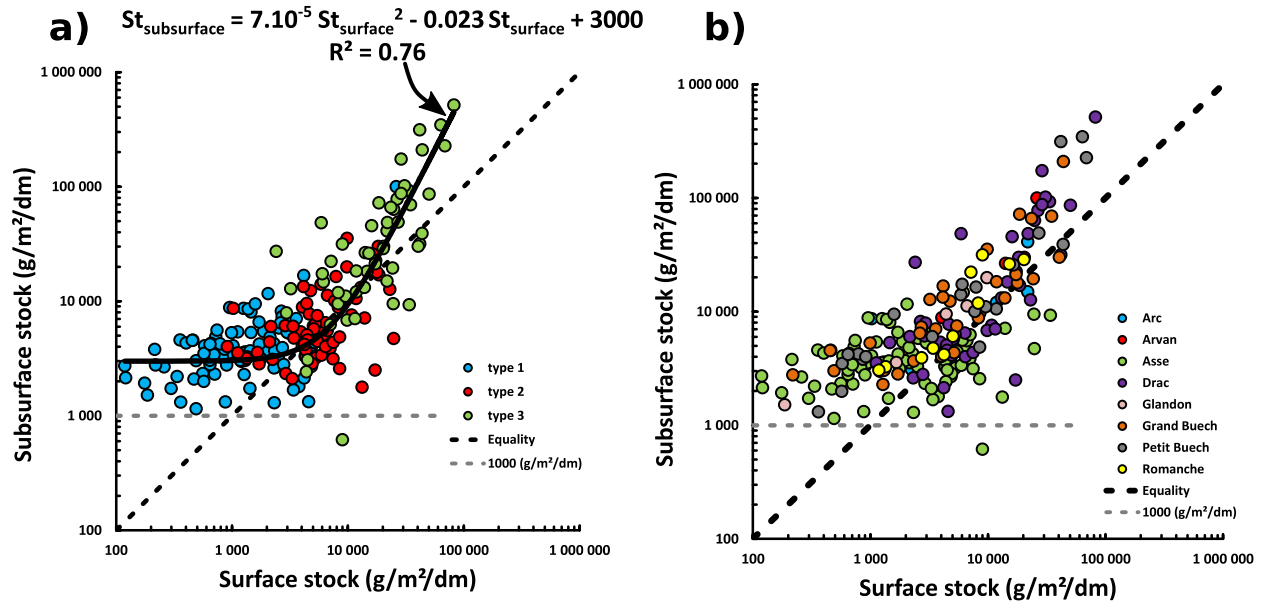


Figure 2.11: Relation between subsurface and surface stocks considering measurements made in the seven rivers (b) or as a function of a visual classification base on the quantity of fine particle found at the bed surface (a). Type 1 corresponds to maximum 25% of fines at the bed surface, type 3 a minimum of 75% and type 2 is for intermediate situations. The horizontal dashed grey line represents a subsurface stock of 1kg/m²/dm. the dashed black line represent equality between surface and subsurface stocks.

2.4.3. AERIAL PHOTO ANALYSIS

The facies area obtained after the supervised classification analysis and active width digitalization revealed large differences in the total river bed area of the seven basins (Figure 2.12, Figure 2.13). The Glandon, Arvan and Romanche which exhibited mainly step pool and plane bed morphologies have relatively small river bed area (respectively $2.0 \cdot 10^5$, $4.4 \cdot 10^5$ and $5.4 \cdot 10^5$ m²). The active width digitalization (Figure 2.13) shows that the morphologies of the Arvan and Glandon rivers were narrow (median active width of respectively 13.7 and 8.4 m) which limited the possibility to perform an automatic classification process. On the opposite, the Drac and Buech exhibited large river bed area related to their braided morphologies (respectively $2.9 \cdot 10^6$ and $4.2 \cdot 10^6$ m²). The Asse and Arc catchments had intermediate area ($1.6 \cdot 10^6$ m² for both). For most rivers that were classified into facies (except for the Romance river), the bars (including DBC) represented the major fraction, especially for the braided morphologies (respectively 59% and 52% for the Drac and Buech). Vegetated bars often represented the smallest fraction.

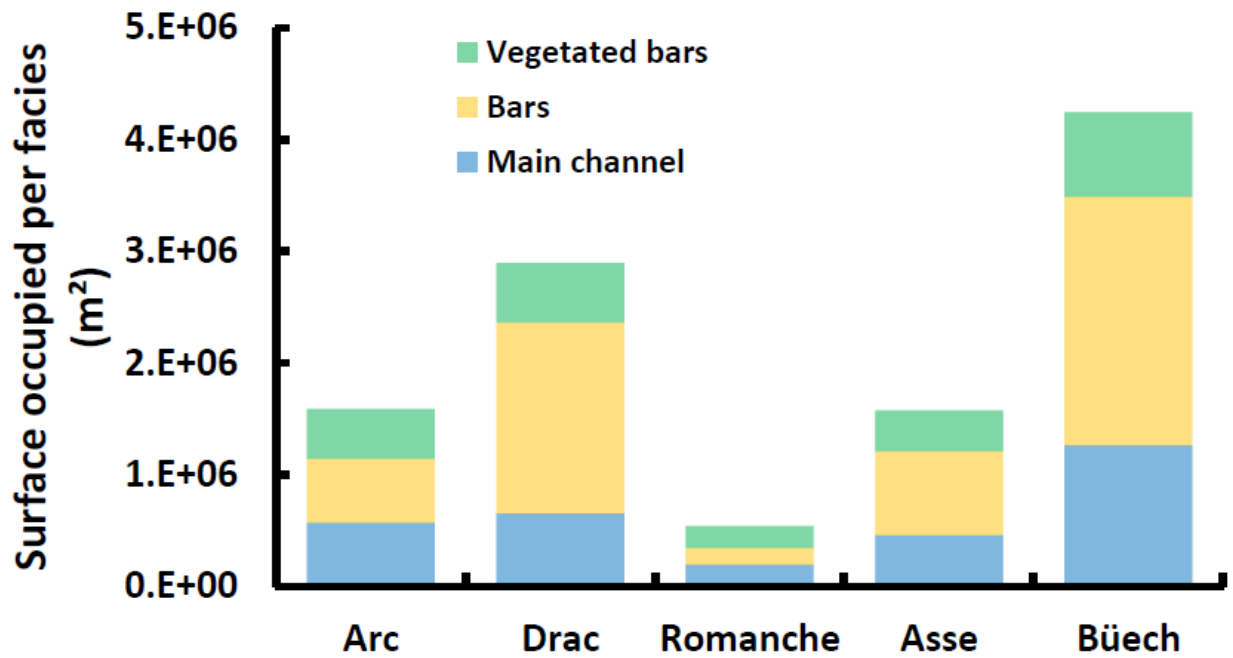


Figure 2.12: Area of the three facies (main channel, bars and vegetated bars) obtained from a supervised classification of orthorectified photographs for the Arc, Drac, Romanche, Asse and Büech catchments.

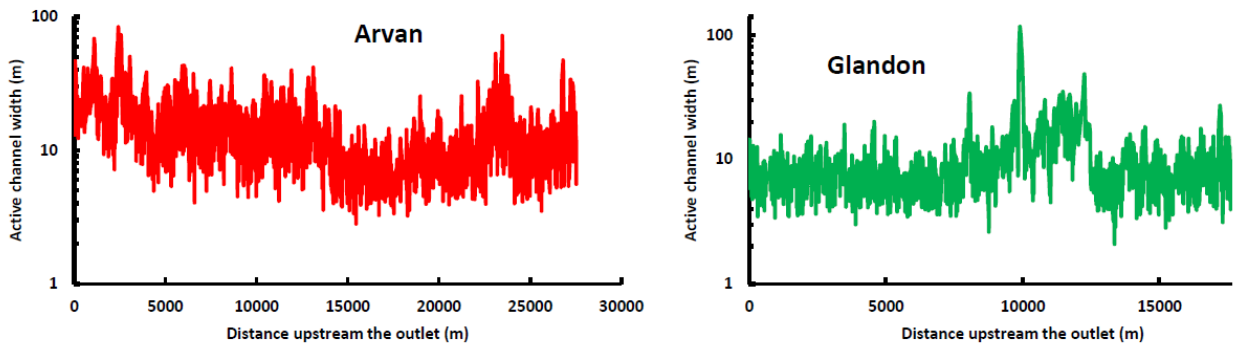


Figure 2.13: Active width of the Glandon and Arvan catchments used for the stock integration.

2.4.4. TOTAL STOCKS AND COMPARISON WITH ANNUAL FLUXES

By considering a depth of 1 dm as often done in similar studies [Collins and Walling, 2007a; Lambert and Walling, 1988; Navratil et al., 2010; Piqué et al., 2014] and combining the mean stocks obtained for each storage facies (Table 2.3) with the area of each facies (Figure 2.12 and Figure 2.13) we estimated the total river bed stocks of fine particles using Eq.2.4 and Eq.2.5 (Figure 2.14-a). While braided rivers have relatively low local stocks compare to others, their large river bed area can store a large amount of fine particles (respectively 50 000 and 100 000 tons for the Drac and Buech). Also, while significant differences in river bed area were observed for the other catchments, quite similar total stocks values were obtained (range 5600 – 8200 tons) except for the Glandon which has much lower total stocks (1200 tons). Using the suspended load time series we could estimate the mean specific sediment yield of the seven catchments (Figure 2.14-b) and compare it with the river bed stocks (Figure 2.14-c). The specific sediment yield was highly variable in a given catchment. Also the seven basins covered a large range between 130 and 2800 t km⁻² year⁻¹. The Arvan exhibited the highest fine sediments production (2800 t km⁻² year⁻¹) and the Asse the second (650 t km⁻² year⁻¹). Other basins had specific sediment yield of nearly 200 t km⁻² year⁻¹ or below. The total stock versus mean annual suspended sediment yield ratios ranged between 1% and 64%. Despite the uncertainties associated to these values, the following observations can be made.

Large braided rivers (Buech and Drac) had significant stocks compared to the mean annual suspended sediment loads suggesting that the river bed could be a significant sediment source with a significant buffering capacity. Other rivers with narrower morphologies and a medium specific sediment yield (Arc, Romanche and Glandon) had ratios around 10%. This suggest that these river beds had a lower buffering capacity than large braided rivers but that they can still be considered as a significant sediment source at shorter time scale. Finally, catchments with a high production of fine sediments (Arvan and Asse) exhibited limited river bed stocks compared to annual suspended sediment loads (1 to 2%). This suggests an efficient transfer of the fine particles produced on hillslopes.

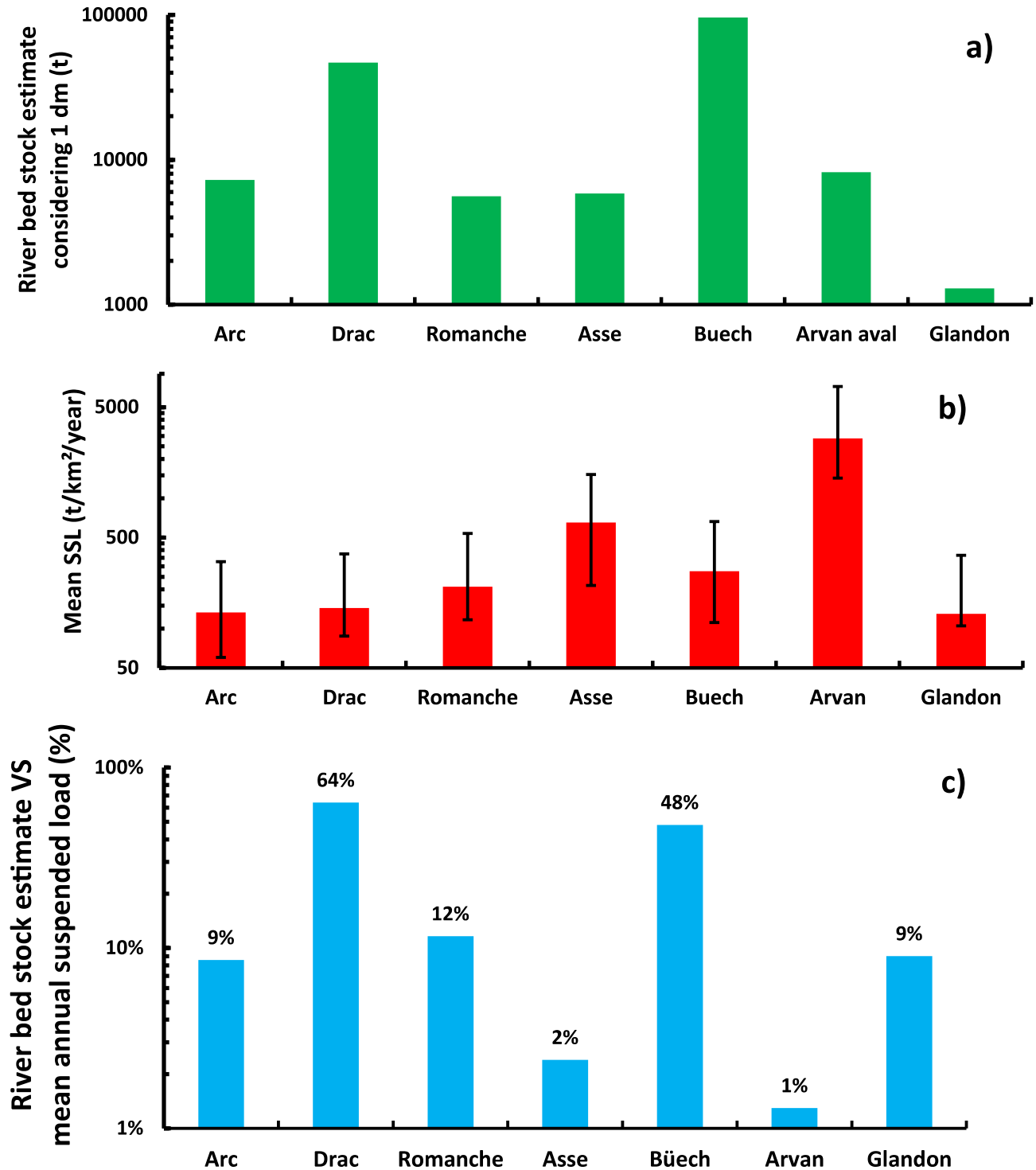


Figure 2.14: a) River bed stocks estimated considering a depth of 1 dm in the seven alpine catchments. b) Mean specific suspended sediment load (SSL) for the seven studied catchments. Error bars indicate the standard deviation. c) Ratio of stock estimate in the river bed (depth of 1dm) versus mean annual suspended sediment load for the seven studied catchments.

2.4.5. ASSESSMENT OF AVAILABLE STOCKS

The previous comparison of river bed stocks and annual suspended sediment loads in the seven catchments allowed to obtain a first estimate of the river bed contribution in the total flux of sediment exported from the catchments. However, the river bed contribution depends on the hydraulic conditions for which these stocks could be released in the flow. The simplified model based on a release of local river bed stocks due to vertical scouring (Figure 2.7) was applied on four of the rivers (Figure 2.15).

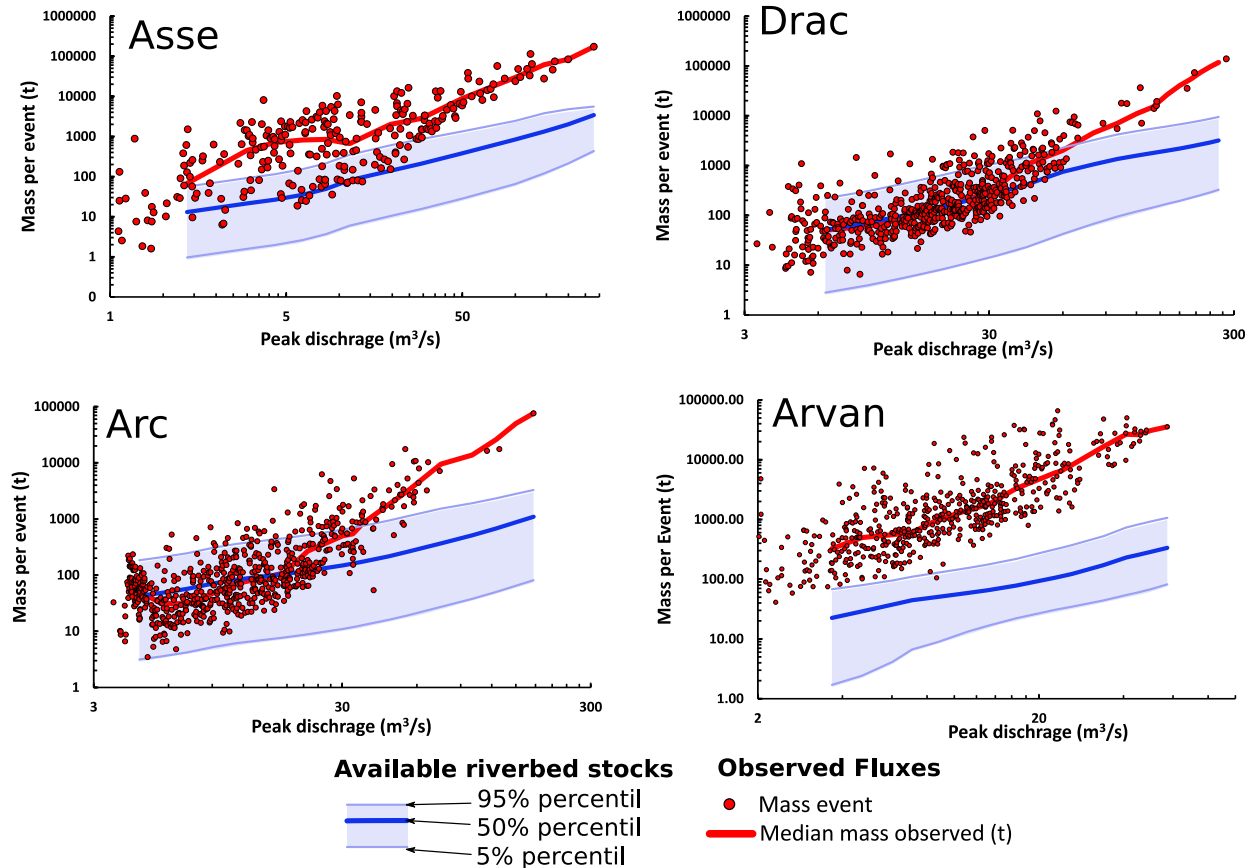


Figure 2.15: Mass per event as a function of the peak discharge considering the measured data and the estimated available river bed stocks.

The range of mass estimated to be available in the river bed as a function of the event peak discharge (blue line and polygon in Figure 2.15) was much lower than the measurements (red points and red line) for the Arvan catchment. Considering the measured median mass per event (red line) and the median available riverbed stock (dark blue line), a maximum ratio between both quantities of 7% was obtained for this catchment. Similar observations were made for the Asse basin while the available stocks represented a larger fraction of suspended fluxes (maximum 19% considering

median values). On the contrary, the Arc and Drac catchments exhibited available stocks similar to measured fluxes for small to moderate events (maximum stock versus flux ratio of around 100%). These results were consistent with the previous ones showing that the Arvan and Drac basins had respectively limited and high river bed stocks relative to fluxes. However, the use of the simplified model that takes into account hydraulics and variable scouring led to different observations than the analysis based on annual fluxes and constant depth for the Asse and particularly for the Arc catchments. Measured fluxes were systematically increasing much steeper than estimated available riverbed stocks for larger peak discharges. This could be due to the use of a simplified riverbed scouring modeling which might not include all riverbed mobilization process as discussed later.

2.5. DISCUSSION

2.5.1. SPATIAL VARIABILITY OF THE RIVER BED STOCKS

The previous results showed the strong storage variability and the importance of subsurface stocks which were in most cases larger than surface ones (true for all facies). This suggests that a significant part of the river bed stocks release is controlled by the mobility of the poorly mobile armor layer. This is particularly true for the bar facies. While no relation was observed between surface and subsurface stocks for low surface storage (lower than $4 \text{ kg m}^{-2} \text{ dm}^{-1}$) both quantities co-evolved for larger surface storage. This relation was interpreted by the presence of a “base level” of storage in the subsurface ($3 \text{ kg m}^{-2} \text{ dm}^{-1}$) and a vertical gradient of stocks resulting from an unimpeded static percolation of fines particles in the gravel matrix when the surface concentration increases [Gibson *et al.*, 2009]. This would be consistent with the strong interactions between fine particles transported as suspension and the gravel matrix reported in several flume and field studies [Frostick *et al.*, 1984; Hill *et al.*, 2017; Mooneyham and Strom, 2018; Park and Hunt, 2017].

The results from this study also confirmed the differences in storage processes that occur in the different zones (the four storage facies) of the river beds as previously observed by Navratil *et al.* (2010). Gravel bars and dry braided channels (DBC) may be submerged sufficiently often so that surface stocks are removed frequently and vegetation cannot develop. The differences between these two facies (DBC showed generally lower ratios between subsurface and surface stocks and larger overall stocks) could be attributed to the differences in hydrodynamics in these two zones. Bars were generally higher in altitude than dry braided channels where flows with low shear stresses and potentially high suspended sediment concentrations could be observed during local storm event (summer) or during the recession of the floods. This could lead to spatially concentrated deposition and partial clogging in these dry braided channels

(explaining the larger amount of fines and the larger surface stocks). For vegetated bars, located higher in altitude than bars, the submersion frequency is much lower. These zones are under water only for large events that generally submerge all the active channel width and are characterized by high suspended sediment concentration. For these conditions, shear stresses are generally low in VB as additional resistance is induced by the vegetation. This enable for massive depositions in these zones which exhibit the highest storage values. Depending on the time scale considered (few years), this facies can be considered as a sink as the fines particles stored here are much less frequently remobilized. Contrary to the other facies, one can expect that the remobilization of this facies might be mainly due to lateral channel migration as discussed in the next section.

Most previous studies that aimed at identifying the river bed stocks significance focused principally on fine sediments stored in the main channel facies [Buendia et al., 2016; Collins and Walling, 2007a; Duerdoth et al., 2015; Lambert and Walling, 1988; Marteau et al., 2018; H. Marttila and Kløve, 2014; Piqué et al., 2014]. Other dry facies were not considered except in Navratil et al. (2010). While estimating fine sediment stocks without considering the dry facies could be acceptable in lowland rivers that have a limited area occupied by bars, dry secondary channels of vegetated bars, our result show that such approach is more questionable in mountainous rivers. Considering only the main channel stocks would have led to much different conclusions in our studied catchments, where the main channel represented only a limited part of the sediment stocks (maximum 5% of the mean annual load, Figure 2.16). This suggests that future studies aiming at identifying the river bed contribution to the total suspended load in rivers exhibiting significant dry river bed areas should not only focus on underwater stocks.

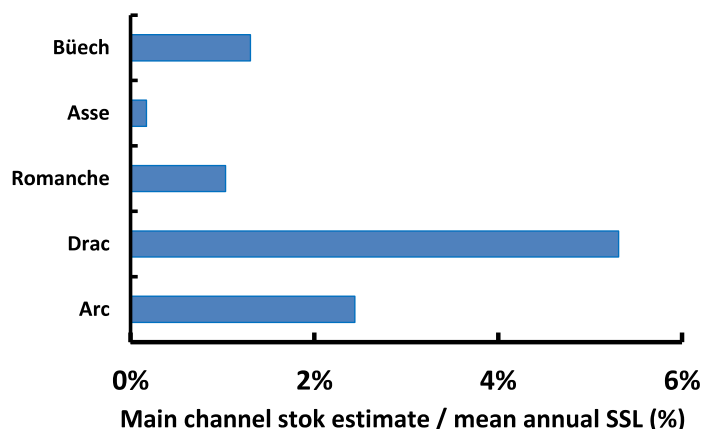


Figure 2.16: Ratio between main channel stock estimate and average annual suspended sediment load for the five catchments for which supervised classification was performed.

2.5.2. TEMPORAL VARIABILITY OF THE RIVER BED STOCKS

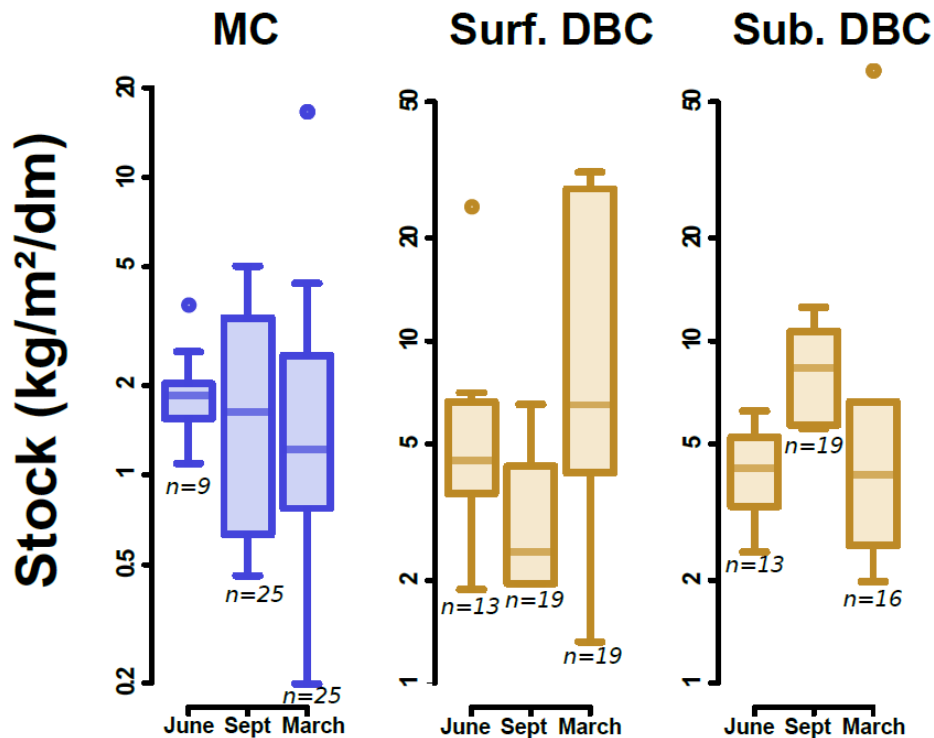


Figure 2.17: Seasonal variability of river bed stocks for the Asse River considering the main channel (MC) and the dry braided channels (DBC) facies. Measurements were conducted in June 2017, Sept 2017 and March 2018. “n” denotes the number of samples, “Sub.” corresponds to surface stocks while “Sub.” corresponds to subsurface stocks. Note, the y axis is in log scale. Measurements were roughly performed at the same locations.

Additional measurements conducted in the Asse river (September 2017 and March 2018) were performed to discuss the results in regards to the seasonal variability of the stocks analyzed previously (Figure 2.17). A decrease between June and September and an increase from September to March of the surface DBC facies were observed (significant differences with a Wilcoxon test with $p_{\text{values}} < 0.05$). On the opposite the subsurface DBC facies showed an increase between June and September and a decrease from September to March (Wilcoxon test with $p_{\text{values}} < 0.05$). No significant differences were observed for the main channel facies (Wilcoxon test with $p_{\text{values}} > 0.5$). These observations are consistent with previous studies showing temporal variations can occur depending on the hydrological and sedimentary conditions [Buendia et al., 2016; Marteau et al., 2018; Piqué et al., 2014]. These variations at the season scale also highlighted that even the dry facies can contribute to store and release fine particles at short time scales. Performing such seasonal analysis should be addressed in future

work, in various Alpine catchments to better understand periods and conditions for which the river bed stocks are flushed and then refilled. Also, this time variability associated to the suspended load variability at the annual and at the event scale (Figure 2.14-b and Figure 2.15) shows the difficulty to estimate the relative contribution of the river bed stocks to the total suspended fluxes as this contribution was probably changing through time (event, season and annual scale).

2.5.3. AVAILABLE RIVER BED STOCKS SIGNIFICANCE

The 339 stocks measurements conducted in seven Alpine gravel bed rivers showed that the subsurface often comprised a high quantity of fine particles stored under a poorly mobile armor layer. Even if the surface stocks were slightly smaller during our field campaigns, they might be more variable in time. The storage and remobilization of fine particles from the surface stock could be more frequent and mainly controlled by the submersion of the facies during runoff events, while the release of sediments from the subsurface would be more controlled by the mobilization of the gravel bed matrix, including lateral erosion of gravel bank matrix. This suggests that two distinct fine sediment release from the river bed should be considered. Also, this suggests that the release of fine particles from gravel bedded streams should not only be modeled by empirical laws such as the one proposed by Partheniades deduced from flume experiments on cohesive material transported above an impervious bed. Our measurements were in agreement with recent flume experiments on porous beds highlighting the large influence of a gravel matrix on the bed capture and release of fine particles [Mooneyham and Strom, 2018].

The previous analysis of bed stocks release using a simplified model at the catchment scale as a function of peak discharge raised several questions on this process. First the choice of the river bed longitudinal length to integrate the calculated bed release was uncertain and questions on the definition of the representative river bed area in a given catchment. Second, it showed that the mobilization depth was a key parameter which is difficult to estimate. Indeed, when analyzing in more details the simplified model results, we observe that the estimated bed production contribution to the total load always becomes negligible for high peak discharges (Figure 2.15). While the conceptual release of fine particles due to vertical scouring seems to be a relevant process for moderate to low floods, it is however not relevant for riverbed widening or lateral channel migration which are important bed reworking processes observed during large events [Bertoldi *et al.*, 2010]. However, the estimation of the magnitude of this lateral erosion remains difficult in practice. Thus, our capacity to estimate the potential release of river bed stocks is in fact highly linked to our knowledge about river bed mobility. As recently suggested by Peirce *et al.* (2018), a valuable way to estimate such morphological changes could be to use reach scale morphodynamics such as stream power or bedload rate.

2.6. CONCLUSION

Hundreds of measurements performed in seven alpine catchments revealed that significant quantities of fine particles could be stored in their river beds. These stocks were highly variable in space, depending on the type of facies (main channel, secondary channel, bars and vegetated bars) in which they were stored. This suggests that storing processes strongly depend on local hydraulics and bed configuration. The low quantity of fine particles found at the surface was interpreted in previous studies as the result of negligible interactions between this sediment fraction and the river bed. However, in the seven alpine studied catchments, large quantities of fine particles were observed in the subsurface (base level of 1-3 km m⁻² dm⁻¹) even if there were no significant stocks at the surface. A general trend was observed between both storage layers with generally higher amounts of fine particles in the subsurface which could result from a free percolation of fine particles in the gravel matrix. Thus a potential significant amount of fine particles could be released to the flow due to river bed mobility.

By integrating these stocks at the catchment scale, we estimated that they could exceed 50% of the mean annual suspended load for large braided rivers while they corresponded to 1% for highly eroded head water streams. While associated to uncertainties, these observations suggest that suspended load dynamic observed at a given point could be driven by the geomorphological configuration of the catchment as the river bed could act as a significant source. This catchment configuration could be conceptualized by the ratio between the capacity of hillslopes to produce suspended fluxes versus the capacity of the river bed to buffer these fluxes which raises question on the wash load concept in alpine rivers with large alluvial stocks. Finally, our analysis aiming at estimating the potential riverbed contribution to total load due to bed reworking shows that the mobilization depth was one of the most critical parameter. However, its estimation remains complex as lateral erosion and channel migration are difficult to model explicitly. A possibility to indirectly quantify the degree of bed reworking and the subsequent fine particle release would be to use reach-scale morphodynamics proxies integrating all riverbed mobilization processes.

2.7. NOTATIONS

The following symbols are used in this manuscript.

SSL	Suspended sediment load (g s^{-1})
SSC	Suspended sediment concentration (g l^{-1})
Q	Flow rate ($\text{m}^3 \text{s}^{-1}$)
S	River bed slope (-)
h_1	Surface layer depth (m)
h_2	Subsurface layer depth (m)
$V_{\text{container } 1}$	Volume of water in the container during the first sampling (l)
$V_{\text{container } 2}$	Volume of water in the container during the second sampling (l)
A	Sampling area (m^2)
$SSC_{\text{container } 1}$	Suspended sediment concentration in the container during the first sampling (g l^{-1})
$SSC_{\text{container } 2}$	Suspended sediment concentration in the container during the second sampling (g l^{-1})
st_{surface}	Local stock of fine particles for the surface layer ($\text{g m}^{-2} \text{dm}^{-1}$)
$st_{\text{subsurface}}$	Local stock of fine particles for the subsurface layer ($\text{g m}^{-2} \text{dm}^{-1}$)
SSC_{cylinder}	Suspended sediment concentration in the cylinder during underwater sampling (g l^{-1})
h_{water}	Water depth in the cylinder during under water sampling (m)
$h_{\text{bed disturbance}}$	River bed disturbance depth for under water sampling (m)
st_{water}	Local stock of fine particles for under water facies ($\text{g m}^{-2} \text{dm}^{-1}$)
\overline{st}_i	Average storage value for the facies i ($\text{g m}^{-2} \text{dm}^{-1}$)
A_i	Area of the facies i (m^2)
$St_{\text{catchment}}$	Integrated fine particles storage at the catchment scale (t dm^{-1})
D_{50}	Sediment diameter of the bed such that 50% of the mixture is finer (m)
D_{84}	Sediment diameter of the bed such that 84% of the mixture is finer (m)
D	Sediment diameter (m)
τ^*	Shields number: dimensionless shear stress (-)
τ_{84}^*	Shields number for D_{84} (-)

Q	Water discharge (m^3/s)
U	Mean water velocity over the section (m/s)
u^*	Friction velocity (m/s)
W	Channel bed width (m)
S	Channel bed slope (m/m)
A	Catchment area (km^2)
ρ	Water density (kg/m^3)
ρ_s	Sediment density (kg/m^3)
s	Relative density of sediment (-)
g	Gravitational acceleration (m/s^2)
d	Mean water depth (m)
R_h	Hydraulic radius (m)
δ	Scouring depth (dm)
$P(\delta)$	Non-exceedance probability to observe δ scouring depth (-)
θ	Scouring exponential distribution parameter (cm^{-1})
$m_{section}$	Mass of fine particles released per unit length for a given cross section ($m_{section}, t m^{-1}$)
$\overline{st_{local i}}$	Cross section averaged local stock for the facies i ($g m^{-2} dm^{-1}$)
$\overline{m_{section}(Q_{peak})}$	Average mass of fine particle released per unit length for all the cross section considered and for a given scouring probability ($t m^{-1}$)
$L_{storage system}$	Length of the active river bed representative of the storage system (m)
$M_{catchment}(Q_{peak})$	Mass of fine particles released at the catchment scale as a function of peak discharge and scouring probability (t)

2.8. APPENDIX

2.8.1. PARAMETERS USED FOR RIVER BED STOCK ESTIMATE

	Facies		
	Main channel (10 ⁵ m ²)	Bars (10 ⁵ m ²)	Vegetated bars (10 ⁵ m ²)
Arc	5.72	5.72	4.42
Drac	6.52	17.1	5.35
Romanche	1.95	1.49	1.95
Asse	4.57	7.55	3.62
Büech	12.6	22.2	7.56

Table 2.5: Facies surface estimate using aerial photographs classification.

	S1	S2	S3	S4
Slope (%)	1.18	0.67	1.07	1.12
D ₈₄ (mm)	153	89.52	109	106.3
Ratio of catchment area	0.31	0.47	0.50	0.63
<i>L_{storage system}</i> (m) = 7000 m (active width larger than 150 m)				

Table 2.6: Characteristics used to estimate the fine particle released from the river bed for the Drac catchment.

	S1	S2	S3
Slope (%)	1.05	1.74	2.06
D ₈₄ (mm)	98	391	378
Ratio of catchment area	0.38	1	1
<i>L_{storage system}</i> (m) = 8600 m (active width larger than 50 m)			

Table 2.7: Characteristics used to estimate the fine particle released from the river bed for the Arc catchment.

	S1	S2	S3
Slope (%)	2.27	3.07	3.32
D ₈₄ (mm)	79	181	337
Ratio of catchment area	0.3	0.5	1
<i>L_{storage system}</i> (m) = 2200 m (active width larger than 30 m)			

Table 2.8: Characteristics used to estimate the fine particle released from the river bed for the Arvan catchment.

	S1	S2
Slope (%)	0.9	1.02
D ₈₄ (mm)	79	66.5
Ratio of catchment area	1	0.25
<i>L_{storage system}</i> (m) = 12000 m (active width larger than 50 m)		

Table 2.9: Characteristics used to estimate the fine particle released from the river bed for the Asse catchment. Note five topographic cross sections and local stocks are used for the calculation.

2.8.2. SETTLING VELOCITY AND FLOCCULATION PROPERTIES OF RIVERBED STOCKS

We report here settling measurements performed on fine particle deposited in river beds using the System Characterizing Aggregates and Flocs (SCAF). A brief description is proposed in the following section and more details can be found in Wendling et al. (2015). The SCAF is a settling column (diameter 3.5 cm and 20 cm high) having 16 infrared emitters and 16 photosensors installed every centimeter along the vertical. The device measures light attenuation (absorbance) through time along the vertical to derive the settling velocity distribution of the mixture. It also enables to detect flocculation process for the finest particles by comparing the settling velocity distribution measured at the top of the settling column and the one at bottom (e.g. bottom settling velocities are higher than surface ones when flocculation occurs). It is thus possible to define a flocculation index as follows:

$$floculation\ index = \frac{W_{s,bottom} - W_{s,surface}}{W_{s,surface}} \quad (2.16)$$

in which $W_{s,bottom}$ is the settling velocity (m/s) at the bottom of the column and $W_{s,surface}$ at the surface (m/s). Non-cohesive material have flocculation index close to one while large positive values indicate cohesive properties [Wendling et al., 2015].

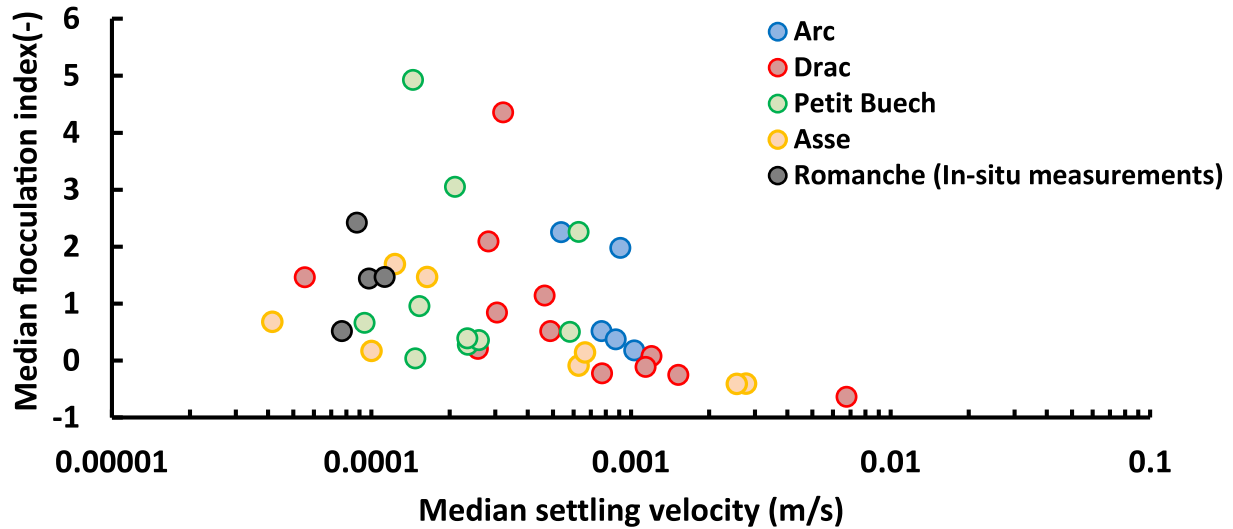


Figure 2.18: Flocculation index as a function of the settling velocity obtained on surface deposits using the SCAF instrument on five of the seven rivers studied. Note: Romanche measurements were performed in-situ on resuspended sediments during the stock measurement protocol.

Most of measurements show settling velocities ranging between 10^{-3} and 10^{-4} m s $^{-1}$ and flocculation index increasing when settling velocity (particle size) decreases.

	w_s mean (m/s)	d_{eq} [μ m]
Arc (n=7)	8.3×10^{-4}	30
Drac (n=12)	1.1×10^{-3}	35
Romanche (n=4, in-situ)	9.4×10^{-5}	10
Asse (n=7)	8.8×10^{-4}	31
Petit buech (n=10)	2.7×10^{-4}	17

Table 2.5: Average median settling velocity obtained on surface deposit using the Scaf instrument. d_{eq} denotes the diameters corresponding to the measured settling velocities using the Stokes law.

Chapter 3

Quantifying bed-related suspended load in gravel bed rivers through an analysis of the bedload-suspended load relationship

Estimating suspended load and its fraction coming from the river bed is often challenging in mountainous gravel bed rivers. It is however often a prerequisite for river management studies. In that third chapter, we investigated the signal of river bed mobility on suspension to detect the river bed related fraction of suspended load. This work is published in Earth Surface Processes and Landforms, by Misset C., Recking A., Legout C., Poirel A., Cazihlac M., Briguet V. and Esteves M. (doi:10.1002/esp.4606).

Estimer les flux en suspension et leur fraction provenant du lit est souvent difficile pour des rivières à graviers de montagne. Pourtant, cette estimation est souvent un prérequis à toute étude relative à la gestion de ces rivières. Dans ce troisième chapitre, nous avons analysé la signature de la mobilité du lit sur les flux en suspension pour détecter quelle fraction de ces flux provenait du lit. Ce travail est publié dans Earth Surface Processes and Landforms, par Misset C., Recking A., Legout C., Poirel A., Cazihlac M., Briguet V. and Esteves M. (doi:10.1002/esp.4606).

3.1. ABSTRACT

Suspended load transport can strongly impact ecosystems, dam filling and water resources. However, contrary to bedload, the use of physically based predicting equations is very challenging because of the complexity of interactions between suspended load and the river system. Through the analysis of extensive data sets, we investigated extent to which one or several river bed or flow parameters could be used as a proxy for quantifying suspended fluxes in gravel bed rivers. For this purpose, we gathered in the literature nearly 2400 instantaneous field measurements collected in 56 gravel bed rivers. Among all standard dimensionless parameters tested, the strongest correlation was observed between the suspended sediment concentration and the dimensionless bedload rate. An empirical relation between these two parameters was calibrated. Used with a reach average bedload transport formula, the approach allowed to successfully reproduce suspended fluxes measured during major flood events in seven gravel bed alpine rivers, morphodynamically active and distant from hillslope sources. These results are discussed in light of the complexity of the processes potentially influencing suspended load in a mountainous context. The approach proposed in this paper will never replace direct field measurements, which can be considered the only confident method to assess sediment fluxes in alpine streams; however, it can increment existing panel tools that help river managers to estimate even rough but not unrealistic suspended fluxes when measurements are totally absent.

3.2. INTRODUCTION

Suspended load is the fraction of the total solid load transported by flow turbulence over long distances. It differs from bedload, which is the fraction transported over short distances close to the bed by rolling and sliding. Suspended sediment transport is associated with important socioeconomic stakes, such as nutrient and pollutant transport included in fine aggregated particles, alteration of spawning habitat by riverbed clogging, main-channel obstruction by vegetation growth in calibrated rivers and reservoir siltation [Kondolf *et al.*, 2014; Owens *et al.*, 2005; Vercauteren *et al.*, 2017; Walling *et al.*, 2003]. Fine sediment transport from river to ocean is also essential in natural geochemical cycles and for coastal or estuarine ecosystems [Le Pape *et al.*, 2013; Ludwig and Probst, 1998]. Therefore, its measurement and prediction has become crucial for water resource management and it would be useful to have tools available to compute even rough but reliable estimates of suspended load using section-averaged parameters, as is often done for bedload transport.

It is often considered that suspended load is an inextricable question because of the diversity of sources of fine sediments, often treated as external inputs not necessarily related to the bed's morphodynamics (washload). Yet, interactions with the bed exist and are far from negligible even for the finest fractions. Collins and Walling (2007)

reported values of in-channel fine sediment stocks ranging from 11% to 39% and from 29% to 97% of the mean annual suspended loads in two catchments in the United Kingdom. In Finland, Marttila and Kløve (2014) found stocks ranging from 13% to 116% of the mean annual suspended load in a 400-km² catchment. On a 300-km² catchment located in Mallorca, Estrany *et al.* (2011) measured storage in the main channel system equivalent to 87% of the sediment input and concluded that fine particles accumulate over several hydrological years until a large enough event remobilizes these stocks. Similar observations were made at the reach scale in the Isabena catchment where changes in fine sediment stocks were correlated with the maximum flood discharge [Buendía *et al.*, 2016]. Most of these field studies were conducted in lowland rivers or considered only fine sediments stored in the wetted channel. Navratil *et al.* (2010) estimated these stocks in a typical mountainous braided river by considering stocks in dried braided channels, bars and vegetated bars in addition to sediments stored in the wetted channel. They found that the stocks at the catchment scale were equivalent to approximately 80% of the mean annual fluxes and that the sediments stored in the 3.5-km reach studied were equivalent to suspended yield for common floods. It is important to note that, even though it is often considered that only coarser materials interact with the bed, all of these field measurements used the Lambert and Walling or the Navratil technique and thus mainly concern the finest fraction (<63 μm) of fine sediments [Lambert and Walling, 1988; Navratil *et al.*, 2010]. The strong interactions observed in these field studies between suspended load and the river bed were also demonstrated in several flume experiments [Glasbergen, 2014; Hamm *et al.*, 2009; Krishnappan and Engel, 2006; Mooneyham and Strom, 2018].

All of these observations demonstrate that the buffering effect of the bed is far from negligible (illustrated in Figure 3.1) and that in some cases the river bed could even act as the main source of fine sediments at the catchment scale. This has motivated several authors to seek a relation between suspended load and bed mobility. Meunier *et al.* (2006) reported a correlation between suspended load and bedload for instantaneous measurements taken in a braided reach of the “torrent de St Pierre”, a gravel bed river (GBR) in the French Alps. They suggested that this correlation was due to fine sediment release when the braided bed of the upstream reach was mobilized. A similar correlation was observed by Métivier *et al.* (2004) in a mountainous river in China. These observations led Turowski *et al.* (2010) to analyze the relation between the two modes of transport in a large data set of instantaneous field measurements (including approximately one-third of the literature data set used below) and to fit a two-trend power law to estimate bedload from suspended load measurements in a given cross-section. Following these field evidences, Park and Hunt (2017) proposed a conceptual model for GBRs by considering an accumulation of fine sediments within the riverbed when the armor layer was stable and a release of fine sediments when this protective layer was broken. Their conceptual model was based on a changing trend observed in

the suspended load versus discharge relationships for 30 California GBRs. The transition between these two phases was found to be correlated with the initiation of gravel mobilization at the reach scale. They concluded that suspended load might be linked with the mobility of the armored layer in GBRs. More recently, Cook *et al.* (2018) used seismometers to study the bedload dynamics during a glacial lake outburst flood in a Himalayan river. During this large event, they observed that the daily suspended sediment concentration was much better correlated with the bedload seismic signal than with flow rate or daily precipitations.



Figure 3.1: a) Picture of a typical gravel bar in a braided reach of the Aigues rivers. A coarse armor layer in surface and large stocks of fine sediments in the subsurface can clearly be distinguished. The picture location is indicated on the right panel by a black star. b) Locations of the alpine catchments used for this study. Note: The Bouinenc, Brusquet, Duyes, Galabre, laval and Moulin catchments are small tributaries of the Bléone rivers.

Following these studies, this paper aims to i) investigate if a macro-descriptor controlling the morphodynamics (such as flow, bedload rate and river bed parameters) could be used to describe suspended sediment concentration (SSC), ii) test such relations in Alpine rivers and iii) qualify situations for which this approach is relevant or not in the light of the complex processes of fine sediment sources activation.

3.3. MATERIAL AND METHODS

3.3.1. DATA SETS

3.3.1.1. Literature data set

A first data set contains data from the literature to investigate which macro descriptors could be used to describe the SSC (Table 3.1). Nearly 2400 instantaneous measurements of bedload, suspended load and related flow and bed parameters measured in 56 rivers were gathered. The main criteria to select rivers was the availability of the following variables: riverbed slope (S), channel width (W), water-discharge (Q), riverbed sediment diameters (D_{50} and D_{84}), instantaneous bedload (Q_b), suspended load (Q_s) and suspended sediment concentration (SSC) measurements. The grain size distribution of the suspended load was not available for most data, as is usually the case in practice. Only GBRs were analyzed in this paper and an arbitrary minimum value of 3 mm for the median sediment bed diameter was considered to exclude sand bed rivers.

Sources	Number of rivers	Number of measurements
Fowler and Wilson, 1995	1	11
King <i>et al.</i> , 2004	33	1793
Smalley <i>et al.</i> , 1994	1	25
Williams and Rosgen, 1989	21	568

Table 3.1: Sources of the literature data set

Part of this data set, mainly composed of measurements published by Williams and Rosgen (1989), was already used by Turowski *et al.* (2010). It was completed with data from Idaho presented by King *et al.* (2004) and from the literature (Table 3.1). Bedload was most often measured with a pressure difference sampler (Helley-Smith bedload sampler). Suspended load was measured using a common isokinetic depth-integrating discharge-weighted sampler at several verticals, from the water surface to within approximately 8 cm of the streambed. These measurements, considered as instantaneous, represent an average value of sediment transport over the time needed to undertake several verticals over the cross section. The data set is presented further on-line as supplementary material and is summarized in Table 3.2.

Variables	Min.	1 st Quartile	Median	Mean	3 rd Quartile	Max.
Q (m ³ s ⁻¹)	0.01	0.99	4.2	164	54	3.8×10 ³
U (m s ⁻¹)	0.13	0.58	0.88	1.04	1.36	3.78
d (m)	0.08	0.27	0.43	0.87	0.96	5.8
S (-)	0.0001	0.004	0.010	0.018	0.024	0.19
W (m)	0.71	6	11	39	41	772
SSC (mg l ⁻¹)	0.1	5	11	178	42	9.9×10 ³
Q _s (t d ⁻¹)	0	0.7	4	9.0×10 ³	118	8.7×10 ⁵
Q _b (t d ⁻¹)	0	0.20	1.3	317	21	2.1×10 ⁴
D ₅₀ (mm)	4.5	48	68	80	94	220
D ₈₄ (mm)	20	100	141	173	207	558
A (km ²)	1.29	46	129	752	386	1.6×10 ⁴
D _{50surf} / D _{50sub} ^(a)	2.5 ^(a)	2.9 ^(a)	4.9 ^(a)	4.8 ^(a)	6.0 ^(a)	7.9 ^(a)

Table 3.2: Main characteristics of the literature data set: discharge (Q), mean flow velocity (U), water depth (d), river bed slope (S), river width (W), suspended sediment concentration (SSC), suspended load (Q_s), bedload (Q_b), river bed sediment diameter corresponding to 50th and 84th percentiles (D_{50} and D_{84}), watershed area (A) and armor ratio (D_{50surf}/D_{50sub}).

^(a) The armor ratio statistics are indicative as these measurements are available for only ten rivers of the dataset [King *et al.*, 2004]. The grain size distributions measured using core samples are considered.

3.3.1.2. Alpine data set

A second data set comprising long-term measurements of suspended load in alpine GBRs was compared with the data from the literature. Seven long-term series of suspended sediment load measured in the French Alps by EDF (Electricity of France), IRSTEA (National Research Institute of Science and Technology for the Environment and Agriculture) and IGE (Institute for Geosciences and Environmental research) were used (Table 3.3). For each river, the following information was available: grain size distribution of the coarse sediments measured using the Wolman count technique, riverbed slope, base flow channel width, total active channel width, catchment size, instantaneous water discharge and suspended sediment concentration. The section and grain size parameters were measured in the nearest alluvial stream upstream from the station. For these alpine rivers, bedload transport was not available. All of these rivers have alluvial riverbeds that could be considered as a significant source of fine sediments.

River	D ₅₀ (mm)	D ₈₄ (mm)	River bed slope (%)	Base flow channel width (m)	Total active width (m)	Catchment area (km ²)	Period	Number of data (×10 ⁴)
Arc	55	377	2.06	18	74	635	2012–2016	3.6
Asse	53	113	1.02	20	100	375	2011–2016	4.0
Bès	26	62	1.4	13	54	165	2007–2009	3.3
Bléone	24	53	0.84	12	163	870	2007–2009	6.9
Buëch	75	213	1.1	21	55	723	2015–2016	1.8
Drac	50	89	0.67	24	150	510	2007–2016	7.7
Romanche	45	138	1.3	12	20	230	2007–2016	7.1

Table 3.3: Alpine data set composed of seven Alpine GBRs.

3.3.2. DATA ANALYSIS

A preliminary analysis of the published data set (Table 3.3) was performed to determine the best macro-descriptor of the SSC in alluvial GBRs. This was done by calculating the Pearson and Spearman rank correlation coefficient between the SSC and flow parameters (Q, q, U, d, P), bed parameters (S, W, D₅₀, D₈₄), catchment area (A) and bedload transport (Q_b). The Spearman rank correlation was used to capture nonlinear relations in addition to Pearson's correlation coefficients. Three dimensionless parameters were also used during this analysis: the Shields number calculated for the coarser sediments of the river bed (D₈₄), a dimensionless flow rate (q*) and a dimensionless bedload rate (q_b*) defined by the following equations:

$$q^* = \frac{q}{\sqrt{gSD_{84}^3}} \quad (3.1)$$

$$q_b^* = \frac{q_b}{\rho_s \sqrt{g(s-1)D_{84}^3}} \quad (3.2)$$

$$\tau_{84}^* = \frac{\rho g d S}{(\rho_s - \rho) g D_{84}} \quad (3.3)$$

In these equations, q is a unit flow rate (m² s⁻¹), g is the gravitational acceleration (m s⁻²), S is the riverbed slope (-), D₈₄ is the sediment diameter of the bed such that 84% of the mixture is finer (m), q_b is the unit bedload rate (kg s⁻¹ m⁻¹), ρ_s is the sediment density (kg m⁻³), ρ is the water density (kg m⁻³), s is the relative density of sediment and d the mean water depth (m).

A second step consisted in analyzing and calibrating a relation between the SSC and its best macro-descriptor for the published instantaneous measurements. A resampling technique was used to determine the uncertainty of the coefficients obtained during this fitting process. This relation was tested on the long-term series of the alpine data set (Table 3.3). The percentage of the ratio between computed and measured values that fell within a range [0.1-10] (E_{10}), [0.2-5] (E_5) and [0.5-2] (E_2) was considered to evaluate the strength of the relation. These indicators have usually been used to evaluate sediment transport formulas for two reasons: sediment transport processes are associated with substantial natural variability and *in situ* measurements are associated with substantial uncertainties [Recking, 2010; Van Rijn, 1984a]. E_{10} , E_5 and E_2 indicators were calculated for instantaneous values and for the suspended sediment yield (SSY) at the flood scale. The inter-annual error (IAE) corresponding to the mean of the relative error on the SSY calculated for each year (i) was also considered:

$$IAE = \frac{1}{n} \times \sum_{i=1}^n \left[\frac{|SSY_{predicted} - SSY_{measured}|}{SSY_{measured}} \right]_i \quad (3.4)$$

where n corresponds to the number of years with suspended load measurements.

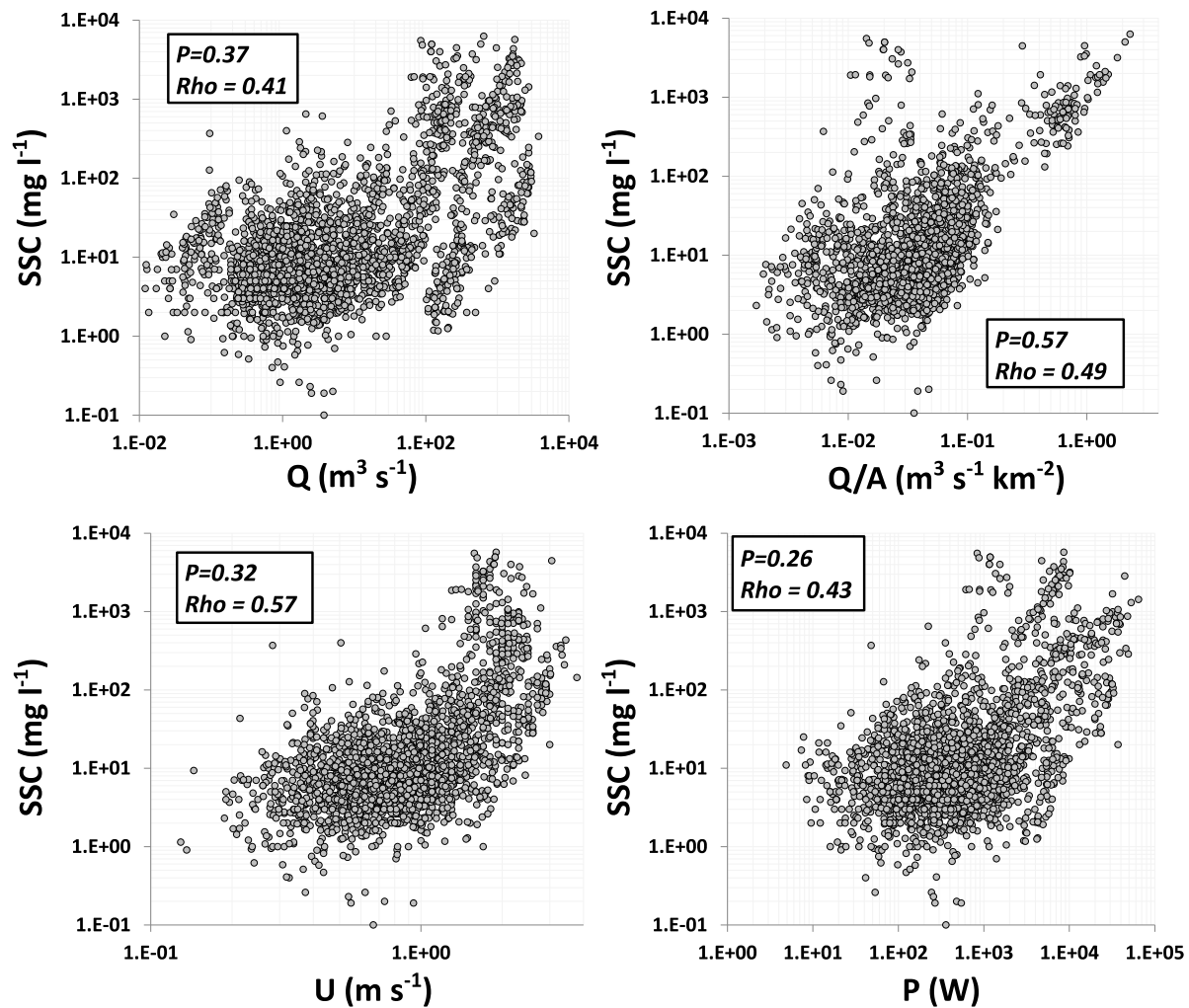
3.4. RESULTS

3.4.1. CORRELATION ANALYSIS

Analyzing the literature data set showed that some relations exist between the SSC and other macro-descriptors for GBRs (Figure 3.2) even though high scattering was observed. No spurious correlation exists between the SSC and the other individual parameters given that the SSC was obtained from independent measurements. Both correlation coefficients (Table 3.4) were low or nonsignificant considering the bed parameters (S , W , D_{50} and D_{84}). Similar results were obtained with hydraulic parameters (Q , q , d , P , τ_{84}^*) except with the mean flow velocity (U), dimensionless flow rate (q^*) and runoff estimate (Q/A), which have slightly higher correlation coefficients. A much better correlation was observed considering the dimensionless bedload transport q_b^* . It suggests that q_b^* includes additional information explaining the SSC better than the flow parameters alone. In addition, using this type of dimensionless parameter makes it possible to be less dependent on the scale of the river considered.

	Q	q	U	d	S	W	D₅₀	D₈₄	A	P	Q_b	q_b[*]	q[*]	τ₈₄[*]	Q/A
SSC (Spearman)	0.41	0.52	0.57	0.41	-0.31	0.26	-0.27	-0.25	0.19	0.43	0.62	0.69	0.50	0.43	0.49
SSC (Pearson)	0.37	0.26	0.32	0.28	-0.17	0.52	-0.20	-0.19	0.23	0.26	0.52	0.67	0.57	0.16	0.57

Table 3.4: Spearman and Pearson correlation coefficients between suspended sediment concentration (SSC) and other flow and bed parameters for the 56 gravel bed rivers of the literature data set: water discharge (Q), water discharge per unit width (q), mean flow velocity (U), mean water depth (d), riverbed slope (S), river width (W), river bed sediment diameter corresponding to 50th and 84th percentiles (D_{50} and D_{84}), catchment area (A), stream power (P), total bedload rate (Q_b), dimensionless bedload (q_b^*), dimensionless discharge (q^*), Shields number (τ_{84}^*) and runoff estimate (Q/A). Bold numbers correspond to significant correlations (p -values < 0.05).



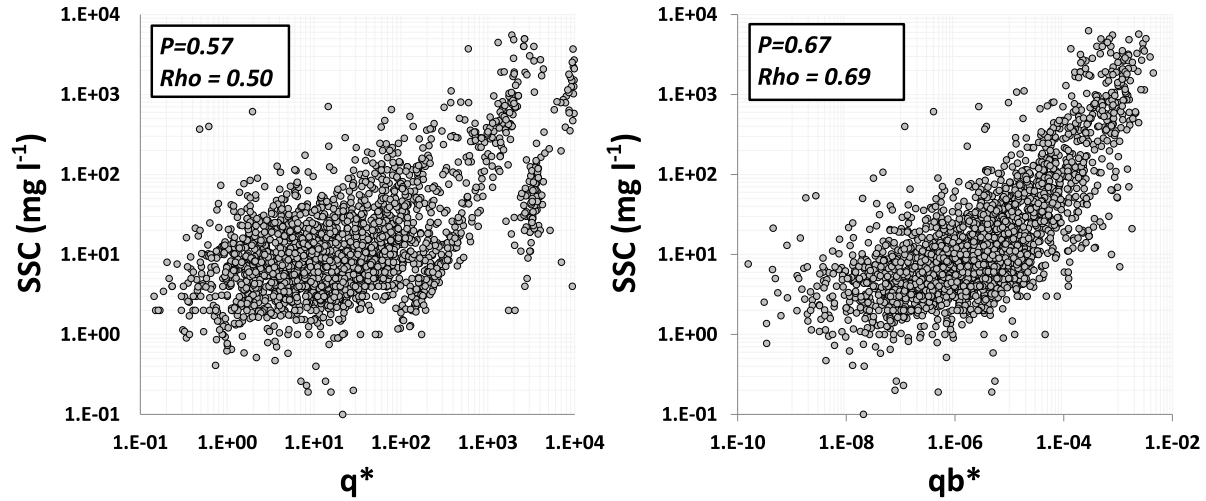


Figure 3.2: Suspended sediment concentration (SSC) as a function of discharge (Q), runoff estimate (Q/A), dimensionless discharge (q^*), Shields number considering the D_{84} (τ_{84}^*), mean flow velocity (U) and dimensionless bedload rate (q_b^*) for the literature data set. P corresponds to the Pearson correlation coefficient while Rho corresponds to the Spearman correlation coefficient. Note: data are plotted with log-log scales.

3.4.2. CALIBRATION OF A RELATION EXPLAINING THE SSC

As a clear changing trend, confirmed by a Davies test (p -value $< 2.2 \times 10^{-16}$) was observed, a piece-wise log-linear model was fitted on the dimensionless suspended sediment concentration ($SSC^* = SSC/\rho_s$) assuming a constant sediment density of 2650 kg.m^{-3} and the dimensionless bedload rate q_b^* (Eq.3.2) from the literature data set:

$$SSC^* = \begin{cases} a_1 \times q_b^{*b_1} & \text{if } q_b^* < b_p \\ a_2 \times q_b^{*b_2} & \text{otherwise} \end{cases} \quad (3.5)$$

One thousand random draws of 2000 values from the GBR data set were done and the 1000 automatic adjustments obtained were used to obtain the range of parameters used in Eq.3.5 (Table 3.5Table).

	$a_1 (\times 10^{-5})$	$a_2 (\times 10^{-2})$	$b_1 (\times 10^{-1})$	$b_2 (\times 10^{-1})$	$b_p (\times 10^{-6})$
2.5% percentile	3.32	7.00	1.75	8.21	7.26
50% percentile	4.04	9.12	1.87	8.49	8.49
97.5% percentile	4.92	11.73	2.01	8.76	10.02

Table 3.5: Fit values for Eq.3.5.

The breaking point (b_p) obtained ranged between 7.10^{-6} and 10^{-5} considering a 95% interval. A steeper increase of the SSC^* as a function of q_b^* was observed after the

breaking point with power law exponents changing from approximately 2 to 8. It was also observed that the correlation between these two variables was much higher for q_b^* values greater than b_p . Pearson and Spearman correlation coefficients were 0.13 and 0.41, respectively, for q_b^* lower than b_p and 0.59 and 0.7, respectively, for q_b^* larger than b_p (all significant with p -values < 0.05). This suggests that dimensionless bedload could be a better proxy for the SSC^* when q_b^* is larger than b_p . However, the dimensionless bedload rate was still the best correlated parameter when q_b^* was lower than b_p .

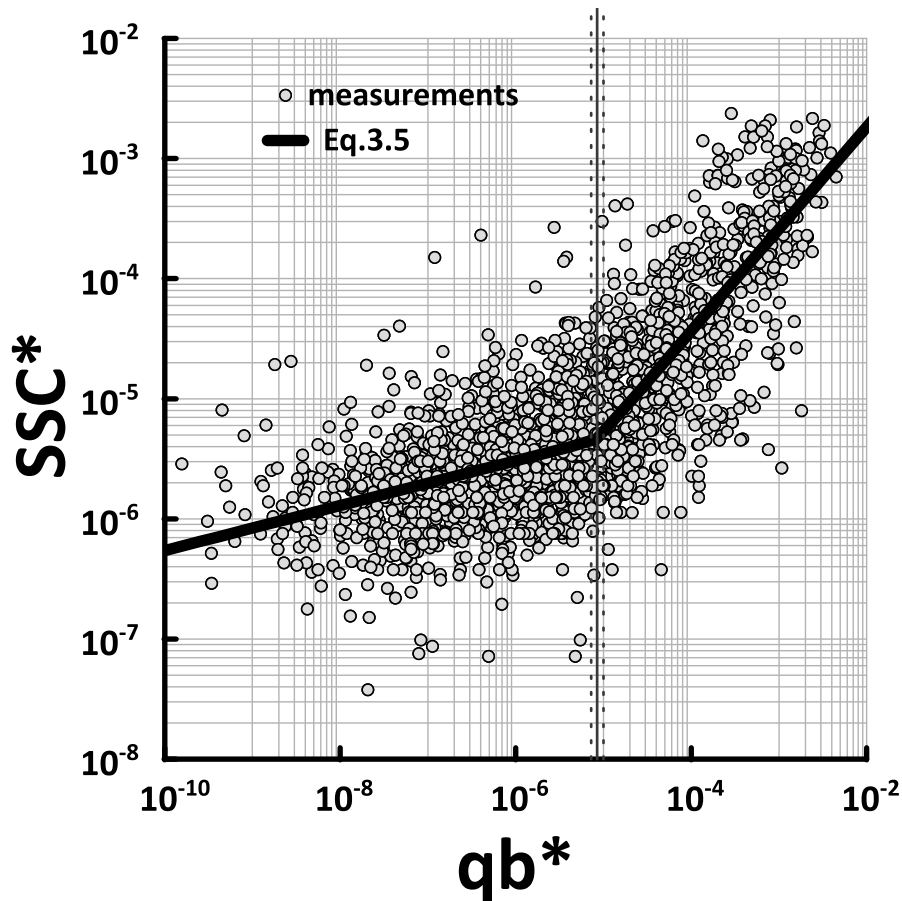


Figure 3.3: Dimensionless suspended sediment concentration SSC^* as a function of dimensionless bedload q_b^* . Eq.3.5 was plotted considering the median fit values obtained (black lines); vertical black line corresponds to the breaking point estimate (bp), vertical dashed grey lines correspond to its 95% confidence interval. Note: data are plotted with log-log scales.

Using a reach average bedload formula (see details later and in the appendix) we back-calculated the Shields number (for bed D_{50}) associated with the breaking point of Figure 3.3. The mean value obtained for the 56 GBRs was 0.046 (standard deviation, 0.04), which roughly corresponds to the threshold condition for mobility of coarse materials in GBRs [Meyer-Peter and Müller, 1948; Lamb et al., 2008; Recking, 2009]. This suggests

that the degree of release of fine sediments in GBRs may be closely related to bed mobility. The same conclusion was drawn by Park and Hunt (2017) from their study of 30 California GBRs.

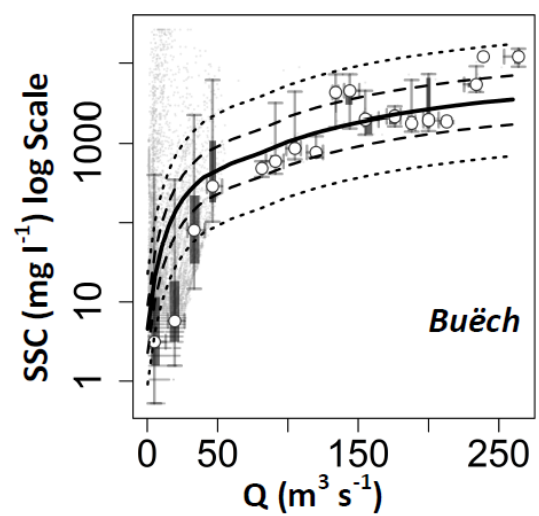
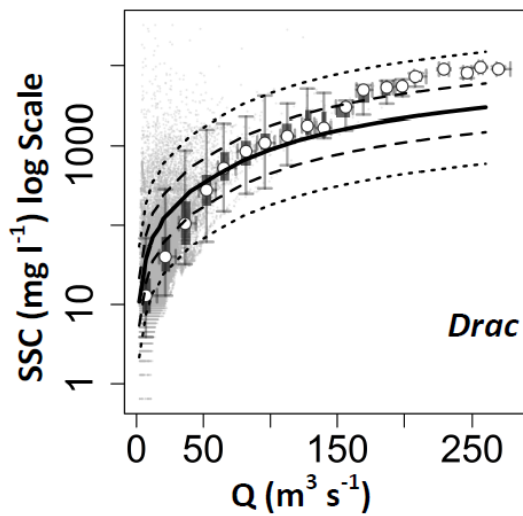
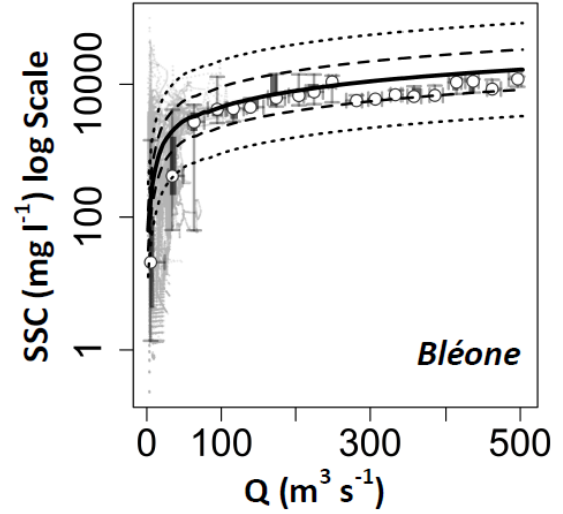
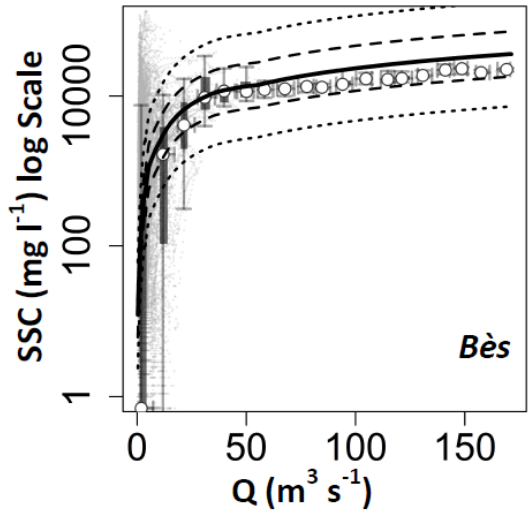
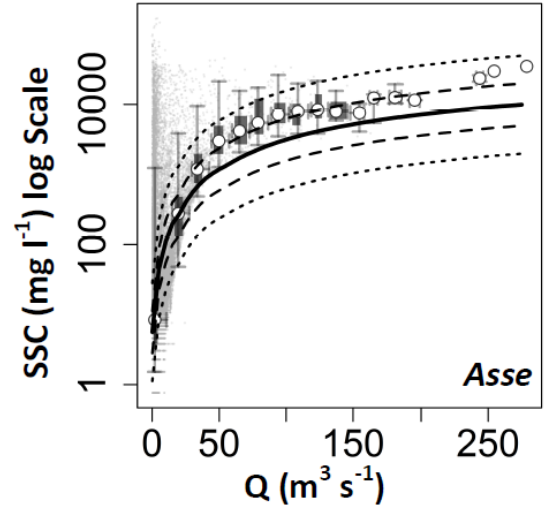
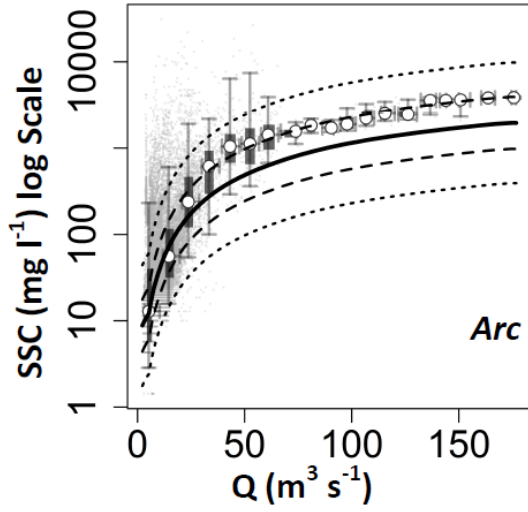
3.4.3. SSC PREDICTION FOR THE ALPINE DATA SET

Since bedload transport is most often not measured but computed, we tested the relevance of Eq.3.5 for long-term series of suspended load measured on seven alluvial alpine GBRs (Table 3.3), with bedload computed from the local bed information. Bedload was computed with a reach average bedload formula proposed by Recking (2013) and Recking *et al.* (2016) and validated on a large field data set (see <http://www.bedloadweb.com/> and details in the appendix). For each time step, the dimensionless bedload rate (q_b^*) was calculated using the reach average bedload formula. The suspended sediment concentration was then deduced with Eq.3.5.

River	Instantaneous			25% Larger flood events			Annual
	E_{10} (%)	E_5 (%)	E_2 (%)	E_{10} (%)	E_5 (%)	E_2 (%)	IAE (%)
Arc	89	85	47	94	85	52	68
Asse	81	62	27	78	65	32	74
Bès	29	24	13	75	59	42	43
Bléone	54	30	13	91	73	50	54
Buëch	48	36	16	90	80	30	53
Drac	95	78	37	98	89	44	37
Romanche	95	86	43	97	91	34	40

Table 3.6: Prediction indexes obtained for the seven alpine GBRs. E_{10} is the percentage of values predicted in the range [0.1–10], E_5 is the percentage of values predicted in the range [0.2–5] and E_2 is the percentage of values predicted in the range [0.5–2]; 25% larger flood events were defined considering the peak discharge. IAE denotes interannual error on suspended fluxes.

Figure 3.4 shows the comparison of the SSCs computed and measured values according to the flow rate Q . Using q_b^* as a proxy for the SSC made it possible to reconstruct the main trends of the suspended load fluxes of these alpine GBRs. Most of the binned data are within or not far from the E_2 range, which can be considered very good considering the large uncertainties related to the hydrology, bedload computation (whose results depends not only on the equation itself, but also on the variability of the input data) and the availability of fine particles for transport. It is worth noting that no spurious correlation was possible here between the SSCs, obtained from independent measurements, and the bedload computation.



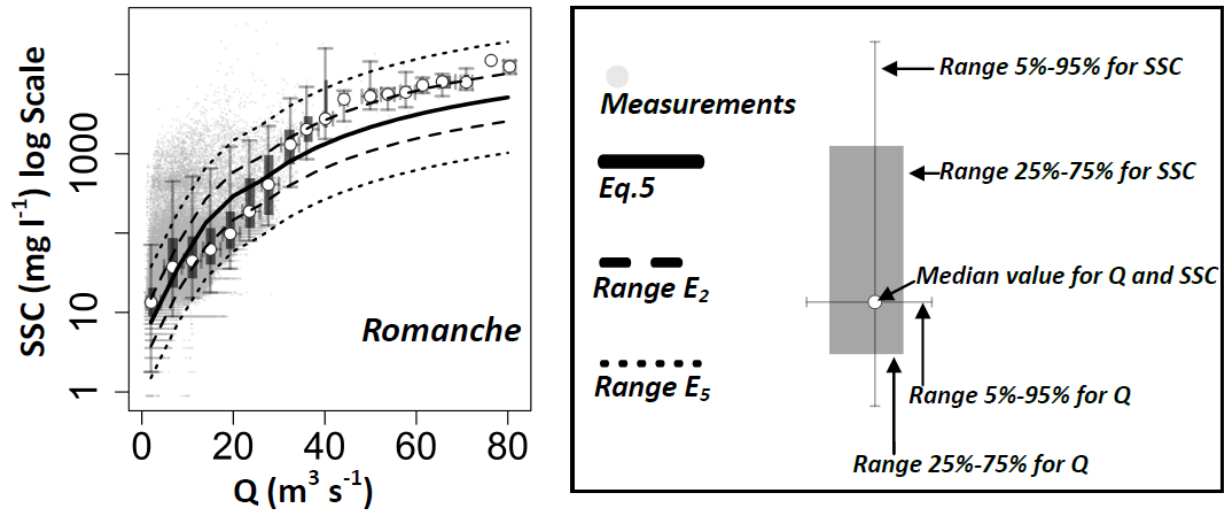


Figure 3.4: Comparison between Eq.3.5 and instantaneous suspended sediment concentration measurements (log scale) in the seven alpine GBRs. Measurements were binned using 20 ranges of equivalent flow rates. Small grey dots correspond to instantaneous measurements; boxplots correspond to binned data considering the 5%, 25%, 75% and 95% percentiles for both flow rate and the suspended concentration; white dots correspond to medians for flow rate and the suspended sediment concentration; the black line corresponds to Eq.3.5 and dashed black lines correspond to its E_2 and E_5 range.

The variability of suspended load and the differences between measured and predicted values using Eq.3.5 were found to decrease for all alpine GBRs when the magnitude of the events increased (Figure 3.5). Thus, using q_b^* to predict suspended load leads to a high percentage of accurately predicted values for all of the alpine GBRs when high flow rates were considered (Table 3.6). This suggests that a substantial proportion of fine particles come from the river bed mobilization rather than from upstream sediment sources during these large events as discussed in the next sections. These events cover a wide range of discharges and correspond to the majority of the total suspended fluxes observed during the measurement periods of the seven alpine GBRs (Table 3.7). Their maximum calculated dimensionless bedload rates were always larger than b_p , which was also the case for most events in these seven GBRs, suggesting that these river beds were often mobilized.

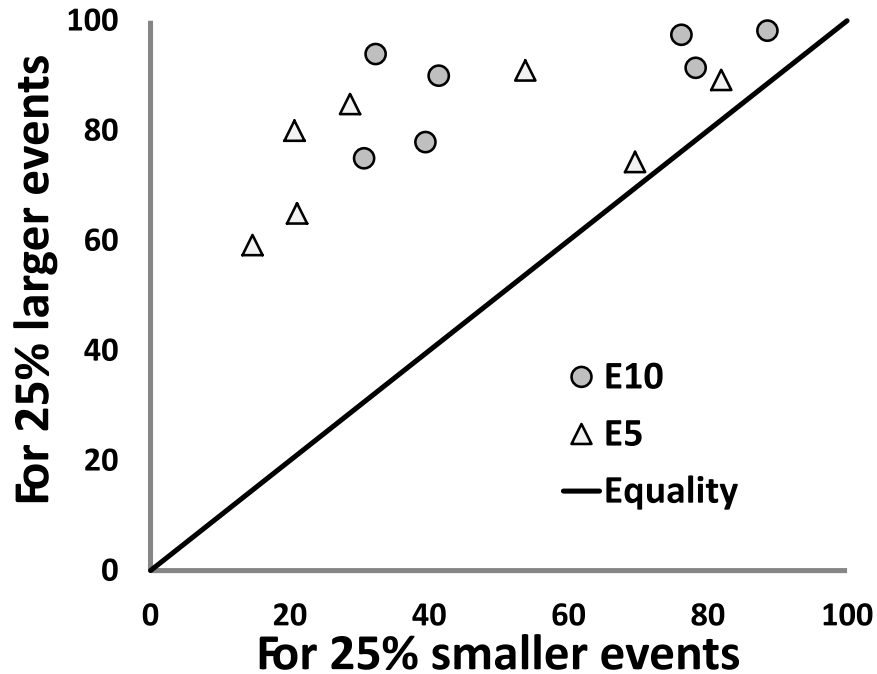


Figure 3.5: Differences of accurately predicted values in a given range considering 25% smaller events and 25% larger events for the seven alpine GBRs.

River	Fraction of all events with $q_b^*_{max} > b_p$ (%)	Fraction of total fluxes corresponding to the 25% smaller events (%)	Fraction of total fluxes corresponding to the 25% larger events (%)	Range of peak discharges corresponding to the 25% larger events ($m^3 s^{-1}$)
Arc	80	2	77	19–177
Asse	73	1.4	85	21–279
Bès	100	1.8	79	8–171
Bléone	100	1	69	36–503
Buëch	78	0.43	57	31–265
Drac	99	2	82	29–280
Romanche	82	2.6	77	17–82

Table 3.7: Fraction of total fluxes transported during 25% smaller or 25% larger events for seven alpine GBRs and fraction of all events with maximum dimensionless bedload rate ($q_b^*_{max}$) higher than the breaking point (b_p) observed in Figure 3.3.

Finally, the average error on annual suspended fluxes (IAE) varied between 74% and 37%. Using other parameters from the literature data set to describe SSCs led to poor results on these seven alpine GBRs. For instance, predictions using Q/A or q^* can be found in the supplementary material. These parameters were not able to reproduce the general trend on the SSC, especially for large events.

3.5. DISCUSSION

3.5.1. SEDIMENT TRANSPORT VARIABILITY

Previous analysis revealed that suspended sediment fluxes and loads are highly variable (Figure 3.2 and Figure 3.3), especially in alpine catchments (Figure 3.4). This variability could be due to measurement uncertainties as well as sediment transport processes. Suspended load measurements are associated with large uncertainties even if turbidity meters are now widely used. It is commonly assumed that the SSC is homogeneous in the cross section, which is not always the case for sandy material. In addition, the SSC–turbidity relationship is highly variable because it depends on the type (i.e., mineralogy, color), shape and size of the sediments. Direct measurements (e.g., with automatic samplers) can also be associated with a grain-size selectivity misrepresenting the suspended concentration [Navratil *et al.*, 2011]. For instance, Clark *et al.* (2009) reported 50% and 20% underestimation on the SSC when using automatic samplers for diameters of 500 μm and 100 μm , respectively. The computation of suspended fluxes with discharges introduces additional uncertainties as stage-discharge rating curves are often doubtful for low flows and floods, especially in mountain streams with unstable cross sections. In this type of stream, similar to those analyzed in this paper, Navratil *et al.* (2011) reported overall uncertainties on SSC measurements of 20% on average (range, 1–30%) and 30% for suspended sediment yield at the flood scale (range, 20–50%) considering 20% uncertainties on discharges. These uncertainties have to be kept in mind when measurements are analyzed.

3.5.2. SEDIMENT SOURCES IN ALPINE RIVERS

Using q_b^* as a macro-descriptor to describe SSC dynamics does not represent all the complex interactions between fine particles and riverbed mobilization. Nevertheless, the dimensionless bedload rate was found to be the best available proxy for the SSC in alluvial GBRs. This relation should not be perceived as the capacity of the flow to maintain a certain quantity of fine particles in suspension but rather as the result of a certain availability of fine particles in the river bed for a given flow condition. Some cases might therefore exist where fine particles could be delivered to the flow from other upstream sources (catchment erosion due to rainfall or runoff, slopes destabilization during debris flows, mudflows or landslides) leading to much higher fluxes than fluxes solely due to bed mobilization. This situation can be observed in head water streams (HWSs) with a steep, narrow and poorly mobile river bed with limited stocks of fine sediments and highly eroded hillslope sources close to the measurement point.

To test this hypothesis, Eq.3.5 was applied on long-term measurements conducted in eight alpine catchments considered as HWSs. Most of these HWSs exhibit a smaller catchment area and steeper slopes than the seven GBRs analyzed previously. Lower

predictions were obtained (Table 3.8). Even if few data were available for catchments with small areas (less than 50 km²), highly eroded areas (greater than 30%) and high bed slopes (higher than 5%), general trends were observed (Figure 3.6). The prediction errors at the annual time scale (IAE) were found to decrease as the catchment size and the riverbed slope decreased while it seems to increase as the percentage of eroded areas increased.

River	Catchment area (km ²)	Eroded area (%)	Slope (%)	Period	IAE (%)
Arvan	220	-	3.3	2011–2015	99
Bouinenc	20	25	2.5	2008–2009	84
Brusquet	1.08	13	3.8	2003–2006	99
Duyes	124	9	1.38	2007–2009	87
Galabre	22	8	2.91	2007–2009	98
Glandon	110	-	5.5	2011–2016	94
Laval	0.86	68	58	1985–2009	18543
Moulin	0.089	54	30	1988–2009	2560

Table 3.8: Validation results for eight alpine GBRs considered as HWS.

The fraction of suspended load that was not explained by the river bed mobilization and attributed to a “global hillslope production” could also be estimated in both GBR and HWS (Table 3.9). The non-bed derived SSC was calculated by subtracting from the measured SSC the SSC predicted with Eq.3.5. The non-bed derived suspended load was then calculated by multiplying the non-bed derived SSC by the flow rate. Despite large uncertainties associated with these estimates, the following observations can be made: i) for the eight HWSs, the major part of the suspended load cannot be explained by the river bed mobilization (Eq.3.5), ii) for the seven alluvial GBRs, the fraction of suspended load not-explained by the river bed mobilization is always smaller for larger events than for smaller ones, iii) overall, the “global hillslope production” in the seven alpine GBRs range between 13% and 68% considering the larger flood events and between 23% and 73% considering all the measurements.

River	25% smaller event (%)	25% larger event (%)	All data (instantaneous) (%)	Type
Arc	90	63	66	GBR
Asse	99	68	73	GBR
Bès	98	20	34	GBR
Bléone	83	13	23	GBR
Buëch	94	58	70	GBR
Drac	68	50	51	GBR
Romanche	85	54	59	GBR
Arvan	99	99	99	HWS
Bouinenc	96	85	86	HWS
Brusquet	100	100	100	HWS
Duyes	100	70	82	HWS
Galabre	100	96	97	HWS
Glandon	90	96	95	HWS

Table 3.9: Supply estimate of non-bed derived suspended load during 25% smaller events, 25% larger events and for all the measurements using Eq.3.5 for fine particles availability in the river bed. Non-bed derived SSC was calculated by subtracting from the measured SSC the SSC predicted with Eq.3.5. The non-bed derived suspended load was then calculated by multiplying the non-bed derived SSC by the flow rate. Note: The Moulin and Laval catchments ($A < 1 \text{ km}^2$, $S > 10\%$) are not considered.

These results suggest that the availability of fine particles in HWSs could be mainly due to other processes than riverbed mobilization such as rainfall, runoff and snow melt eroding bare soils or terrain destabilization during exceptional events (debris flows, mudflows, landslides). For the seven GBRs, both processes could be significant but for different ranges of flow rate. Predictions using Eq.3.5 and thus, the suspended load fraction explained by the river bed mobilization, were always much better for the large events than for the small ones (Figure 3.5, Table 3.9). This could stem from a more significant availability of fine particles due to riverbed mobilization compared to hillslope erosion during large events than during small ones. This hypothesis is consistent with the conceptual models used by Park and Hunt (2018) and Picouet *et al.* (2009) and the conclusions drawn by Vaughan *et al.* (2017). In an analysis of 45 river gages in Minnesota, the latter reported that near channel morphology controls the steepness and the shape of the power law relating suspended load to discharge, suggesting that near channel morphology controls changes in the SSC when the flow increases. They also observed that land use was the main controlling factor of the SSC for low and moderate flows. The low predictions obtained in this study for catchments with high percentage of eroded areas (Figure 3.6), also suggests that using bedload as a proxy of SSC in

landscapes having large areas covered by bare soils, such as arid, semi-arid or large agricultural catchments might not be suitable.

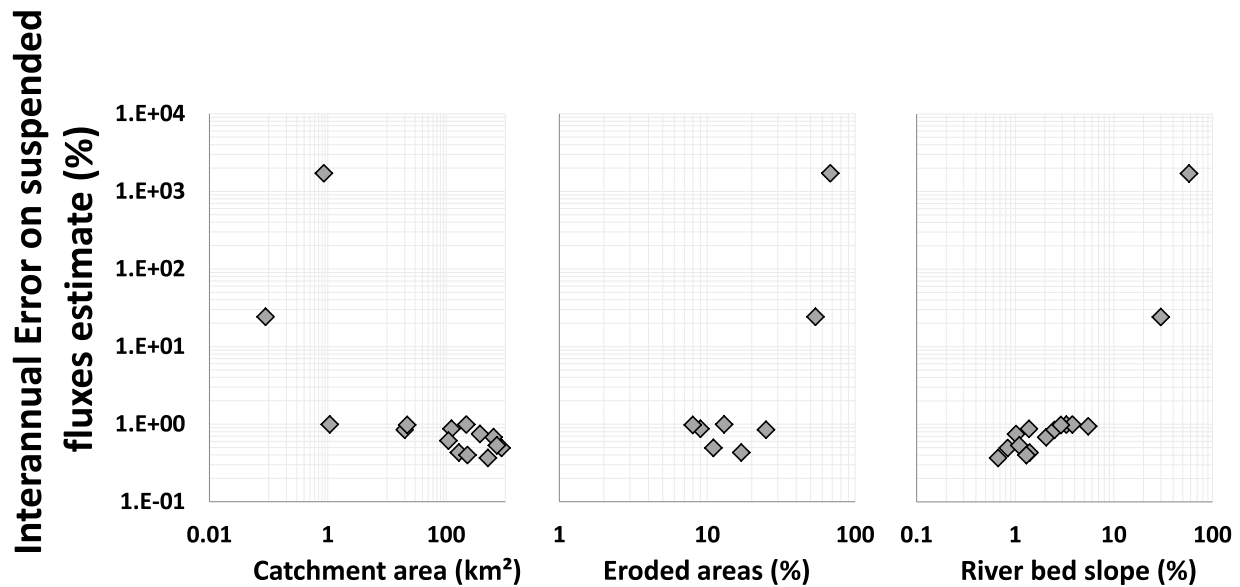


Figure 3.6: Errors using Eq.3.5 to estimate suspended annual fluxes as a function of catchment area, percentage of eroded area and riverbed slope for the alpine rivers presented in Table 3.3 and Table 3.8; IAE = interannual error. Note: data are plotted with log-log scales.

3.5.3. RIVER BED MOBILITY

The data used to obtain Eq.3.5 include bedload rates ranging from low (40% lower than $1\text{g s}^{-1}\text{ m}^{-1}$) to more intense transport (7% larger than $100\text{g s}^{-1}\text{ m}^{-1}$). These data are thus representative of the most common conditions (from transport of sand and fine gravel over a stable armor layer to partial transport during local armor destabilization and subsurface material release) found in GBRs. However, the prediction (annual or event scale) of suspended load assuming a riverbed mobilization in mountainous rivers could depend on the degree of stability of the river bed and the frequency of coarse particles mobilization. As observed previously, it seems that there is a more significant availability of fine particles in the river bed when q_b^* exceeds b_p . This value of q_b^* will be attained depending on the streams and the hydrological forcing considered. If b_p is rarely exceeded, low predictions are obtained using Eq.3.5 (Figure 3.7). This highlights the fact that in addition to depending on the proximity of active hillslope sources, using q_b^* as a macro-descriptor for fine particle availability could be relevant in morphologically active alluvial streams, where bedload is associated with frequent bed reworking.

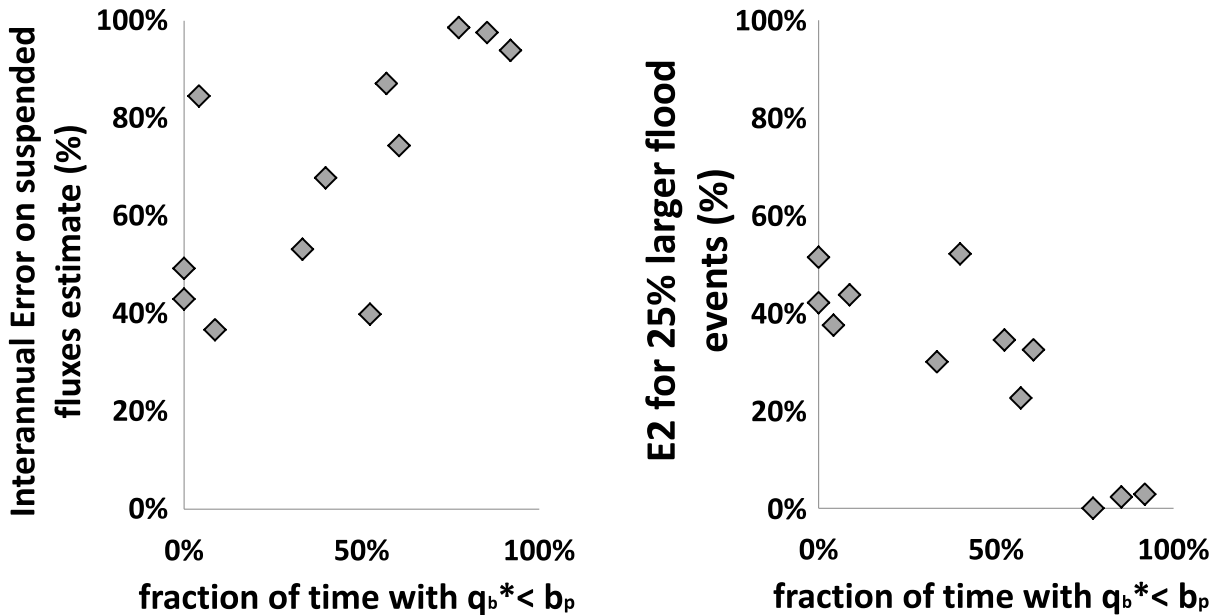


Figure 3.7: Predictions using Eq.3.5 as a function of time for which the dimensionless bedload rate (q_b^*) exceeds the breaking point (b_p) observed during the literature data set analysis. All alpine GBRs and HWSs were considered except the Bursquet, Laval and Moulin catchments which had very small areas ($A \leq 1 \text{ km}^2$).

3.5.4. ON THE ORIGIN OF FINE SEDIMENTS

All the above results and analysis finally questions the origin of fine sediments in alpine streams. Only few studies such as the one of Navratil *et al.* (2010) focused on fine sediment stocks in mountainous rivers to better understand bed related suspended load. On the Bès river, the latter reported that during mainly low magnitude floods, suspended load was finer (7% of clay, 86% of silt and 7% of sand) than the surface deposits in a dry braided channel (2% of clay, 16% of silt and 82% of sand) suggesting a limited release of fine particles from these zones of the braided reach. However, it would be of interest to compare not only the surface but also the subsurface river bed particle types to the suspended load, not only in terms of grain size distributions but also in terms of their nature and origin (e.g. using fine sediments fingerprinting techniques). Making these comparisons for various flow conditions would help to quantify more precisely the suspended fraction resulting from the gravel bed mobilization and the related physical processes. The stocks of fine sediments in the river bed may be reconstructed due to infiltration of fine particles in the empty pore spaces of the gravel matrix, during the falling limb of the hydrographs or during low-flow periods, as suggested by Park and Hunt (2017). This hypothesis is consistent with observations made in several flume and field studies considering sand, silt or clay particle infiltration in porous beds [Frostick *et*

al., 1984; *Glasbergen*, 2014; *Hamm et al.*, 2009; *Harvey et al.*, 2012; *Krishnappan and Engel*, 2006; *Mooneyham and Strom*, 2018]. This infiltration process was found to occur even for very low Rouse numbers (~ 0.01), especially when pore spaces were empty [*Khullar*, 2007; *Mooneyham and Strom*, 2018]. These alternative infiltration and bed mobilization processes could induce a buffering behavior for fine particle transport in the river bed [*Guillon et al.*, 2018; *Orwin and Smart*, 2004b]. However, the river bed could also be a zone in which fine particles are directly produced and not only temporarily stored. Coarse sediments at rest in the river bed are, for instance, degraded by repeated vibrations or abrasion during the transport of other particles, potentially generating fine sediments [*Brewer et al.*, 1992; *Schümm and Stevens*, 1973]. Abrasion during bedload transport also generates a non-negligible amount of fine particles depending on the lithology considered [*Attal and Lavé*, 2009; *Le Bouteiller et al.*, 2011]. For instance, during 18 flume experiments on 10-mm to 20-mm pebbles collected in the Buëch River (also analyzed in our study), *Attal and Lavé* (2009) observed a production of fine particles mainly in the clay-silt range.

3.6. CONCLUSION

In this paper, the flow and bed parameters that best correlate with suspended sediment concentration were investigated using a large data set comprising 2400 instantaneous measurements on 57 gravel bed rivers (GBRs) found in the literature. Among all the available parameters tested, the dimensionless bedload rate (q_b^*) was found to be the best correlated with the suspended sediment concentration (SSC) for these GBRs. A much higher increase of the SSC with q_b^* was observed when a certain value of q_b^* was exceeded. This breaking point seemed to occur approximately when the median river bed sediment is mobilized. An empirical relation was derived between these variables (q_b^* vs SSC). This relation used with a reach average bedload formula was able to reproduce the main trends of suspended load measurements made in alluvial rivers from the French Alps, especially for large events. This relation could be seen as a lower limit of suspended load because it could represent the availability of fine particles in the river bed for a given bed mobilization and not the capacity of the flow to maintain fine particles in suspension. Consequently, in cases where other upstream sources could feed the flow with fine particles, much higher fluxes could be measured. Our results suggest that the limitation of this approach mainly concerns small flood events or small headwater streams directly connected to active hillslope sources. The relative contribution of the bed mobilization of fine particles to total suspension yield also seems to depend on the frequency of coarse sediment mobility.

Finally, we conclude that the dimensionless bedload transport rate q_b^* is a reliable macro-descriptor that could be useful for practitioners to get a suspended load estimate during large flood events when such measurements are not available. Because suspended load results from various complex processes at the catchment scale, the

inherent limitations of such simple approach should be carefully considered. Thus, its application should be restricted to morphodynamically active river reaches considered far enough from direct hillslope supply. This approach could also be useful to perform a rapid assessment of the relative contribution of the river bed and the watershed production when suspended load measurements are available.

3.7. APPENDIX

3.7.1. BED LOAD CALCULATION

Many equations have been proposed in the literature and could be used to predict bedload. We chose to use the one proposed in Recking (2010), Recking (2013) and Recking *et al.* (2016) (Eq.3.6 to Eq.3.9) because it was specifically developed from field data for reach average computation and was validated with a large independent data set. The input parameters are Q , W , S , D_{50} and D_{84} .

$$q_b^* = \frac{q_b}{\rho_s \sqrt{g(s-1)D_{84}^3}} = \frac{14\tau^{*2.5}}{1 + \left(\frac{\tau_m^*}{\tau^*}\right)^4} \quad (3.6)$$

$$\tau_{84}^* = \frac{\rho g d S}{(\rho_s - \rho) g D_{84}} \quad (3.7)$$

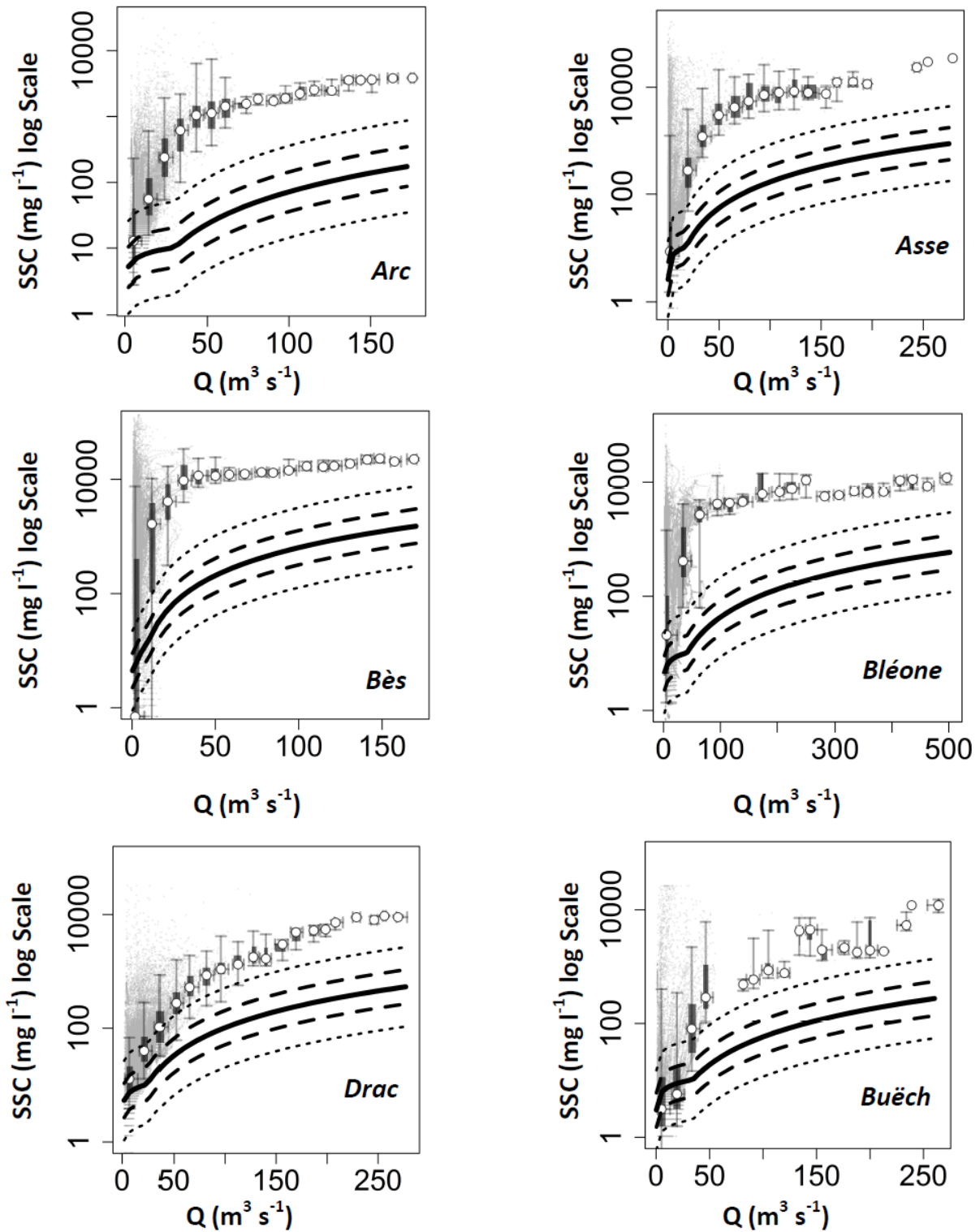
where q_b ($\text{kg s}^{-1} \text{m}^{-1}$) is the unit bedload transport per unit width, $s = \rho_s/\rho$, ρ_s is the sediment density, ρ is the water density, and g is the gravity acceleration. In Eq.3.6 the parameter τ_m^* defines the transition between partial transport and full mobility. It depends on the morphology of the stream [Recking *et al.*, 2016].

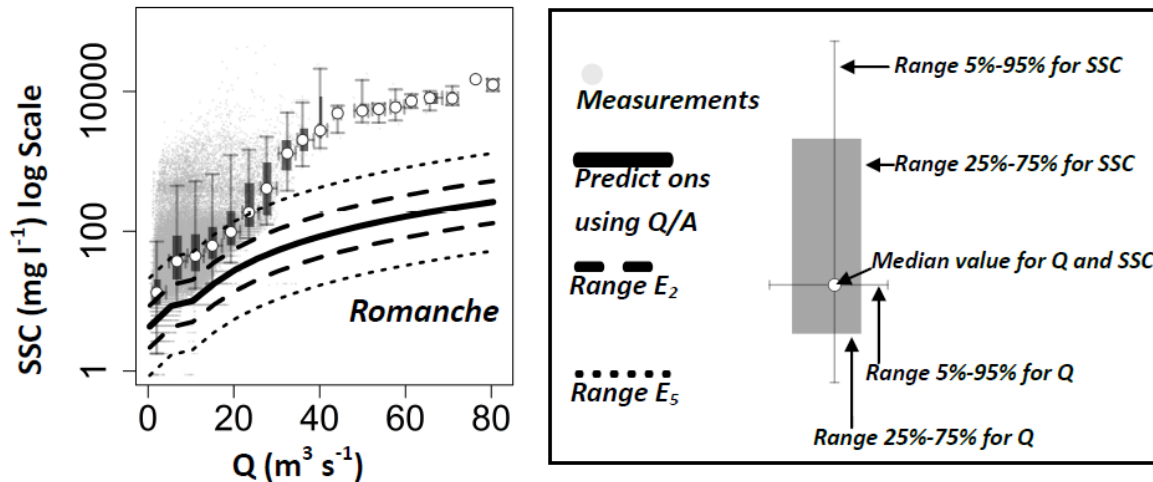
$$\tau_m^* = \begin{cases} (5S + 0.06) \left(\frac{D_{84}}{D_{50}}\right)^{4.4\sqrt{S}-1.5} & \text{for riffle pool} \\ 1.5S^{0.75} & \text{for other morphology} \end{cases} \quad (3.8)$$

The Shields number τ^* in Eq.3.7 was computed with a discharge measurement and with d deduced from Eq.3.9, which is an approximation of the flow resistance equation proposed by Rickenmann and Recking (2011) and valid for all flow regimes [Recking *et al.*, 2016].

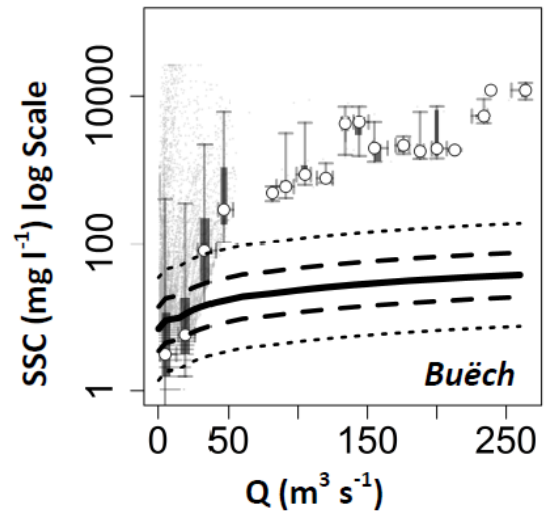
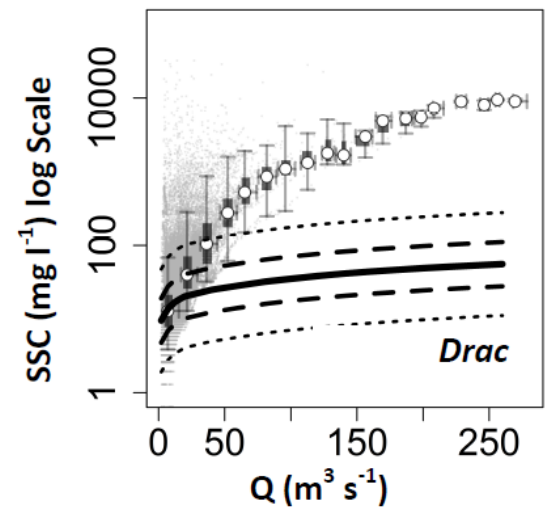
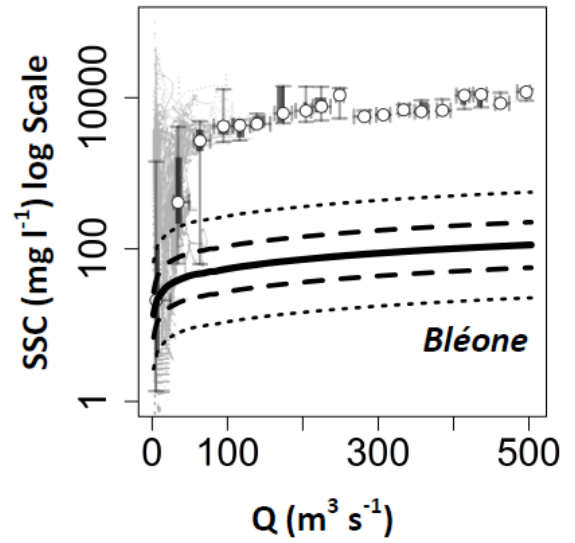
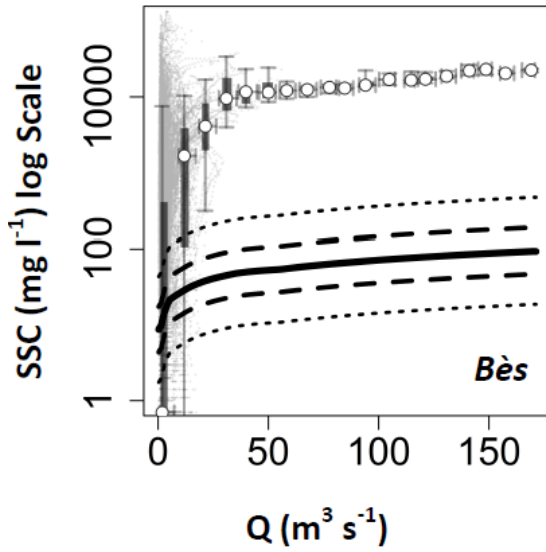
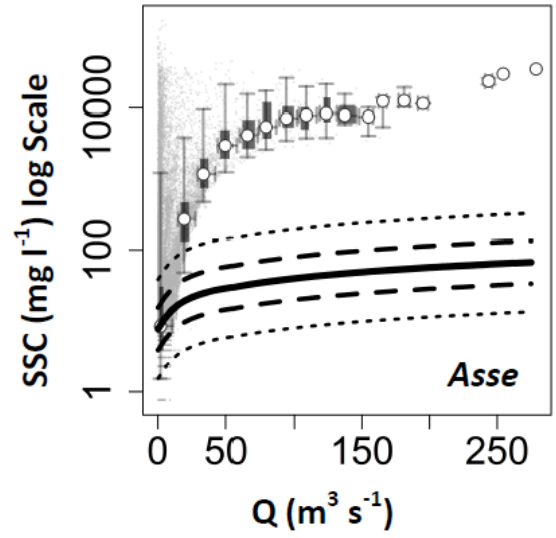
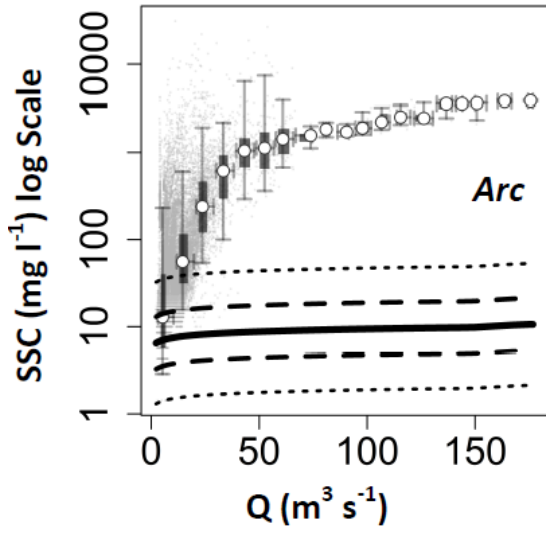
$$\begin{cases} d = 0.015 D_{84} \frac{q^{*2p}}{p^{2.5}} \\ q^* = \frac{q}{\sqrt{g S D_{84}^3}} \\ p = 0.24 \text{ if } q^* < 100 \text{ and } p = 0.31 \text{ otherwise} \end{cases} \quad (3.9)$$

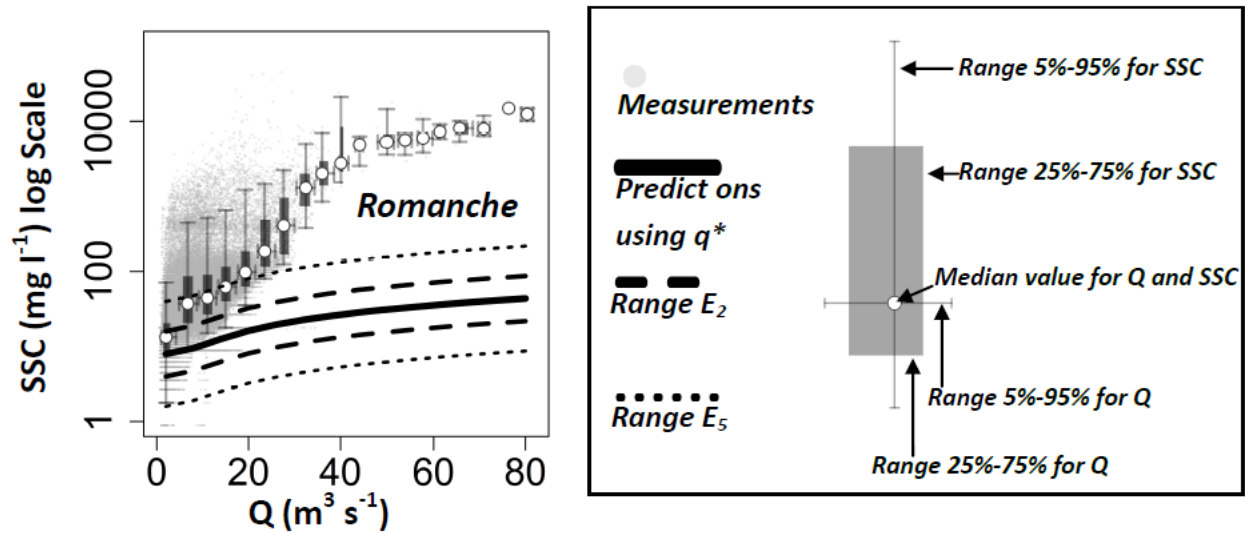
3.7.2. PREDICTION IN ALPINE RIVERS USING PROXIES DERIVED FROM THE FLOW RATE





Supplementary material 1: Comparison of instantaneous suspended sediment concentration measurements (log scale) in the seven alpine GBRs and a piece-wise log-linear model fitted on the literature data set between the SSC and Q/A. Measurements were binned using 20 ranges of equivalent flow rates. Small grey dots correspond to instantaneous measurements; boxplots correspond to binned data considering the 5%, 25%, 75% and 95% percentiles for both flow rate and the suspended concentration; white dots correspond to medians for flow rate and the suspended sediment concentration; the black line corresponds to the best fit between SSC and Q/A for the literature data set and dashed black lines correspond to its E_2 and E_5 range.





Supplementary material 2: Comparison of instantaneous suspended sediment concentration measurements (log scale) in the seven alpine GBRs and a piece-wise log-linear model fitted on the literature data set between the SSC and q^* . Measurements were binned using 20 ranges of equivalent flow rates. Small grey dots correspond to instantaneous measurements; boxplots correspond to binned data considering the 5%, 25%, 75% and 95% percentiles for both flow rate and the suspended concentration; white dots correspond to medians for flow rate and the suspended sediment concentration; black line corresponds to the best fit between the SSC and q^* for the literature data set and dashed black lines correspond to its E_2 and E_5 range.

3.8. NOTATIONS

The following symbols are used in this paper.

D_{50}	Sediment diameter of the bed such that 50% of the mixture is finer [m]
D_{84}	Sediment diameter of the bed such that 84% of the mixture is finer [m]
D	Sediment diameter [m]
τ^*	Shields number: dimensionless shear stress [-]
τ_{84}^*	Shields number for D_{84} [-]
τ_m^*	Dimensionless transition parameter between partial and full mobility [-]
Q	Water discharge [$\text{m}^3 \text{s}^{-1}$]
U	Mean water velocity over the section [m s^{-1}]
u^*	Friction velocity [m/s]
W	Channel bed width [m]
S	Channel bed slope [-]
A	Catchment area [km^2]
ρ	Water density [kg m^{-3}]
ρ_s	Sediment density [kg m^{-3}]
s	Relative density of sediment [-]
g	Gravitational acceleration [m s^{-2}]

d	Mean water depth [m]
p	Dimensionless transition parameter between intermediate and high submersion [-]
q^*	Dimensionless water unit discharge [-]
q	Unit water discharge [$m^3 s^{-1} m^{-1}$]
Q_s	Suspended load [$t d^{-1}$]
Q_b	Bedload [$t d^{-1}$]
q_s	Unit suspended load [$kg s^{-1} m^{-1}$]
q_b	Unit bedload [$kg s^{-1} m^{-1}$]
q_b^*	Dimensionless bedload [-]
SSC	Suspended sediment concentration [$mg l^{-1}$]
SSC^*	Dimensionless suspended sediment concentration [-]
P	Stream power [w]

PART 2

Chapter 4

Combining multi-physical measurements to quantify bedload transport and morphodynamics interactions in an Alpine braiding river reach

This fourth chapter reports a detailed description of morphodynamic and bedload transport in a typical alpine braided river (La Séveraisse). This riverbed mobility description will then be used to interpret concomitant observations made on suspended load (next chapter). Strong interactions between bedload transport and morphological changes were observed using a wide range of direct and indirect technics showing the interest to combine multi-physical measurements. This work has been published in Geomorphology (DOI: 10.1016/j.geomorph.2019.106877) by Missot C., Recking A., Legout C., Bakker M., Bodereau N., Borgniet L., Cassel M., Geay T., Gimbert F., Navratil O., Piegay H., Valsangkar N., Cazilhac M., Poirel A. and Zanker S.

Ce quatrième chapitre rapport des observations détaillées de la morphodynamique et du transport par charriage dans une rivière en tresse typique des Alpes (La Séveraisse). Cette description de la mobilité de la rivière est ensuite utilisée dans le chapitre suivant pour interpréter des observations concomitantes sur les flux en suspension. De fortes interactions entre charriage et changements morphologiques ont été observées à l'aide d'un large panel de mesures directes et indirectes montrant l'intérêt de combiner des mesures multi-physiques. Ce travail a été publié dans Geomorphology (DOI: 10.1016/j.geomorph.2019.106877, contributeurs Missot C., Recking A., Legout C., Bakker M., Bodereau N., Borgniet L., Cassel M., Geay T., Gimbert F., Navratil O., Piegay H., Valsangkar N., Cazilhac M., Poirel A. and Zanker S.).

4.1. ABSTRACT

Understanding the interactions between bedload transport and morphodynamics in braided streams has important applications in river management and restoration. Direct field measurements addressing this question are however scarce as they are often challenging to perform. Here, we report an extensive two-month field campaign in an alpine braided reach (La Séveraisse river, French Alps) that experienced predictable daily peak discharge (48 events observed) generating significant bedload transport and morphological changes during the melting season. We monitored these processes using a wide range of direct and indirect techniques: bedload sampling, continuous seismic measurements, pebbles tracking, topographic surveys and remote sensing using ground control cameras and drone flights. Doing so, surrogate measurements allowed to extend temporally discrete manual bedload sampling, and to extend spatially local riverbed cross section measurements. These measurements provide unique complementary constraints on the targeted physics, at various spatial and temporal scales which enabled us to draw robust conclusions. Data showed a progressive decrease in bedload transport for a given flow rate along the two months period. Simultaneously, river morphology in the braided sections changed from an incised to a more distributed configuration which led to a decrease of local maxima in dimensionless shear stresses in the braided reach for similar flow conditions. This control of bedload transport by maximum local shear stresses was in line with tracked pebble surveys indicating that coarse bedload particles were mostly transported in the main active channel. At the reach scale, this transport was found to be more efficient in laterally constrained sections than in braided ones which has important implications in terms of bedload estimation in alternative constrained and braided rivers. Finally, this study highlight the interest to combine a large variety of traditional and innovative measurements techniques to better understand complex sediment transport processes in the field.

4.2. INTRODUCTION

In Alpine environments, sediment supplied from hillslopes is generally transferred through the river system via a complex cascade of processes. Sediment passes through successive types of riverbed morphologies [Montgomery and Buffington, 1997], each of which affecting transfer efficiency due to changes in river bed characteristics [Recking et al., 2016]. Among these, braiding river reaches play a key role due to their high capacity to store sediments in terraces, bars, and channels [Hoey, 1992; Lisle and Church, 2002; Wilkinson et al., 2006]. Braided rivers are characterized by multiple channels, separated by unstable bars, that interact with one another at to confluences and bifurcations of the flow [Ashmore, 1991]. Braided systems are present in various settings, from steep Alpine headwaters to piedmont rivers that emerge from mountain ranges. In addition, mountain systems often show alternating braiding and non-braiding reaches (Figure 4.1). As a consequence, understanding the relation between bedload transport rates

and braiding morphology is a keystone for river management and restoration programs. The study of braided reaches is not only useful for the braided reaches themselves, but also further downstream, where river morphological development depends strongly on the upstream storage and release of sediment.



Figure 4.1: Braided reaches (white lines) alternating with narrow constrained reaches (black lines) in the Séveraise river (Google earth 2016). A water intake is located downstream the study area.

Conditions for braiding are related to a high supply of bedload material, a high stream power, low bank resistance and limited in-channel riparian vegetation [Bertoldi *et al.*, 2011; Eaton *et al.*, 2010; Gran and Paola, 2001]. Braided morphology observed at a given time results from complex interactions between the river morphology, the hydraulic conditions, and the solid flux. Thus, large fluctuations in bedload flux have been observed in flume experiments for constant water discharge [Gomez *et al.*, 1989; Recking *et al.*, 2009]. Average cross section hydraulic parameters (stream power or bed shear stress) are typically used for bedload transport modeling in single channel morphologies when there are no available measurements. However, this approach leads to large under-predictions of bedload fluxes in flume experiment of braiding morphologies [Bertoldi *et al.*, 2009]. This is likely due to bedload transport being localized in narrow zones within the cross section where shear stresses are high [Warburton, 1992], which is not well captured by the averaged hydraulic parameters [Recking, 2013a]. Also, for braiding morphologies in the field, the choice of the cross section where bedload equations should be applied is poorly documented and may lead to large uncertainties in such streams [Recking *et al.*, 2016]. In addition, it has been observed that depending on the upstream bedload fluxes, braided rivers may experience aggradational or degradational phases [Liebault *et al.*, 2013]. During aggradation, a decrease in flow depth for a given flow rate reduces the capacity of the channel to export bed material while during degradation, the flow concentrates in incised channels, leading to increased transport capacity [Pryor *et al.*, 2011]. These observations support the notion that there is no single relationship between the water discharge and transport

capacity in such streams and that morphological changes have strong and direct effects on bedload transport.

Although the relation between bedload transport and braiding morphodynamics has been investigated for decades using flume experiments [Ashmore, 1982; Bertoldi *et al.*, 2009; Warburton and Davies, 1994] few field studies such as the one of Lane *et al.* (1996) reported simultaneous bedload transport and braiding morphodynamics measurements. This lack of field observation is largely due to difficulties associated with direct sampling being highly challenging in such highly dynamic streams with unstable bed morphology. This limitation led to the use of remote sensing technics such as photogrammetry [Bakker and Lane, 2017; Lane *et al.*, 1996; Lane *et al.*, 2003], lidar [Bertoldi *et al.*, 2011; Lallias-Tacon *et al.*, 2014; Milan *et al.*, 2007] or ground-based imagery [Ashmore *et al.*, 2011; Luchi *et al.*, 2007] to specifically study morphological changes in braided streams. On the other hand, some studies have focused on the measurement of bedload transport in braiding rivers by using classical sampling methods when feasible [Meunier *et al.*, 2006], indirect seismic measurements [A. Burtin *et al.*, 2011] or pebble tracers to detect bedload particle path [Chapuis *et al.*, 2015; Liébault *et al.*, 2012]. Direct samplings give an estimate of transport and topography respectively, but with limited time and space resolution. Surrogate techniques give access to large temporal and spatial observations, but need calibration with local measurements. Thus combining direct (bedload sampling, topographic survey) and indirect techniques (seismic measurements, remote-sensing imagery, pebble tracking) permits to optimize field based measurements for a well-documented data set required to better understand the complexity of morphodynamics of braiding streams.

In this paper, we present a comprehensive measurement campaign in an Alpine braided river reach (La Séveraisse, Ecrin Massif, SE French Alps). Daily floods of various magnitudes occur each year during a 2-month snowmelt season (May to June). Such regular seasonal and daily occurrence allow preparing the field campaigns to test a combination of techniques/approaches that can most of the time not be combined in the same field site, during the same period. Then traditional and novel techniques were used to conduct complementary hydrological and sediment transport measurements (bedload sampling, continuous seismic measurements, pebbles tracking, topographic surveys, remote sensing using ground control cameras and drone flights). Those measurements have been made at several key places throughout the reach and continuously over a 2-month long period during the snowmelt season (May to June). The objectives of the study were to: i) assess the interest of such multi-physical measurement approach and its application in future geomorphological studies; ii) to provide new insights into characterizing bedload transport and braided bed morphology dynamics during the course of a snow-melt season; and (iii) to analyze relations

between the various physical quantities, confronting them with laboratory-derived hydraulic / bedload formulas.

4.3. STUDY AREA

The Séveraise catchment in the Ecrin Massif (SE French Alps) is well suited for this study because it has low-human impact (no dams or water intakes upstream the study area, limited embankments), it is well-accessible from the river banks, and it provides opportunities for direct bedload sampling from bridges (Figure 4.2). A pre-existing gauging station (managed by EDF, a French electric power company) provides water discharge measurements (at 10-min time-step) that recorded high daily flow events from the melt of the large snowpack that fell during the 2018 winter. At the gauging station, the drainage area is 130 km². The valley morphology is shaped by glacial erosion and the river is still fed by glaciers located in the upper parts of the catchment (maximum elevation of 3579 m a.s.l). The geology mainly comprises crystalline rocks (gneiss, granite) and few patches of softer rocks (marls). The upper part of the catchment is highly erosive and delivers large amounts of sediment via rock falls, debris flows [Helsen *et al.*, 2002], and tributaries. These areas are well-connected with downstream river reaches, showing several sequences of well-developed braiding morphologies and straight (constrained) river channels in the more laterally-constrained sections of the valley. In this study we considered a constrained-braided-constrained sequence located few hundred meters upstream of the gauging station (Figure 4.2).

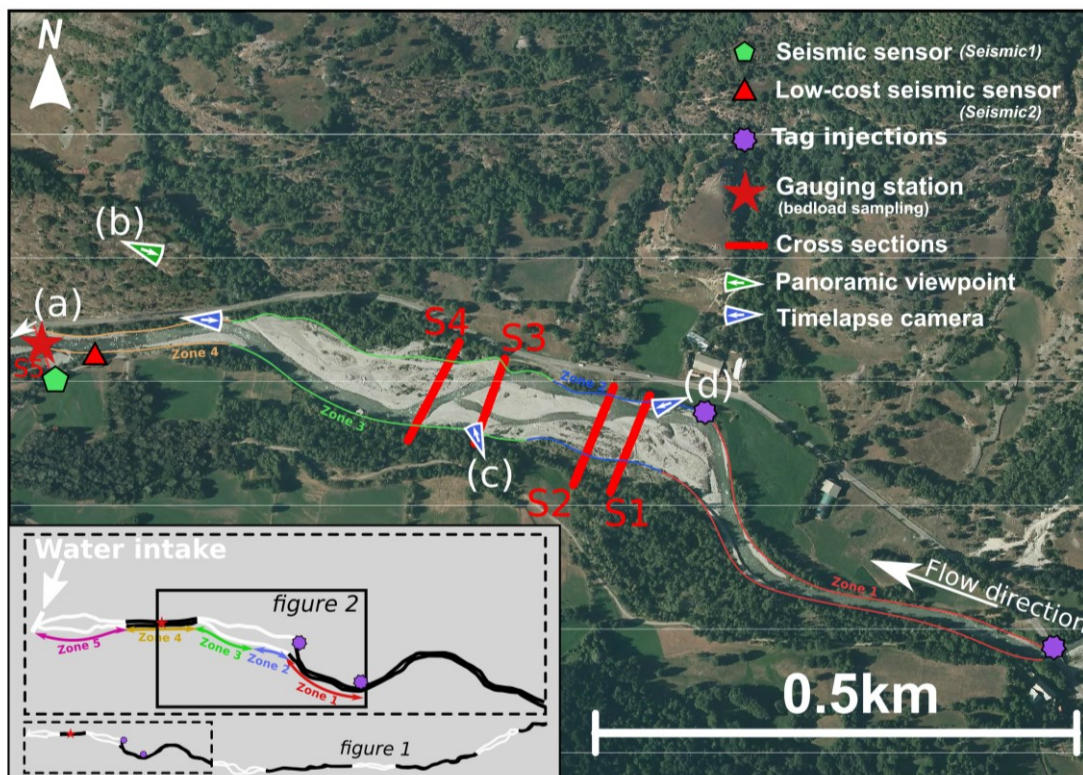




Figure 4.2 : Location of the instruments and measurements within the studied reach of the Séveraise. S1 to S5 correspond to cross-section surveys located from upstream to downstream; (a) is the narrow and paved downstream section where flow rate measurements and bedload sampling were performed, (b) is a view of the braided reach, (c) is a picture taken from a time-lapse camera in the middle of the braided reach and (d) is a picture taken from a time-lapse camera in the upstream part of the braided reach. The five zones used to analyze tracking pebble surveys are indicated with different colors. These zones have different morphologies: zone 1 and 4 are narrow and constrained, zone 2 is the entrance of the braided reach, and zone 3 is the downstream part of the braided reach. Zone 5 is located downstream the gauging station few meters upstream the water intake and is the most downstream prospected zone.

4.4. MATERIAL AND METHODS

4.4.1. DIRECT BEDLOAD TRANSPORT SAMPLING

Bedload fluxes were sampled downstream from the studied reach (S5 in Figure 4.2), on the bridge besides the gauging station managed by *Electricité de France* (EDF) which provided discharge measurements (repeated gauging using dilution, ADCP, velocity profilers techniques and coupled with continuous pressure level sensors at 10 min time-interval). No change in the rating curve was observed as confirmed by daily bed

topography controls performed by the field team. A pressure difference sampler (Elwha 20.7×12 centimeter) with a mesh size of 0.5 mm was deployed at approximately 1.5 m intervals across the channel width. The bedload flux was integrated over the cross section using Eq.4.1:

$$q_b = \frac{1}{L_t} \sum_{i=1}^N \frac{Q_{be\ i}}{L_e} L_i \quad (4.1)$$

in which q_b is the bedload rate per unit width ($\text{g s}^{-1} \text{m}^{-1}$), N is the number of samples, $Q_{be\ i}$ is the bedload rate for each sample (g s^{-1}), L_t is the cross section width (m), L_e is the sampler width (m) and L_i is the width considered representative for the sampling point i (m). The time of sampling (from 15 to 300 seconds) was adapted to bedload transport conditions to avoid trapping efficiency decreases. Between the 27th of April and the 26th of June, 60 measurements of the cross-sectional bedload flux (q_b) were performed. These measurements were performed for a wide range of water discharges (9-25 m^3/s), allowing us to elaborate rating curves and to observe temporal changes in bedload rates. A resampling technique detailed in appendix A was used to test the significance of temporal trend in bedload samples. This method is based on an analysis of the relation between time and residuals obtained from a power law fitted between bedload and the flow rate.

The cross-sectional bedload grain-size distribution was measured for a subset of the samples (17 of the 60 samples). We mainly focused on samples collected in the central part of the cross section with the largest unit bedload rates. Bed load samples were sieved with 1.6mm, 10mm, 20mm, 32mm, 45mm, 64mm, 91mm, 128mm and 181mm mesh sizes. The 50th and 84th percentiles of the transported diameters in terms of mass could then be calculated (D_{50} and D_{84}).

4.4.2. INDIRECT BEDLOAD TRANSPORT MEASUREMENTS

To complement the previous direct in-stream sampling, we thus performed continuous, indirect measurements based on seismic monitoring to assess the variability of bedload transport in time [A. Burtin *et al.*, 2008; A. Burtin *et al.*, 2011; Cook *et al.*, 2018]. In this study, we led two types of seismic measurements with geophones: (i) a complete and classical seismic measurement station similar to the one used by Cook *et al.* (2018) with high-frequency acquisition (we called Seismic1 at Figure 4.2) and (ii) a low-cost seismic measurement derived from debris-flows monitoring applications (Seismic2) and tested here to study its use for spatially extending seismic measurements [Bel *et al.*, 2017; Navratil *et al.*, 2013]. The geophones allow ground-motion vibrations to be investigated within the range ca. 5-200 Hz which encompasses frequencies expected for bedload transport [Gimbert *et al.*, 2019; Tsai *et al.*, 2012] and flow turbulence [Gimbert *et al.*, 2014]. At Seismic1, the classical seismic station, a PE-

6/B geophone was installed on the river floodplain (25 m from the left channel bank, Figure 4.2) to monitor bedload-induced seismic vibrations. The data was recorded with a frequency of 400 Hz on a DiGOS DATA-CUBE³. Given that bedload-induced noise is thought to be of a higher frequency than turbulent-flow-induced noise [Cook *et al.*, 2018; Gimbert *et al.*, 2014] we calculate seismic power P_b at relatively high frequencies. We evaluate P_b in the 20-80 Hz frequency range allowing maximum sensitivity to bedload while minimizing the contribution of strong site effects (anthropogenic noise) at the very high frequencies (> 100 Hz). If primarily caused by bedload, seismic power P_b is set by impact forces exerted by transported bed material on the river bed, and is expected to scale with bedload flux (Q_b) and transported grain diameter (D) as [Tsai *et al.*, 2012]:

$$P_b \sim Q_b \times D^3 \quad (4.2)$$

4.4.3. COARSE PARTICLES DISPLACEMENT

To quantify the transport and mobility of coarse particles in the braiding stream, 29 natural pebbles were equipped with active ultra-high frequency transponders also known as a-UHF tags [Cassel *et al.*, 2017a]. Their average b -axis is 77mm, approximately twice the D_{50} value of the study site. The transponders were of the COIN-ID model, emitting a beacon signal at 433.92 MHz every 2.2s. The tags were placed into a 40mm diameter hole drilled in the pebbles and then filled with the mixture polyurethane resin and corundum [Cassel *et al.*, 2017b]. Sediment tracers were injected on the 12th of June 2018 at two locations on the study site. Fifteen tracers were injected in a narrow section located 500 meters upstream the entrance of the braided reach. Fourteen of them were injected from the embankment in the river bed a few meters upstream the entrance of the studied reach (Figure 4.2). Following tracer injection, 5 tracking-surveys were conducted within a period of 2 weeks (Table 4.1). The first three periods covered one water discharge peak and the following two a series of 4 and 6 peaks respectively.

	Injection		Tracking			
Date	12/06/18 (Am)	12/06/18 (Pm)	13/06/18 (Day)	14/06/18 (Day)	18/06/18 (Day)	25/06/18 (Day)
Prospected zones	-	Partial (Z1 and Z2)	Full	Full	Partial (Z1 to Z4)	Full
Recovery rate	29/29 (100%)	13/29 (45%)	21/29 (72%)	22/29 (76%)	23/29 (79%)	25/29 (86%)
Number of peaks discharge	-	1	1	1	4	6
Maximum peak discharge (m³/s)	-	19.5	22.6	20	19.5	24.2

Table 4.1: Synthesis of the pebbles tracking campaign. There were five prospection zones, Z1 to Z5 from upstream to downstream. Zones Z1 to Z4 are indicated in Figure 4.2.

The tracers were tracked using a reading system (composed of a Slender III antenna and SCIEL reader connected at laptop) and a GPS (Leica Zeno 20), carried by three operators, from the main channel bank (Figure 4.2-a). The antenna was moved and oriented such as to maximize the a-UHF tag signal intensity by real-time visual monitoring of the received signal strength indication (so called RSSI). The main advantages of this method are its rapidity, allowing prospection of the entire study reach between two floods event, and its detection range, estimated at 10m for transponders immersed in 50cm of water. The tracer localization was performed in a single longitudinal profile along the river as proposed by Piégay *et al.* (2016), with an uncertainty of approximately 10m. Therefore, an uncertainty of 20m was considered for the tracers 1D travelled distance between surveys. The data of the travelled distance are analyzed with respect to the tracer injection locations, the zones of the study reach where tracers have been deposited or entrained and the duration between tracking surveys to determine virtual velocities, as well as the channel in which they traveled.

4.4.4. QUANTIFYING MORPHOLOGICAL CHANGES

Repeated topographical surveys were conducted along five cross-sections (S1 to S5; Figure 4.2) to quantify the morphological changes over the snow melting period. A topographic total station (Leica Geosystems) was used with fixed marks on both banks allowing accurate morphological comparison through time. Measurements were performed during low-flow periods for safety reasons. Vertical resolution of the measurements is limited to the size of the coarse bed-particles. It is estimated to be approximately ca.10 cm (twice the median surface particle size D_{50}). Non-truncated Wolman pebble counts of surface grain-size were also performed at the beginning and

at the end of the campaign to detect potential grain-size changes associated with morphological changes. Each time, four hundred particles were sampled along four transects (two in the main channel and two on top bars) approximately located at the same positions.

Three cameras, similar to the ones used by Benacchio *et al.* (2017) were installed to record local morphological changes at the upstream, middle, and downstream locations of the braided reach (Figure 4.2). Pictures were taken every 20 min from 6 AM to 10 PM. In addition, several pictures were taken ($n=4$) from a vantage point at the downstream end of the reach to qualitatively observe morphological changes (Figure 4.2-a).

To characterize global morphological changes, two drone flights were performed before and after the melting season on respectively the 27th of April and 25th of July. We assume that morphological changes that occurred after the field campaign were limited in comparison to those occurring during this period as only one significant ($Q=17\text{m}^3/\text{s}$) and three other lower intensity ($Q<15\text{m}^3/\text{s}$) peak discharges were recorded in July. A drone-based camera (ILCE-7, focal length 35 mm, resolution 6000×4000) was used to take pictures (respectively 426 and 676 in April and July) with an overlap of minimum 85%, enabling the reconstruction of orthorectified images with a 2cm-resolution. Images were aligned by using Structure from Motion photogrammetry software (Agisoft Photoscan) and c. 30 ground control points measured in the field using a differential GPS. GPS point's accuracy (3D position) was on average 1.6 cm. The accuracy on 2D position (XY) of the orthorectified images obtained (estimated by the root mean squared errors of ground control points used in orthorectification) was respectively 10.3 and 10.1 cm in April and July. A laserScan (Yellowscan) installed under the drone was also used to performed a scan of the river bed to construct digital elevation models (DEMs) and calculate the elevation differences between the two flights. An average point density of 60 points/ m^2 was obtained. DEMs were filtered, aligned and their elevation difference was calculated on a 1m-radius using Cloud Compare software considering a 25cm-limit of detection.

4.4.5. HYDRAULIC CALCULATIONS

To estimate the main hydraulic parameters (velocity, hydraulic radius and water depth) at the five surveyed cross sections (S1 to S5) from the measured discharge Q , we used the flow resistance equation proposed by Ferguson (2007) (detail in appendix A) by iteratively adjusting water level, assumed to be uniform over the cross section and using a mean reach slope and an average grain size distribution. We chose to use this flow resistance equation as it has been shown to be suitable for flow having small relative submergence [Ferguson, 2010; Rickenmann and Recking, 2011] as is the case in the braided gravel bedded stream studied. Because of high lateral variability in hydraulics, several homogeneous vertical panels were considered independently to compute locally

averaged parameters as proposed by Bertoldi et al. (2009) for braided morphology. This allowed us to estimate a local or average Shield parameter considering the 84th percentile of the grain size distribution (τ_{84}^*) in each cross-section and to compare this parameter with bedload transport rates (see appendix A for details on the calculation of τ_{84}^*).

4.5. RESULTS

4.5.1. OVERVIEW

Figure 4.3 shows the time-series of all the measurements conducted during the field campaign. Water discharge varies between 8 and 26 $\text{m}^3 \text{s}^{-1}$ and exhibits daily peak discharge due to snowmelt, and sometimes due to rain events. The maximum instantaneous peak discharge measured corresponds to approximately a 2-year return period as calculated by the French hydrometric services (<http://www.hydro.eaufrance.fr>) based on 49 years of measurements. This suggests that our field campaign documents common flow conditions and exclude extreme events (5-year, 10-year and 20-year return period of 44, 56 and 68 m^3/s respectively). Indirect, seismic measurements also exhibit daily fluctuation, varying about three orders of magnitude, suggesting that the flow rate exerts a significant control on bedload transport in this river. The temporal seismic variability is also consistent with direct bedload sampling measurements.

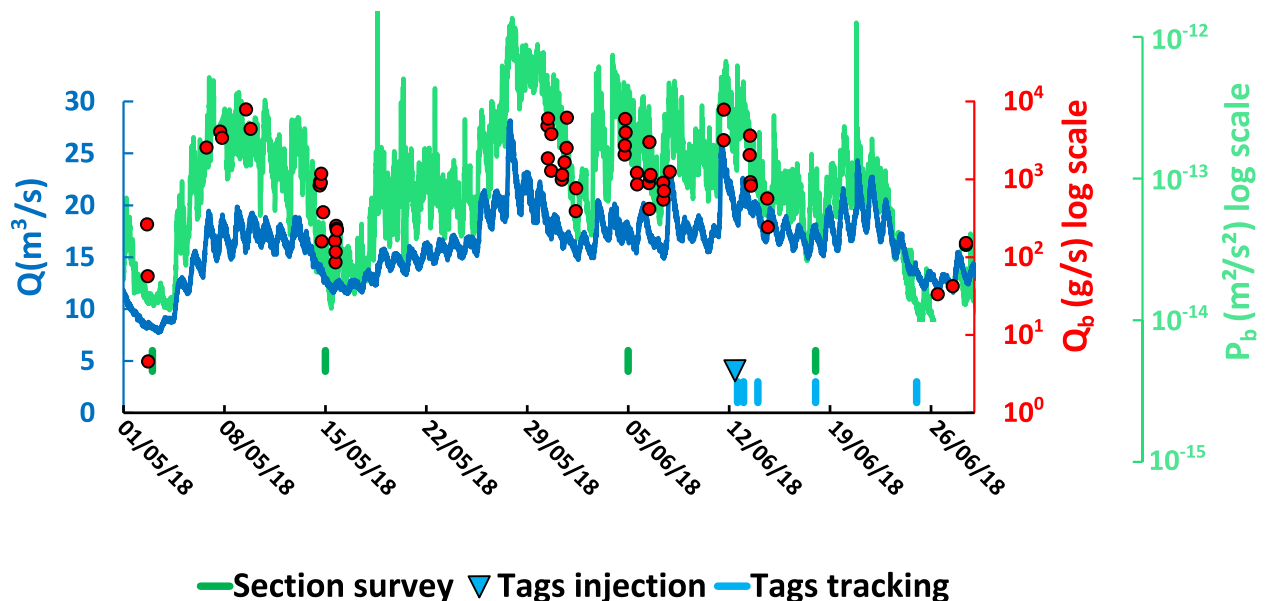


Figure 4.3: Time series of flow rate (Q , m^3/s), seismic power at seismic1 (P_b , m^2/s^2) (20–80Hz) and direct bedload sampling measurements (Q_b , g/s). The dates of cross section survey, tag injection and tracking are indicated.

The main topographic and bed grain size distribution characteristics (detailed in the following sections) exhibit significant differences between the braided and the constrained sections (Table 4.2). The braided sections have wider active widths, gentler slopes, and finer bed materials which suggests a more active morphology in this area.

	Slope (%)	Bed D_{50} range (mm)	Bed D_{84} range (mm)	Total active width range (m)
Braided sections (S1 to S4)	1.05	37-49	94-123	50-90
Constrained section (S5)	1.2	110	303	12

Table 4.2: General river bed characteristics of the studied reach for braided sections (S1 to S4, located in Figure 4.2) and the constrained section (S5). Bed D_{50} and D_{84} range correspond to the 50th and 84th percentiles of nun-truncated wolman counts performed in early May and late June in both channel sides and top bars (details can be found in appendix C).

4.5.2. BEDLOAD DYNAMIC

Bedload transport rates range from 0.3 to 592 g s⁻¹ m⁻¹ (Figure 4.4) and are available as supplementary material. The general increase of unit bedload rate (q_b) with flow rate (Q) exhibits a power law with an exponent of 5.3 by fitting a log linear model. We observe a variability in bedload transport flux of one order of magnitude at a given flow rate, as is often found in gravel bedded streams [Recking, 2013b]. Part of this variability is time-dependent, as relatively larger transport rates occur at the beginning of the field campaign as confirmed by the resampling technique detailed in Appendix A.

The average transported diameters are respectively 33 and 77 mm ($n=17$) for D_{50} and D_{84} , which is similar to the bed material sampled in the main channel of the braided sections, where D_{50} was between 28 and 43 mm and D_{84} between 63 and 123 mm, considering the start and the end of the campaign (Figure 4.5-a). These measurements are available as supplementary material. On the opposite, the constrained section has a much coarser bed ($D_{50}=110$ mm and $D_{84}=303$ mm), which suggests that bedload samples at S5 do not come from a local bed mobilization of this constrained section but from the material mobilized from the upstream braided sections. While the estimation of the coarsest transported diameter might be potentially underestimated due to the size of the sampler intake compare to bedload particles size, no significant trend is observed between the transported grain size and the flow rate even when only samples with small diameters are considered (Figure 4.5-b). The absence of such a relationship indicates a more or less equal mobility of bed material when delivered to the flow following local morphological changes such as bank failure or armor breakup.

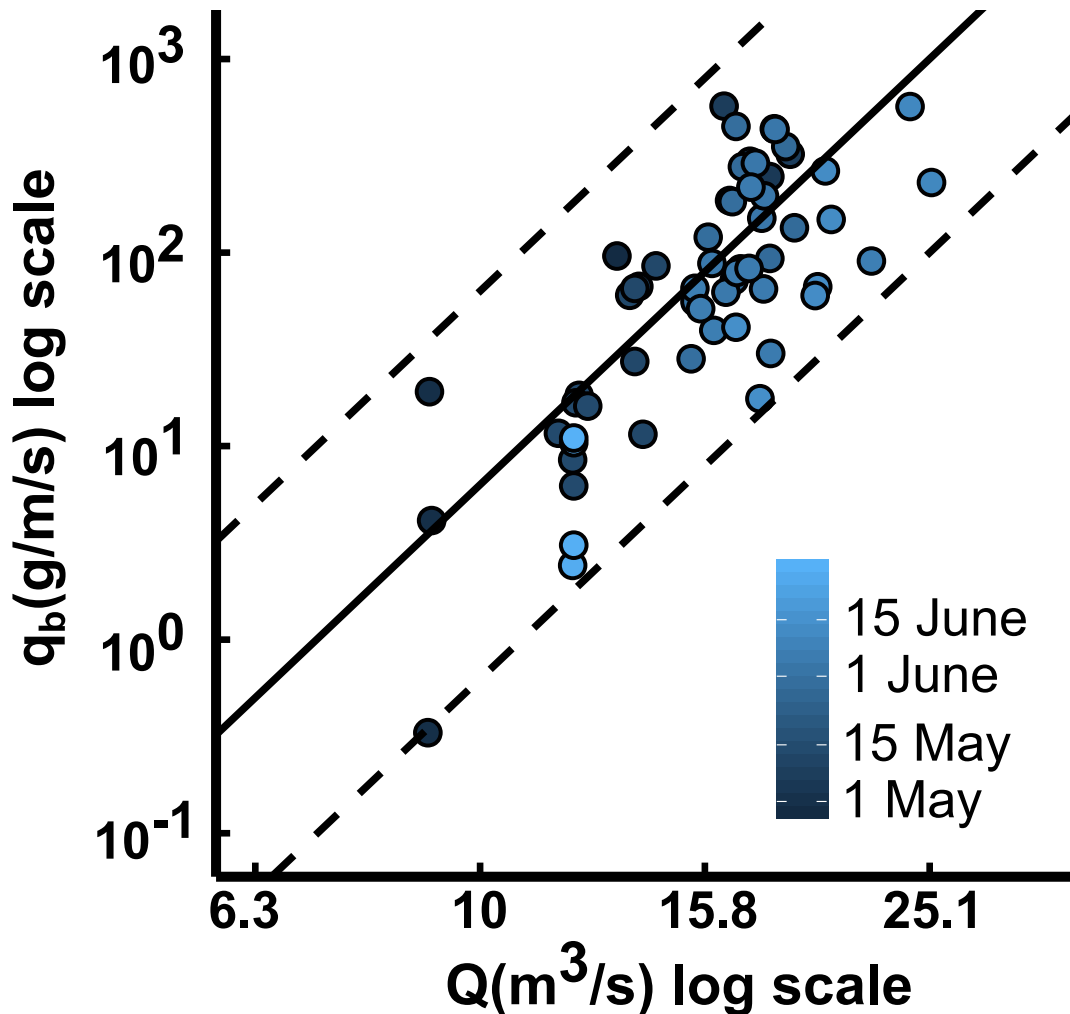


Figure 4.4: Sampled unit bedload transport rates measured at the gauging station (S5) as a function of flow rate for the whole field campaign. The black line is the best log-linear fit using all the data, dashed lines correspond to one order of magnitude around this best fit.

For a given bedload transport rate, calculated Shields numbers in the upstream cross sections of the braided reach (S1 and S2) are similar although slightly larger than the ones in the more downstream (S4) cross section (Figure 4.5-c). On the contrary, much lower Shields numbers for equivalent bedload transport rates is observed in the narrow, paved and laterally constrained section where bedload sampling were conducted (S5).

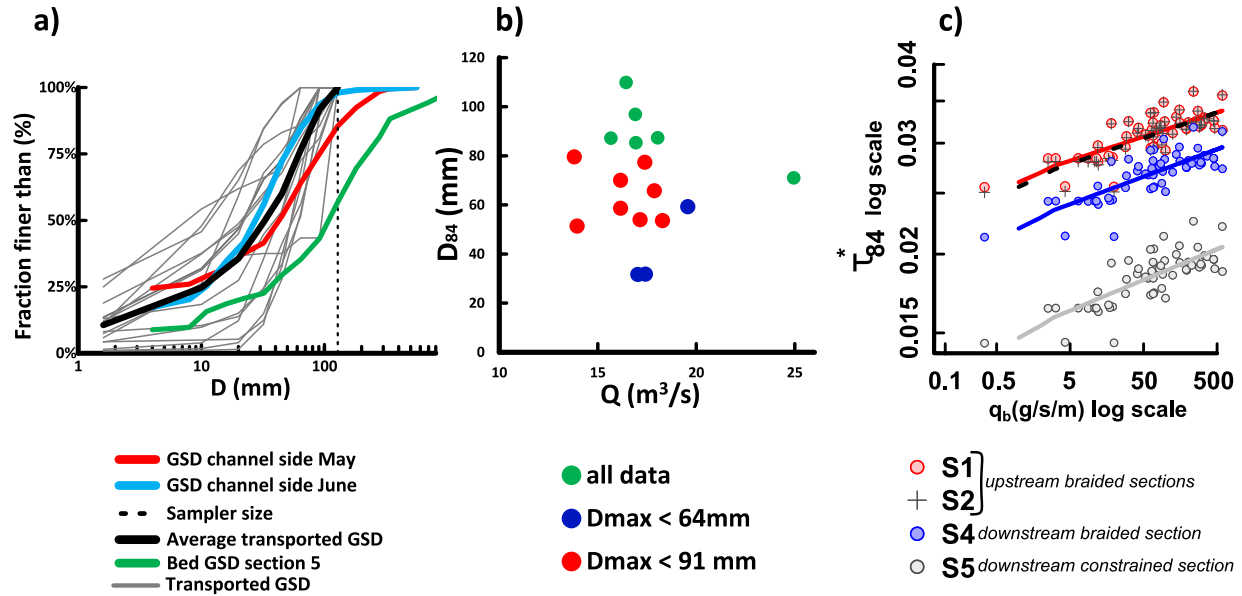


Figure 4.5: (a) River bed and transported grain size distributions. (b) 84th percentile of the transported diameter as a function of flow rate depending, points color indicates the range of maximum diameter sampled. (c) Shields number in the main active channel calculated considering four cross sections (beginning of the campaign, location in Figure 4.2) as a function of bedload fluxes measured.

4.5.3. SEISMIC OBSERVATIONS

We observe that seismic power at *Seismic1* station is a power law function of flow discharge (Figure 4.6). Where grain size does not significantly vary with flow discharge (Figure 4.5), previous theory and laboratory experiments indicate that bedload-induced seismic power scales linearly with bedload flux (see Eq.4.2, Tsai *et al.* 2012 and Gimbert *et al.* (2018)), i.e. P_b scales with Q with a similar exponent than q_b does. For our measurements, best data fit with a log-linear model gives a power law exponent of 3.9, which is significantly larger than the 7/5 exponent theoretically expected for seismic power from turbulent flow (Gimbert *et al.*, 2016), but is significantly lower than the 5.3 exponent observed in this study between sediment transport flux and flow discharge (Figure 4.4). It is thus likely that a source other than turbulent flow generates significant ground seismic motion. Although the 3.9 power-law exponent is not quite as high as the 5.3, this indicates bedload is a prominent source of the observed seismic signal in the 20-80 Hz frequency range. Yet we cannot conclude whether the observed discrepancy in P_b and q_b versus Q exponents is due to turbulent flow or any other potential river source significantly contributing to seismic power or local site-effects that impact upon the seismic signal.

We also observe a temporal trend in the P_b versus Q relationship with a decrease of the intercept along the two months highlighted by the two power laws fitted for the 10 first days of May and the 10 last days of June (Figure 4.6). Similar seasonal trend was previously observed in the Trisuli River in Nepal by Burtin *et al.* (2008). Time dependency has also been observed at shorter timescales in various river settings (Hsu *et al.*, 2011, Roth *et al.*, 2014, Diaz *et al.*, 2014) and has often been attributed to bedload variability, although in these previous studies no independent direct measurements allowed confirming such an interpretation. Our present observations provide such a confirmation, since the temporal trend P_b versus Q occurs concomitantly with the temporal shift of the relationship between q_b and Q (Figure 4.4 and Figure 4.6). The decrease of the intercept through time could be indicative of a decrease in upstream sediment supply. Continuous observations from seismic signals may provide a unique mean to investigate the intra-seasonal activation and deactivation of upstream sediment sources.

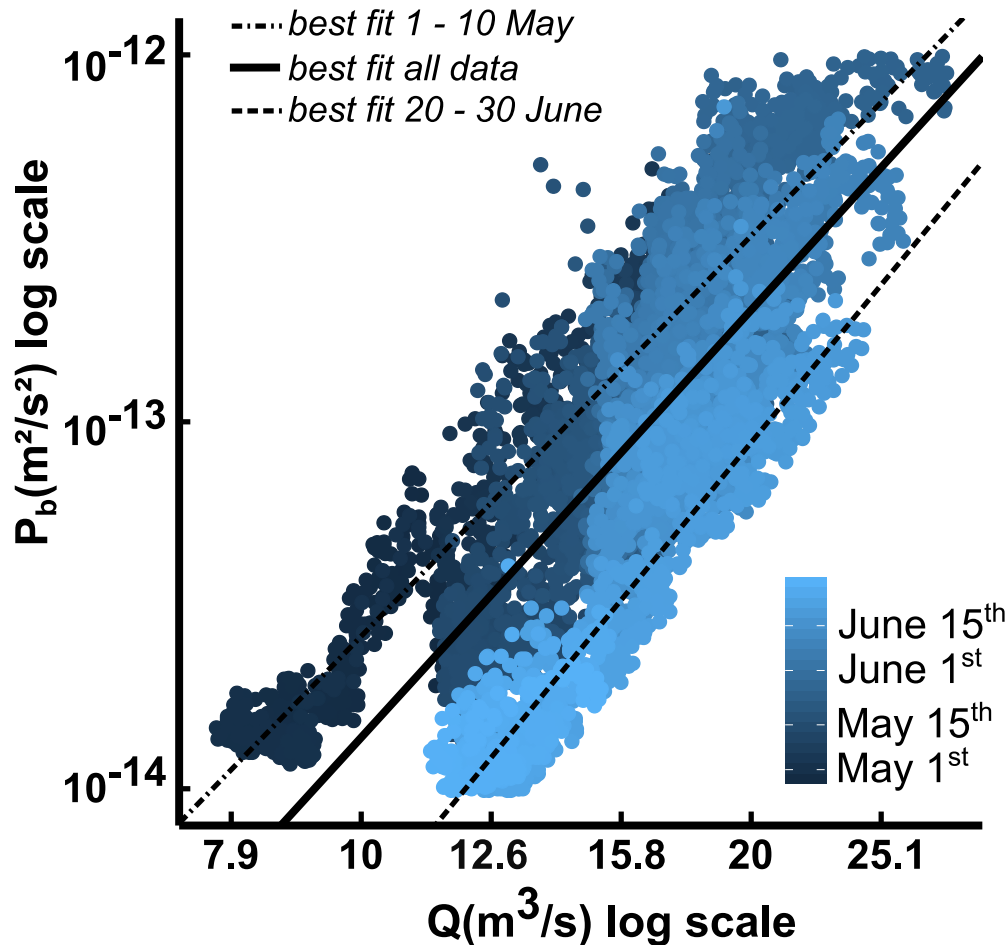


Figure 4.6: Seismic power at Seismic1 on a frequency range 20-80Hz as a function of the flow rate on a 10-minute basis.

4.5.4. *BEDLOAD PARTICLE MOBILITY*

Pebble tracking surveys confirm the high bedload transport intensity during this field campaign. Following the tag tracers injection, most of the tracers were retrieved when the whole reach was prospected thanks to their active UHF signal (return rate between 72% and 86%). This high recovery rate permits to be confident on the representativeness of these measurements. The pebbles were highly mobile with a maximum distance of nearly 2 km traveled over the course of one day (see T2, Figure 4.7). Thus, after the second day, several tags might have moved beyond the prospected zone and their travel distances or velocities cannot be observed. Assuming that the second full prospection (13th of June) is representative of the pebble dispersion (not too much tags downstream the prospected zone), a mean velocity can be estimated for the upstream and downstream injection point of respectively 27 and 13 meters per hour.

During the prospection, no pebbles were found in secondary channels or on bars indicating that these coarse grains were mainly transported through the main channel. It was also observed that the number of tracked pebbles detected may depend on the zones (1 to 4) of the reach considered (Figure 4.7). It appears that pebbles transit through the narrow constrained upstream and downstream parts of the reach (zone 1 and 4) more quickly than through the braided parts of the reach (zone 2 and 3). Considering all tags, almost half of them (14/29) were still at the entrance of the braided reach (zone 2) after the last prospection while only few tags were still detected in other zones. However, different behavior was observed depending on the injection point. 78% of the tags injected few meters upstream of zone 2 (downstream injection) stayed at the entrance of the braided reach (zone 2) or traveled through the entire prospection zone. Conversely, a smaller proportion of tags injected from the upstream point (in the constrained reach almost 500 meters upstream zone 2) stayed in zone 2. However, the entrance of the braided reach was still the zone in which most tags stayed until the end of the survey. It must also be highlighted that the entrance of the braided reach (zone 2) is only 200-meter-long compare to respectively 400, 400 and 500 meters for zone 1,3 and 4.

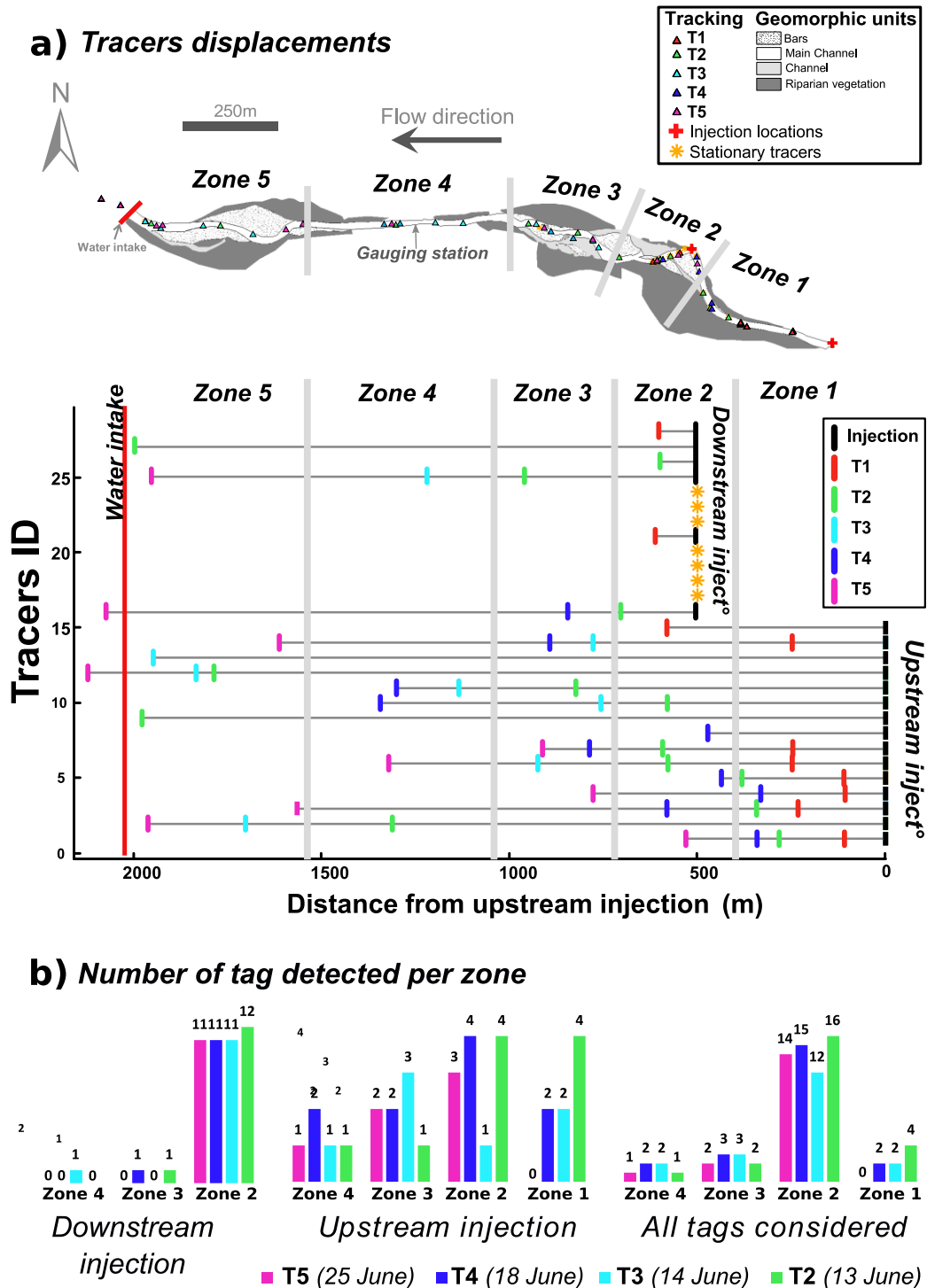


Figure 4.7: (a) Tracers displacements during the five tracking surveys (T1 to T5) following the injection. (b) Number of tags detected in each zone of the studied reach considering all tags or upstream and downstream injection separately. Note that the following tags were still found in Zone 2 on the 30th of august: 8, 15, 17, 19, 20, 21, 23, 24, 26, 28 and 29.

4.5.5. MORPHOLOGICAL CHANGES

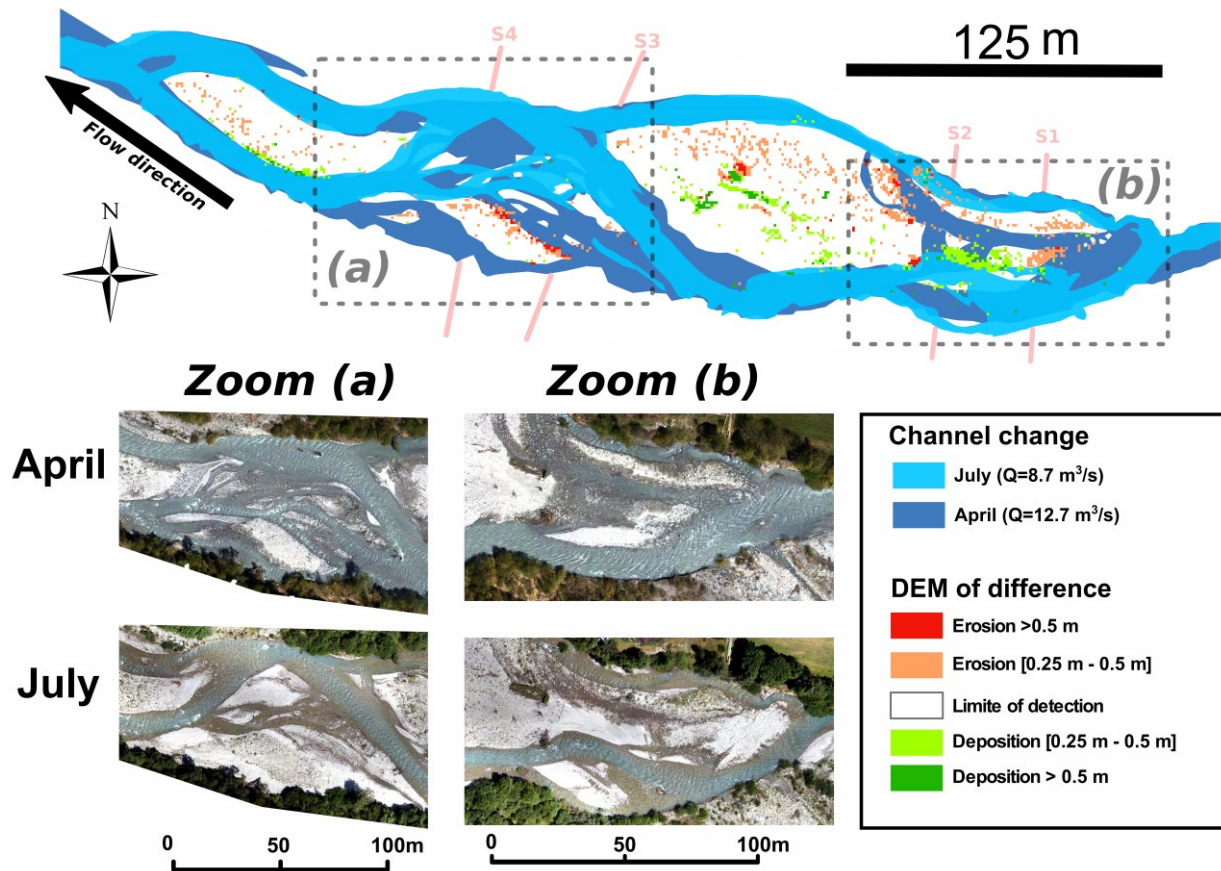


Figure 4.8: Diachronic analysis of the channels displacement between April and July using orthophotographs digitalisation and digital elevation model (DEM) of difference between April and July. Surveyed cross sections (S1 to S4) are indicated by red lines.

Orthophotographs, repeated topographic surveys, ground-based pictures show that the braided reach experienced significant planar and elevational changes during the study period (Figure 4.8, Figure 4.9 and Figure 4.10). First, the entrance and the middle part of the braided reach (respectively zones a and b in Figure 4.8) exhibit high braiding intensity with complex multi-channel flows leading to several confluences and bifurcations. These zones are particularly active with bars formation or banks and bars erosion. Second, the entrance of the braided reach experienced significant morphological changes, as shown in cross section surveys and ground-based pictures (Figure 4.10, Figure 4.9, Figure a and b). In this area, net deposition was observed with bed aggradation of locally more than one meter (average depth change of respectively +11 cm and +13 cm for section 1 and 2). Morphological changes occurred from an incised channel configuration in May (one main channel on the left and one not well-

connected secondary channel on the right) to a more distributed channel in June, associated with water being more evenly spread over the cross section (two main channels on the left and one active secondary channel on the right). Lateral channel migration took place near the entrance zone, amounting to 2.9 meters and 1.4 m of left bank erosion for section 1 and 2. Third, other cross sections (3 and 4) in the downstream active zone were more stable as no major bed elevation changes were detected (Figure 4.10-c and d) while bank erosion and lateral migration was significant for section 4 with almost 6 meters of right bank erosion. Lidar measurements on emerged top bars showed limited elevation changes for these zones suggesting that underwater areas were the most active zones in this braided reach.

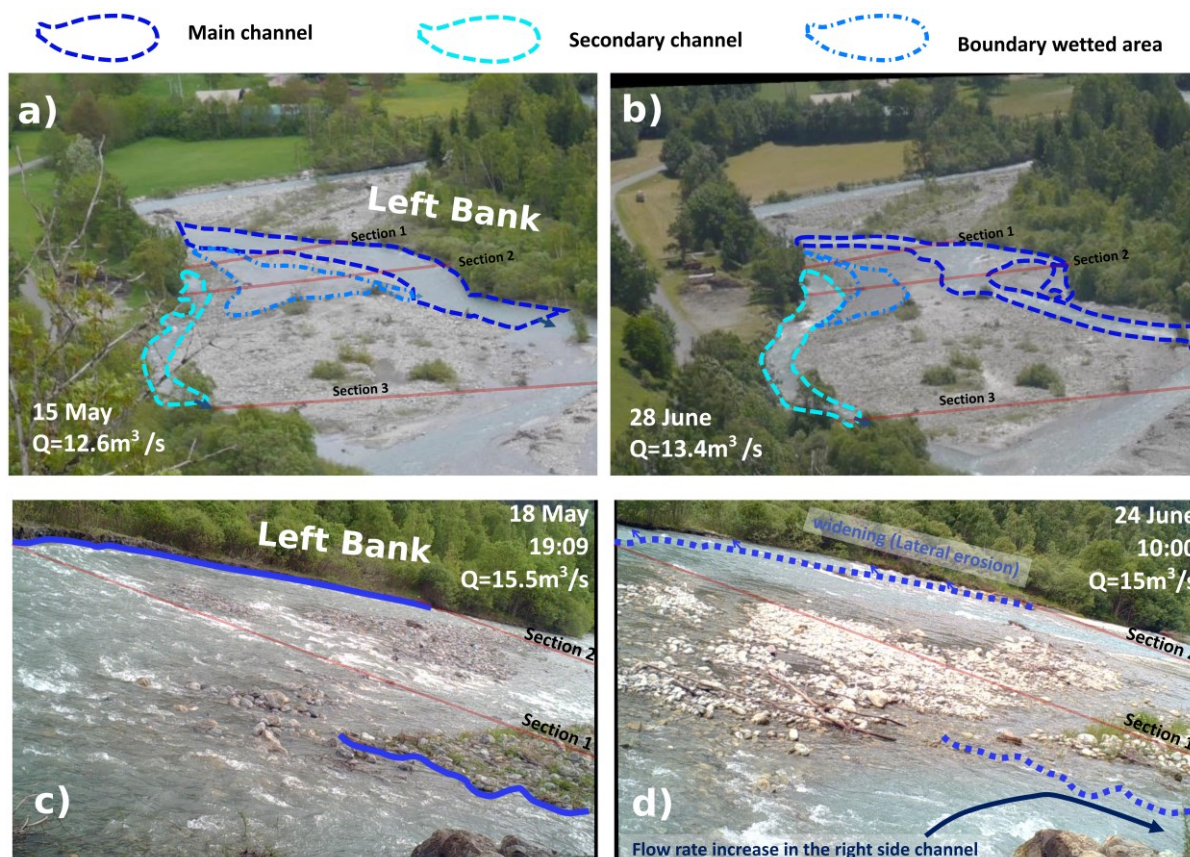


Figure 4.9: Morphological changes observed at the entrance of the downstream braided reach. Top view of the entrance of the downstream braided reach at the beginning (a) and at the end (b) of the campaign. View of the entrance of the downstream braided reach at the beginning (c) and at the end (d) of the campaign for the same discharge. Other ground-based pictures of the downstream part of the reach can be found in appendix B.

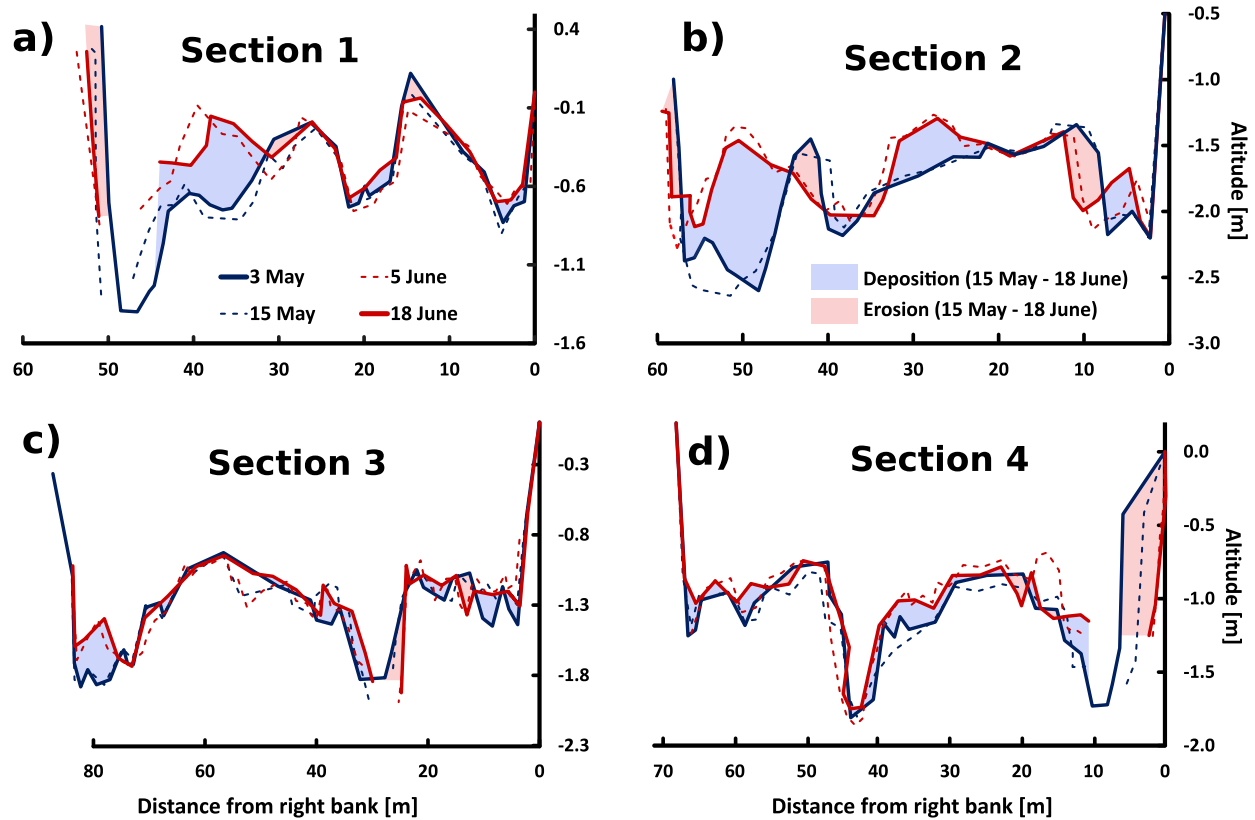


Figure 4.10: Topography evolution at the entrance of the downstream braided reach for section 1 (a), section 2 (b), section 3 (c) and section 4 (d).

Surface grain size analysis of the braided reach show a decrease in D_{50} and D_{84} from respectively 49mm and 123 mm at the beginning of the campaign to 37 and 94 mm at the end of the campaign (Figure 4.12-a). Top bars exhibited more or less constant coarse grain size distribution while much less fine particles (<10mm) were observed in June. Conversely, in the main channel, the fine fraction was constant while a decrease in coarse grain size was observed.

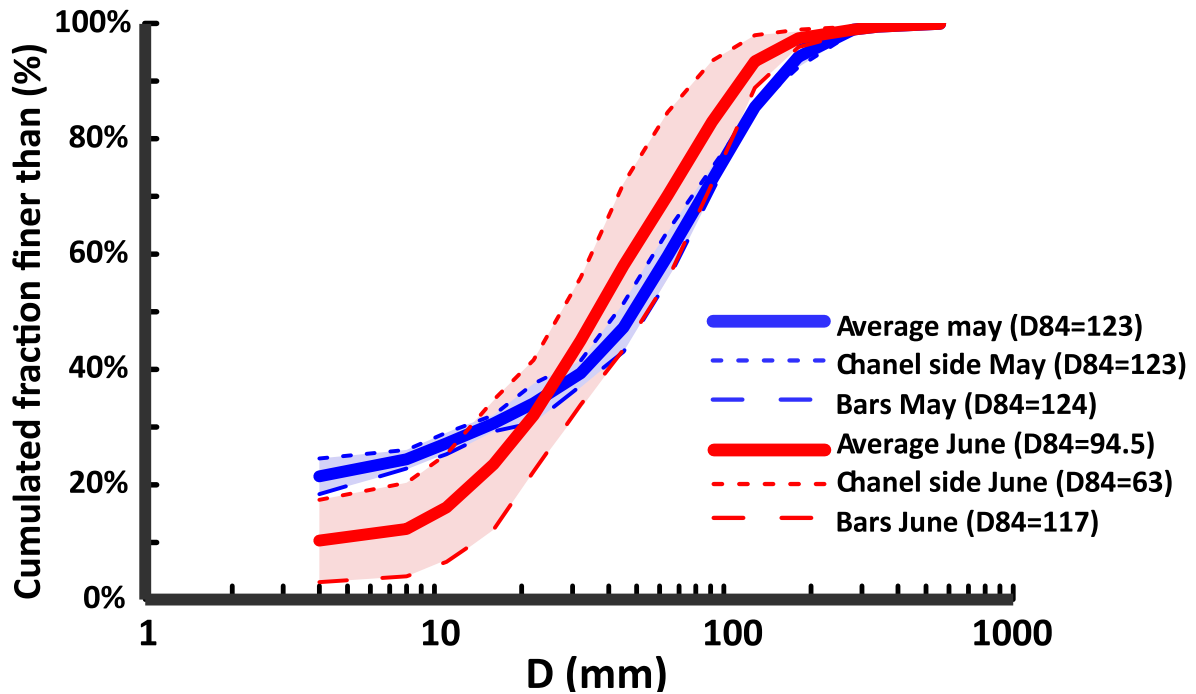


Figure 4.11: Surface grain size distribution of the studied reach at the beginning and the end of the field campaign, considering the main channel side and top bars.

4.5.6. HYDRAULIC CHANGES

The variability of transport capacity was computed by considering the morphological changes observed previously. The morphological changes observed in the cross section 2 lead to higher average Shields numbers as calculated (for a given flow rate) in early May compared to late June (Figure 4.12-c), despite the smaller grain size in June (Figure 4.11). Local Shields number distributions (τ_{84}^* , calculation detailed in appendix A) also showed differences over the whole cross section due to morphological changes (Figure 4.12-a, Figure 4.12-b). Shields numbers were more uniformly distributed around 0.025 (for $Q=10\text{m}^3/\text{s}$) in late June with fewer low and high values. A similar trend was observed at $20\text{m}^3/\text{s}$ discharge. The decrease of high-percentile Shields numbers during the season was consistent with a decrease in bedload rate for similar flow rates, as observed in Figure 4.4. This suggests that high-percentile Shields numbers control the bedload fluxes exported from such braided reaches as observed in flume experiments by Bertoldi et al. (2009). It is also consistent with the fact that tracked pebbles were found only within the main active channel.

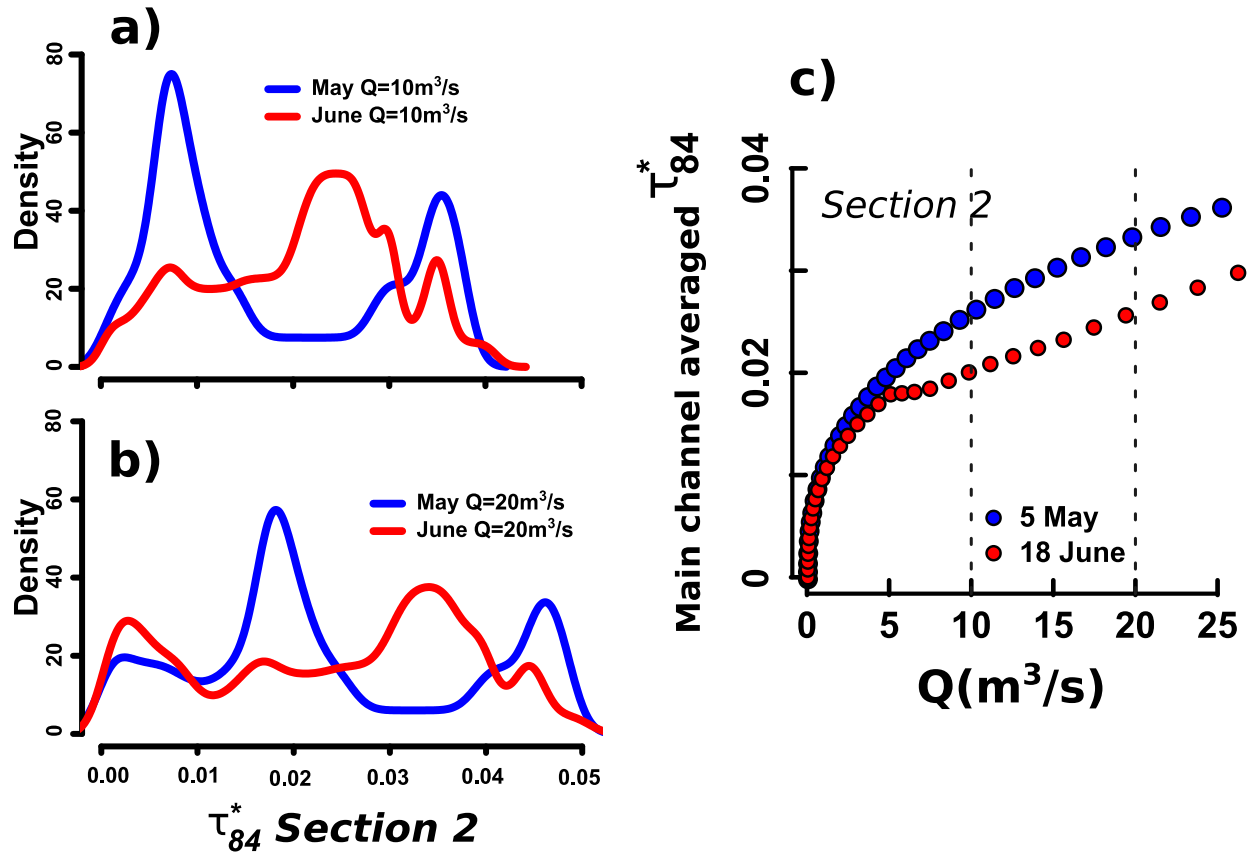


Figure 4.12: Probability density distribution of local Shield number calculated for a flow rate of (a) $10 \text{ m}^3/\text{s}$ and (b) $20 \text{ m}^3/\text{s}$ at the beginning and at the end of the campaign. (c) Averaged Shields number calculated in the main channel as a function of the flow rate, considering cross section 2 and grain size distribution at the beginning and at the end of the campaign.

4.6. DISCUSSION

4.6.1. ON THE INTEREST TO COMBINE MULTIPLE FIELD TECHNIQUES

To quantify the interactions between bedload and morphology, both high spatial and temporal resolutions are required as bedload transport is highly variable at various time scales (instantaneous, event-based, or seasonal scale) and morphological changes have a large spatial extent. This field campaign on a particularly suitable site (high predictable flow and sediment transport variability during 2 months, accessible riverbed, feasible direct sampling) shows that the combination of novel, continuous indirect measurements (seismics), direct field measurements (bedload sampling, cross section survey, pebble tracking), and drone-based and ground-based remote sensing imagery

provides an informative set of observations on the dynamics of a complex braiding system. The combination of these measurements is a promising way to quantify bedload and morphology interactions. Indeed the joint measurements of bedload directly and seismic signals allowed us to detect unambiguous decrease through time over the two months period of the bedload activity which would have been difficult to conclude using only one of the two measurements. As direct measurements of bedload are time consuming and not always achievable, they are often sparse in time. Even though a rather high number of bedload direct measurement (60) could have been done during this field campaign given the good access facilities to the site and the presence of a field team on site, less measurements were available for example by the end of the June (Figure 4.4). The fact that the continuous seismic monitoring provided measurements at that period and showing the same trend, allowed us to be more confident on the decrease with time of the bedload activity. Conversely, while seismic monitoring is continuous, it cannot easily be inverted to estimate bedload flux and benefited from the comparison with direct measurements. Future studies should focus on using direct sampling to better understand the seismic signal so that this type of data can be properly inverted into bedload flux.

Also, interesting perspectives were observed concerning the use of the low-cost geophone (*Seismic2* station in Figure 4.2). This environmental monitoring station was installed with a solar panel power-supply and a vertical geophone GS20-DX Geospace® (8 Hz natural frequency). This low-cost and low-power consumption station has the advantage to allow seismic recording during long time-period in remote environmental conditions. *Seismic2* is installed close to the main channel, on the left river bank (few meters from the main channel, 40m upstream the gauging station, Figure 4.2). A three-step signal conditioning was performed with an electronic interface (Navratil et al, 2013): i) the signal of the geophone is rectified; ii) a low-pass filter (from $f_c=0.5\text{Hz}$ to 80Hz) is applied; iii) the signal is amplified and finally recorded (5-Hz sampling frequency) with a Arduino Uno® open-source microcontroller. The signal amplitude (in mV) thus directly derived from the seismic energy integrated in the frequency band 0-80Hz. This low cost station also detected the decrease with time of bedload intensity (Figure 4.13). While the inversion of this signal needs future development, such low-cost device could for instance be used to develop a monitoring network at a larger spatial scale to detect when bedload occurs in the different branches of a catchment.

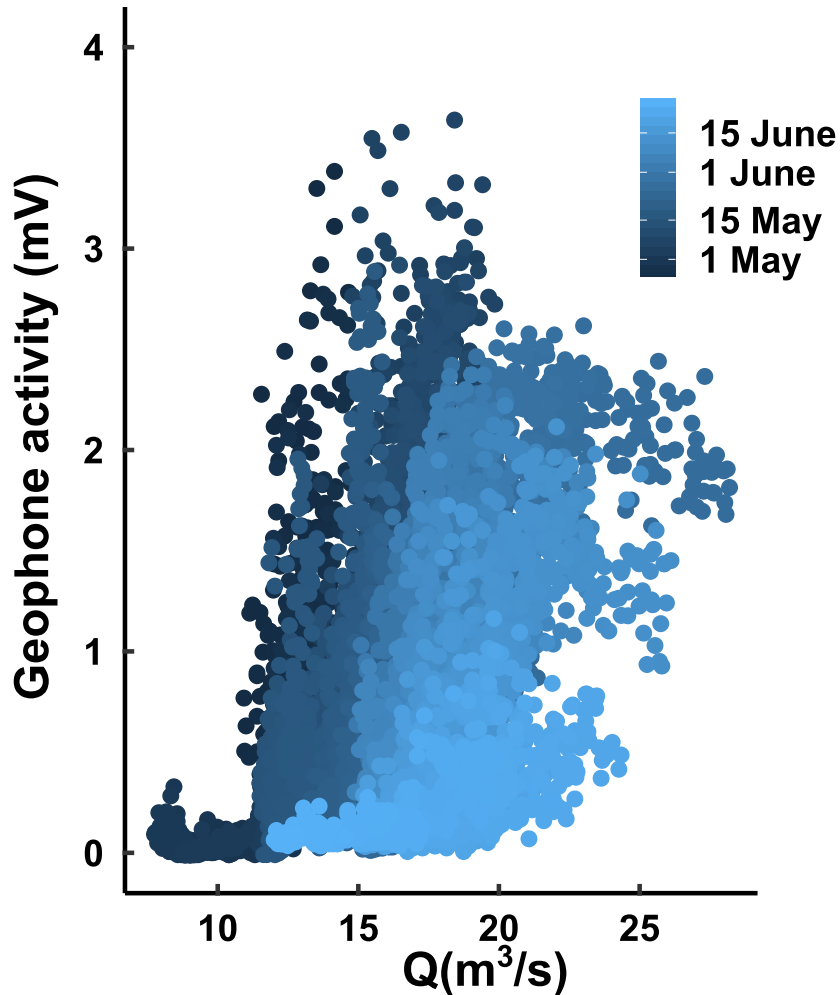


Figure 4.13: Low-cost geophone activity (Seismic2 in Figure 4.2) as a function of flow rate during the two-month field campaign.

By combining complementary techniques such as pebble tracking, ground time-lapse cameras, direct cross section surveys, and drone imagery, we were able to quantify spatial morphological changes (bed mobility, lateral and vertical changes). Similarly to bedload measurements, we should stress that it would not have been possible to draw clear and robust conclusions by using only one of these techniques alone. Lidar data permitted to quantify elevation changes with a large spatial extent but were sparse in time (2 dates) and concerned only emerged bars excluding most changes in our case (Figure 4.8). Consequently, the repeated cross section surveys to quantify locally underwater elevation changes appeared to be essential as other remote measurements were not efficient in these zones considering our field campaign conditions: no signal return for Lidar, too high turbidity for any bathymetric estimation using SFM or colorimetry techniques. They were also essential to estimate hydraulic parameters

related to bedload transport. While ground-based camera is challenging to use as a quantitative measurement [Benacchio *et al.*, 2017] such technique was really useful to qualitatively confirm the other observations with a high temporal resolution. Adding information of pebble tracking, a dynamic measurement of morphology changes, permitted to analyze the longitudinal dynamic and the location of bedload transport in the reach. It confirmed that the main channel was the most active area which corroborates that average hydraulic parameters related to bedload transport should preferentially be calculated in that zone. Future studies using similar tracking protocol should carefully consider the injection point as it could have a significant effect on the tags propagation.

4.6.2. INTERACTION OF BRAIDED RIVER BED MORPHOLOGY WITH BEDLOAD FLUXES

The whole set of results acquired during the field campaign suggests that bedload fluxes and morphological changes are co-evolving during the two months melting season. In this period, a significant decrease in the bedload rate for a given discharge was observed with both direct sampling and indirect seismic measurements. Simultaneously, the braided bed morphology evolved from an incised to a more homogeneous river bed configuration. Similar aggradation processes in braided reaches during melting season have already been observed in Switzerland by Warburton (1994) or on longer time scale in California by Pryor *et al.* (2011). In the studied reach, aggradation caused a decrease in flow depth and a subsequent decrease of the high percentiles of Shields numbers for a given flow rate. This simultaneous decrease in both bedload rate and high percentiles of shield numbers is consistent with observations made in flume experiments showing that, excluding extreme events, only few zones were actually active in braided streams [Bertoldi *et al.*, 2009]. This is confirmed by the fact that during the a-UHF tags prospection, no pebbles were found in secondary channels or on bars indicating that coarse bedload was transported predominantly in the main channel and that average hydraulic parameters controlling bedload transport (Shield number, dimensionless stream power) should preferentially be calculated in that zone. Pebble tracing also suggested that the active braided zones may act as buffers and that pebbles are transferred efficiently between these buffer zones.

All of these observations show that a strong link exists between bedload and morphological changes in braided streams, which is in agreement with previous field and flume studies [Bertoldi *et al.*, 2009; Lane *et al.*, 1996; Liebault *et al.*, 2013]. Also, our study suggests that bedload rate and morphological changes are more closely related in the braiding sections (S1, S2, S4) than in the constrained ones (S5), in which bedload fluxes may not result from local bed mobilization. The following observations support this conclusion:

- (i) No morphological changes were observed in the constrained section while large changes were observed in the braiding one,
- (ii) Tracked pebbles resided longer in the braiding section as compared to the constrained one,
- (iii) The average transported grain size distribution was similar to the bed grain size distribution found in the main channel side of the braided reach while the constrained section had a much coarser bed,
- (iv) Much lower Shields values for a given bedload rate were determined for the constrained section compare to the alluvial ones,

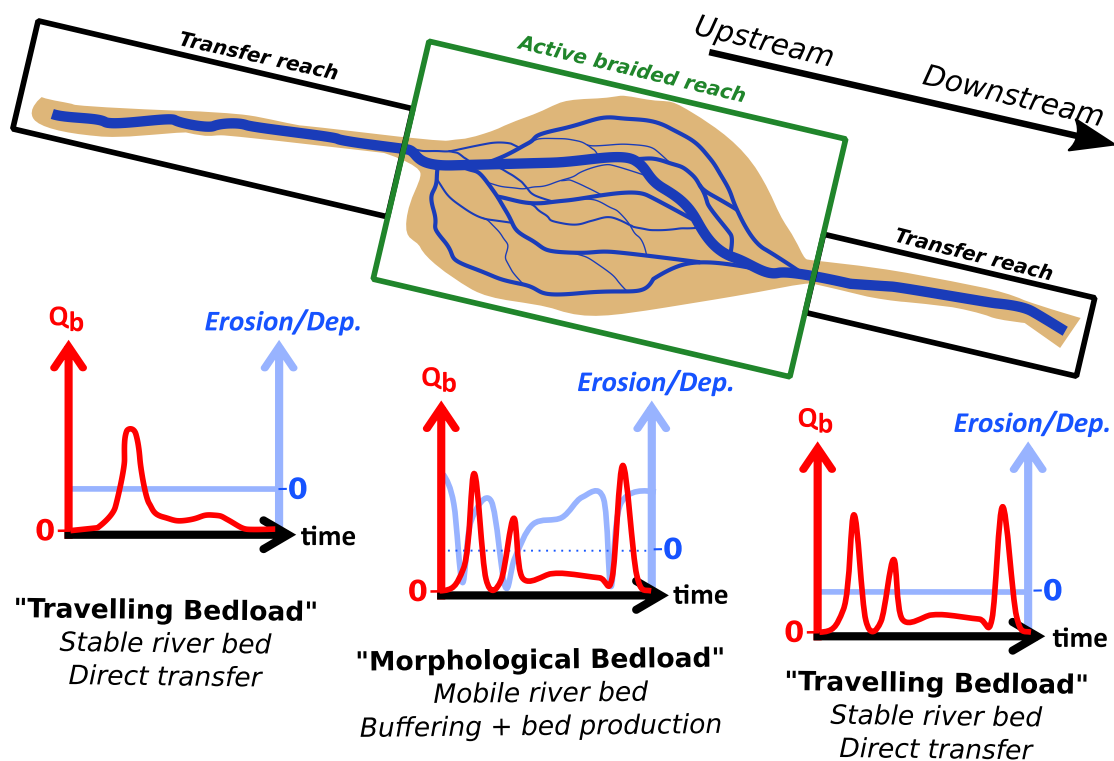


Figure 4.14: Conceptual diagram illustrating the influence of braiding on bedload transfer in alternating constrained (transfer) and unconstrained (alluvial) reaches typically found in Alpine streams. The transfer reaches are for most floods non-active in terms of morphology and can efficiently transfer bedload material from upstream (supply limited). There is no relation between bedload fluxes and bed morphology changes. The alluvial reaches (here braiding) can adapt their morphology to hydraulics and upstream sediment fluxes resulting in a strong relation between morphological changes and bedload exported downstream (transport capacity limited). " Q_b " denotes bedload fluxes; "Erosion/Dep." denotes erosion and deposition processes leading to morphological changes.

Figure 4.14 shows a conceptual scheme, linking bedload and bed morphology in rivers with alternatively unconstrained and constrained sections. Alluvial reaches have bed morphology that may respond rapidly, through flow width, grain size distribution, etc., to local hydraulic forcing and upstream bedload fluxes. Such reaches could thus buffer upstream bedload fluxes and can be considered a source of sediment for downstream reaches: a strong link exists between morphological changes and bedload fluxes (morphological bedload, transport capacity limited). On the contrary, bed morphology in constrained reaches cannot adapt to local hydraulics and upstream bedload forcing under most conditions (extreme events excluded): upstream bedload fluxes are efficiently transferred without bed morphological changes according to the travelling bedload concept (supply limited) proposed for steep torrents, highly connected to hillslope sources [*Piton and Recking, 2017*].

4.6.3. *IMPLICATIONS FOR REACH-AVERAGED BEDLOAD MODELING*

A noticeable interest of the complete data set acquired during this study is that it allows to build and run physically based and fully distributed numerical models to go further in the understanding of the bedload and morphology interactions and to test assumptions about the drivers of these interactions. This analysis will be conducted in the near future. Nevertheless, we should stress that our results also have general and immediate implications for the estimation of bedload rates in systems with alternating constrained and unconstrained sections for which direct bedload measurements are scarce. A key consideration is to choose where bedload calculation should be made to estimate bedload transport [*Recking et al., 2016*] as confirmed by the variability of Shields number associated with a given measured bedload transport rate (Figure 4.5-c). As discussed previously, bedload transport is better related to morphodynamics in the braided sections than in the constrained sampling cross section S5. We thus applied in both the braided and constrained sections the Recking bedload formula (presented in Appendix A) which is a relation between average Shield parameters and bedload transport rate (calibrated and validated on a large field dataset). Predictions were significantly improved when considering alluvial sections (S1, S2 and S4) compared to the constrained and paved one (S5) (Figure 4.15) which is consistent with a limited production of bed material in the transfer reach compared to in the studied upstream braiding reach. The seasonal variability of the cross section and grain size distribution was considered for cross section 2. This led to small differences in term of predictions, compare to spatial differences due to the choice of cross section. This shows that applying bedload formula in such system should preferably be done in alluvial, morphodynamically active zones.

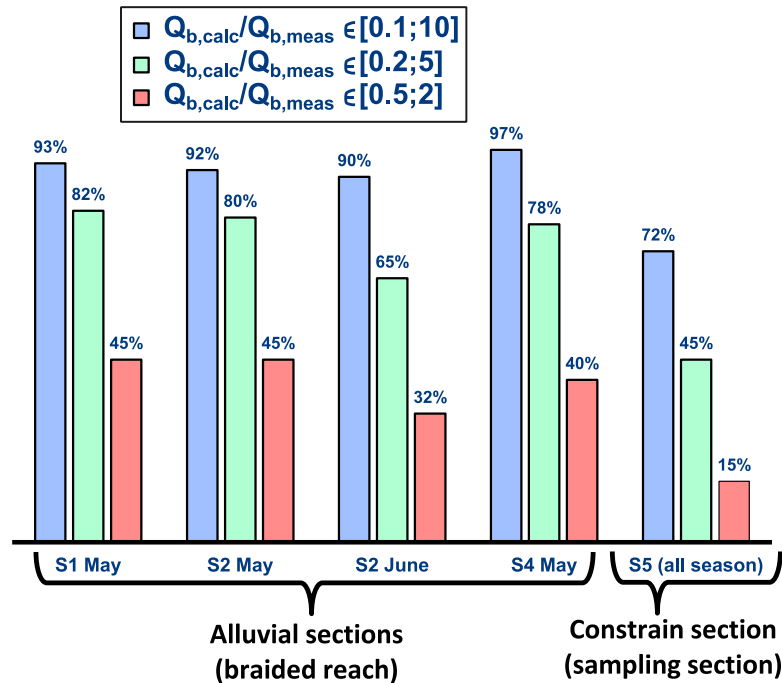


Figure 4.15: Predictions obtained with the Recking bedload formula depending on the cross section and date considered. To quantify the goodness of predictions, we calculated the percentages of ratios $Q_{b, calculated}/Q_{b, measured}$ that fell in the ranges [0.1-10], [0.2-5] and [0.5-2]. S1, S2 and S4 correspond to alluvial cross sections (in the braided reach) while S5 is the cross section where bedload fluxes were measured (constrained and paved reach).

4.7. CONCLUSION

In this paper we analyzed the relation between bedload transport and morphodynamic in a typical Alpine braided river by combining multi-physical measurements. We show that such approach combining both traditional direct measurements with novel indirect techniques permits a much deeper understanding of the physical processes often difficult to capture in the field with a single instrument. This study also highlights the interest to measure simultaneously bedload transport processes and river bed morphology changes. This is particularly relevant in braided river: strong interactions were observed between bedload transport and morphodynamics on the study site. These detailed observations confirm flume-derived hypotheses stating that bedload particles in braided rivers are mostly transported in concentrated zones where shear stresses are high. Our observations showing that aggradational or degradational phases exert a significant control on bedload fluxes exported downstream are also in line with longer-term field observations. Finally, these results have been shown to have important implications for modeling bedload in braiding rivers in the field.

While consistent observations were made in this study, braided rivers morphodynamic and bedload transport stay highly complex processes. For this reason, we think that future research should continue to combine such a large panel of techniques. For instance, this could consist of inverting the seismic signal by using direct sampling or combining high-frequency imagery, pebble tracking, and a seismic array to localize with a high temporal resolution bedload transport path and intensity.

4.8. ACKNOWLEDGMENTS AND DATA

This project was founded by IRSTEA and Électricité de France. Data supporting the content of this paper can be obtained by contacting IRSTEA (C. Misset or A. Recking). The authors are grateful to D. Vázquez-Tarrío, E. Gronlier, J. Paloucek and F. Bonazzi who helped for the field measurements; E. Mermin, F. Ousset and P. Tardif who helped to perform the drone flights.

4.9. NOTATIONS

The following symbols are used in this paper.

D_{50}	Sediment diameter of the bed such that 50% of the mixture is finer [m]
D_{84}	Sediment diameter of the bed such that 84% of the mixture is finer [m]
D	Sediment diameter [m]
τ^*	Shields number: dimensionless shear stress [-]
τ_{84}^*	Shields number for D_{84} [-]
τ_m^*	Dimensionless transition parameter between partial and full mobility [-]
Q	Water discharge [m^3/s]
U	Mean water velocity over the section [m/s]
u^*	Friction velocity [m/s]
W	Channel bed width [m]
S	Channel bed slope [m/m]
ρ	Water density [kg/m^3]
ρ_s	Sediment density [kg/m^3]
s	Relative density of sediment [-]
g	Gravitational acceleration [m/s^2]

d	Mean water depth [m]
q	Unit water discharge [$m^3/s/m$]
Q_b	Bedload [kg/s]
q_b	Unit bedload [kg/s/m]
q_b^*	Dimensionless bedload [-]
P_b	Seismic power [m^2/s^2]
L_t	Cross section width [m]
L_i	Width considered representative for the sampling point I [m]
L_e	Sampler width [m]
$Q_{be i}$	Bedload rate for each sample [g/s]

4.10. APPENDIX A

4.10.1. HYDRAULICS CALCULATION

To estimate the main hydraulics parameters (velocity, hydraulic radius and water depth) at a given cross section from the measured discharge Q , we used the Ferguson (2007) flow resistance equation in an iterative way:

$$\frac{U}{\sqrt{gR_h S}} = \frac{2.5 \frac{R_h}{D_{84}}}{\sqrt{1 + 0.15 \left(\frac{R_h}{D_{84}}\right)^{5/3}}} \quad (4.3)$$

Where S (-) is the river bed slope, D_{84} (m) the 84% percentile of the grain size distribution, R_h (m) the hydraulic radius, U ($m s^{-1}$) the mean flow velocity and g ($m s^{-2}$) the gravity acceleration.

It was then possible to estimate a local or an average Shield number (τ_{84}^*) with respectively the local water depth (d) in the cross section or an averaged hydraulic radius (R_h) in the main channel:

$$\tau_{84}^* = \frac{\rho g d S}{(\rho_s - \rho) g D_{84}} \quad (4.4)$$

where ρ is the water density, ρ_s is the sediment density. This method was used to compare the bed mobility associated to morphological changes between the beginning and the end of the campaign.

4.10.2. BED LOAD CALCULATION

Many equations have been proposed in the literature and could be used to predict bedload. To test where bedload calculation should be used in alternatively braiding and constrained sections, we choose to test the one proposed in Recking (2010), Recking (2013) and Recking *et al.* (2016), Eq.(4.5) and Eq.(4.6). It was specifically developed from field data for reach average computation and was validated with a large independent data set. The input parameters are Q , W , S , D_{50} and D_{84} .

$$q_b^* = \frac{q_b}{\rho_s \sqrt{g(s-1)D_{84}^3}} = \frac{14\tau^{*2.5}}{1 + \left(\frac{\tau_m^*}{\tau^*}\right)^4} \quad (4.5)$$

where q_b ($\text{kg s}^{-1} \text{m}^{-1}$) is the unit bedload transport per unit width, $s = \rho_s/\rho$, ρ_s is the sediment density, ρ is the water density, and g is the gravity acceleration. In Eq.4.5 the parameter τ_m^* defines the transition between partial transport and full mobility. It depends on the morphology of the stream [Recking *et al.*, 2016] and was calculated using the following equation:

$$\tau_m^* = 1.5S^{0.75} \quad (4.6)$$

This formula was used with the averaged hydraulics parameters in the main active channel (calculations were made on the website: www.bedloadweb.com). The percentages of well predicted values that fell in a given range were calculated considering a range [0.1-10] (E10), [0.2-5] (E5) and [0.5-2] (E2) as often done to evaluate sediment transport formula.

4.10.3. RESAMPLING TECHNIQUE TO DETECT TEMPORAL TREND ON BEDLOAD SAMPLING

To test the significance of a temporal trend in bedload transport flux, the following resampling procedure was adopted on the bedload samples (N=60):

- i) 5000 selections of N_r random samples are performed ($N_r < N$),
- ii) For each random selection, a log-linear model is fitted between the N_r bedload rates and flow rates,
- iii) For each regression, a linear model is fitted between the residuals and the time,

- iv) The significance of this relation of residuals through time is analyzed through its p_{value} . The temporal trend is considered significant if the 5000 p_{values} obtained are lower than 0.05,
- v) These steps are repeated by varying N_r from 59 to 40.

4.11. APPENDIX B

4.11.1. GROUND-BASED CAMERA OBSERVATIONS



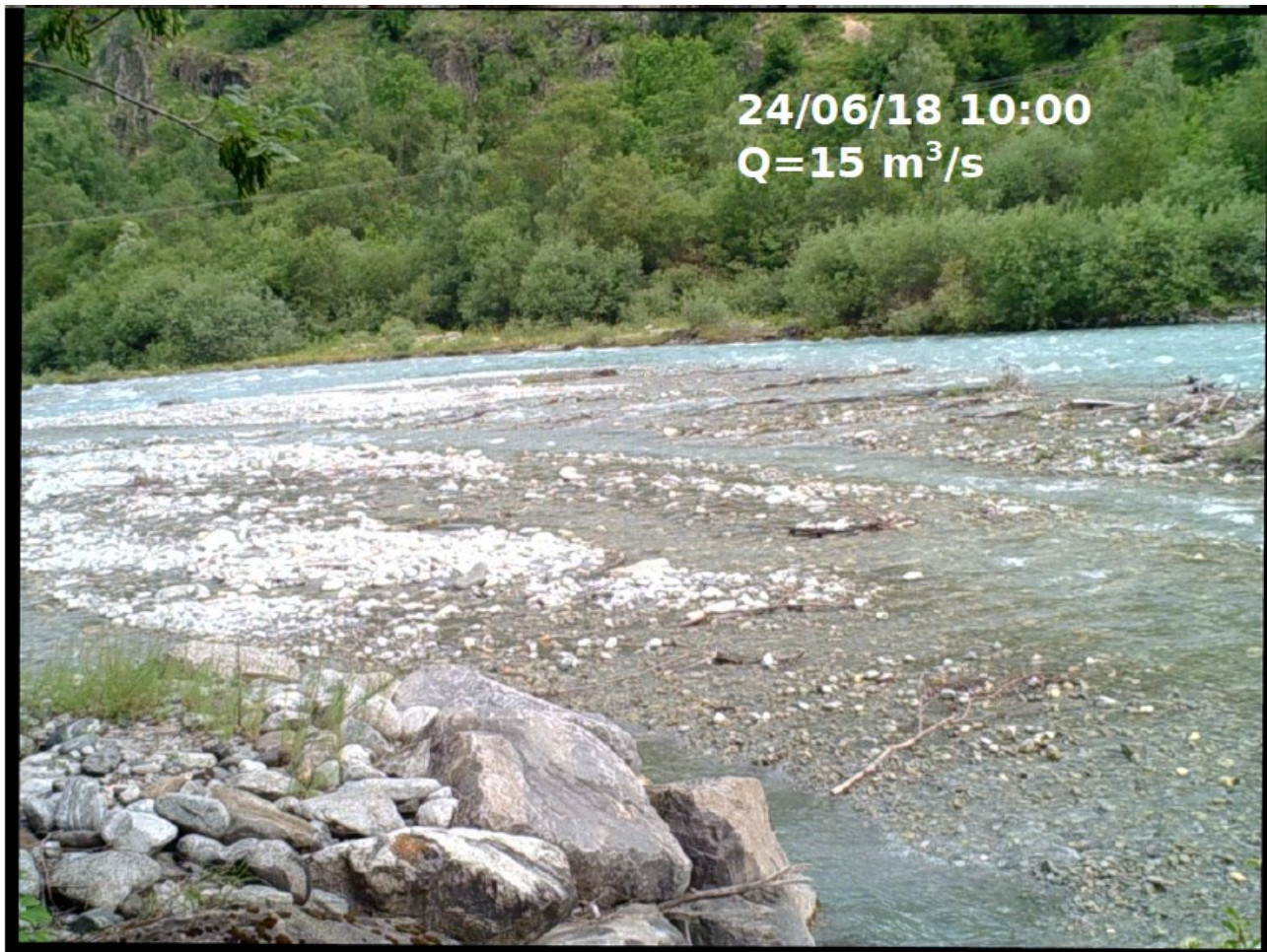


Figure 4.B.1: Ground-based camera pictures of the middle of the braided reach, (c) in Figure 4.2.





Figure 4.B.2: Ground-based camera pictures of the outlet of the braided reach.

4.12. APPENDIX C

4.12.1. BED LOAD MEASUREMENT

Date (UTC+1)	h (m)	Q station (m ³ /s)	Q _b (g/s)
30/04/2018 18:00	0.87	13.20	1327
02/05/2018 14:20	0.72	8.99	264
02/05/2018 15:10	0.72	9.03	57
02/05/2018 16:10	0.72	8.96	5
06/05/2018 17:10	1.03	16.63	2568
07/05/2018 16:00	1.04	17.34	4098
07/05/2018 18:50	1.07	18.05	3415
09/05/2018 11:00	1.02	16.44	7897
09/05/2018 18:30	1.08	18.82	4458
14/05/2018 16:50	0.92	13.92	159
14/05/2018 19:20	0.92	13.69	378
14/05/2018 13:30	0.92	13.55	832
14/05/2018 14:10	0.92	13.81	925
14/05/2018 15:20	0.92	13.69	903
14/05/2018 15:50	0.93	14.30	1180
15/05/2018 14:50	0.87	11.71	161
15/05/2018 15:40	0.87	12.08	86
15/05/2018 16:10	0.87	12.05	117
15/05/2018 16:50	0.87	12.22	253
15/05/2018 17:30	0.87	12.14	232
15/05/2018 18:20	0.87	12.43	223
30/05/2018 08:45	1.08	18.65	4883
30/05/2018 09:10	1.08	18.99	1857
30/05/2018 09:32	1.09	18.22	6031
30/05/2018 14:39	1.03	18.05	1290
30/05/2018 15:00	1.03	17.07	3837
31/05/2018 08:32	1.02	16.78	994
31/05/2018 09:00	1.02	17.00	1140

31/05/2018 13:10	0.99	15.91	1661
31/05/2018 16:20	1.03	16.72	2535
31/05/2018 16:55	1.02	16.85	6208
01/06/2018 07:48	0.96	15.37	391
01/06/2018 08:13	0.96	15.49	770
04/06/2018 17:00	1.02	17.76	2081
04/06/2018 17:30	1.02	17.86	2715
04/06/2018 18:10	1.04	18.25	5985
04/06/2018 18:30	1.04	17.53	4004
05/06/2018 13:26	1	16.04	1215
05/06/2018 13:45	1	16.50	863
06/06/2018 09:18	1.02	17.82	897
06/06/2018 10:25	1.03	17.37	3013
06/06/2018 09:52	1.02	18.09	417
06/06/2018 11:30	1.03	16.88	1093
06/06/2018 12:00	1.01	17.30	1145
07/06/2018 09:02	0.94	15.49	903
07/06/2018 09:35	0.97	16.10	548
07/06/2018 10:15	0.98	15.67	709
07/06/2018 20:12	1.18	22.23	1251
11/06/2018 13:42	1.27	25.15	3183
11/06/2018 14:08	1.27	24.07	7856
13/06/2018 09:00	1.13	20.47	2051
13/06/2018 09:43	1.13	20.23	3651
13/06/2018 10:30	1.1	19.92	921
13/06/2018 11:18	1.13	19.81	830
14/06/2018 14:20	0.97	16.85	569
14/06/2018 15:15	1.05	17.69	243
26/06/2018 10:08	0.87	12.05	33
28/06/2018 09:00	0.88	12.08	144
28/06/2018 09:00	0.88	12.08	152
27/06/2018 11:00	0.87	12.08	43

Table C.1: Direct bedload transport measurement

Time (UTC+1)	Q(m³/s)	Qs (g/s/m)	D₅₀(mm)	D₈₄(mm)	% Sand (<1.6mm)
06/05/2018 17:15	17.6	192.4	12	32	27.9%
07/05/2018 16:30	17.8	307.0	40	70	4.2%
07/05/2018 19:00	18.2	255.8	22	59	13.5%
09/05/2018 11:00	16.9	591.5	42	85	1.5%
09/05/2018 19:00	18.8	333.9	22	54	13.5%
14/05/2018 16:20	13.9	88.4	55	80	0.9%
14/05/2018 14:20	18.8	333.9	11	51	11.1%
30/05/2018 9:32	18.0	451.8	23	66	18.9%
31/05/2018 16:20	17.0	189.9	17	32	5.8%
04/06/2018 17:00	16.9	155.9	40	97	13.1%
04/06/2018 17:50	17.5	203.4	62	87	8.2%
05/06/2018 14:00	16.6	64.7	71	110	7.4%
06/06/2018 10:25	17.5	225.7	54	77	1.0%
07/06/2018 9:00	17.0	85.8	62	87	4.3%
11/06/2018 14:08	24.8	588.5	21	71	11.7%
14/06/2018 14:20	17.3	42.6	9	54	25.0%
13/06/2018 9:43	19.6	273.5	23	59	12.2%

Table C.2: Transported diameter measured.

4.12.2. *BED GRAIN SIZE DISTRIBUTION*

Early May	Percent finer than			
	D (mm)	Gravel bars	Channel side	total
	4	0.18	0.25	0.21
	8	0.23	0.26	0.24
	11	0.25	0.29	0.27
	16	0.29	0.32	0.31
	22	0.31	0.38	0.34
	32	0.37	0.42	0.39
	45	0.43	0.52	0.47
	64	0.55	0.64	0.60

91	0.71	0.75	0.73
128	0.86	0.86	0.86
181	0.96	0.93	0.94
280	1.00	0.99	0.99
340	1.00	1.00	1.00

Table C.3: Bed grain size distribution measured using Wolman count technique in early May in the braided reach (more than 400 pebbles). These measurements were conducted along four lines, two along the main active channel side and two along higher gravel bars.

Late June D (mm)	Percent finer than		
	Gravel bars	Channel side	total
4	0.03	0.17	0.10
8	0.04	0.20	0.12
11	0.07	0.25	0.16
16	0.12	0.35	0.24
22	0.22	0.42	0.32
32	0.34	0.56	0.45
45	0.43	0.72	0.58
64	0.56	0.85	0.70
91	0.72	0.94	0.83
128	0.89	0.98	0.94
181	0.96	0.99	0.98
280	0.98	1.00	0.99
340	0.99	1.00	1.00
560	1.00	1.00	1.00

Table C.4: Bed grain size distribution measured using Wolman count technique in late June in the braided reach (more than 400 pebbles). These measurements were conducted along four lines, two along the main active channel side and two along higher gravel bars.

Chapter 5

Quantifying erosion and deposition of fine sediments in a typical alpine river

This fifth chapter reports a detailed description of fine particles transport and intermediate storage at the event scale in a typical alpine braided river reach (La Séveraisse). The occurrence of interactions between suspended particles and the river bed has been measured and confronted with riverbed mobility and morphodynamic changes. This work has been published in Water Resources Research (DOI: 10.1029/2019WR025222) by Misset C., Recking A., Legout C., Valsangkar N., Bodereau N., Zanker S., Poirel A. and Borgniet L.

Ce cinquième chapitre présente une description détaillée du transport et du stockage intermédiaire de particules fines à l'échelle de l'évènement dans une rivière en tresse typique des Alpes (La séveraisse). L'occurrence d'interactions entre particules transportées par suspension et le lit de la rivière a été mesurée et confrontée aux changements de mobilité et de morphodynamique du lit. Ce travail a été publié dans Water Resources Research (DOI: 10.1029/2019WR025222, contributeurs Misset C., Recking A., Legout C., Valsangkar N., Bodereau N., Zanker S., Poirel A. and Borgniet L).

5.1. ABSTRACT

The transport of fine particles as suspension is associated with important social, economic and environmental issues, especially in mountainous rivers. It is still unclear, however, how fine particles eroded on hillslopes are transferred downstream through the river system. Whereas the finest fraction has long been considered as washload, with limited interactions with the river bed, recent field and flume studies have demonstrated that in gravel bedded streams, large quantities of these fine materials can be found in the bed matrix, suggesting the opposite. Both the quantification of these interactions and control parameters remain poorly known. In this study, we aimed to investigate these processes by applying a sediment budget approach to a typical 3.5-km-long alpine braided reach located in the French Alps. Using high-frequency suspended load measurements combined with Monte Carlo simulations for uncertainty propagation, we showed that the buffering behavior of the braided reach studied was non-negligible at various time scales. Thirty-three of the 48 events observed during the 2 months of the campaign showed significant differences between upstream and downstream suspended sediment yield (SSY) even if the reach studied was short compared to the upstream drainage area (130 km²). These differences at the event scale varied between a net erosion equivalent to 51% of upstream SSY and a net deposition equivalent to 71%. At a nearly instantaneous time scale, the flow rates and sediment concentrations were found to control deposition and remobilization of fine sediments in a different way: the erosion fluxes increased as the water discharge increased until a given suspended sediment concentration from which deposition fluxes increased as the concentration rose, whatever the discharge. Finally, coarse particle mobility and morphological changes in the braided reach appeared to have a strong influence on the conditions allowing erosion or deposition of fine particles. These observations have important implications for our understanding of the transfer of fine particles in gravel bedded streams.

5.2. INTRODUCTION

Suspended sediment loads in rivers have been widely studied in the last decades given that they are associated with important socioeconomic and environmental issues [Kondolf *et al.*, 2014; Vercauteren *et al.*, 2017; Walling *et al.*, 2003]. This is particularly true in mountainous and Mediterranean catchments where high suspended sediment yields (SSYs) are generally observed [Vanmaercke *et al.*, 2011]. The transport of the finest particles has long been considered as washload, i.e., the fraction of the load transported by the flow over long distances without interacting with the river bed. However, this concept has been largely questioned in the recent literature with several studies demonstrating that suspension can strongly interact with the bed, even for the finest fractions. Unraveling the relative significance of washload in fine sediment dynamics is very important because it has strong implications for modeling suspended

load transport. It also conditions our capacity to plan what could be the real impacts of sediment release in the river network, such as during dam flushing operations. This question has motivated this work, which is based on a detailed description of fine sediment dynamics at the reach scale of a typical alpine stream, the Severaisse River in France.

The washload concept is based on a very comprehensive analysis of several material and hydrodynamic properties, such as the percentage of fines at the bed surface [Einstein *et al.*, 1940], the critical Rouse number [Wang and Dittrich, 1992; Wang *et al.*, 2007], the absolute particle size [Partheniades, 1977], a critical size ratio (bed material vs washload material) or the balance between sediment supply and transport capacity [Hill *et al.*, 2017]. However, recent field and flume studies have demonstrated that even the finest particles are present in large quantities in the bed sediment matrix of gravel bed rivers [Hill *et al.*, 2017; Mooneyham and Strom, 2018; Navratil *et al.*, 2010]. Of course part of this material could result from local production (mechanical and chemical alteration of the coarser particle in place or organic matter degradation), but it also questions the real dynamics of fine sediments transported in presence of a coarse material mixture, especially in alpine streams, where very turbulent shallow flows strongly interact with the bed [Legout *et al.*, 2018]. Therefore, questions arise as to the real interactions with the local morphology (deposition/remobilization) and the related grain processes (infiltration, kinetic sorting). Direct field observations of such interactions are still needed to quantify these processes, especially in a mountainous context.

Most field investigations were conducted at the catchment scale considering the outlet of the catchment and the main tributaries [Navratil *et al.*, 2012; Piqué *et al.*, 2014; Smith *et al.*, 2003]. Fewer approaches were applied on smaller reaches to understand the mechanisms controlling deposition and resuspension. Most of them were conducted in a small proglacial area for glacial denudation rate estimation [Guillon *et al.*, 2018; Orwin and Smart, 2004b]. This approach was also used downstream of a small tributary reconnection in northwest England [Marteau *et al.*, 2018]. All of these studies reported a significant contribution of the reach studied in the sediment budget for an annual or a seasonal time scale. Guillon *et al.* (2018) concluded that the reach studied acted as a buffer for suspended fluxes while Orwin *et al.* (2004) concluded that the proglacial reach studied controlled the fluxes exported in that it delivered 80% of downstream fluxes during the 2 months of their field study. This type of information is still missing in mountainous alluvial rivers. Therefore, the objectives of the present study were to i) analyze the dynamics of fine sediments passing through a typical braided river reach characterized by its morphology, hydrology and bed mobility, ii) assess the extent to which erosion and deposition of fine sediments could be demonstrated and iii) isolate parameters controlling erosion and deposition of fine particles and their relation with the general morphodynamics. This was done by measuring, during a 2-month melting

season, transport rates, erosion and deposition of fine particles in a representative alpine braided reach using a sediment budget approach considering the local morphology changes and bedload transport coupled with an uncertainty analysis based on Monte Carlo simulations.

5.3. AREA STUDIED

The Séveraisse catchment located in the southeast French Alps in the Ecrins massif was chosen to investigate the importance of erosion and deposition processes of fine particles (Figure 5.1). The downstream station has a 130-km² catchment area characterized by a low human impact (no dams or water intakes) and highly active sediment sources on the upstream part of the catchment [Helsen *et al.*, 2002]. The river has alternative braiding and more constrained sections with a slope between 1% and 2%. Some glaciers are located on the upper part of the basin (maximum altitude, 3579 m NGF). The hydrology is characterized by a melting period (May–June), which was chosen for the field campaign to ensure high flow variability. The reach studied, nearly 3.5 km long, comprises two braiding sections connected by a narrower constrained reach.

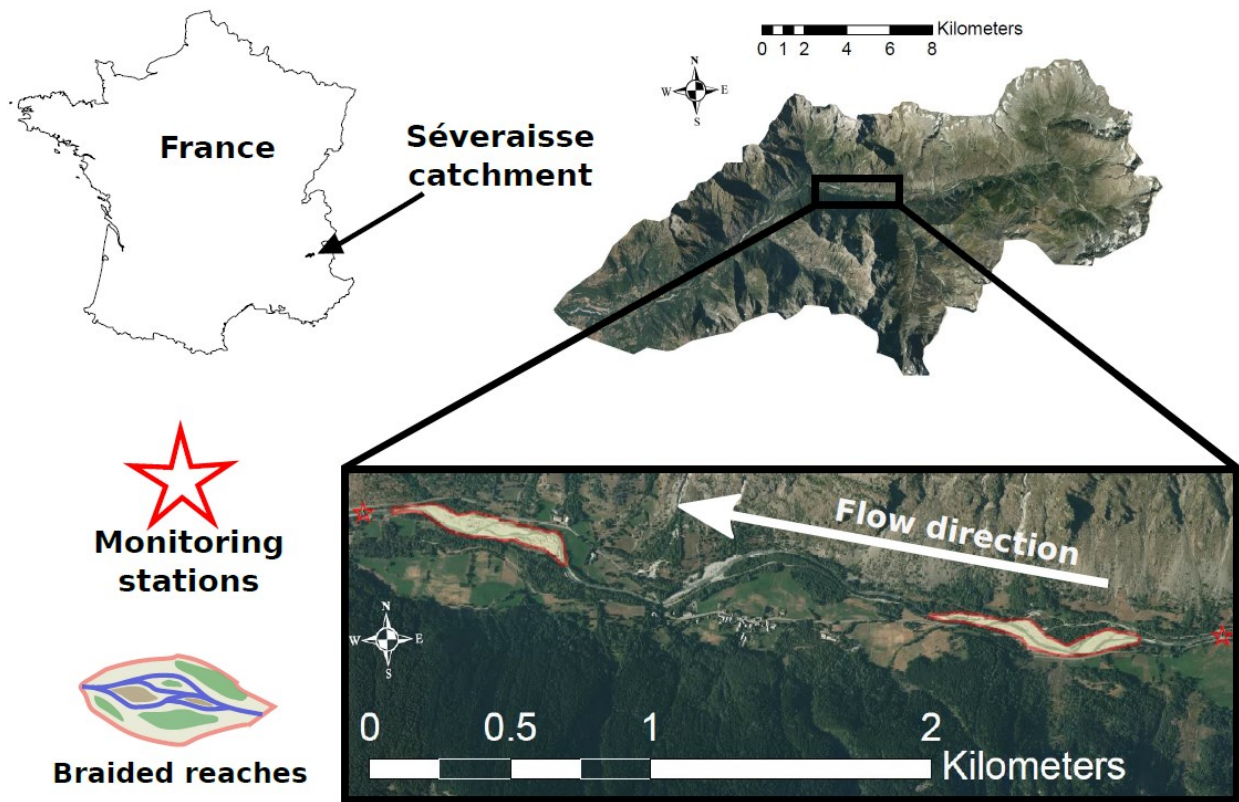


Figure 5.1: Catchment location

5.4. MATERIAL AND METHODS

5.4.1. FINE SEDIMENT BUDGET FRAMEWORK

The following framework was applied to the Séveraisse reach. Upstream ($SSL_{upstream}$) and downstream ($SSL_{downstream}$) suspended sediment loads were measured to investigate erosion fluxes (E) and deposition (D) fluxes occurring in the reach (red stars in Figure 5.1). Of course this approach is valid if no or negligible intermediate sources of fine sediments are present. Small lateral tributaries were monitored with time lapse cameras (one picture every 20 min) to be sure that they were not active during the field campaign.

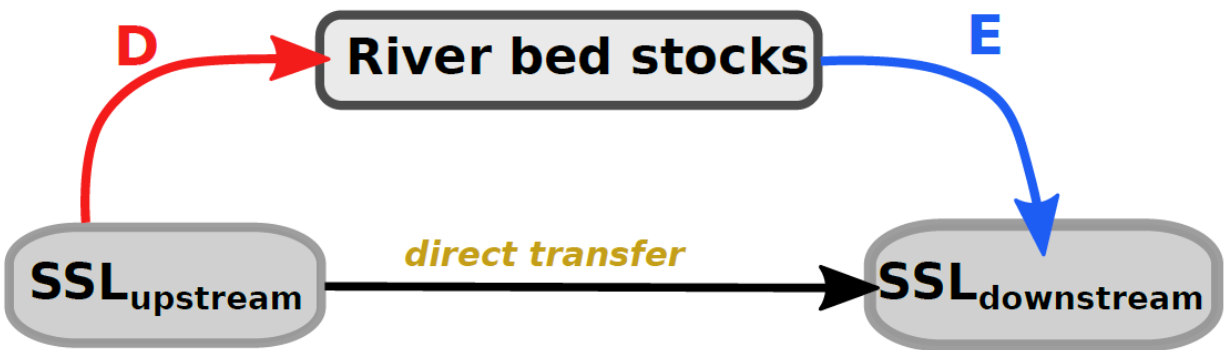


Figure 5.2: Sediment budget approach.

It was then possible to apply the sediment budget approach presented in Figure 5.2 and in the following equations:

$$SSL_{upstream} + E = SSL_{downstream} + D \quad (5.1)$$

$$SSL_{downstream} - SSL_{upstream} = E - D \quad (5.2)$$

$$\frac{SSL_{downstream}}{SSL_{upstream}} = \frac{E - D}{SSL_{upstream}} + 1 \quad (5.3)$$

According to Eq.5.2 and Eq.5.3, dominant erosion generates a positive difference between exiting and incoming fluxes as well as a ratio between these fluxes higher than 1, while deposition generates a negative difference and a ratio lower than 1. If the system is at equilibrium, a ratio of 1 and a difference equal to 0 will be observed.

5.4.2. SUSPENDED LOAD MEASUREMENT

Two suspended load stations were installed upstream and downstream of the reach to measure $SSL_{downstream}$ and $SSL_{upstream}$ (red stars in Figure 5.1). The suspended sediment concentration (SSC) was measured using turbidimeters (Hach Lange Solitax) coupled with sequential samplers (ISCO 3700W) containing 24 1-L bottles. An average value of turbidity measured for 1 min was recorded every 10 min. Sequential samplers took water samples every 2 h during flood events spread over the field campaign (hundreds of samples covering a wide range of suspended concentrations). The water samples were filtered using preweighed 0.7- μm fiberglass filters dried at 100°C for approximately 5 h so that all the water contained in the sample was removed. A calibration curve between turbidity and the SSC was then built, as often done in such field work [Lewis, 1996; Mano *et al.*, 2009; Navratil *et al.*, 2011]. The turbidimeters and sequential sampler's water intakes were fixed at the same location in the cross section, approximately 50 cm above the bottom of the river bed. We assumed that SSC was homogenous over the cross section due to well-mixed and highly turbulent flows and that our SSC measurements were representative of the average SSC over the cross section. This assumption was confirmed by water samples taken twice at three locations in the cross sections, indicating a 6% coefficient of variation (average value over standard deviation) for the SSC in the cross section. However, larger uncertainties associated with the representativeness of the sampling point in the cross section were considered (detailed in the following sections). The suspended sediment load for time step i (SSL_i , kg s^{-1}) was thus computed by multiplying the average SSC (SSC_i , g L^{-1}) by the flow rate (Q_i , $\text{m}^3 \text{s}^{-1}$) at that time step using the following equation:

$$SSL_i = SSC_i \times Q_i \tag{5.4}$$

Downstream flow discharges were provided by Electricité de France (EDF) while the upstream station was maintained during the 2-month campaign by a field team. For both stations, water pressure sensors with 10-min instantaneous measurement frequencies were coupled with several flow rate gauging performed during the field campaign to obtain flow rate time series. Several techniques including salt dilution, the acoustic Doppler current profiler (ADCP), large-scale particle image velocimetry (LSPIV) and current meters were used to measure the flow rates. Rating curves between water levels and flow rates were built. Potential changes in the rating curve due to riverbed mobility were verified daily by local bed topography control.

Suspended load grain size distribution (GSD) was estimated at the upstream station on sediments collected during the field survey with a trap of 10L installed 70 cm above the water intake sampler and the turbidity sensor. The trap intake (5mm²) was positioned vertically and started to capture fine sediments for flow rates exceeding approximately 14m³/s. At the end of the field campaign, a fraction of these sediments were sieved (566

g) using the following mesh sizes: 40 μm , 63 μm , 100 μm , 250 μm , 400 μm , 500 μm , 800 μm , 1250 μm and 2000 μm .

5.4.3. UNCERTAINTY ANALYSIS FOR SUSPENDED FLUXES

Uncertainties associated with suspended load measurements were quantified and propagated using Monte Carlo simulations similar to those used by Navratil *et al.* (2011) and detailed in Appendix 5.9.1. A turbidity fluctuation signal with a 6% coefficient of variation (average value over standard deviation) was measured for the range of turbidity measurements. Concerning the SSC measurements obtained by sampling the turbid water, conservative uncertainties found in the literature (a short review can be found in Appendix 5.9.1) were considered: a $\pm 15\%$ standard deviation due to the representativeness of the sampling point, a $\pm 20\%$ standard deviation due to technical problems with the sampling procedure in the field and a $\pm 3\%$ standard deviation due to laboratory analysis errors. Finally, summing these uncertainties ($\sqrt{15\%^2 + 20\%^2 + 3\%^2}$) leads to a conservative uncertainty of $\pm 25\%$ for the SSC samples. We should stress that this uncertainty does not include the errors related to the regression curve used between turbidity and SSC samples. Using these uncertainty terms on SSC sampling and turbidity measurements, statistical distributions describing the global SSC uncertainties were derived from a first set of Monte Carlo simulations following a procedure presented in Appendix 5.9.1. These distributions (gamma distributions fitted for each turbidity unit and presented in Appendix 5.9.1) account for uncertainties related to the turbidity measurements, the SSC sampling procedure (representativeness of the sampling point, technical problems and laboratory analysis errors) and the regression curve used between turbidity and SSC. They were used to propagate uncertainties associated with SSC measurements on the suspended load at each time step.

Concerning flow rate measurements, a $\pm 3.5\text{-cm}$ standard deviation on the water level was estimated for the two stations. This corresponds to water level fluctuation over 1 min and to the sensor uncertainty. Errors associated with individual gauging (95% interval) varied from $\pm 15\%$ for LSPIV [Jodeau *et al.*, 2017] to $\pm 5\%$ for the other techniques used [Di Baldassarre and Montanari, 2009]. Using these uncertainty terms on Q and water level measurements, statistical distributions describing the global Q uncertainties were derived from a second set of Monte Carlo simulations following a procedure presented in Appendix 5.9.1. These distributions (logistic distributions fitted every centimeter for the water level and presented in Appendix 5.9.1) account for uncertainties related to the water level measurements, the gauging procedure and the regression curve used between flow rate and water level measurements. To extrapolate the rating curve when no gauging was available, the Ferguson (2007) variable power friction law equation (detailed in Appendix 5.9.1) was used with the local grain size distribution, the local river bed slope and the local bathymetry. This equation was

chosen because it is adapted to steep streams with low relative submersion and large bed roughness [Ferguson, 2007; Rickenmann and Recking, 2011]. A $\pm 25\%$ uncertainty on the mean flow velocity calculated was considered. This was based on the analysis of the errors associated with this equation detailed in Rickenmann and Recking (2011) for the local conditions of our sites. These distributions were then used to propagate uncertainties associated with flow rate measurements on suspended load at each time step. Also, before applying any flux analysis, it was verified that upstream and downstream flow rates were consistent together. No trend (increasing or decreasing) on their differences was observed during the 2 months of the field campaign. On average this flow rate difference was $2.1 \text{ m}^3 \text{ s}^{-1}$, which is consistent with the 14-km^2 intermediate drainage area and several flow rate gauging performed on small tributaries draining the alluvial aquifer.

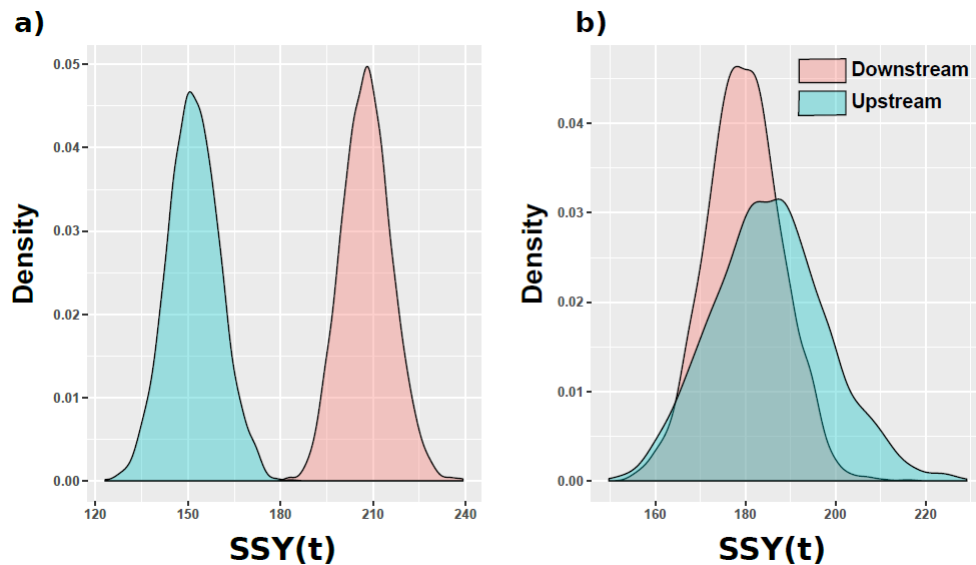


Figure 5.3: Probability density functions of upstream and downstream suspended sediment yield (SSY) obtained after the Monte Carlo procedures for a significant (a) and a nonsignificant (b) difference between upstream and downstream SSY: (a) and (b) correspond to event number 7, which occurred on 11/05/2018 and event number 32, which occurred on 09/06/2018, respectively.

Using the above statistical distributions that describe the global uncertainties on SSC and flow rate, a third set of Monte Carlo simulations was conducted to propagate uncertainties on suspended load (detailed in Appendix 5.9.1). At each time step, statistical models were used to build samples comprising 2000 values of upstream and downstream suspended load, from which we deduced statistical distributions of the upstream and downstream SSY (after integration of the suspended sediment load over a given time period). For each event, this allowed us to build a statistical distribution of differences between upstream and downstream SSY. Upstream and downstream SSY

were considered to be significantly different if the statistical distribution of differences was different from 0 (the distribution of differences is significantly positive or negative). The criterion considered was that the quantiles 2.5% and 97.5% of the statistical distribution of differences had the same sign. Otherwise the difference was considered nonsignificant. Examples of distributions of the upstream and downstream SSY for one significant and one nonsignificant event are presented in Figure 5.3.

5.4.4. FINE SEDIMENT STOCK ESTIMATE

To estimate the available river bed stocks of fine sediments in the reach (Figure 5.2), a sampling strategy proposed by Navratil *et al.* (2010) for that kind of river was used at the beginning of the campaign. The total stock estimates of each river bed sediment facies could then be compared with suspended sediment fluxes and their differences. This stock at the reach scale (St_{reach}) ($t\ dm^{-1}$) was calculated by integrating the mean local stocks for a given storage facies i (\overline{st}_i , $kg\ m^{-2}\ dm^{-1}$) over their area (A_i , m^2) using the following equation:

$$St_{reach} = \sum_{i=1}^4 \overline{st}_i \times A_i \quad (5.5)$$

Four facies were identified in the reach studied. Dried zones were divided considering the percentage of area having a certain cover of fine particles. Type 1 was defined with a maximum 25% of the area covered by fines, type 3 with a minimum 75% of the area covered by fines and type 2 for intermediate situations (Figure 5.4). The fourth facies corresponded to wetted channels at the time of the field measurements. Local stocks for dried facies were measured using a resuspension technique in a container filled with clean water, while underwater stocks were estimated using the Lambert and Walling technique (further detail can be found in Appendix 0). The area occupied by each facies was determined for the downstream braided reach, which was assumed to be representative of both the braided reaches studied. To do so, we used orthophotography built with aerial photographs obtained with a drone flight performed at the beginning of the field campaign. Then the four facies areas were determined from a supervised classification using 115 manually classified samples and the ArcGIS 10.3 maximum likelihood classification toolbox. This stock was integrated on the two braided zones between the gauging stations (Figure 5.1).

To estimate the GSD representative of these stocks measurements, all stocks samples were put together after being dried in the lab and sieved using the following mesh sizes: 50 μ m, 100 μ m and 200 μ m. We also performed surface sampling and estimate the surface dispersed GSD using a laser diffraction sizer (Malvern, Mastersizer 2000) on 6 randomly chosen samples in the reach studied. The dispersed GSD was obtained

following the protocol proposed by Grangeon et al. (2012), i.e. after 10 minutes of pumping, stirring and sonication at maximum level.

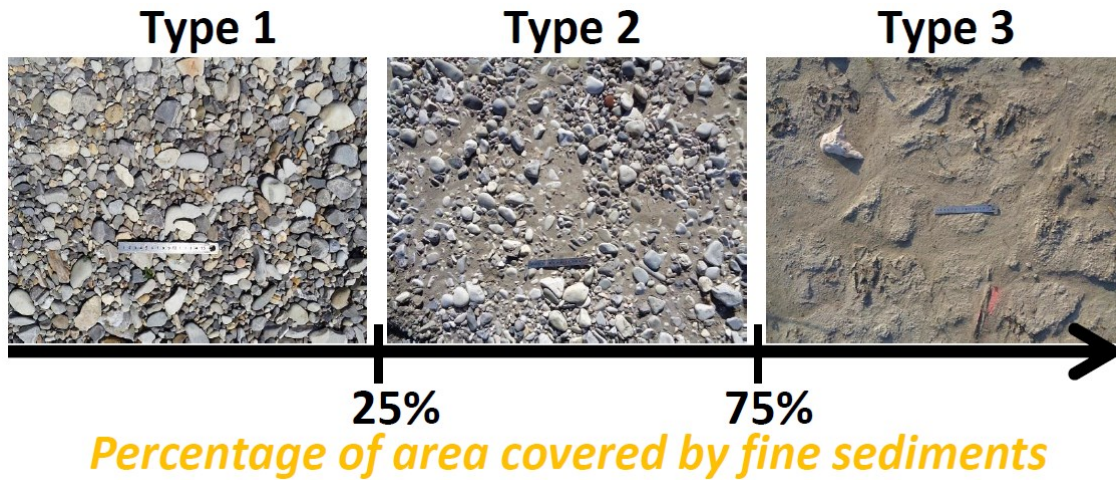


Figure 5.4: Storage facies classification.

5.4.5. BEDLOAD TRANSPORT MEASUREMENT

To quantify the mobility of the river bed and the associated potential release of fine particles, bedload transport was measured at the downstream station during the field campaign (May–June). A pressure difference sampler (Elwah 20.7×12 cm) with a 0.5-mm mesh size was deployed over eight verticals (approximately every 1.5 m) to sample the bedload flux passing through the cross section. The methodology was based on the SEWI method [Edwards and Glysson, 1999] with the sampling duration for each vertical adapted for each transport intensity. The total bedload rate Q_b (g s^{-1}) was calculated using Eq.5.6 in which N is the number of verticals, $Q_{bE i}$ is the bedload rate for each measurement point (g s^{-1}), L_E is the sampler width (m) and L_i is the width considered to be representative of the sampling point i (m):

$$Q_b = \sum_{i=1}^N \frac{Q_{bE i}}{L_E} L_i \tag{5.6}$$

5.5. RESULTS

5.5.1. RATING CURVES

Discharge-water levels and SSC-turbidity rating curves were built for both stations including uncertainties obtained with the Monte Carlo simulations (Figure 5.5). For each of the two stations, a unique rating curve was used between SSC and turbidity since the

relation was stable over time, indicating a more or less constant diameter for suspended particles [Lewis, 1996]. One hundred nine and 105 samples spread over the study period were used for the upstream and downstream stations, respectively. Examples of the statistical distributions representing SSC uncertainties for the downstream station can be found in Appendix 0.

A unique discharge rating curve (12 flow rate gauging used) was built for the downstream station for the whole study period given the high stability of the paved section. Three rating curves (total of flow rate 19 gauging used) were built for the upstream station because the cross section bathymetry changed twice during the field campaign. Transient periods with uncertain relations between flow rate and water level were not considered in further analysis (3.5 days corresponding to approximately 6% of the campaign period, shown in Figure 5.6). An example of the statistical distributions describing the flow rate uncertainties of the downstream station can be found in Appendix 0.

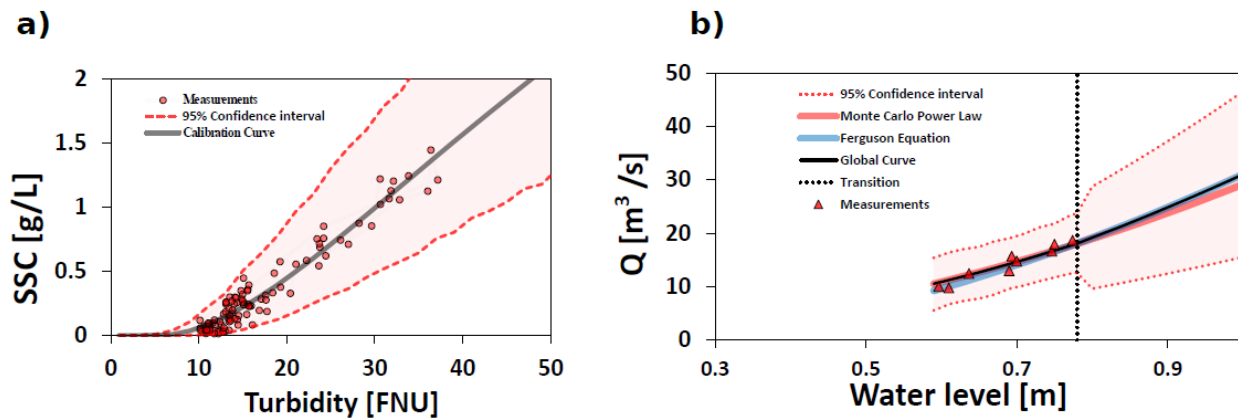


Figure 5.5: Example of rating curve and associated uncertainties for the upstream station (a) between SSC and turbidity or (b) between Q and the water level (enlargement of the envelope corresponds to an increase in uncertainty with absence of data and the use of a friction law).

5.5.2. HYDROSEDIMENTARY DYNAMICS

During the 2-month period, high variability was observed for Q and SSC at the season and the event scales (Figure 5.6-a). For the downstream station, SSC ranged from 0.02 g L^{-1} to nearly 1.2 g L^{-1} during the period while Q ranged from $8 \text{ m}^3/\text{s}$ to $26 \text{ m}^3 \text{ s}^{-1}$. Fluctuations associated with daily snowmelt could be observed on both signals. SSC associated with a given Q was found to decrease as the season advanced. A clear rising and falling limb due to snowmelt could be observed on hydrographs every day. Minimum daily flow rate values were generally observed around 12 am while peak flow rates generally occurred around 10 pm. It was therefore easy to manually define the

beginning, the peak and the end of 48 events during this period (see Appendix 5.9.3 for the main characteristics of the 48 events). An average time delay of 90 min for peak discharge propagation was observed and used to propagate the start and the end of each event from upstream to downstream.

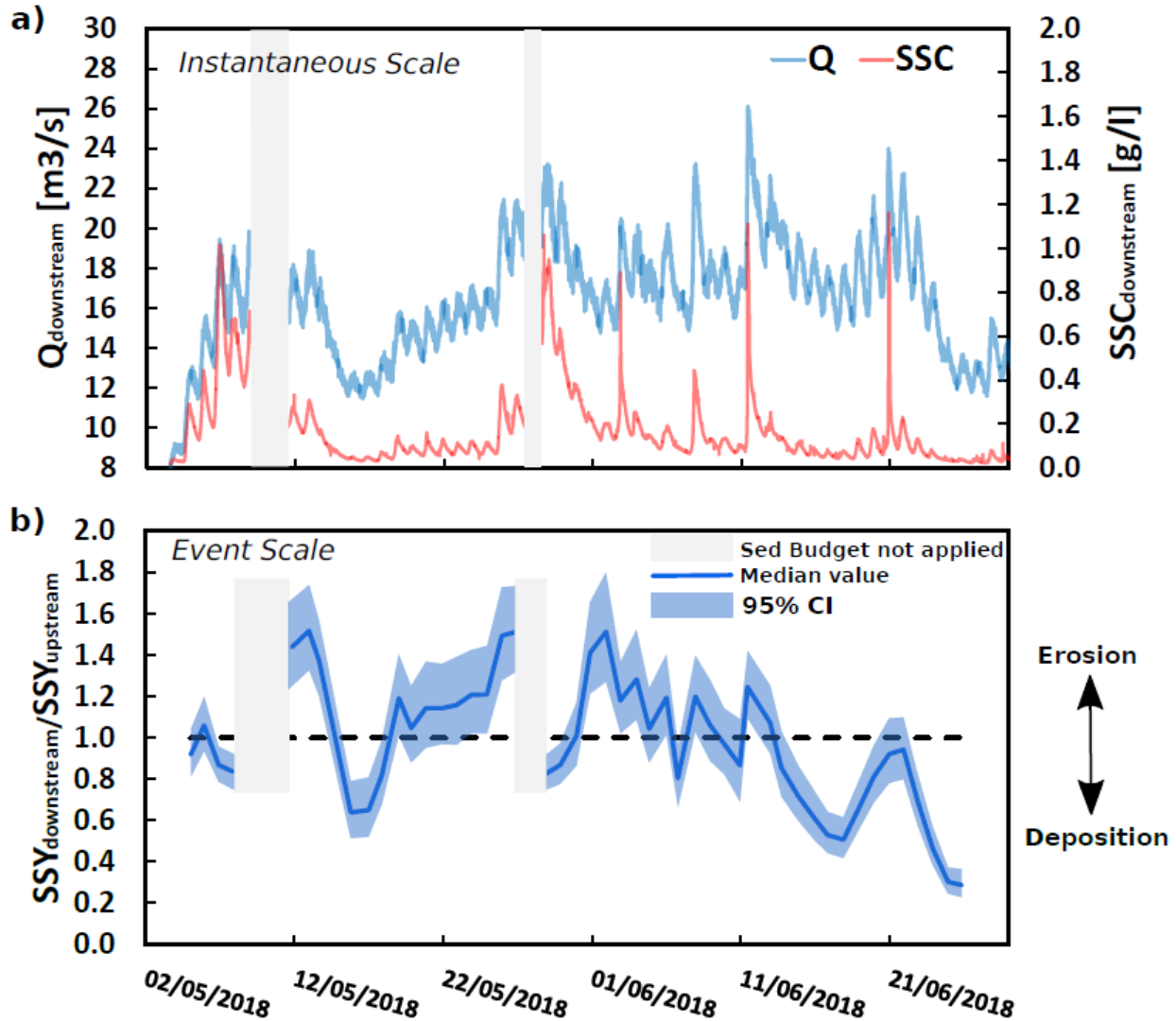


Figure 5.6: (a) Time series of the flow rate (Q) and the suspended sediment concentration (SSC) measured during the field campaign on the downstream station every 10 min. (b) Ratio of downstream over upstream suspended sediment yield (SSY) for each of the 48 events identified. The blue line corresponds to the median value obtained with the Monte Carlo simulations; the light blue polygon indicates the 95% confidence interval (CI) obtained with the Monte Carlo simulations; the horizontal dashed line corresponds to equal upstream and downstream SSY . Light grey polygons indicate periods for which the sediment budget approach was not applied due to an uncertain flow rate rating on the upstream station.

5.5.3. SEDIMENT BUDGET

A highly contrasted dynamic was observed considering the sediment budget of the reach (Figure 5.6-b). According to the estimated uncertainties, 33 of the 48 events observed during the field campaign were found to have significant differences between upstream and downstream SSY. For individual events we measured a net deposition accounting for up to 71% of the upstream SSY, while others exhibited net erosion accounting for up to 51% of the upstream SSY (considering median values of SSY obtained with Monte Carlo simulations). It was also observed that the suspended sediment yield ratios ($\frac{SSY_{downstream}}{SSY_{upstream}}$) were statistically larger during the rising limb than during the falling limb for the 48 events (Figure 5.7), as confirmed by a Mann-Whitney test (p -value<0.01). This indicates that the reach exported fine sediments more easily during the rising limbs while it stored these sediments more efficiently during the falling limb.

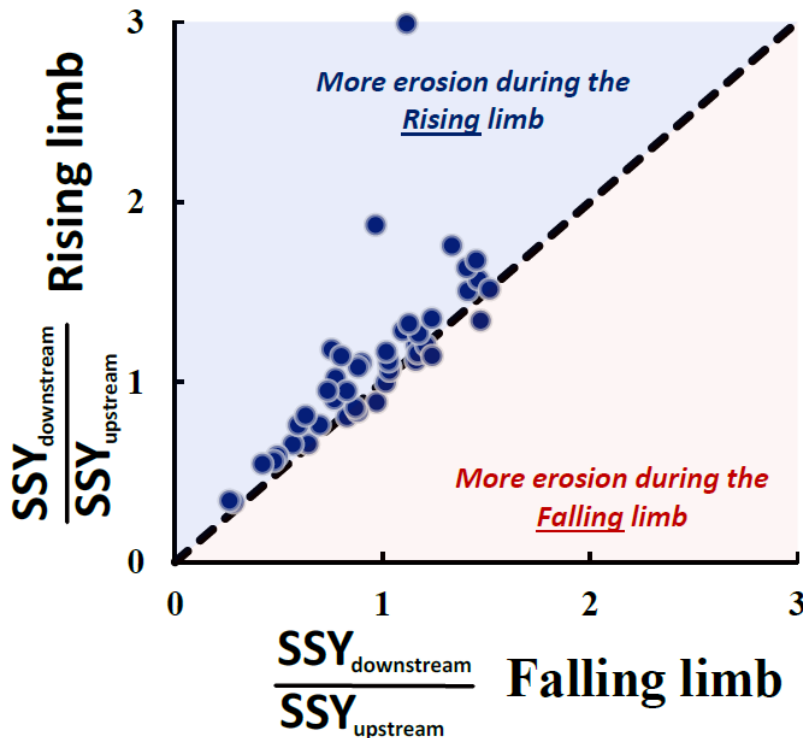


Figure 5.7: SSY ratio ($\frac{SSY_{downstream}}{SSY_{upstream}}$) of the reach during the rising limb as a function of the flux ratio during the falling limb of the hydrograph for each of the 48 events. Dashed black line corresponds to equality. Data correspond to median SSY ratio obtained with the Monte Carlo simulations.

At the campaign scale (transient periods associated with an uncertain upstream discharge rating curve not considered, light grey polygons in Figure 5.6), the deposition events were equivalent to 11% of the upstream fluxes (1500 t) while erosion events were equivalent to 9% of the upstream fluxes (1200 t). This budget at the whole campaign scale is not complete as one major event (May 27th) and two other smaller events could not be included in this analysis (missing data or uncertain upstream flow rate measurements). However, the available data obtained at the event or at the season scale show that erosion and deposition of fine particles was non-negligible in such streams, even though a relatively short distance (3.5 km) was considered compared with the upstream drainage area (130 km²). In addition, the two braided reaches studied were relatively small: 600 m×80 m for the downstream reach and 700 m×80 m for the upstream reach.

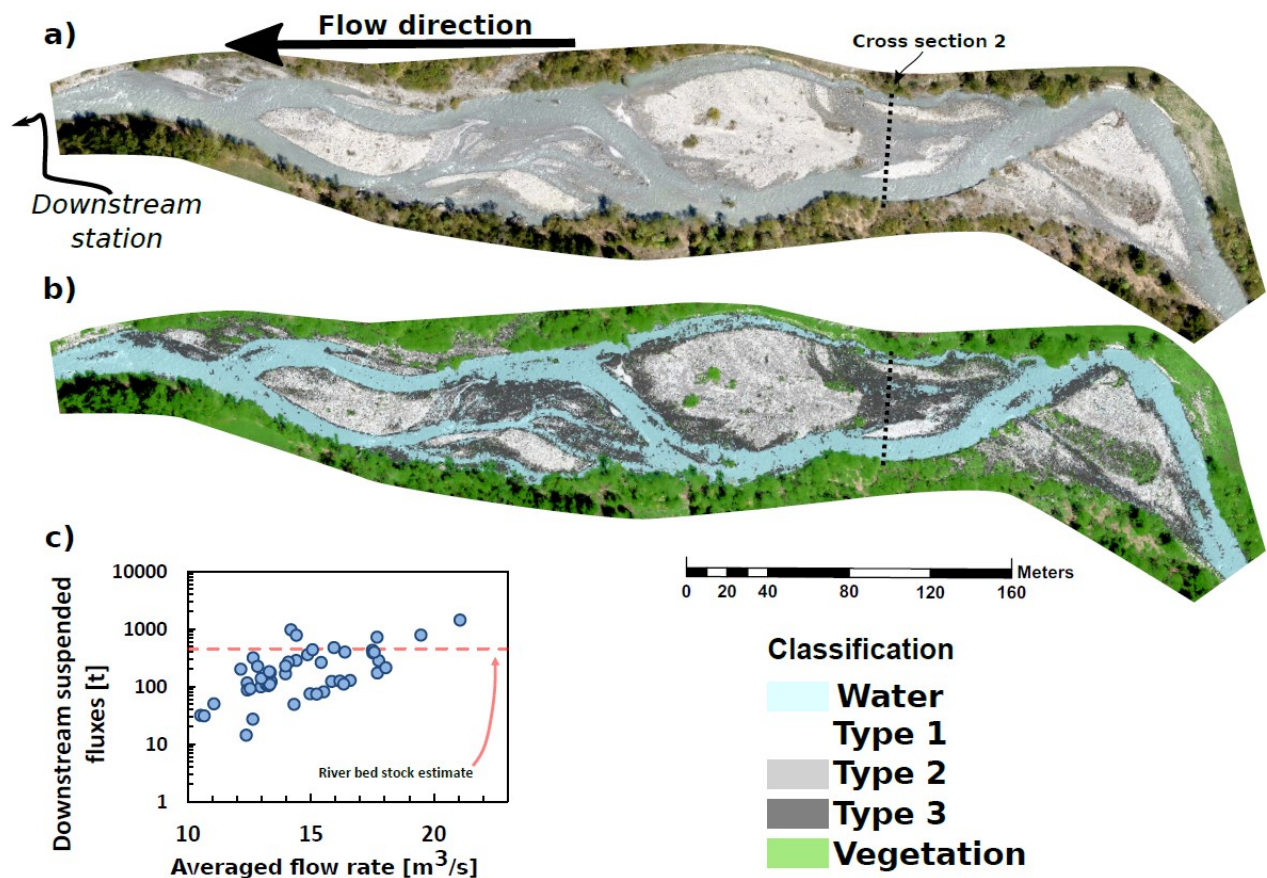


Figure 5.8: (a) Ortho-photograph of the downstream braided reach (27 April), (b) classification in four storage facies and (c) SSY as a function of the averaged flow rate during the 48 events of the field campaign.

The sediment budgets were compared to the amounts of fine particles stored in the two braided reaches. Mean stocks (considering an average value of surface and subsurface

storage) of $3.3 \text{ kg m}^{-2} \text{ dm}^{-1}$ for type 1 storage ($n=1$), $6.3 \text{ kg m}^{-2} \text{ dm}^{-1}$ for type 2 storage ($n=7$), $10.3 \text{ kg m}^{-2} \text{ dm}^{-1}$ for type 3 storage ($n=8$) and $3.2 \text{ kg m}^{-2} \text{ dm}^{-1}$ for underwater storage ($n=8$) were observed in the two braided zones (Figure 5.8Figure -a and Figure 5.8-b). The respective area occupied by each facies obtained from the supervised classification of ortho-photographs from the downstream reach were 42% (underwater), 7% (type 1), 19% (type 2) and 32% (type 3). Considering the area of the two braided reaches ($74,000 \text{ m}^2$), an arbitrary depth of 10 cm, as often considered in other studies [Buendia et al., 2016; Collins and Walling, 2007a; Lambert and Walling, 1988; Navratil et al., 2010], and using Eq.5.5, we estimated a stock of 450 t dm^{-1} for the two braided reaches (Figure 5.8-c).

After sieving all of the 16 stocks samples (350g) we obtained the following GSD: 23% finer than $50\mu\text{m}$, 51% finer than $100\mu\text{m}$ and 90% finer than $200\mu\text{m}$. Using the Stokes law to estimate the settling velocities, we considered that particles coarser than $250\mu\text{m}$ were not sampled by using this protocol as we waited 4s for coarse sand to settle (protocol details in appendix 5.9.2). Considering only the GSD below $250\mu\text{m}$, we observed that the particles of the river bed stock were very similar to those from the trapped suspended sediment one: 36% finer than $40\mu\text{m}$, 43% finer than $63\mu\text{m}$ and 52% finer than $100\mu\text{m}$. This result shows that river bed stock measurements can reasonably be compared with suspended fluxes especially since river bed stocks are underestimated due to an upper limit for sampled grain size. We could also compare the non-truncated surface GSD obtained with the laser diffraction sizer for 6 samples with the non-truncated trapped suspended one (appendix 5.9.1). Surface samples showed a certain variability as median diameters (D_{50}) ranged between 104 and $214 \mu\text{m}$ but were in the same range as trapped suspended median diameter ($208\mu\text{m}$) confirming that the river bed can deliver these fine particles.

5.5.4. TEMPORAL CHANGES

The hydrosedimentary behavior of the river reach was found to evolve during the season. At the event scale, larger averaged flow rates were required at the end of the campaign for the reach to export fine sediments (Figure 5.9-a). Events exhibiting net erosion occurred approximately at discharges higher than $13 \text{ m}^3 \text{ s}^{-1}$ in May while they required $20 \text{ m}^3 \text{ s}^{-1}$ in late June. Considering only events with no significant differences in terms of fluxes (the SSY difference distribution obtained from Monte Carlo simulations was not significantly positive or negative), Figure 5.9-b shows a statistically significant linear relation between averaged discharge and time ($R^2 = 0.86$). It was then possible to estimate an equilibrium flow rate (Q_{eq}) needed so that the upstream flux equal to the downstream flux at the event scale for a given time t in the season:

$$Q_{eq}(t) = at + b, \quad \frac{SSL_{downstream}}{SSL_{upstream}}(Q_{eq}(t)) \rightarrow 1 \quad (5.7)$$

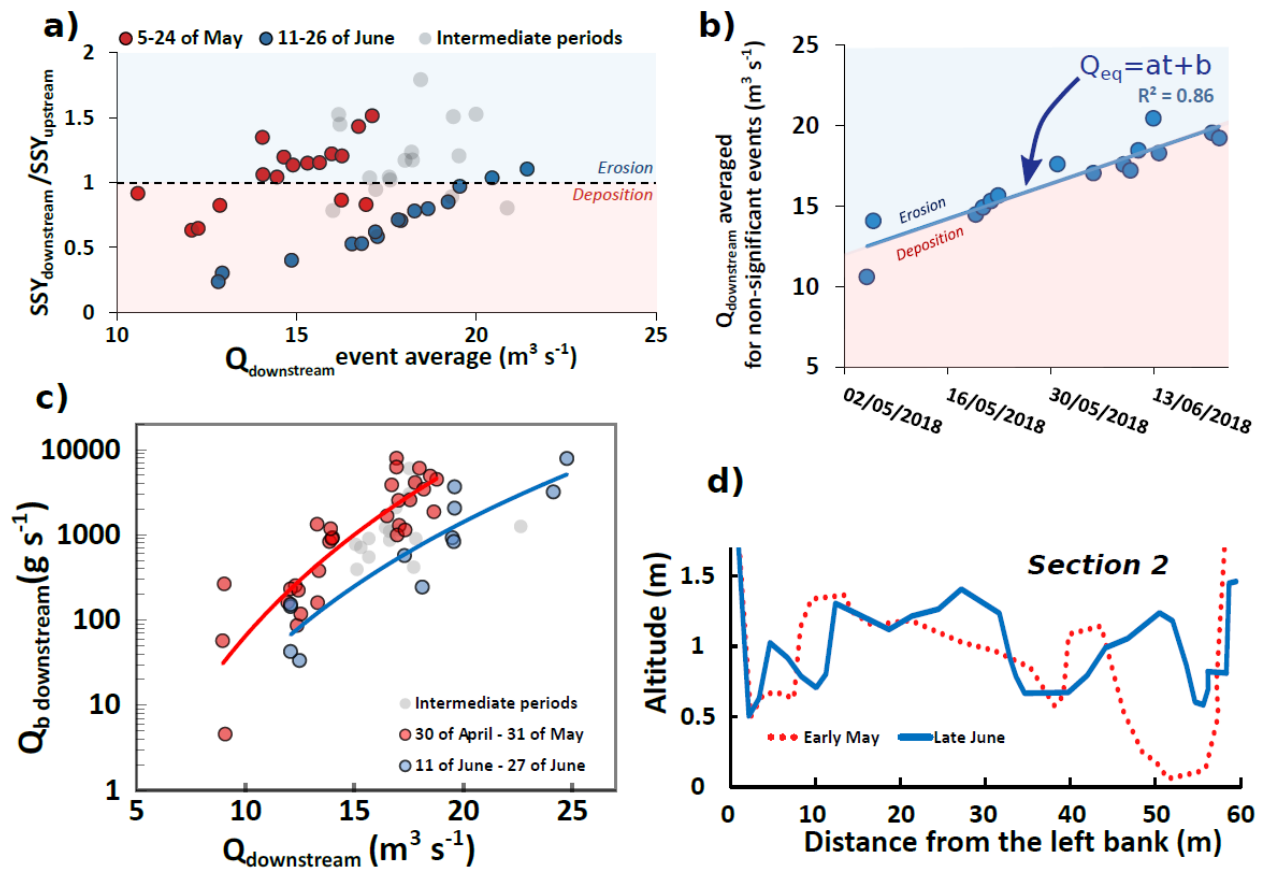


Figure 5.9: (a) Relation between averaged flow rate and ratio between upstream and downstream fluxes at the event scale. (b) Averaged discharge corresponding to nonsignificant events in terms of suspended flux differences (Q_{eq}) over time. (c) Bedload transport rate measured at the downstream station as a function of the flow rate. Red dots and red line correspond, respectively, to measurements in May and the best fitted power law for this period. Blue dots and blue line correspond, respectively, to measurements in late June and the best fitted power law for this period. (d) Topographic changes between early May and late June of cross section 2 in the downstream braided reach (location in Figure 5.8). Note: events were considered nonsignificant when the SSY difference distribution obtained from Monte Carlo simulations was not significantly positive or negative (more detail in the Methods and Appendix sections).

These seasonal changes for the fine sediment reach budget dynamics were consistent with morphodynamic modifications observed in the reach. Significant morphological transformations were observed on the downstream braided reach. For instance, Figure 5.9-d shows a significant aggradation of cross section 2 (location in Figure 5.8) between the start and the end of the campaign. Also, bedload measurements taken at the

downstream station show a decrease of the bedload intensity for a given flow rate throughout the campaign (Figure 5.9-c). This indicates that the bed mobility of the reach decreases for similar discharges between the start and the end of the campaign, which could explain that higher flow rates are needed to erode fine sediments from the reach.

5.5.5. FACTORS CONTROLLING EROSION AND DEPOSITION PROCESSES

Considering 2-h averaged values and an average time delay of 90 min for peak discharge propagation, interesting trends were observed (Figure 5.10): the flux ratio ($\frac{SSL_{downstream}}{SSL_{upstream}}$) increased with the normalized flow rate $Q_{downstream}/Q_{eq}$ (Q_{eq} given by Eq.5.7) until a given upstream concentration from which $\frac{SSL_{downstream}}{SSL_{upstream}}$ decreased whatever the discharge.

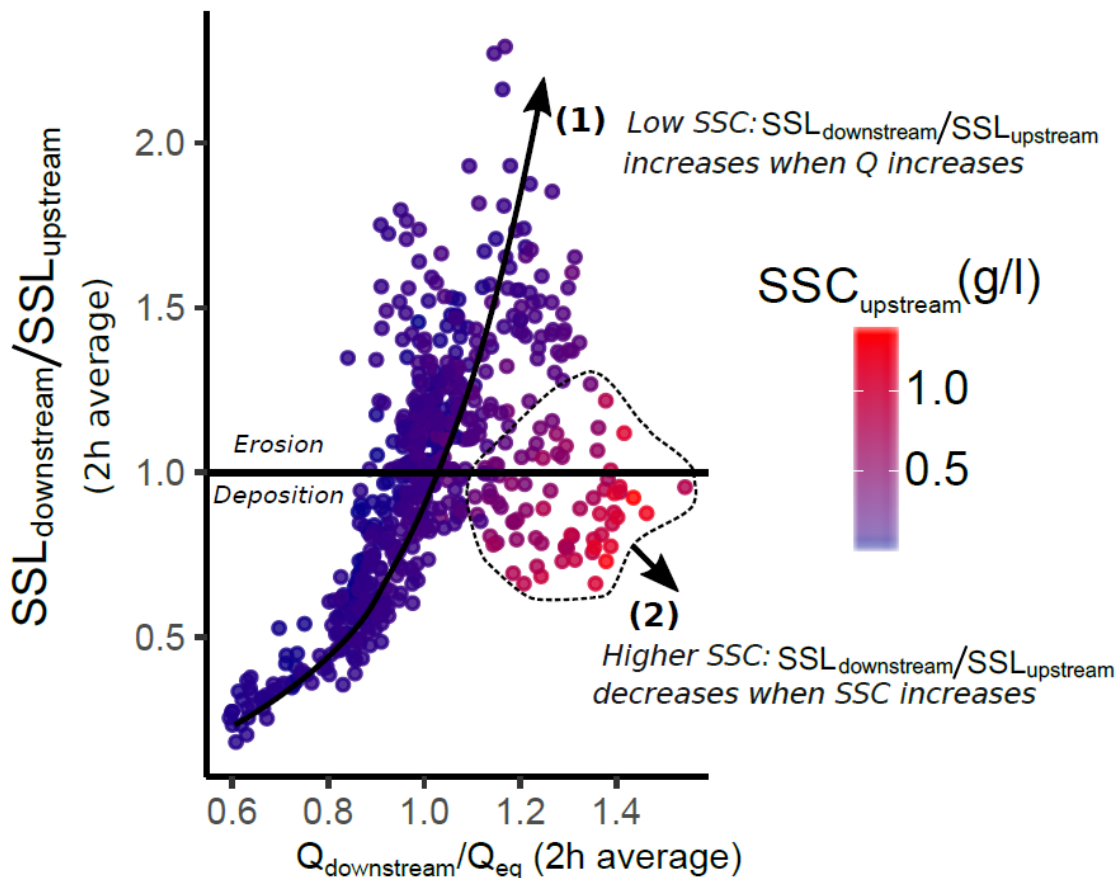


Figure 5.10: Ratio of downstream over upstream fluxes ($SSL_{downstream}/SSL_{upstream}$) as a function of the downstream flow rate normalized by the flow rate for equilibrium at that time ($Q_{downstream}/Q_{eq}$). Dots were colored according to the upstream suspended sediment concentration ($SSC_{upstream}$) and 2-h averaged values were considered.

Considering a limit $SSC_{upstream}$ value of approximately 0.2 g L^{-1} to split data between the two phases observed in Figure 5.10, Spearman rank correlation tests confirmed these visual trends (Table 5.1). For $SSC_{upstream}$ smaller than 0.2 g L^{-1} (79% of the data), the flux ratio was highly positively correlated with the normalized flow rate ($\rho = 0.83$) while it was less correlated with the suspended sediment concentration ($\rho = 0.35$). For $SSC_{upstream}$ larger than 0.2 g L^{-1} (21% of the data), the flux ratio had a nonsignificant correlation with the normalized flow rate ($p_{value} > 0.05$) while it was highly and negatively correlated with the SSC ($\rho = -0.72$). These observations suggest that both the flow rate and SSC control erosion and deposition of fine particles at the reach scale, but in opposite ways.

	$SSC_{upstream} < 0.2 \text{ g l}^{-1}, n = 474$		$SSC_{upstream} > 0.2 \text{ g l}^{-1}, n = 123$	
	$Q_{downstream} / Q_{eq}$	$SSC_{upstream}$	$Q_{downstream} / Q_{eq}$	$SSC_{upstream}$
$\frac{SSL_{downstream}}{SSL_{upstream}}$	0.83	0.35	-0.13	-0.72

Table 5.1: Spearman rank correlation coefficients between the flux ratio of downstream over upstream fluxes ($\frac{SSL_{downstream}}{SSL_{upstream}}$), the downstream flow rate normalized by the flow rate for equilibrium at that time ($Q_{downstream}/Q_{eq}$) and the upstream SSC ($SSC_{upstream}$). Data with $SSC_{upstream}$ higher or lower than 0.2 g L^{-1} were considered separately. n corresponds to the number of data for each case, bold values are significant correlations with p -value < 0.05 .

5.6. DISCUSSION

5.6.1. IMPORTANCE OF EROSION AND DEPOSITION PROCESSES

The sediment budget demonstrated that erosion and deposition processes of fine particles were far from negligible in this typical alpine gravel bedded reach. Most of the events analyzed showed significant differences between upstream and downstream fluxes and complex interactions with the bed controlled by both the SSC and flow rate. Larger events than those recorded during the period studied with potentially greater bed mobilization or short and highly erosive stormy events with a limited flow rate might lead to an even greater buffering effect of the river bed. In addition, one must keep in mind that all these observations concern a short 3.5-km braided reach. For longer streams and wider braiding morphologies, the cumulative effect might be substantial.

Even if the stock of 450 t dm^{-1} of fine particles estimated for the two braided reaches is associated with large uncertainties and only corresponds to a measurement taken at a given moment, interesting conclusions can be drawn. The stock is rather high compared

to the fluxes exported during most individual events of the field campaign (Figure 5.8-c) and it is on the same order of magnitude as the range of both maximum individual event depositions of 317 tons (159–482 t with 95% confidence interval) and erosion of 157 t (62–248 t with 95% confidence interval). This means that the reach studied can act as a fine sediment buffer. Considering an equivalent average fine sediment storage in the river bed of $6 \text{ kg m}^{-2} \text{ dm}^{-1}$ and that the whole reach area is mobilized, the maximum remobilization event (157 t) might correspond to an approximate remobilization depth between 1.5 cm and 5.5 cm (considering only uncertainties on flux differences, 62–248 t). Even though the mobilization of the sediment matrix might occur at some locations and not in the whole area of the braided zone, this order of magnitude is also consistent with the topographic changes observed.

5.6.2. CONCEPTUAL DESCRIPTION OF THE PROCESSES INVOLVED

Following the results detailed above, we could hypothesize that erosion and deposition processes occur simultaneously in the river bed in variable proportions at various locations depending on the hydrosedimentary forcing (Figure 5.11).

(A) For low flow rates (Q) and low SSC, only limited zones of the main channel exhibit high shear stresses leading to a low erosion flux. Deposition fluxes occur in zones with low shear stresses such as secondary channels or main channel boundaries. In that case, the reach is globally storing fine particles. (B) For moderate flow rates associated with relatively low SSCs, the river bed is mobilized in the main channel and secondary channels leading to significant erosion fluxes. Deposition fluxes are low because they are limited in space and intensity. In that case, the reach is globally releasing fine particles. (C) For high flow rates associated with high SSCs, the river bed is actively mobilized with possible migration of the main channel and scouring of secondary channels leading to high erosion fluxes. Deposition fluxes are even larger because they have a large spatial extent (submersion of the entire cross section) and because they have a high intensity (high SSC). In that case, the reach is globally storing fine particles. This conceptual description highlights the impact of the bed morphology and bed mobility on both erosion and deposition of fine particles: (i) deposition controlled by the shear stress distribution in the cross section and (ii) erosion controlled by the bed (coarse particles) mobility.

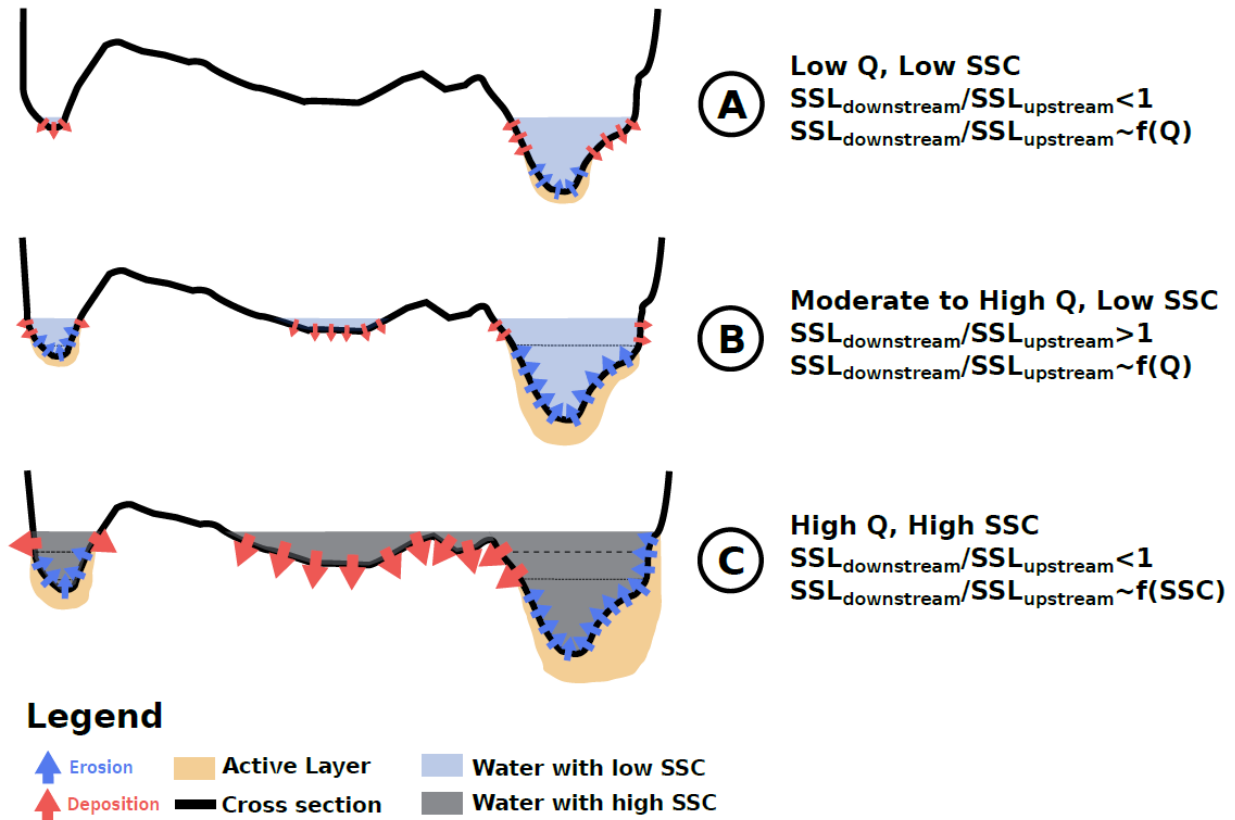


Figure 5.11: Conceptual description of the erosion and deposition processes occurring in a cross section of the reach for various hydrosedimentary forcings. Q denotes the flow rate; SSC denotes the suspended sediment concentration; $\frac{SSL_{downstream}}{SSL_{upstream}}$ corresponds to the flux ratio of downstream over upstream fluxes. Note: the nonlinearity of the relation SSC vs Q explains why it is possible to have (A) low Q with low SSC , (B) moderate Q with low SSC and (C) high Q with high SSC .

5.6.3. IMPLICATION FOR SUSPENDED LOAD MODELING

These observations suggest that models (conceptual, statistical and physically based) that attempt to reproduce or predict the suspended load transfer through gravel bedded streams might take into account such erosion and deposition processes. This could be particularly true for catchments with active river bed morphologies. The conceptual storage reservoir usually used in conceptual models to reproduce storage and release of fine particles [Asselman, 1999; Park and Hunt, 2018; Picouet et al., 2009] is for now poorly understood. To the best of the authors knowledge, Park and Hunt (2018) were the first to propose a simplified description of this storage and release behavior at the catchment scale, based on physical processes: gravel bed scouring and gravel matrix infiltration. They proposed that under a certain critical flow rate corresponding to gravel bed mobilization, fine particles infiltrate the gravel matrix if pore spaces are empty. For

higher flow rates, they considered that these stored particles were released in the flow depending on the scouring depth, which was defined as a function of the flow rate magnitude. This increase of the bed production of fine particles as the flow rate increases is supported by the measurements recorded in the alpine river reach studied (Figure 5.10). The conceptual model proposed by Park and Hunt also considers that during a flood event, fluxes at the outlet of the reach due to bed mobilization are larger during the rising limb than during the falling limb of the hydrograph. Then the previously flushed gravel matrix captures fine particles coming from upstream more easily. Such differences between rising limb and falling limb were also observed on the reach studied (Figure 5.7).

Future research might focus on determining the buffering capacity of river reaches at various time scales (instantaneous, event, season and annual) and for a variety of gravel bedded streams. This will help to characterize both the river bed properties (morphology, coarse grain size distribution) and the upstream forcing properties (fine grain size distribution, hydrology and SSC range) that generally control the shape of the erosion and deposition functions.

5.7. CONCLUSION

To quantify the processes of erosion and deposition of fine particles in gravel bedded streams, a fine sediment budget approach was applied on a 3.5-km typical braided stream from the French Alps using high-frequency suspended load measurements taken over 2 months of the melting season. Monte Carlo simulations were used to propagate uncertainties and determine precisely if deposition or erosion occurs during each of the 48 events identified. The results indicate that even over short distances (the reach considered was relatively small compared to the upstream catchment area) most events (33 out of 48) exhibited significant flux differences. These differences at the event scale ranged between net deposition equivalent to 71% of upstream suspended yield and net erosion equivalent to 51%. For most events, the reach tends to export fine sediments more easily during the rising limb than during the falling limb, which could result from a gravel matrix flushing process followed by fine particle entrapment in empty pore spaces. At a nearly instantaneous time scale, the fine sediment budget of the reach was found to be controlled by both flow rate and upstream SSC in a complex way: erosion fluxes increase as the water discharge increases, while deposition fluxes increase as SSC increases. Also, during the 2 months, the sediment budget equilibrium of the reach exhibited significant changes that occurred concomitantly with morphodynamic changes in the reach (topography and bedload transport).

Finally, these field observations demonstrate that the dynamic of suspended load in this type of alluvial alpine river is complex and exhibits strong interactions with the gravel bed matrix. It raises questions about the relevance of the washload concept in gravel

bedded streams and suggests that modeling efforts at the catchment or the reach scale should necessarily take into account such interactions between fine particles and the gravel bed.

5.8. NOTATIONS

The following symbols are used in this paper.

SSY	Suspended sediment yield (t)
SSL	Suspended sediment load (kg/s)
SSC	Suspended sediment concentration (g/l)
Q	Flow rate (m ³ /s)
$X_{upstream}$	Variable X for the upstream station
$X_{downstream}$	Variable X for the downstream station
E	Erosion flux
D	Deposition flux
St_{reach}	Fine sediment stock estimate of the reach (t/dm)
\overline{st}_i	Average local stock for the storage facies I (kg/m ² /dm)
A_i	Area of the storage facies I (m ²)
t	Time

5.9. APPENDIX

5.9.1. ERROR QUANTIFICATION FOR SUSPENDED LOAD MEASUREMENTS

5.9.1.1. Uncertainties associated with SSC measurements

Reference	Type of study	Observations
[Horowitz <i>et al.</i> , 1992]	Field	SD: ±10%. Errors on SSC measurements and regression between turbidity and SSC using automated water sampler compared to isokinetic samplers (EDI/EWI).
[Horowitz, 2008; Horowitz <i>et al.</i> , 2001]	Field	SD: ±10%. Errors concerning the reproducibility of isokinetic sampler (EDI/EWI)
[Navratil <i>et al.</i> , 2011]	Lab	17% overall underestimation for SSC using automated water sampler. Uncertainty quantified as a function of the SSC (g/L): $Sd = 0.23 * SSC^{0.79}$
[Clark <i>et al.</i> , 2009]	Field / Lab	Underestimation on SSC of 20% and 50% for automated water sampler for particles of 100 µm and 500 µm (d_{50}), respectively.
[Bossong <i>et al.</i> , 2006]	Field / Lab	SD: ±32% on SSC for field and lab errors for automated water sampler compared to isokinetic samplers (EDI/EWI).
[Allen and Petersen, 1981]	Field	SD: ±8% on SSC for field and lab errors for automated water sampler compared to isokinetic samplers (EDI/EWI).

Table 5.2: Short review of uncertainties associated with SSC sampling found in the literature.

5.9.1.2. Monte Carlo framework for suspended load uncertainty propagation

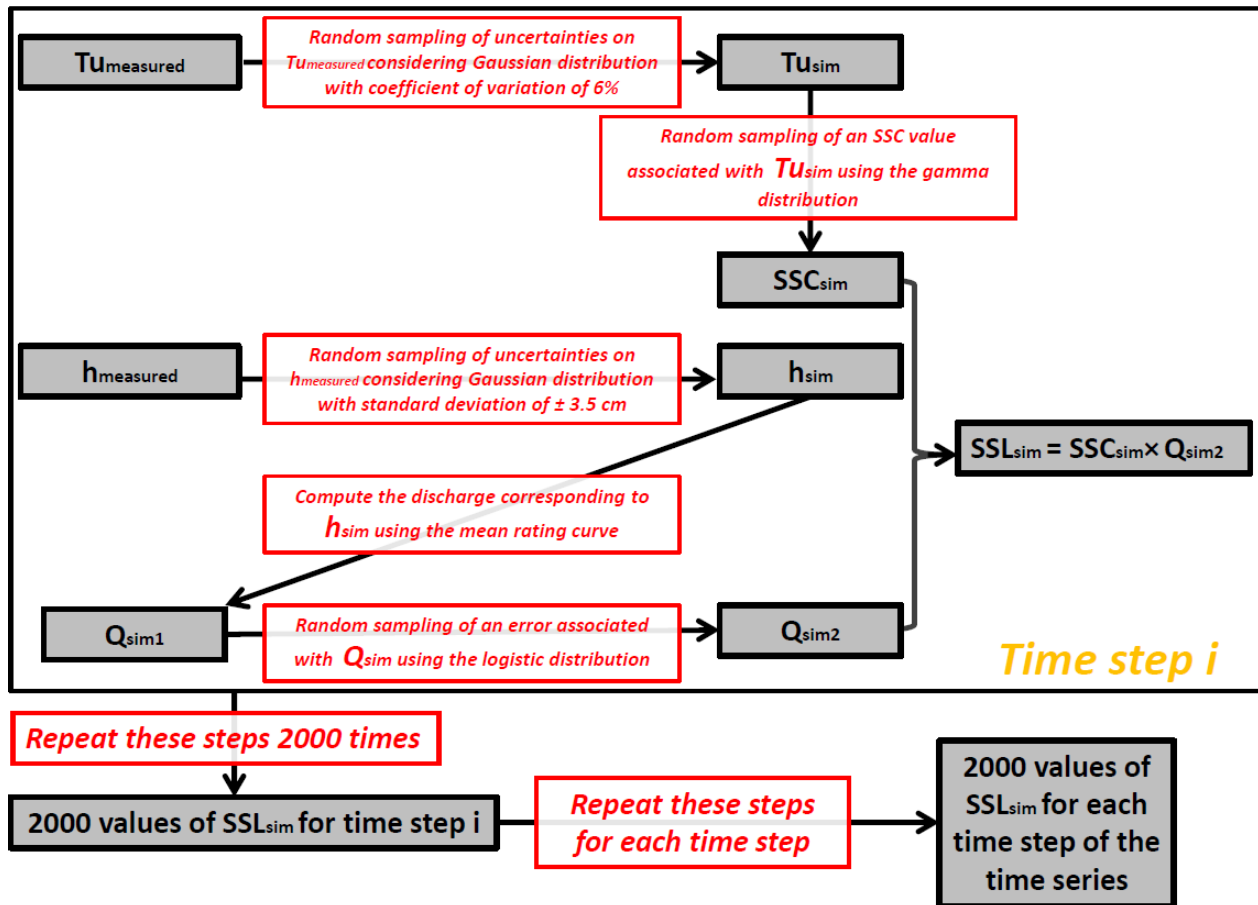


Figure 5.12: Monte Carlo simulation used to propagate uncertainties on suspended load. $TU_{measured}$ corresponds to the turbidity measured, TU_{sim} indicates the turbidity simulated after randomly adding its uncertainty corresponding to a Gaussian distribution with a 6% coefficient of variation, SSC_{sim} indicates the SSC simulated after randomly sampling a value in the gamma distribution corresponding to TU_{sim} . $h_{measured}$ corresponds to the water level measured, h_{sim} to the water level simulated after randomly adding its uncertainty corresponding to a Gaussian distribution with a standard error of ± 3.5 cm, Q_{sim1} corresponds to the discharge calculated with the mean rating curve for h_{sim} and Q_{sim2} indicates water discharge simulated after adding a randomly sampled error in the logistic distribution corresponding to Q_{sim1} . SSL_{sim} is the flux of suspended sediment simulated.

5.9.1.3. Suspended sediment concentration uncertainty propagations

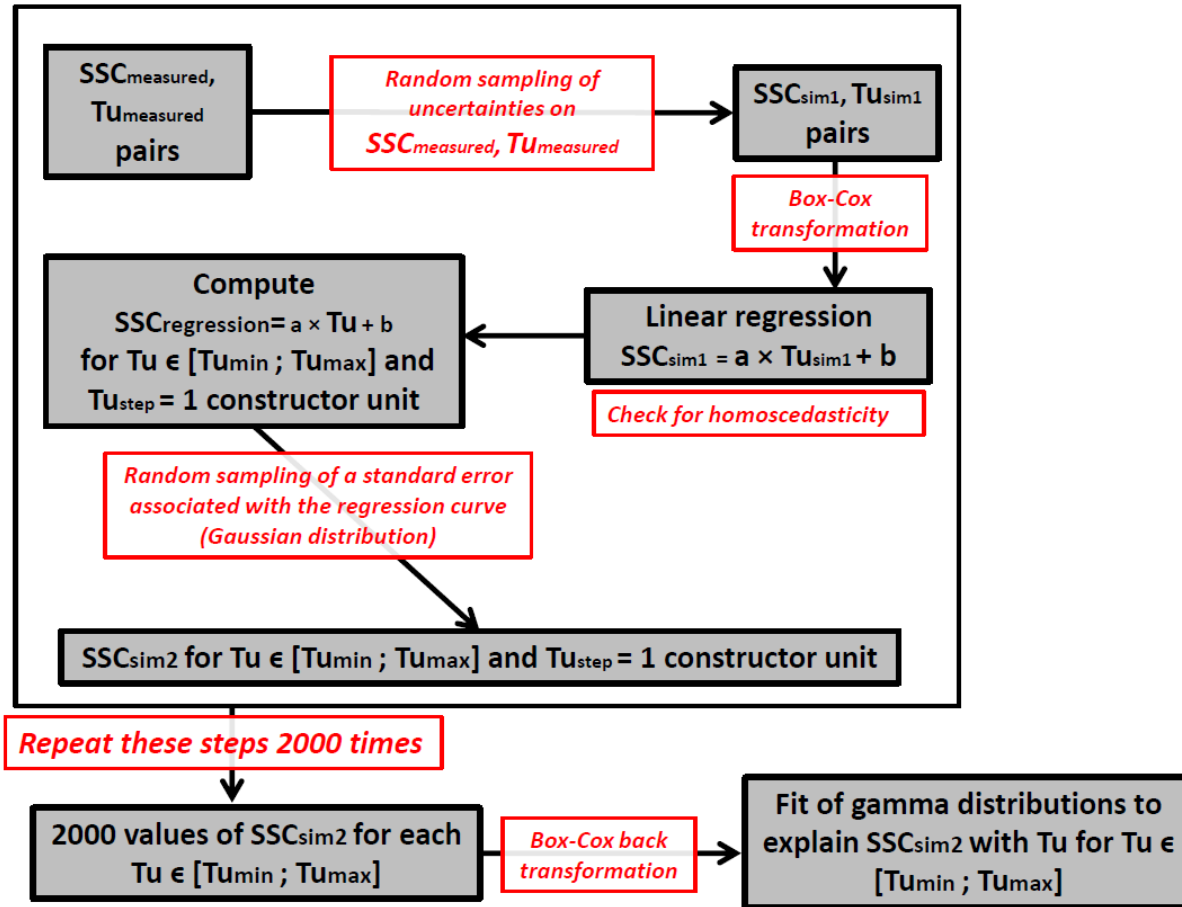


Figure 5.13: Framework used to propagate uncertainties on turbidity, SSC measurements and regression curve used between SSC and the turbidity measurements. This analysis was applied to all turbidity and water sample pairs for which SSC was measured. 1) For each turbidity and SSC pair, a random sampling in truncated (only positive values) normal distributions associated with turbidity (6% coefficient of variation) and SSC uncertainty (25% standard deviation). 2) a Box-Cox transformation is done on these first simulated values (Tu_{sim1} and SSC_{sim1}) to prevent heteroscedasticity. 3) A linear regression is done on these simulated and transformed turbidity and SSC pairs and homoscedasticity is checked. 4) For each turbidity unit, an SSC value predicted using the previously fitted regression curve is calculated. The regression error is added to this value to obtain SSC_{sim2} (using a random drawn in a Gaussian distribution associated with the standard error of the regression curve). 5) These steps are repeated 2000 times to obtain 2000 values of simulated SSC (that take into account turbidity, SSC and regression curve uncertainties) for each turbidity unit. 6) The data obtained are back-transformed and gamma distributions explaining simulated SSC (SSC_{sim2}) are fitted for each turbidity unit. These gamma distributions can then be used in the Monte Carlo simulations (Figure 5.12).

To propagate uncertainties on SSC, gamma distributions were fitted to describe possible SSC values including uncertainties on turbidity measurements, SSC samples and the regression curve used between turbidity and SSC (framework detailed in Figure 5.13). Gamma distributions were used as they were found to be the best statistical distributions to represent these uncertainties. These distributions were fitted for each turbidity unit in the measurement range using the Anderson-Darling criteria and the R package “fitdistrplus” from Delignette-Muller and Dutang (2014). If the Anderson-Darling criterion was not fulfilled, the null hypothesis considering that empirical error distribution was similar to the fitted distribution was rejected. The fitted distributions were then used to propagate uncertainties associated with SSC measurements on suspended load at each time step.

The probability density function of the gamma distribution used to propagate uncertainties on SSC values is defined by the following equation:

$$f(x | k, \beta) = \frac{\beta^k}{\Gamma(k)} x^{k-1} \exp(-\beta x) \tag{5.8}$$

in which k is a shape parameter (positive) and β is a rate parameter (positive) fitted for each turbidity unit (Figure 5.14) after statistical analysis detailed in Figure 5.13.

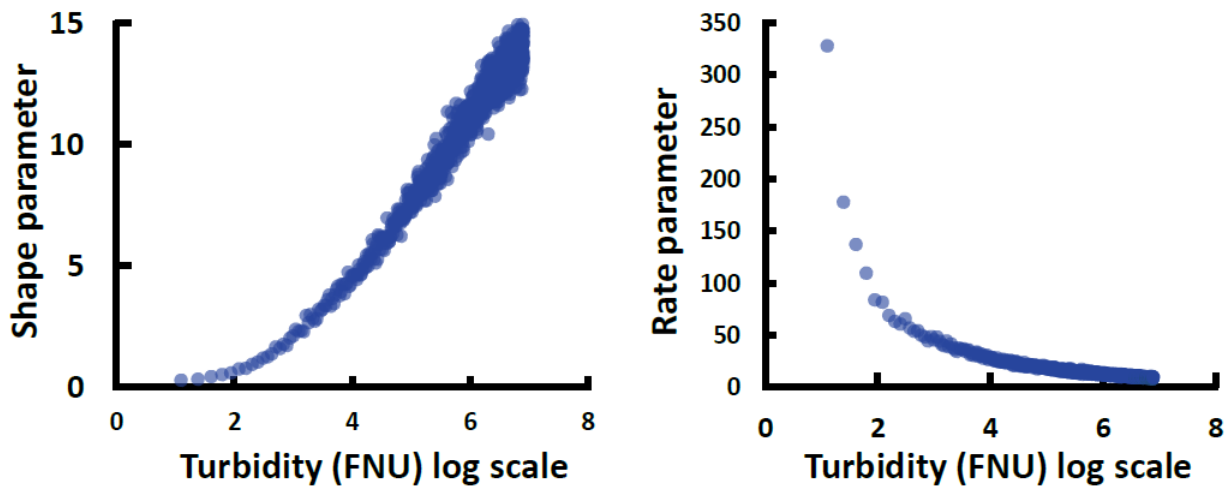


Figure 5.14: Examples of fitted shape and rate parameters of the gamma function used for the turbidity uncertainty propagation of the downstream station.

5.9.1.4. Flow rate uncertainty propagations

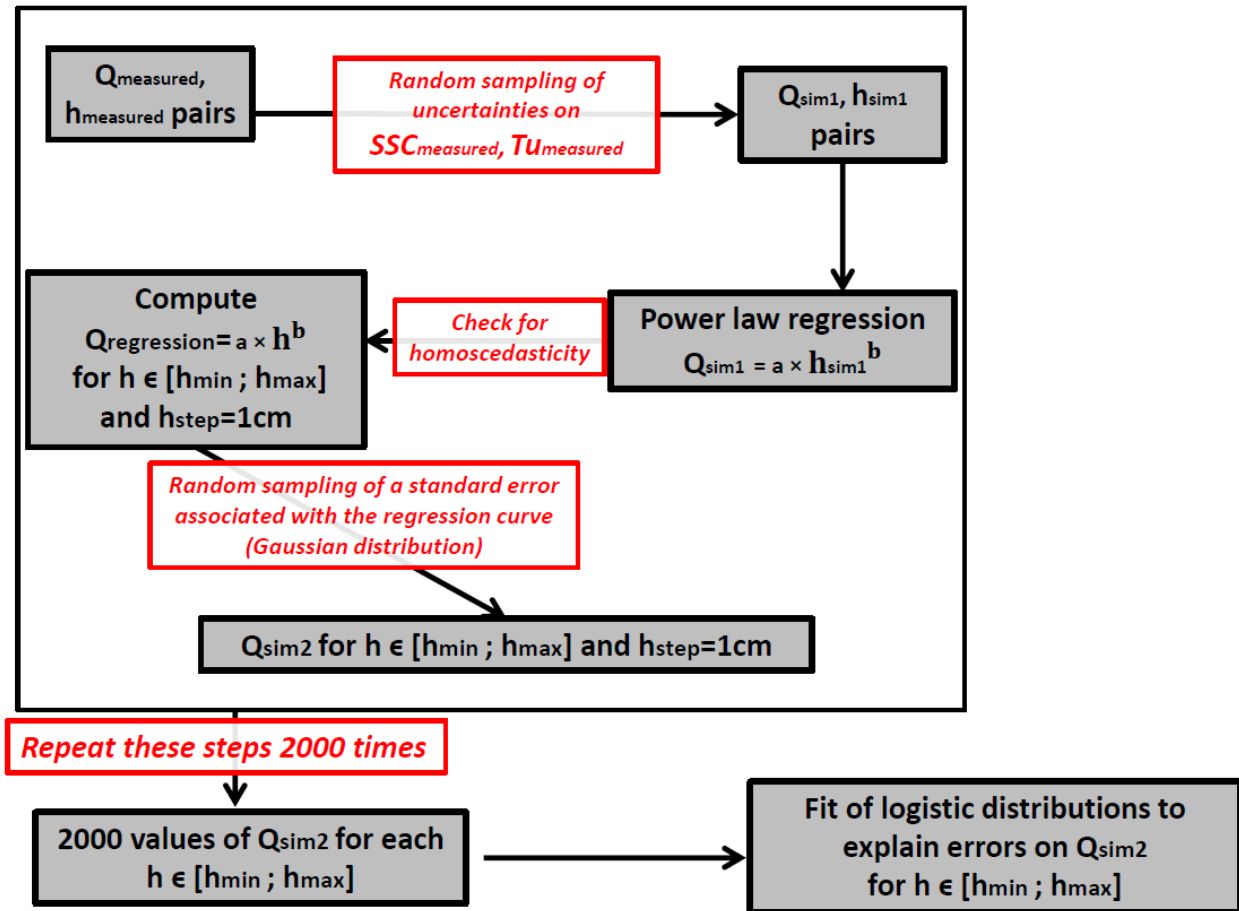


Figure 5.15: Framework used to propagate uncertainties on water level, the flow rate measurements and regression curve used between the water level and the flow rate measurements. This analysis was applied on all water level and flow rate pairs for which gauging was performed. 1) For each water level and flow rate pair, random sampling in truncated (only positive values) normal distributions associated with water level (standard deviation, ± 3.5 cm) and Q uncertainty (standard deviation, 5–15% depending on the type of gauging). 2) A power law is fitted on these simulated water level and Q pairs and homoscedasticity is checked. 3) For each centimeter a Q value predicted using the previously fitted power law is calculated. The regression error is added to this value to obtain Q_{sim2} (using a random drawn in a Gaussian distribution associated with the standard error of the fitted power law). 4) These steps are repeated 2000 times to obtain 2000 values of simulated Q (that take into account water level, flow rate and regression curve uncertainties) every centimeter. 5) A power law is fitted on the averaged Q_{sim2} obtained every centimeter. Logistic distributions explaining the errors around this power law are fitted every centimeter. These logistic distributions can then be used in the Monte Carlo simulations (Figure 5.12).

Logistic distributions were fitted to describe uncertainties on flow rate values due to water level measurements, flow rate measurements and the regression curve used to relate flow rate and water level (framework detailed in Figure 5.15). Logistics distributions were used because they were found to be the best statistical distributions to represent these uncertainties. These distributions were fitted every centimeter in the measurement range using the Anderson-Darling criteria and the R package “fitdistrplus” from Delignette-Muller and Dutang (2014). These distributions were then used to propagate uncertainties on flow rate values used for suspended load calculation at each time step.

The probability density function of the logistic distribution used for error distribution in flow rate uncertainty propagation is defined by the following equation:

$$f(x | \mu, s) = \frac{\exp\left(\frac{-(x - \mu)}{s}\right)}{s \left(1 + \exp\left(\frac{-(x - \mu)}{s}\right)\right)^2} \quad (5.9)$$

in which μ is the location parameter (equal to zero in our case) and s the scale parameter (positive) fitted every centimeter (Figure 5.16) after the Monte Carlo simulations detailed in Figure 5.15.

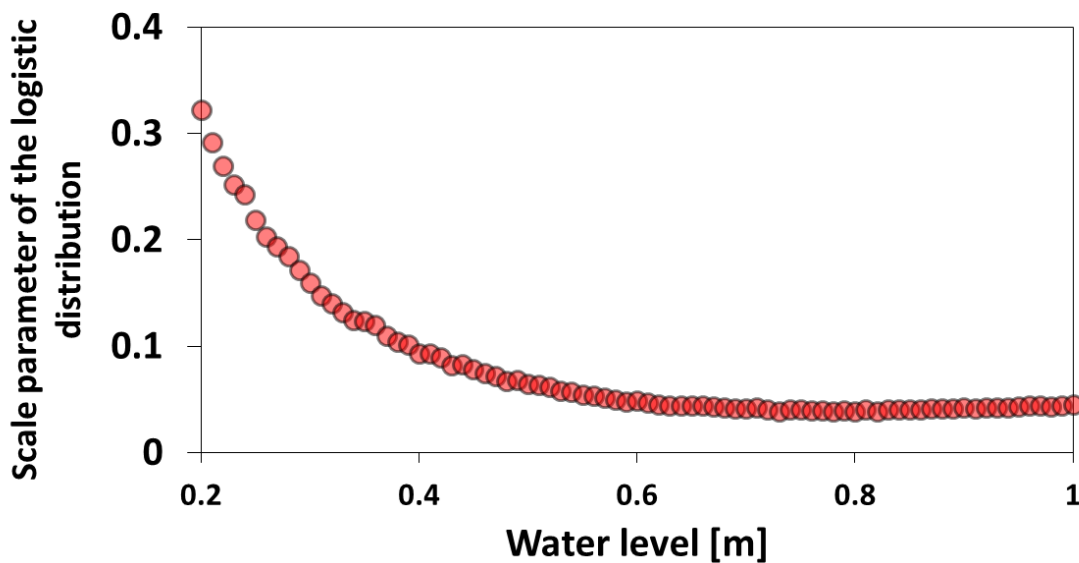


Figure 5.16: Example of fitted shape parameters of the logistic distributions used for flow rate uncertainty propagation for the downstream station.

5.9.2. FINE SEDIMENT STOCK ESTIMATE

The sampling technique proposed by Navratil *et al.* (2010) was used to measure local stocks of fine sediments in dried storage facies. No distinction was made during the analysis between surface and subsurface stocks given that an average value was considered.

Measurements consist of a first sampling of the bed material (area, 28×34 cm), which includes the gravel armor layer and all sediments deposited on this layer. These bed materials are then put in a container filled with 20 L of clear water and the mixture is agitated for 10 s using a shovel. After waiting 4s for coarse particles to settle, a turbid water sample (250 mL) is then taken at the container surface and brought to the lab to determine its suspended sediment concentration. All previous steps are repeated for the subsurface layer (approximately 10 cm deep). It is then possible to estimate a local value of fine particle storage using the following equations:

$$st_{surface} = \frac{SSC_{container\ 1} \times V_{container\ 1}}{A \times h_1} \quad (5.10)$$

$$st_{subsurface} = \frac{(SSC_{container\ 2} - SSC_{container\ 1}) \times V_{container\ 2}}{A \times h_2} \quad (5.11)$$

in which $st_{surface}$ is the local stock estimate in the surface ($\text{g m}^{-2} \text{ dm}^{-1}$), $SSC_{container\ 1}$ is the SSC in the first water sample (g L^{-1}), $V_{container\ 1}$ is the volume of water in the container (L), A is the surface of sampling (m^2), h_1 is the depth of the first sampling (dm), $st_{subsurface}$ is the local stock estimate in the subsurface ($\text{g m}^{-2} \text{ dm}^{-1}$), $SSC_{container\ 2}$ is the SSC in the second water sample (g L^{-1}), $V_{container\ 2}$ is the volume of water in the container after the first water sample was taken (L) and h_2 is the depth of the second sampling (dm).

The Lambert and Walling (1988) protocol already used in several field studies was used to estimate underwater storage [Collins and Walling, 2007a; Duerdoth *et al.*, 2015; Piqué *et al.*, 2014; Walling *et al.*, 1998]. A cylinder 29 cm in diameter ($A_{cylinder}$, m) was pushed in the river bed to separate the sampling area from the flow. Then a trowel was used to disturb and agitate the bed before a turbid water sample was taken in a 250-mL bottle to estimate its concentration in the lab ($SSC_{cylinder}$, g/L). No differences were made between the surface and subsurface. The depth of bed agitation ($h_{bed\ agitation}$, dm) was estimated as well as the water volume in the cylinder ($V_{cylinder}$, L) to finally obtain the local stock estimates st_{water} ($\text{g m}^{-2} \text{ dm}^{-1}$):

$$st_{water} = \frac{SSC_{cylinder} \times V_{cylinder}}{A_{cylinder} \times h_{bed\ agitation}} \quad (5.12)$$

5.9.1. FINE PARTICLE GRAIN SIZE DISTRIBUTION

In this section we report grain size distributions (GSD) of fine particles stored in the riverbed and transported in suspension. In Figure 5.17 measurements obtained with the laser diffraction sizer (Dep. 1 to 6) or by sample sieving are presented. The left panel shows truncated GSD of surface deposits (grey lines), river bed stocks (blue line, surface and subsurface are mixed) and trapped suspended sediments (red line). These GSD were relatively similar while some surface samples (Dep.1 to Dep.3) were a bit coarser and trapped suspended sediments exhibited a slightly higher fine content. The right panel shows non-truncated GSD of surface deposits and trapped suspended particles. These GSD were in the same range while the GSD of surface deposit were significantly variable.

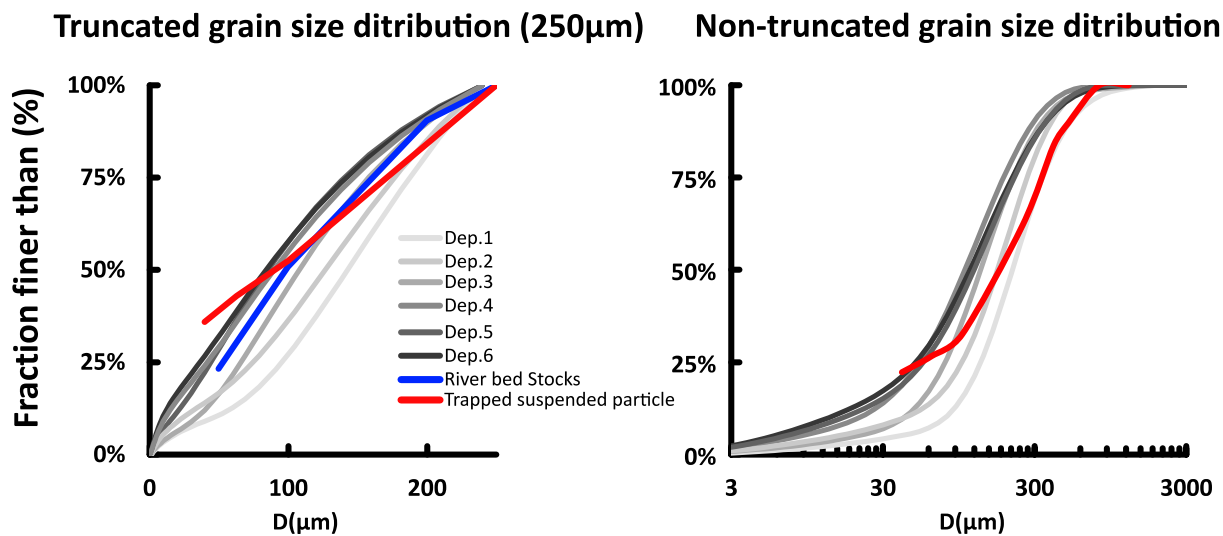


Figure 5.17: Truncated (left panel) and non-truncated (right panel) grain size distribution of suspended sediments captured in a trap (red lines), stored at the river bed surface (grey lines) or measured with the river bed stock resuspension protocol (blue line).

5.9.2. FERGUSON EQUATION

To extrapolate the rating curve obtained between water depth and flow rates, the variable power equation proposed by Ferguson (2007) was used in an iterative way. The parameters needed are the slope (S) of the water surface (-), the coarser surface grain size distribution (D_{84} , the 84% percentile, m) determined using the Wolman count technique [Wolman, 1954] and the cross section's topography. The water level corresponding to a given flow rate was calculated using Eq.5.13:

$$\frac{U}{\sqrt{gR_hS}} = \frac{2.5 \frac{R_h}{D_{84}}}{\sqrt{1 + 0.15 \left(\frac{R_h}{D_{84}}\right)^{5/3}}} \quad (5.13)$$

5.9.3. MAIN EVENT CHARACTERISTICS

Date of Peak	Downstream	Upstream	Upstream vs downstream			Signif ?
	m	SSY _{q50%} (t)	ΔSSY _{q50%} (t)	$\frac{SSY_{down}}{SSY_{up}}_{q50\%}$	$\frac{\Delta SSY}{SSY_{up}}_{q50\%}$	
05/05 01:10	203	221	-18	0.92	-8%	No
05/05 22:40	315	297	18	1.06	6%	No
06/05 21:50	965	1114	-149	0.87	-13%	Yes
07/05 20:20	779	932	-155	0.83	-16%	Yes
11/05 20:30	285	198	87	1.44	44%	Yes
12/05 23:40	360	239	122	1.52	51%	Yes
13/05 16:10	208	152	56	1.37	37%	Yes
15/05 19:00	32	50	-18	0.64	-36%	Yes
17/05 00:00	31	48	-17	0.65	-35%	Yes
17/05 21:00	50	61	-11	0.82	-18%	Yes
19/05 00:30	113	95	18	1.19	18%	Yes
19/05 20:30	88	84	4	1.05	5%	No
20/05 20:20	99	86	12	1.15	14%	No
21/05 22:10	109	95	14	1.14	14%	No
22/05 21:30	103	89	14	1.16	16%	No
23/05 21:40	121	101	20	1.21	20%	Yes
24/05 22:40	109	90	19	1.20	21%	Yes
25/05 22:40	379	253	125	1.50	49%	Yes
26/05 19:30	420	278	142	1.51	51%	Yes
28/05 18:50	1453	1769	-317	0.82	-18%	Yes
29/05 20:50	834	960	-125	0.87	-13%	Yes
30/05 23:00	422	418	5	1.01	1%	No
31/05 20:50	286	203	83	1.41	41%	Yes
01/06 22:30	225	149	76	1.51	51%	Yes
02/06 21:50	463	392	71	1.18	18%	Yes
04/06 00:00	275	215	61	1.28	28%	Yes
04/06 20:20	178	171	8	1.04	4%	No
06/06 00:00	229	192	38	1.19	19%	Yes
06/06 18:30	100	125	-25	0.80	-20%	Yes
07/06 22:30	422	352	69	1.19	19%	Yes
08/06 22:30	147	139	9	1.06	6%	No
09/06 21:00	180	185	-5	0.97	-3%	No
10/06 22:40	75	87	-12	0.87	-14%	No

11/06 11:00	801	644	159	1.25	24%	Yes
12/06 23:20	297	277	20	1.07	7%	No
13/06 17:40	154	181	-26	0.86	-14%	No
14/06 20:20	127	177	-50	0.72	-28%	Yes
15/06 22:50	88	144	-56	0.61	-39%	Yes
16/06 20:00	75	141	-67	0.53	-47%	Yes
17/06 21:30	70	138	-68	0.51	-49%	Yes
18/06 22:30	116	175	-60	0.66	-34%	Yes
19/06 22:00	170	209	-39	0.81	-19%	Yes
20/06 23:10	364	394	-31	0.93	-7%	No
21/06 22:20	246	261	-15	0.94	-6%	No
22/06 21:10	131	189	-58	0.69	-31%	Yes
23/06 21:20	63	135	-72	0.47	-53%	Yes
24/06 22:00	29	96	-67	0.30	-70%	Yes
25/06 20:00	23	80	-57	0.29	-71%	Yes

Table 5.3: Main characteristics of the 48 events observed during the field campaign on upstream and downstream stations. $SSY_{q50\%}$ corresponds to the median value obtained during Monte Carlo simulations for the SSY of each event. $\Delta SSY_{q50\%}$ corresponds to the median value obtained during Monte Carlo simulations for the difference between downstream and upstream SSY, $\frac{SSY_{down}}{SSY_{up}}_{q50\%}$ indicates the median value obtained during Monte Carlo simulations for the suspended sediment yield ratio and $\frac{\Delta SSY}{SSY_{up}}_{q50\%}$ the median value obtained during Monte Carlo simulations for the relative SSY difference (with regard to the upstream SSY). “Signif” indicates that the upstream and downstream SSY distributions are significantly different considering the measurements uncertainties.

Chapter 6

Identifying bed-related suspended load by using continuous turbidity and seismic measurements in a gravel bedded alpine stream

This sixth chapter presents the use of concomitant continuous seismic and turbidity measurements to identify interactions between fine suspended particles and the river bed mobility in a braided Alpine river (La Séveraisse). This work shows how the use of these two non-time-consuming continuous measurements opens up interesting opportunities concerning the understanding of suspended load dynamic and sediment source in the field. These measurements are consistent with previous local and large scale observations confirming that strong interactions exist between suspension and river bed mobility in Alpine gravel bed rivers. This chapter corresponds to an article in preparation by Misset C., Recking A., Legout C., Gimbert F., Geay T., Bakker M., Cazilhac M., Poirel A. and Zanker S.

Ce sixième chapitre présente l'utilisation conjointe de mesures continues de turbidité et de vibrations sismiques afin d'identifier les interactions entre les sédiments fins et la mobilité du lit d'une rivière en tresse alpine (La Séveraisse). Ce travail montre que l'utilisation de ces deux mesures continues faciles à mettre en œuvre sur le terrain ouvre des opportunités intéressantes concernant la compréhension de la dynamique du transport par suspension et de l'activation de différentes sources sédimentaires. Ces mesures sont cohérentes avec les précédentes observations locales et à large échelle. Elles confirment les fortes interactions entre suspension et mobilité du lit des rivières à gravier alpines. Ce chapitre est un article en cours de préparation (contributeurs Misset C., Recking A., Legout C., Gimbert F., Geay T., Bakker M., Cazilhac M., Poirel A. and Zanker S.).

6.1. INTRODUCTION

Studying sediment partitioning has been a major research topic for decades because this conceptual description is crucial for our understanding of sediment transport processes. Coarse particles (Boulder to sand sizes) are often considered to be transported as bedload by sliding, rolling or saltating with strong interactions with the river bed and its morphology. Finer particles (sand to clay size) are often considered to be transported as suspension in the water column. This fraction has been subdivided into bed-material suspended load and wash load depending on the occurrence of interactions that suspension has with the riverbed [Einstein *et al.*, 1940]. This conceptual subdivision led to differences in the way these processes are modelled: bed-material suspended load is considered to be controlled by the flow capacity while wash load is considered to be a function of sediments availability in the watershed. Many theoretical and practical criteria have been proposed for partitioning suspension into wash load and bed-material suspended load. These are mostly based on the sediment size fraction absent from the river bed surface [Einstein *et al.*, 1940], a critical particle size [Partheniades, 1977], a critical Rouse number [Wang and Dittrich, 1992; Wang *et al.*, 2007], a size ratio between bed and suspended material or a balance between transport capacity and sediment availability [Hill *et al.*, 2017]. These criteria help to define the conditions for wash load but are mainly based on flume experiments or on punctual field measurements. Consequently, it is usually difficult in the field to conclude on interactions between suspended load and the river bed. This led to the use of a wide variety of variables describing both hillslope and river bed erosion to predict suspension in the past few decades such as rain, temperature or flow rate [Asselman, 1999; Buendia *et al.*, 2016; Costa *et al.*, 2018; Khosravi *et al.*, 2018; Mano *et al.*, 2009; Park and Hunt, 2018; Picouet *et al.*, 2009].

One valuable way to quantify the presence or absence of interactions between suspension and the river bed would be to measure concomitantly riverbed mobility and suspended load. Indeed, several studies suggest that in gravel bedded streams, the mobility of coarse particles exert a significant control on suspended load by controlling the storage and release of subsurface material [Mooneyham and Strom, 2018; Navratil *et al.*, 2010; Park and Hunt, 2017] and a relation between bedload and suspended load transport has been observed in previous studies [Métivier *et al.*, 2004; Meunier *et al.*, 2006; Misset *et al.*, 2019; Turowski *et al.*, 2010].

To study these interactions and better characterize the fraction of suspension related to the river bed mobilization, we propose to use continuous indirect measurements of the river bed mobility (seismic measurement) and suspended load (turbidity measurement). The main advantages of these measurement techniques are the high temporal resolution and limited field efforts. Thus, this work addresses the following questions: (i) can we use continuous indirect measurements to quantify interactions between coarse

particles mobility and fine particles dynamic? (ii) How do river bed and hillslope respectively contribute to the suspended load in gravel bedded alpine rivers?

6.2. FIELD SITE AND METHODS

These questions were addressed on an alpine river (La Séveraisse) located in the Ecrin massif in the French Alps (Figure 6.1) during the April-August period. At the monitoring station (red point in Figure 6.1) the drainage area is 130km² and comprises some glaciers located on the upper part of the basin (maximum altitude, 3579 m NGF). This catchment is characterized by a low human impact and active eroded areas on hillslopes (Figure 6.1-a) generating large quantities of sediments during debris flow [Helsen *et al.*, 2002] or rock fall events. The river bed in the downstream part of the valley has a slope between 1 and 2% and alternate between braiding with active width of approximately 100m (Figure 6.1-b) and narrower constrained sections 20m wide. The river bed grain size distribution (GSD) obtained from non-truncated Wolman counts (more than 1600 particles performed in May and June) in the two braided sections upstream the measurements station has a median diameter of 37mm and a 84th percentile of 113mm. GSD of fine particles deposited at the riverbed surface has a median diameter ranging between 100 and 200µm (6 samples) which was found to be similar to fine particles transported as suspension and captured in a trap (median diameter around 200µm on 500g sieved). River bed stock measurements (16 samples) and trapped suspended particles exhibit similar size distributions. The hydrology is influenced by snowmelt during the late spring to the beginning of summer and by the ice-melt and storms during the late summer and autumn. Low flow periods are observed when the basin has a snow cover in winter.

A preexisting hydrometric station (red point in Figure 6.1) maintained by EDF (French hydro-electricity company) measured a 1-min average water level every 10-minutes using pressure sensor. Repeated gauging were performed using salt dilution, current meter or Acoustic Doppler Current Profiler techniques to build a rating curve between the water level (h) and the flow rate (Q):

$$h = f(Q) \tag{6.1}$$

A turbidity meter (Hach Lange Solitax) was installed approximately 50 cm above the bottom of the river bed near the water pressure sensor. Such sensor has a detector aligned at an angle to the beam to measure the scattered light. It also has an automatic cleaning system preventing the development of biofilm on the sensor which was also checked regularly by the field team. An average value of turbidity (Tu) measured for 1 min was recorded every 10 min. Turbidity measurement is a function of suspended sediment concentration (SSC) and suspended particle size ($D_{\text{suspension}}$) [Landers and Sturm, 2013; Lewis, 1996]:

$$Tu = f(SSC, D_{suspension}) \quad (6.2)$$

It is thus commonly used coupled with direct sampling to estimate suspended load [Landers and Sturm, 2013; Lewis, 1996; Mano et al., 2009; Navratil et al., 2011; Orwin and Smart, 2004a]. As direct sampling of SSC were only available from May to late June, it was not possible to ensure that the SSC-turbidity relationship was stable over the whole study period. Thus, we preferred to use the raw turbidity signal as a surrogate of SSC including possible particle size changes through time. According to observations conducted by Landers and Sturm (2013) for a given SSC a decrease in suspended sediment size will induce an increase of the measured turbidity.

A seismic sensor (PE-6/B geophone) was installed 25 m from the left channel bank near the turbidity and water pressure sensors. This geophone records ground-motion vibration in the range ca. 5–200 Hz including frequencies expected for bedload transport [Gimbert et al., 2019; Tsai et al., 2012] and flow turbulence [Gimbert et al., 2014]. The data were recorded with a 400-Hz frequency on a DiGOS DATA-CUBE³. The raw seismic signal of vertical ground vibrations (m/s) calculated using geophone specifications and data logger settings was analyzed in the time frequency domain. Spectrograms with a 3s temporal resolution were obtained using Fast Fourier Transform and the method of Welch (1967) as in Burtin et al. (2016). The median value of this signal on a 10-min time step was used to remove anthropogenic noises. We then calculated the seismic power P_b in the 20- to 80-Hz frequency range allowing maximum sensitivity to bedload while minimizing the contribution of strong site effects at higher frequencies and flow turbulence at lower frequencies [Cook et al., 2018; Gimbert et al., 2014]. Seismic power caused by bedload transport (P_b) results from impacts exerted by the transported material on the river bed. It is expected to be a function of the bedload flux (Q_b) and of the coarsest fraction of the transported material ($D_{bedload}$) to the power 3 [Tsai et al., 2012]:

$$P_b = f(Q_b \times D_{bedload}^3) \quad (6.3)$$

Air temperature and rain data were also provided by EDF with a 6-min time step. These measurements were conducted on a station located approximately 5km upstream the outlet of the catchment (green point in Figure 6.1).

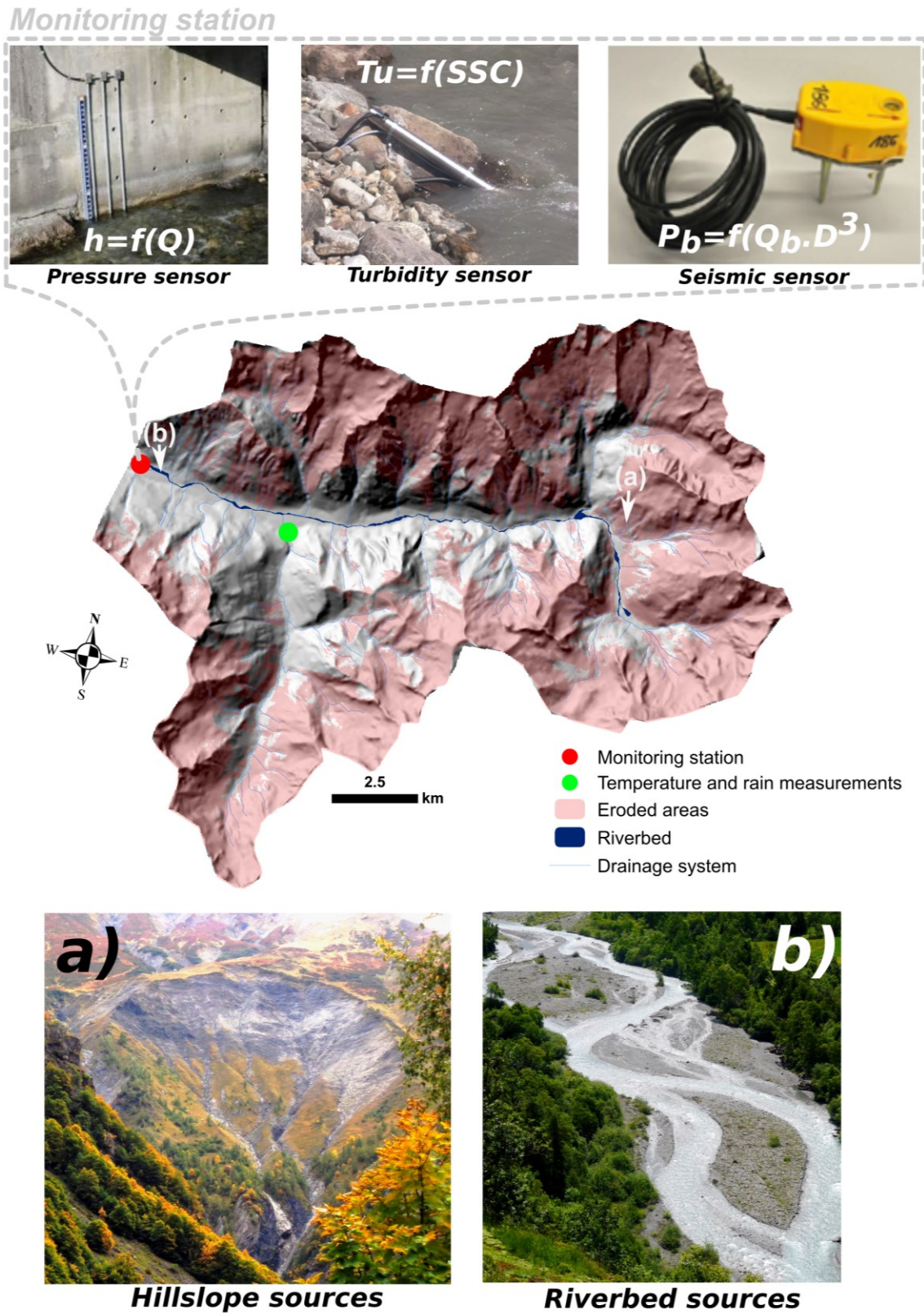


Figure 6.1: Presentation of the field site and the monitoring configuration.

6.3. RESULTS

During the May-August period, the temperature ranged between 0 and nearly 30°C, the flow rate ranged between 5 and 41m³/s and rainfall attained a maximum of 13.8mm/6min (Figure 6.2). Turbidity varied over more than two orders of magnitude (6-600 FNU) and seismic power over nearly three ($5 \cdot 10^{-15}$ - $2 \cdot 10^{-12}$ m²/s²). A first look at these data revealed that flow rate, turbidity and seismic signals exhibited daily fluctuations related to snowmelt or ice-melt. Two periods could be identified. During the melting period (May-June), the flow rate was rather high (>10m³/s), rainfall relatively limited and the turbidity evolved concomitantly with the seismic power. During the late season (July-August) the flow rate was on average lower except during storm events with intense rainfall that occurred mainly in late July to early August. Turbidity and seismic power evolved in a different way during this period as high turbidity could be observed while seismic power was relatively low.

A more detailed analysis (Figure 6.3) indicates that the relation between turbidity and flow rate was highly variable, with two orders of magnitude being observed for a given flow rate. Tu values indicated a seasonal variation, with a Tu-Q relation decreasing from May to June. It then increased during the July-August period (Figure 6.3-a). While such high variability of turbidity time series has been observed in several previous studies [Guillon *et al.*, 2018; Mano *et al.*, 2009; Mao and Carrillo, 2016; Navratil *et al.*, 2011], flow rate was often the only available variable that was used to interpret suspended load dynamic.

The relation between seismic power and flow rate (Figure 6.3-b) shows a similar seasonal decreasing trend during the May-June period while P_b was relatively high ($>10^{-14}$ m²/s²). P_b -Q relation was more variable during the second period and high P_b could be observed for low Q. Considering the lower P_b values measured for a given flow rate, a breaking point is observed with a steeper increase of P_b for Q larger than approximately 10 to 12m³/s. This might be explained by a predominant contribution of turbulence induced vibrations for the lower part and an initiation of bedload inducing additional ground vibrations for the upper part (Bakker *et al.* 2019 under review).

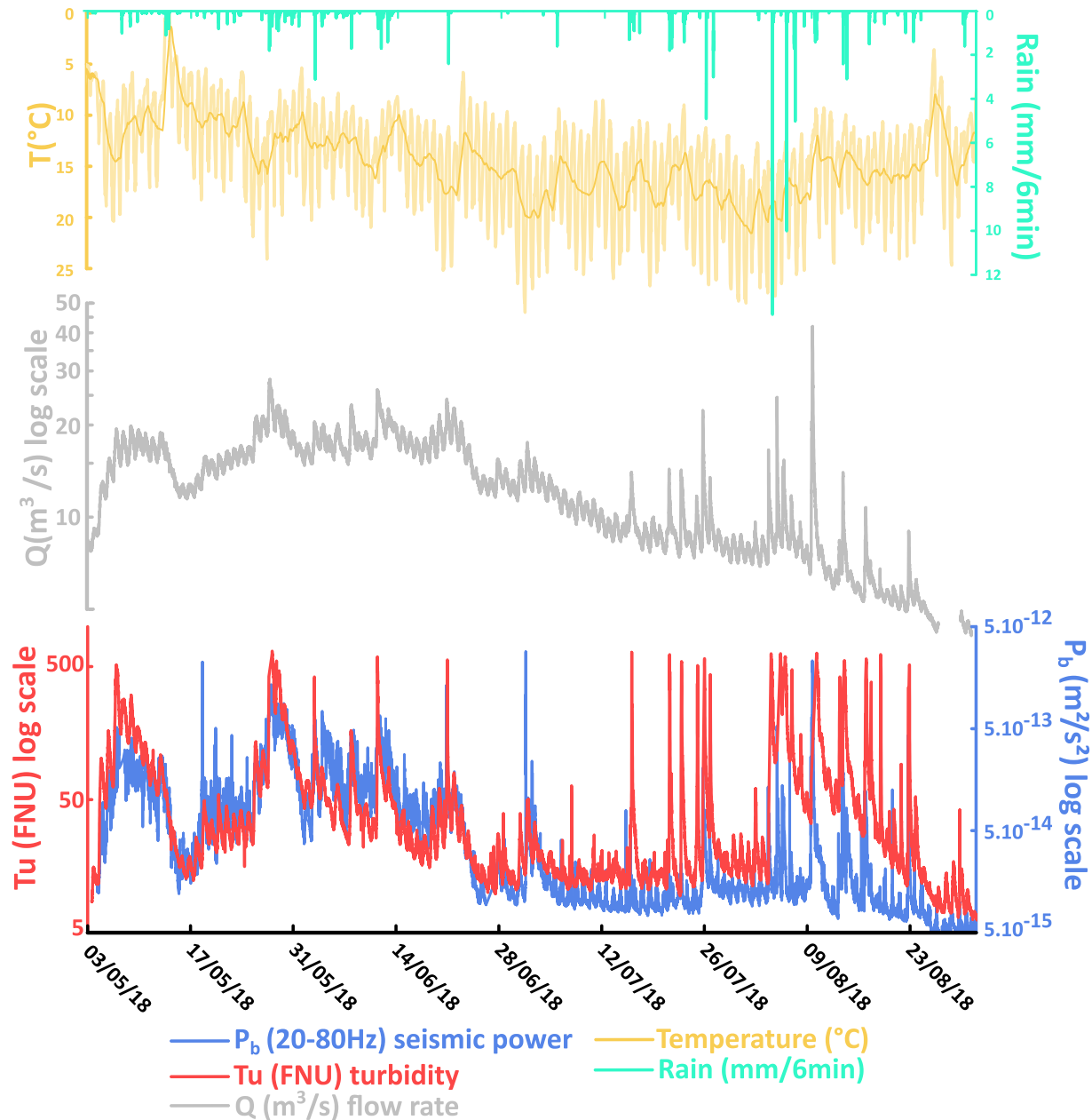


Figure 6.2: Time series of the measurements conducted in the Séveraisse catchment.

When analyzing the relation Tu - P_b in Figure 6.3-c, two well defined behaviors could be observed. For high seismic power ($P_b > 1.5 \times 10^{-14} \text{ m}^2/\text{s}^2$ and $Tu < 1.07 \times 10^{22} P_b^{1.5}$) associated with significant bed mobilization, Tu and P_b co-evolved and were well correlated (Spearman and Pearson correlation coefficient of respectively 0.8 and 0.7). This mainly concerns the melting period events (dark blue) including some measurements in early August during a large storm. For lower seismic power associated with limited bed mobilization ($Tu > 20 \text{ FNU}$ and $Tu > 1.07 \times 10^{22} P_b^{1.5}$), a high variability of turbidity was observed. This mainly concerns the July-August period (light blue)

characterized by several storm events (Figure 6.2). Tu and P_b were much less correlated in that part of the scatter plot (Spearman and Pearson correlation coefficient of respectively 0.47 and 0.48).

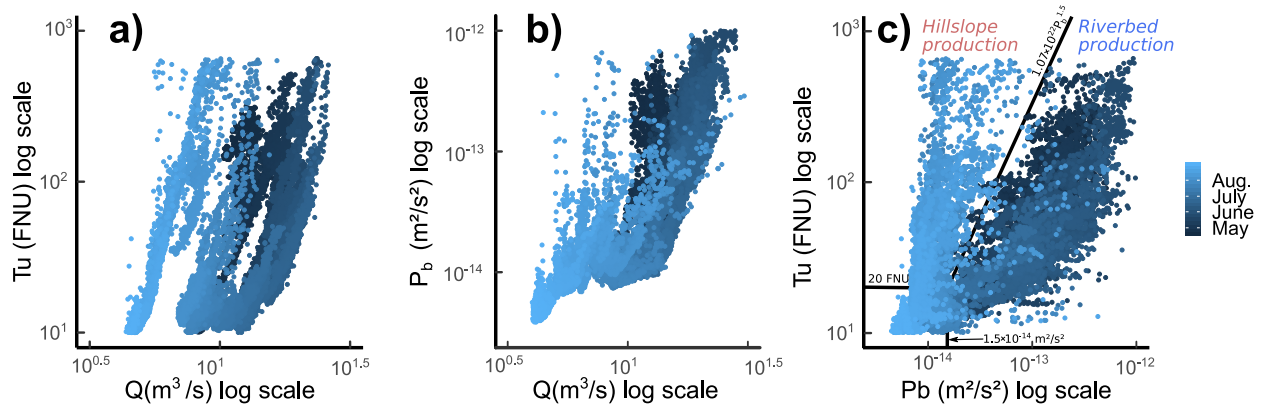


Figure 6.3: Relations between turbidity, flow rate and seismic power during the May-August period. Point color is a function of time. The part considered as river bed production is defined by $P_b > 1.5 \times 10^{-14} m^2/s^2$ and $Tu < 1.07 \times 10^{22} P_b^{1.5}$. The part considered as a global hillslope production is defined by $Tu > 20$ FNU and $Tu > 1.07 \times 10^{22} P_b^{1.5}$.

6.4. DISCUSSION

6.4.1. EVOLUTION OF THE ORIGIN OF SUSPENDED PARTICLES DURING A 4 MONTH PERIOD

As turbidity and seismic power exhibited different behaviors depending on the period (i.e. May-June and July August, Figure 6.3-c), we tested the assumption that this could be the signature of different production processes of fine particles. We interpreted Tu co-evolving with P_b when P_b was high ($P_b > 1.5 \times 10^{-14} m^2/s^2$ and $Tu < 1.07 \times 10^{22} P_b^{1.5}$) as a production of fine particles mainly controlled by their release from the river bed. On the contrary, the high variability of Tu when P_b was low ($Tu > 20$ FNU and $Tu > 1.07 \times 10^{22} P_b^{1.5}$) suggested a production of fine particles mainly controlled by a different source from the river reach measured with the seismic sensor. This production could be related to either the contribution of upstream river reaches or a global hillslope production. Because we did not have SSC measurements during the July-August period we could not conclude whether the higher turbidity for a given seismic power observed in that period was solely due to a much higher SSC or a to significant decrease in the suspended sediment GSD (Eq.6.2). However, both hypotheses support the above interpretation of two different dominant production processes.

Based on this partition, we could classify instantaneous measurements of 155 peak flow events observed during the 4-month campaign into “dominant river bed” and “dominant global hillslope” production of fine particles. Assuming that the SSC-Tu relation obtained in May-June was representative of the whole period, we could infer a dominant river bed production corresponding to 77% of the total fluxes while the dominant global hillslope production corresponded to 16% (7% undetermined when T_u and P_b were both really low). We should stress that the possible decrease of suspended particle size in the July-August period would have led to a dominant global hillslope production representing an even smaller fraction of total fluxes.

To test the relevance of this partition, we analyzed the hydro-meteorological conditions corresponding to each production processes. Results indicate that river bed production was generally characterized by relatively low cumulated rainfall, high average flow rate and limited flow variability (Figure 6.4). On the contrary, the global hillslope production was characterized by relatively higher cumulated rainfall, lower average flow rate and high flow variability. The temperature was only slightly higher for the global hillslope production. This analysis was consistent with the partition into two production processes obtained by using independent turbidity and seismic data: dominant river bed production was likely to govern suspension for high flow rates and low rainfall intensity while the dominant hillslope production was likely to govern suspension when the river bed was not mobilized and when erosion on hillslopes due to rainfall was maximal. We should also stress that during the first part of the measurement period (May-June) a significant part of hillslope sources were protected by a snow cover which progressively melted so that hillslope sources were unprotected during the second July-August period.

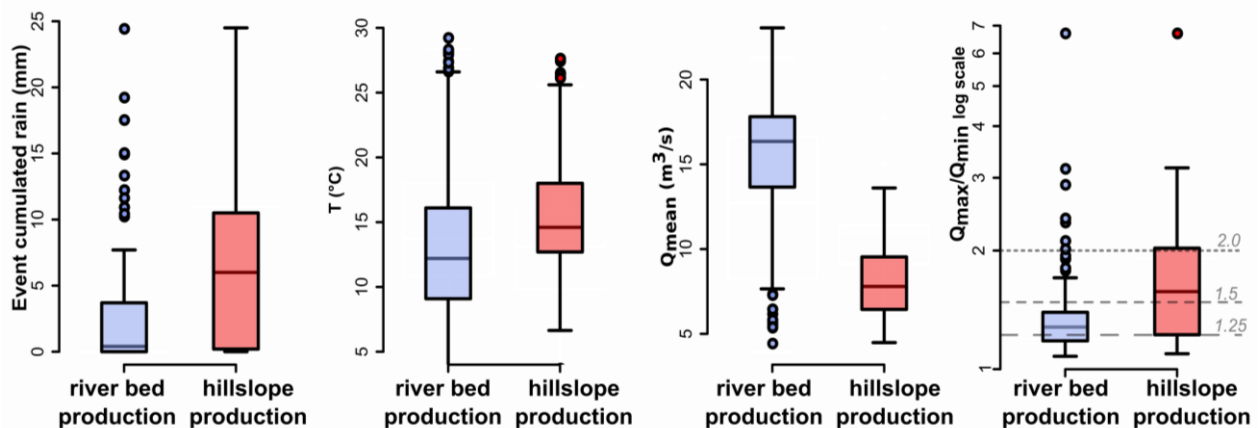


Figure 6.4: Hydro-meteorological conditions corresponding to the two different fine particle production processes inferred using turbidity and seismic measurements to partition instantaneous measurements.

6.4.2. INTEREST OF THE COMBINED USE OF TURBIDITY AND SEISMIC MEASUREMENTS

These results show the interest in terms of methodology to combine seismic measurements and commonly used flow rate and turbidity measurements. It allows to record with a high temporal resolution transport interactions between fine and coarse sediments and to detect various sediment sources activation in the field. Inverting seismic power into bedload flux is often challenging. The transported diameter is often unknown and seismic power associated to bedload is theoretically expect to scale with the coarsest fraction of transported material to the power 3 (Eq.6.3) [Tsai *et al.*, 2012]. In fact, this high sensitivity of the method to the coarsest fraction could be considered as an opportunity to use seismic measurement as a relevant proxy of the global river bed mobility and subsurface material availability.

These field observations have implications concerning our understanding of the sediment transport processes. Experiments of Mooneyham and Kyle (2018) among several others flume and field observations [Diplas, 1994; Frostick *et al.*, 1984; Glasbergen, 2014; Krishnappan and Engel, 2006; Navratil *et al.*, 2010] have shown that fine particles infiltrate in the gravel matrix even for very low Rouse number and stay in the subsurface until the surface coarse bed particles are mobilized. Our observations suggest that the degree of river bed mobility controls the release of these fine particles infiltrated in the subsurface of gravel bedded streams. While this process is often neglected for the finest fraction of suspension, it is consistent with the generally admitted idea that the armor layer mobility controls the availability of subsurface material in that kind of river [Lenzi *et al.*, 1999; Misset *et al.*, 2019; Park and Hunt, 2017; Pitlick *et al.*, 2008; Recking, 2013b]. It is also in-line with recent studies focused on the wash load concept concluding to strong interactions between that fraction and the river bed [Mooneyham and Strom, 2018; Navratil *et al.*, 2010; Orwin and Smart, 2004b; Park and Hunt, 2017]. These studies and our observations question on the definition of the wash load concept. When referring to the recent multicriteria of Hill *et al.* (2017), the suspended load measured in our study should be considered as wash load (see appendix 6.6 for details) while it co-evolved with the river bed mobility for approximately half of the measurement period.

6.5. CONCLUSIONS

Continuous field measurements using turbidity and seismic sensors in a gravel bedded alpine river revealed strong interactions between suspended load and river bed mobility. This highlighted the significance of the release of fines particles when coarse particles of the river bed were mobilized, a sediment transport processes often neglected for the finest fraction of suspension in such mountainous context. This study shows that using continuous measurements such as turbidity combined with seismic or another proxy of

the river bed mobility (hydrophone, geophone plates) could be a valuable way to identify the river bed related suspended fraction with a high temporal resolution. It opens up some considerable opportunities to improve our understanding of complex interaction between the different modes of sediment transport.

6.6. APPENDIX

Theoretical partitioning into wash load and bed material load:

To partition the suspended load measured into wash load and suspended bed material we used the recent criteria proposed by Hill et al. (2017). They observed during flume experiments that the transition between the lubrication regime (decrease of the river bed slope due to the ad of fine particles staying on the river bed surface) to the wash load regime (which they define as the addition of fine particles having no effect on the river bed slope in their flume) occurred when the three following criteria are fulfilled: sediment ratios between bed and suspended particle size (D^* , Eq.6.4) larger than 30, Rouse numbers for suspended material (R_o , Eq.6.5) lower than 0.8 and supply versus transport capacity ratio for suspended material (qs^* , Eq.6.6) lower than 0.05.

$$D^* = \frac{D_{bed}}{D_{suspension}} \quad (6.4)$$

$$R_o = \frac{w_s}{\kappa u^*} \quad (6.5)$$

$$qs^* = \frac{qs_{supply}}{qs_{capacity}} \quad (6.6)$$

D_{bed} (m) is the median river bed diameter, $D_{suspension}$ (m) the median suspended diameter, w_s (m/s) the fall velocity for suspended particles calculated using the method described in Ferguson and Church (2004) as in Hill et al. (2017), κ (-) is the Von Karman constant of 0.4, u^* (m/s) the friction velocity estimated from the shear stress calculated in the main channel, qs_{supply} (m²/s) the suspended load measured in the field estimated for a upper and a lower limit (Figure 6.5) and $qs_{capacity}$ (m²/s) the capacity of the flow to transport particles calculated by using the Engelund and Hansen (1967) formula (Eq.6.7) as was done by Hill et al. (2017):

$$qs_{capacity} = \sqrt{g(s-1)D_{suspension}^3 \frac{0.05}{C_f} (\tau^*)^{5/2}} \quad (6.7)$$

In which, g (m/s^2) is the acceleration due to gravity, s (-) the relative sediment density, C_f (-) the averaged friction coefficient in the main channel and τ^* (-) the averaged shield number in the main channel considering the suspended diameter.

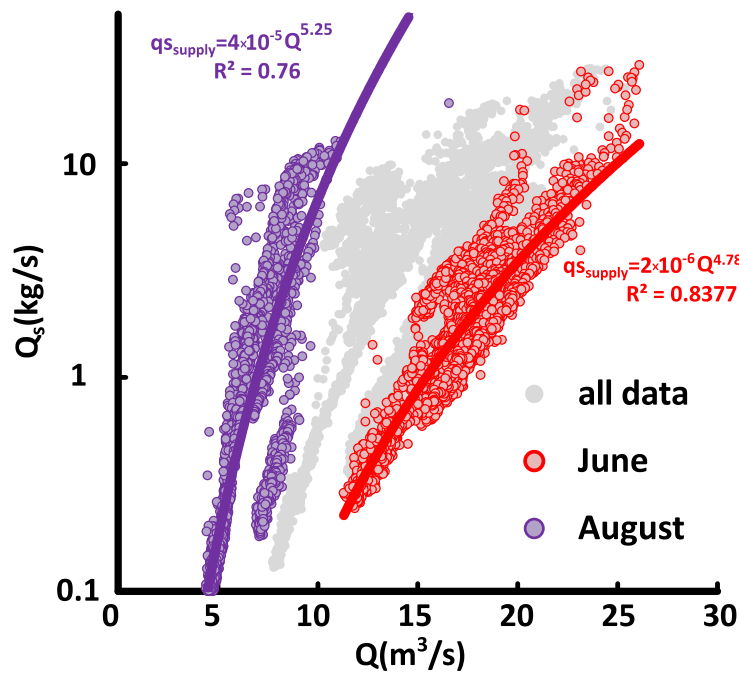


Figure 6.5: Suspended sediment supply measured and its upper and lower limit considered.

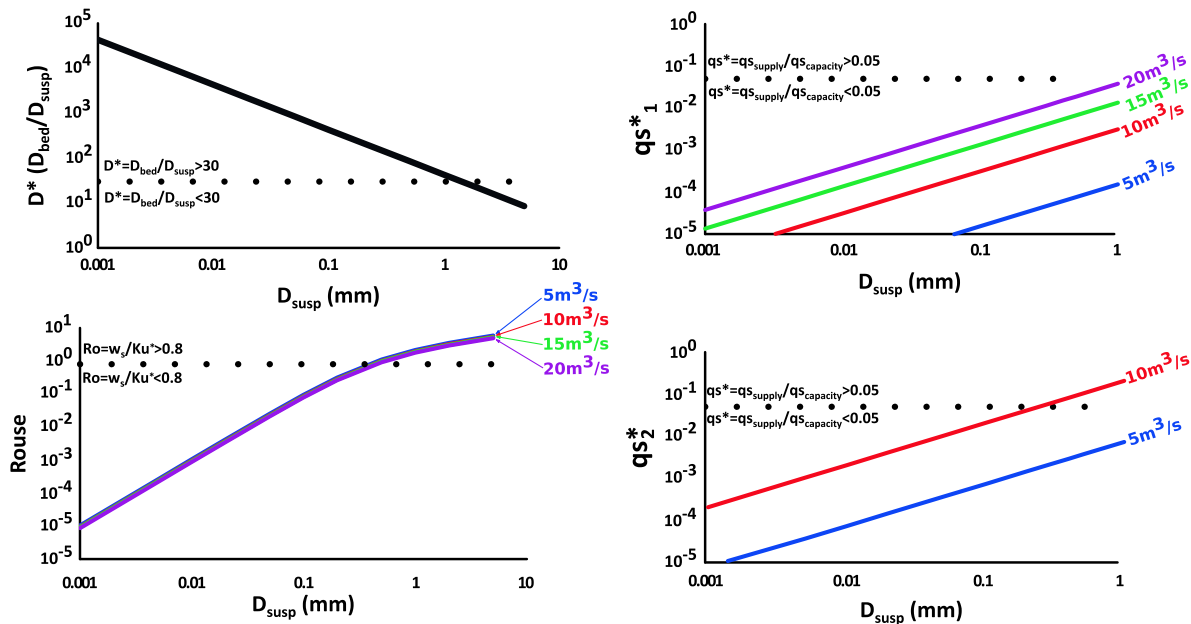


Figure 6.6: Calculation of hill criteria for wash load regime definition varying the suspended sediment size and the flow rate. Note: qs^*_1 and qs^*_2 denote respectively the lower and upper supply (Figure 6.5).

Because the suspended sediment diameter was not continuously available and because flow rates were unsteady as it is often the case in the field we made calculations varying these two variables (Figure 6.6) to compare with critical values defining the wash load domain according to Hill et al. (2017). Criteria on Rouse number and D^* indicate that whatever the flow rate, suspended load can be considered as wash load for $D_{\text{suspension}}$ smaller than approximately $500\mu\text{m}$. The capacity vs supply criteria is more complex as it significantly varies with $D_{\text{suspension}}$ and Q . The supply is also changing through time with a lower limit mainly in the May-June period and an upper limit in the July-August period (Figure 6.5). The most critical condition is attained considering the upper supply (qs^*_1 in Figure 6.6) observed for a maximum flow rate of approximately $10\text{m}^3/\text{s}$ (higher flow rates are not attained for that supply). For these conditions particles coarser than $200\mu\text{m}$ are not considered as wash load. The lower supply (red line in Figure 6.5) corresponds to a critical particle size of $400\mu\text{m}$ for wash load. Consequently, according to measurements of grain size distribution of trapped sediments ($D_{50}=200\mu\text{m}$) that can be considered representative of the averaged size transported, our suspension should be considered as wash load in May-June period while it interact significantly with the river bed. On the contrary, in the July-August period, when limited bed mobility is observed suspended particle sizes are those that start to be considered as non-wash load.

Conclusion and perspectives

SYNTHESIS

CONSISTENCY BETWEEN OBSERVATIONS MADE AT THE CATCHMENT AND AT THE REACH SCALE

The two parts of this manuscript report observations and analysis performed at different scales. In the following section, the extent to which they are consistent is discussed. In part 1, we observed a link between suspended load hysteresis and sediment sources configuration. In the second part we observed at a local scale significant buffering processes in the Séveraisse. Figure 7.1 shows that this basin can be well described by the hysteresis-sediment source configuration relation obtained in part 1 (chapter 1).

The Séveraisse catchment has a relatively low sediment source index of 3.7 (considering 70% of the catchment) which is similar to the Drac catchment and which was interpreted as a significant capacity to produce distant fluxes and to buffer these fluxes in the main fluvial system. This interpretation of the hysteresis-sediment sources configuration relation is consistent with the observation of significant intermediate storage processes in the Séveraisse (chapter 5).

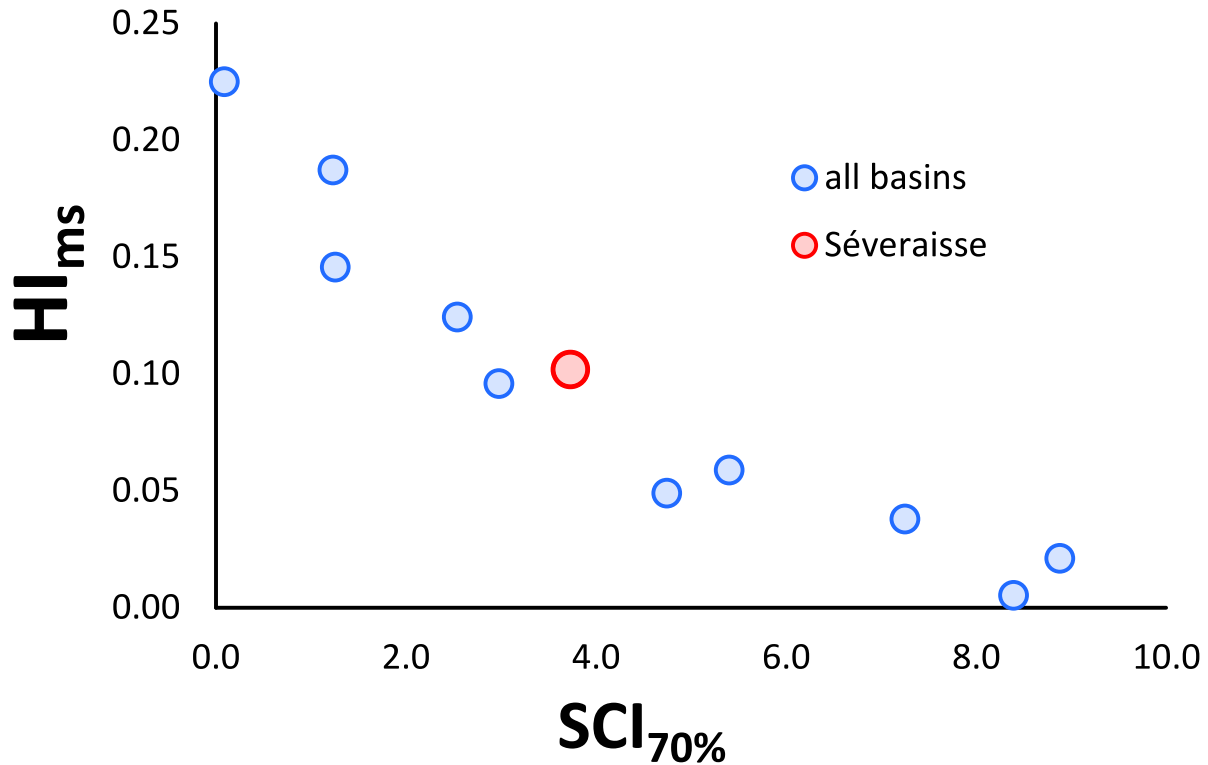


Figure 7.1: Relation between the mass weighted hysteresis index (HI_{ms}) and the sediment source configuration considering 70% of the catchment ($SCI_{70\%}$) for the studied basins of chapter 1 (blue points) and for the Séveraisse (red point).

In the first part of the manuscript, we observed a relation between suspended sediment concentration and dimensionless bedload rate (chapter 3). Applying this relation to the Séveraisse with cross section parameters changing through time (detailed in chapter 4), led to reasonable estimations of the measured suspended fluxes and their dynamics (Figure 7.2). 12600 and 5500 tons were measured in May and June respectively while modeling using the cross section 1 and 2 defined in chapter 4 led on average to 13200 and 6200 tons respectively. The decrease of suspended load was well reproduced by this model based on riverbed mobility even though June was characterized by higher flow rates and water volumes transported than during May ($Q_{max,May} = 25.8\text{m}^3/\text{s}$, $Q_{max,June} = 26.1\text{m}^3/\text{s}$, $Q_{mean,May} = 15.3\text{m}^3/\text{s}$, $Q_{mean,June} = 16.9\text{m}^3/\text{s}$) and water volume transported 8% lower in May. Independently from this analysis, continuous seismic and turbidity measurements also show a strong relation between fine and coarse particles transport in the Séveraisse (chapter 6) which makes the coarse and fine particle transport interactions consistent in the two parts of the manuscript.

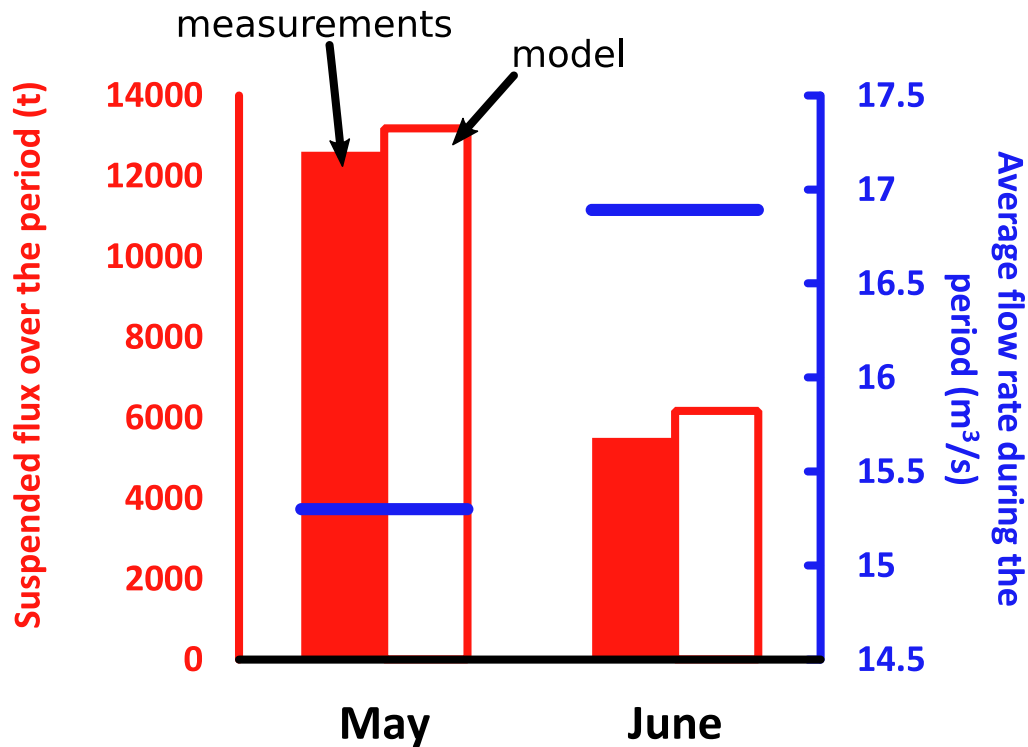


Figure 7.2: Comparison between suspended fluxes measured in the Séveraisse during May and June (chapter 4 to 6) and suspended fluxes estimated using the relation between riverbed mobility and suspension (chapter 3). Increasing average flow rate during the period is also indicated (blue lines).

MAIN CONCLUSIONS CONCERNING THE PROCESSES OBSERVED

The main objective of this work was to understand the role of the river bed on suspended sediment transfer in Alpine catchments. This key question for both scientists and practitioners raised interrogations on how fine particles eroded on hillslopes are transferred downstream, on the conditions for which deposition and erosion of fine particles are significant and on how fine and coarse particles interact. All chapters of this manuscript are self-standing and focused on one of these specific questions. They have their own conclusions which are synthetized in the following section.

Our observations show that suspended load can strongly interact with the river bed in alluvial Alpine rivers. Fine particles eroded on hillslopes are not necessarily directly transferred downstream. They can be stored in the fluvial system over longer time scales as suggested by the large quantities of fine particles found in alluvial Alpine streams. Even if they are absent at the bed surface, significant quantities can be found in the subsurface under a poorly mobile armored layer (Chapter 2). This shows that the buffering capacity of alluvial streams on fine particle transfer cannot be neglected in

Alpine rivers. Consequently, because of this river bed buffering capacity, the transfer of suspended particles eroded on hillslopes strongly depends on the geomorphological catchment configuration and thus on the location of the observation point considered along the drainage system. This suggests that the suspended load dynamics at a given point will be driven by both the relative capacity of the catchment to produce fine sediments on the slopes and the capacity to buffer these upstream fluxes in the fluvial system to cross. This conclusion is supported by the relation observed between suspended load hysteresis patterns and sediment sources configuration (chapter 1), by the river bed stocks measurements (chapter 2) and the relation observed between suspended load and bedload (chapter 3). It is also consistent with several recent studies [Mooneyham and Strom, 2018; Navratil et al., 2012; Park and Hunt, 2017]. It highlights that a wash load assumption is not always straightforward in Alpine catchments which has important implications for both scientists and practitioners.

The analyses performed in this work suggest that erosion and deposition of fine particles are significant in large alluvial streams having gentle slopes (chapters 1, 2, 3 and 5). In these streams, deposition seems to preferentially occur in secondary channels and in vegetated bars (chapter 2). Also, the detailed measurements presented in chapter 5 suggest that deposition could be more significant during the falling limb of flood events than during the rising limb due to more space availability in the gravel matrix which is in line with the conceptual model of Park and Hunt (2017, 2018). These measurements also show that the balance between erosion and deposition can be significantly influenced by the riverbed morphology, mobility and by the upstream hydro-sedimentary forcings (flow rate vs suspended sediment concentration). Indeed, we could derive a behavioral functioning for the studied Séveraisse reach. Below a threshold concentration the system releases more fine particles when increasing the flow rate while above this threshold concentration, the system stores fine particles when increasing the concentration. However, the transferability of these observations should be tested in other geomorphological and hydrosedimentary configurations and over longer time scales as discussed in the following sections.

Finally, the data collected in this work show that coarse particles mobility can have a significant effect on suspended load dynamics. This was the case in alluvial Alpine rivers where large stocks of fine sediments were observed (Chapter 2) and whose availability was found to be controlled by the mobility of the surface armor layer (chapter 3). This was also confirmed at the reach scale by showing i) significant erosion and deposition of fine particles evolving with river bed morphology and coarse particle transport (Chapter 5) and ii) a relation between continuous measurements of suspended load and river bed mobility (Chapter 6).

The control exerted by coarse particles mobility on the availability of fine subsurface sediments was evidenced using reach scale morphodynamics such as the

dimensionless bedload rate (chapter 3) of the seismic power associated with bedload transport (chapter 6). Nevertheless, this process remains complex to measure and to model precisely at a local scale. The main challenge in modeling the proportion of fine particles released by the riverbed (chapter 2) remains the ability to estimate the mobilization depth as a function of flow conditions in Alpine streams. While highly uncertain to estimate, bed widening and lateral channel migration might be first orders bed reworking processes considering large events. Also, Chapter 4 shows how difficult are the measurements of underwater bed reworking in mountainous streams. Improving our understanding of this process could be archived by using new measurement techniques, by applying spatially distributed modeling on well constrained datasets or through experimental flume experiments as discussed later.

PERSPECTIVES

PRACTICAL APPLICATION

Measurements or modeling approaches as well as observations made in this work could be useful in practice. Some potential applications and future challenges are discussed in the following section.

Suspended load modeling – application and limitations in practice

Simple geomorphological GIS-based indexes presented in the chapter 1 and used to identify the main contributing sources could be useful in Alpine environments prior to i) the installation and design of the sensors to equip a monitoring station, ii) the definition of a modeling strategy or iii) the planning of catchment management strategies. Also, while performing field measurements remains the most reliable way to estimate suspended load, they are often not available. In that case, the method presented in the chapter 3 could be useful to get an estimate of suspended load at some locations in alluvial streams distant from active hillslope sources. This can help for river management, hydraulic structure design or for environmental studies. However, such estimation remains difficult when no measurements are available in highly eroded and connected head water streams having limited alluvial sections. One possibility for practitioners would be to use empirical relations based on hillslopes properties such as the one of Duvert et al. (2012) using peak discharge and badland cover fraction. In future work, such relation could be improved in an Alpine context by integrating several contrasted catchments and morphometric indexes such as the ones of Cavalli et al. (2013), Heckmann and Schwanghart (2013) combined with those from chapter 1.

When measurements are available, a simple and promising way to make predictions would be to use conceptual models calibrated on data as often done in hydrology for water discharge prediction. Several conceptual approaches have been already

developed in various contexts [Asselman, 1999; Mano, 2008; Park and Hunt, 2018; Picouet et al., 2009]. Amongst these approaches, the one developed by Park and Hunt (2018) is particularly promising as it considers the infiltration and release of fine particles in gravel bedded streams by using few statistically calibrated parameters. This model considers a critical flow rate under which fine particles resulting from the catchment erosion (a base level concentration function of the flow rate) infiltrate in the gravel matrix filling a conceptual storage reservoir. Above this critical flow rate, a certain quantity of fine particles is released in the flow due to bed disturbance and is added to the catchment production. These fine particles resuspended from the river bed are then removed from the conceptual storage reservoir and are thus not available until this stock has been reconstructed after further infiltration. As an example of future promising work that could be conducted, a modified version of this model (detailed in appendix page 216) giving predictions at the event scale was applied in the Asse catchment (Figure 7.3, Table 7.1). Instead of using an exponential law as was initially proposed by Park and Hunt, we used a power law to model the river bed release function. Such formulation permitted a much better fit with our data and was also consistent with observations made in chapters 2 and 3. We also considered that the catchment production of fine particles had a seasonal trend while it was considered constant by Park and Hunt. Such seasonal trend was highly marked on our catchments, particularly during summers which were characterized by really high suspended sediment concentrations. Finally we considered that the quantity of fine sediment that could be released from the river bed was a function of the river bed stock reservoir filling. This means that for the same flow rate, it was easier to flush fine sediments when the river bed stock reservoir was full than when it was nearly empty. This conceptual model was calibrated on the 2011-2013 period and validated on the 2014-2016 period. The quality of the model was evaluated using the following criteria:

$$RSR = \frac{\sqrt{\sum (M_{event, observed} - M_{event, modeled})^2}}{\sqrt{\sum (M_{event, observed} - \bar{M}_{event, observed})^2}} \quad (7.1)$$

$$R = \left| 1 - \frac{\sum M_{event, modeled}}{\sum M_{event, observed}} \right| \quad (7.2)$$

in which, $M_{event, observed}$ is the event mass of suspended sediment observed and $M_{event, modeled}$ the event mass modelled. A perfect model is characterized by a 0 value for all these indicators. Also, RSR values below 0.7 are considered acceptable [Moriasi et al., 2007]. To evaluate the interest of using such modelling approach, we compared it with a simple power law between peak discharge and the event mass of suspended sediment as proposed by Duvert et al. (2012).

	Calibration		validation	
	RSR	R	RSR	R
Conceptual model	0.41	0.00	0.61	0.00
Power law	0.49	0.45	0.74	0.61

Table 7.1: Models performance on the Asse catchment.

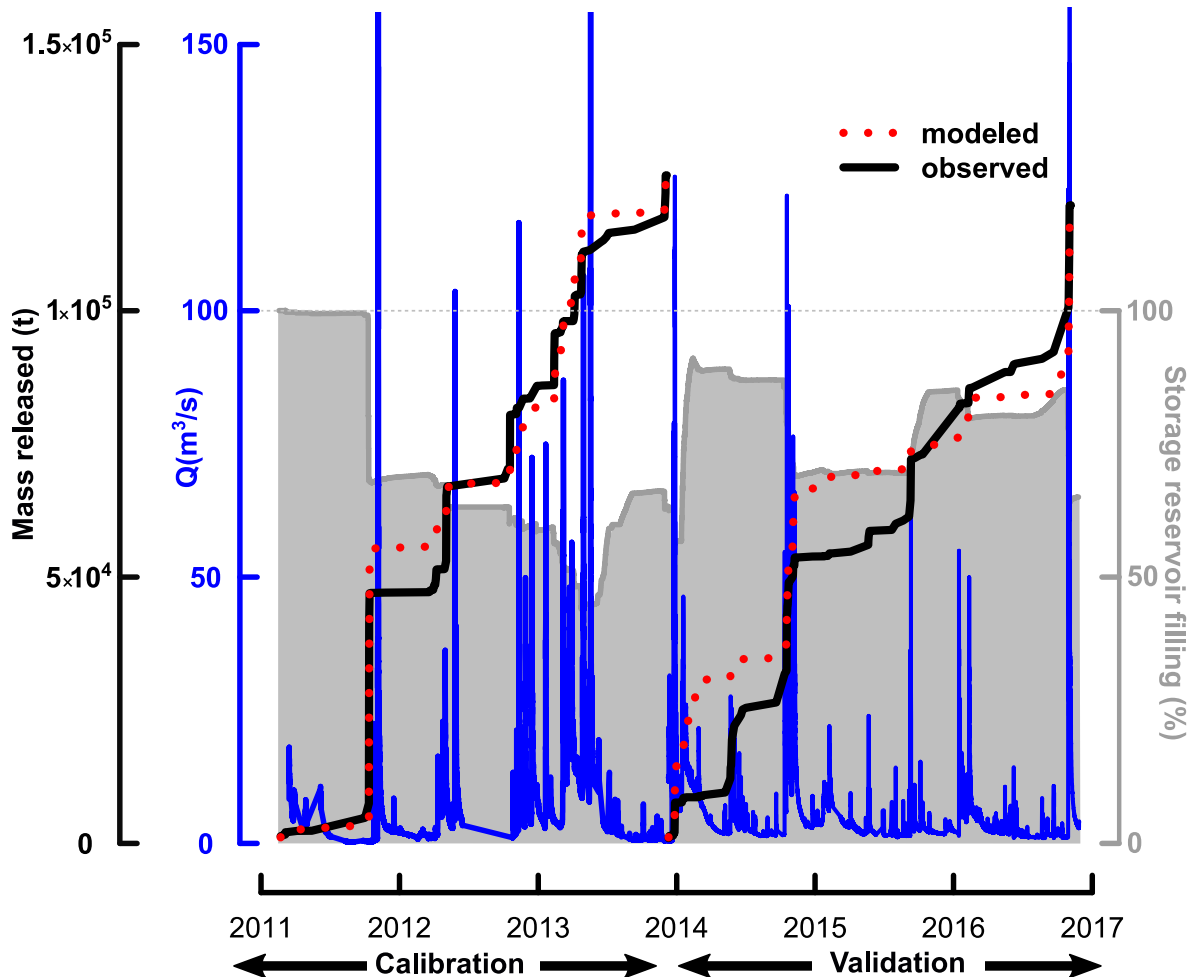


Figure 7.3: Application of a modified version of the conceptual model of Park and Hunt (2018) on the Asse catchment.

The conceptual model reproduces the mass measured with acceptable errors for both the calibration and validation period. It is also much more accurate than the power law model which shows lower predictability during the validation period. Such conceptual model gives information on riverbed stocks evolution through time which can be useful for river or dam management. In the future, such approach which only needs suspended load and flow rate input data should be tested in other Alpine catchments to determine if

it is widely applicable and to analyze how the model parameters are influenced by riverbed and catchment characteristics.

Practical measurements opportunities

A wide range of protocols and measurement techniques have been used in this work. Interesting potential operational applications are proposed below. We have seen that the combined analysis of various measurements is a valuable way to study complex sediment transport processes in the field. The use of continuous proxies of both suspended load (turbidity meter) and river bed mobility (hydrophone, seismic sensor) which are non-time consuming and provide high temporal resolution is particularly interesting (chapter 6). It could be used during dam flushing operations, targeted water releases to flush fine sediments [Loire *et al.*, 2019] or more generally to improve the way water and fine sediments are managed in rivers. The methodology based on Monte Carlo simulations to propagate uncertainties and detect erosion and deposition of fine sediments at the reach scale (chapter 5) could also be useful in other contexts. It could for instance be applied on water intake channels, dams or reservoirs to quantify siltation and conditions favorable to erosion and deposition of fine sediments. This approach could also be transposed on calibrated indirect measurements of bedload transport (hydrophones or seismic sensors).

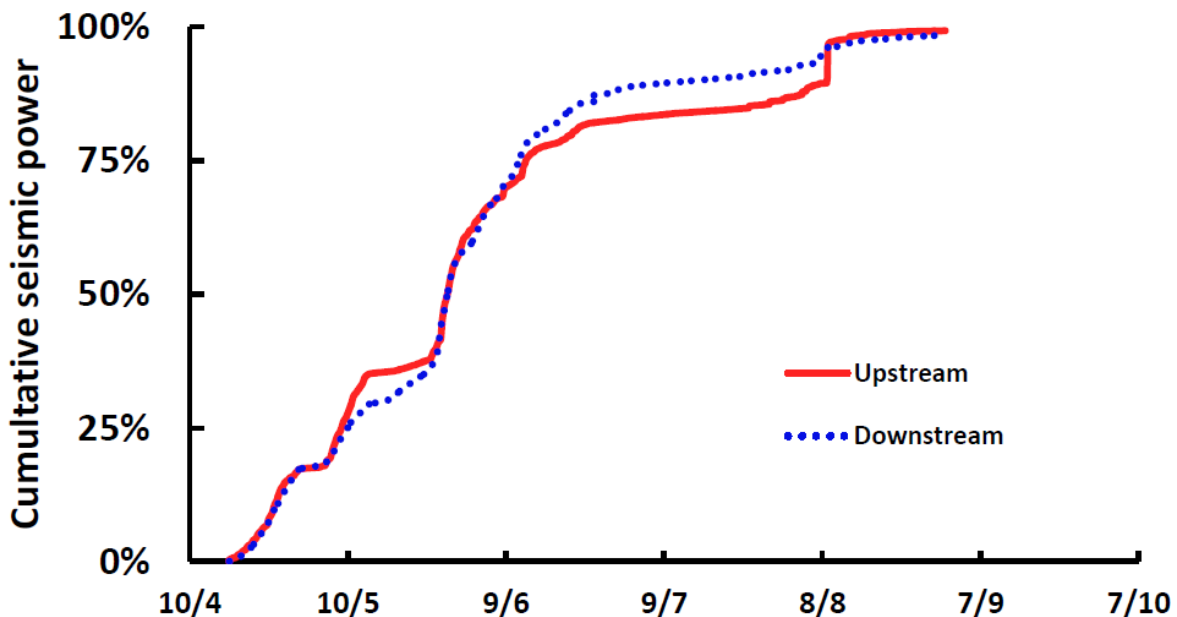


Figure 7.4: Cumulated seismic power of upstream and downstream station on the Séveraisse stream during the 2018 campaign. Potential storages and erosion in the reach are indicated when both curves are not synchronized. Part of these data is presented in chapter 4 and in Bakker *et al.* (under review).

As an example, a sediment budget of coarse particles with a high temporal resolution could be applied on seismic data obtained on the Séveraisse reach (Figure 7.4). This opens up interesting opportunities for practical engineering works or river restoration. Finally, the fine particle storage method (chapter 2) could also be useful to quantify the impact of dam flushing, dragging operation or in-stream construction works on downstream river bed clogging

FUTURE CHALLENGES

Future studies aiming at understanding the role of the river bed on fine particle transfer could use measurement techniques that were not tested in this work. For instance identifying differences in term of fine sediment properties (color, chemistry, size) between those resuspended from the river bed and those directly transferred from the slopes could open up some considerable opportunities. Measuring settling velocities with a high temporal resolution could also help to better understand conditions leading to a direct transfer, to erosion or to deposition, as changes in suspended particle sizes significantly affect these processes. Moreover, using indirect geophysical techniques to integrate river bed stocks with a high spatial resolution would help to better understand interactions between fine sediments and river beds. A more precise quantification of riverbed reworking depth could be archived by using echosonders or active scouring chains as was done by Brousse *et al.* (2018). Also, from a general point of view, we think that future studies would stand to benefit from using a combination of measurements rather than a single observation. Such combination is a real opportunity to improve our knowledge in sediment transport science in which processes are generally complex to observed, highly variable in space and through time, but strongly interacting with each other. As an example, a measurement framework used in this work to quantify bedload transport and morphodynamics (chapter 4) is presented in Figure 7.5:

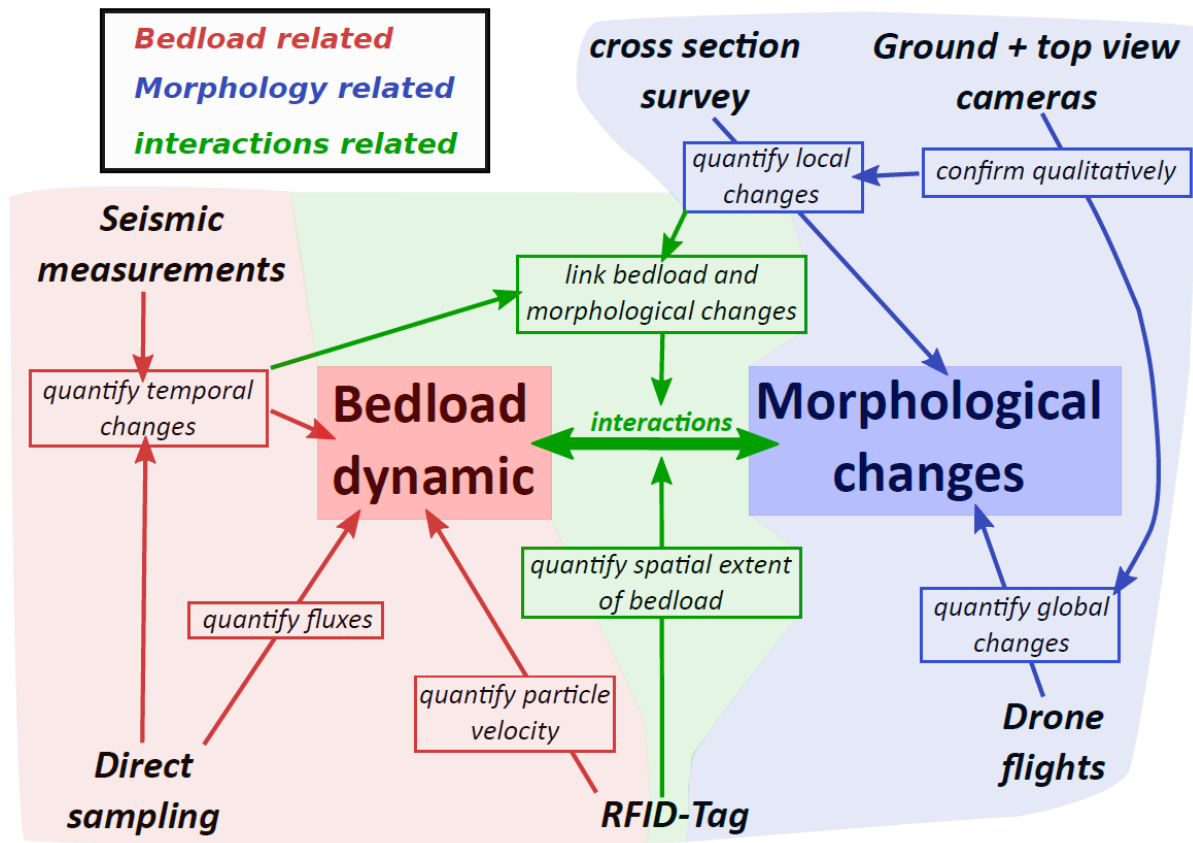


Figure 7.5: Example of a multi-measurement framework to study bedload transport and morphodynamics interactions (Chapter 4).

To continue this work and improve our understanding on fine particles-riverbed interactions as well as conditions leading to deposition or erosion of suspended sediments in Alpine rivers, field approaches similar to those used in chapter 5 and 6 could be applied in other types of catchments. Actually, measurements performed on the Séveraisse river are representative of catchments having relatively low upstream suspended sediment yields, coarse suspended particles strongly interacting with the coarser ones and significant capacities to buffer hillslope fluxes. Consequently, it would be of interest to investigate if similar deposition/erosion processes could be observed in settings with finer suspended sediments, higher upstream suspended sediment yields and less active river bed morphologies. This could help to quantify more generally the conditions leading to deposition and erosion of suspended sediments in Alpine rivers. Also, it would be of interest to apply these approaches over longer time scales as significant seasonal and inter-annual variabilities are observed in suspended load dynamics. This could be particularly relevant in catchments having a Mediterranean hydrological regime such as the Asse, Bléone, Galabre or Bès characterized by rare and intense exports of suspended fluxes.

In order to understand at a local scale how the mobility of coarse particles controls the release of fine particles from the river bed, an interesting perspective for the near future would be to use the well documented dataset presented in chapter 4 to 6 to apply spatially distributed modeling. This could be useful to determine which local law (deposition, infiltration, erosion and release) could be used to reproduce the reach-scale behavior observed. The relevance of classical Partheniade and Krone formulations could be tested as well as more recent laws that specifically model infiltration of fine particles in gravel beds [Núñez-González, 2016]. This modeling approach could also be useful to test quantitative formulations describing at a local scale the release of fine particles when the gravel matrix starts to move. Such functions could be based on coarse river bed particles mobility criteria as was done in chapter 2 and 3, integrating lateral bars erosion and channel migrations. Moreover, while many flume studies have quantified the process of fine particles infiltration in gravel beds [Gibson *et al.*, 2009; Hill *et al.*, 2017; Krishnappan and Engel, 2006; Mooneyham and Strom, 2018; Núñez-González, 2016] only few have qualitatively described the release phase [Diplas, 1994; Schalchli, 1992]. Consequently, an interesting perspective would be to perform new flume experiments specifically focused on that release phase quantification.

Combining the previously mentioned flume, numerical and field approaches would probably be a comprehensive way to quantify the “stop and go” steps regarding the transfer of suspended particles in Alpine catchments, whose are often non-negligible as suggested by the present work. These steps should be taken into account when estimating the transit time of particulate contaminants or nutrients that could be stored in river beds over long time periods after their initial release in the fluvial system. In the same way, landscape denudation rates derived from short time flux measurements might be biased if these intermediate storage processes are neglected.

Appendix

CONCEPTUAL MODELLING

This appendix presents a modified version of the conceptual model initially developed by Park and Hunt (2017-2018) and tested on the Asse catchment. This model is based on two main observations. The first one is that above a critical flow rate corresponding to initiation of gravel bed mobility, the relation between flow rate and suspended load is increasing steeper due to a fine particle release from the river bed (Figure 8.1). The second one is that during the recession limb of peak flow event, the suspended sediment concentration is asymptotically reaching a watershed base level concentration function of the flow rate (Figure 8.2).

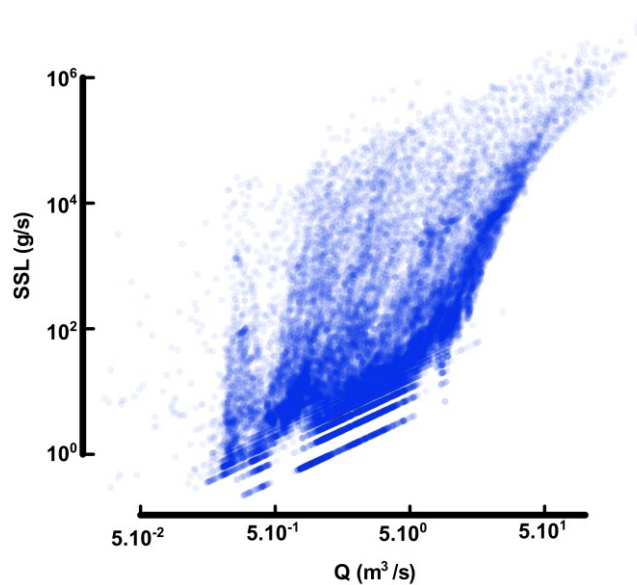


Figure 8.1: Relation between suspended load (SSL) and the flow rate in the Asse catchment. A clear braking point can be observed for flow rates around 10 m³/s.

Figure 8.2: Relation between suspended sediment concentration and flow rate during the recession limb of flood events in the Drac catchment. Each color corresponds to an event. The base level concentration (C_b) is indicated by a black line.

The conceptual model considers three different phases:

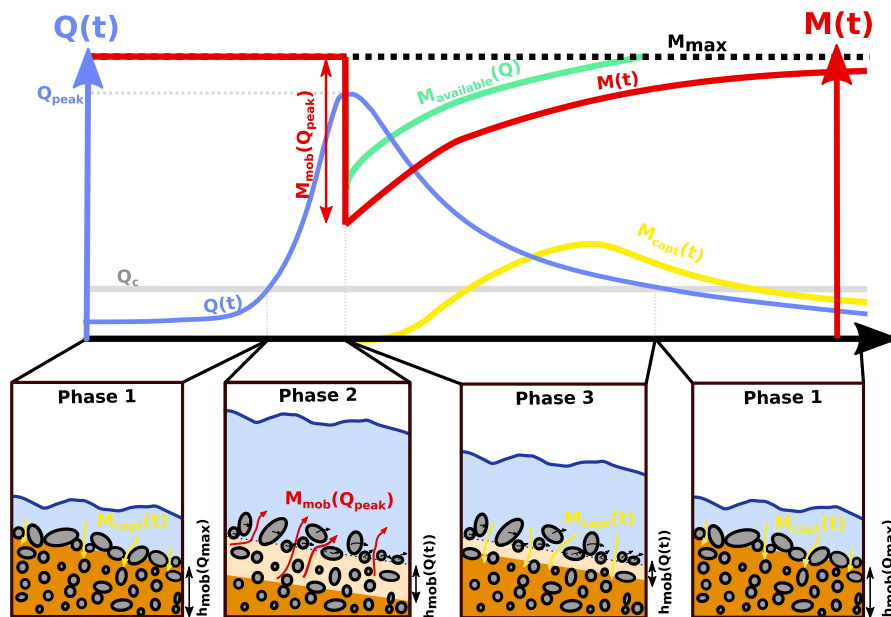


Figure 8.3: Conceptual model description.

During the first phase when the flow rate is below a critical value ($Q < Q_c$), the conceptual reservoir representing the mass of fine particles stored in the gravel bed (M) is increased with the mass of fine particles infiltrated ($M_{capt}(t)$):

$$M(t) = M(t - 1) + M_{capt}(t) \quad (8.1)$$

The mass captured is estimated as a function of the available storage space $(1 - \frac{M(t-1)}{M_{max}})$, an infiltration parameter (α) and the suspended sediment concentration in the flow, a linear function of the flow rate ($k_1 Q(t)$):

$$M(t) = M(t - 1) + \alpha k_1 Q(t) \left[1 - \frac{M(t - 1)}{M_{max}} \right] \quad (8.2)$$

Because we observed high seasonal variability in that base level concentration, the parameter k_1 was defined as a function of the season (winter, spring, summer and autumn) instead of a constant value as initially proposed by Park and Hunt.

The second phase starts when the flow rate exceeds a critical value ($Q > Q_c$). The model estimates the quantity of fine particles released from the riverbed (M_{mob}) due to bed mobilization as a function of the peak discharge:

$$M(t) = M(t - 1) - M_{mob}(t) \quad (8.3)$$

Based on the scouring model developed by Haschenburger (1999), Park and Hunt initially proposed to use an exponential function to compute the mass released. Based on a comparison with our data and observations made in chapter 2, 3 and 5 we preferred to use a power law formulation to estimate the representative mobilized layer (h_{mob}):

$$M_{mob}(Q(t)) = f(h_{mob}(Q(t))) = k_2' Q(t)^{k_3} \quad (8.4)$$

in which k_2' and k_3 are power law coefficients. The maximum mass that can be released (M_{max}) can then be estimated as follow:

$$M_{max} = M_{mob}(Q_{max}) = f(h_{mob}(Q_{max})) = k_2' Q_{max}^{k_3} \quad (8.5)$$

in which Q_{max} is the maximum observed peak discharge. We can then compute the relative mass mobilized:

$$\frac{M_{mob}(t)}{M_{mob}(Q_{max})} = \frac{M_{mob}(t)}{M_{max}} = \left(\frac{Q(t)}{Q_{max}} \right)^{k_3} \quad (8.6)$$

This formulation, similarly to the one proposed by Park and Hunt leads to an equivalent mass released independently to the filling of the storage reservoir (until the reservoir is empty). We made the assumption that the mass that could be released was also a linear function of the degree of storage filling (lower quantities are released when the river bed has been recently flushed even if it is not empty):

$$M_{mob}(t) = f\left(k_2 \left(\frac{M(t-1)}{M_{max}}\right)\right) \quad (8.7)$$

in which k_2 is the linear coefficient. Combining Eq.8.6 and Eq.8.7 we obtain:

$$M_{mob}(t) = k_2 M(t-1) \left(\frac{Q(t)}{Q_{max}}\right)^{k_3} \quad (8.8)$$

The third phase starts just after the peak discharge ($Q < Q_{max}$) when the flow rates are still higher than the critical value ($Q > Q_c$). During that phase, fine particles infiltrate in the empty pore spaces created by the previous bed mobilization:

$$M(t) = M(t-1) + M_{capt}(t) \quad (8.9)$$

However, because the bed is still mobilized a part of the storage reservoir is not available. Available pore spaces ($M_{available}$) for fines particles to infiltrate depend on the layer mobilized (h_{mob}):

$$M_{available}(Q) = f(h_{mob}(Q_{max}) - h_{mob}(Q)) \quad (8.10)$$

Using Eq.8.4, Eq.8.5 and Eq.8.8 we deduce:

$$M_{available}(t) = k_2' Q_{max}^{k_3} - k_2' Q(t)^{k_3} \quad (8.11)$$

$$M_{available}(t) = k_2' Q_{max}^{k_3} \left(1 - \left(\frac{Q(t)}{Q_{max}}\right)^{k_3}\right) \quad (8.12)$$

$$M_{available}(t) = M_{max} \left(1 - \left(\frac{Q(t)}{Q_{max}}\right)^{k_3}\right) \quad (8.13)$$

We then substitute the maximum available space (M_{max}) in Eq.8.2 by the effective available space considering the still mobile river bed ($M_{available}$) during that phase to compute the mass captured into the river bed:

$$M(t) = M(t - 1) + \alpha k_1 Q(t) \left[1 - \frac{M(t - 1)}{M_{available}(t)} \right] \quad (8.14)$$

References

- Aguilera, R., and J. M. Melack (2018), Concentration-Discharge Responses to Storm Events in Coastal California Watersheds, *Water Resources Research*, 54(1), 407-424, doi:10.1002/2017wr021578.
- Aich, V., A. Zimmermann, and H. Elsenbeer (2014), Quantification and interpretation of suspended-sediment discharge hysteresis patterns: How much data do we need?, *Catena*, 122, 120-129, doi:10.1016/j.catena.2014.06.020.
- Allen, P. B., and D. V. Petersen (1981), A study of the variability of suspended sediment measurements, *Erosion and Sediment Transport Measurement (Proceedings of the Florence Symposium, June 1981)*. IAHS Publ. no. 133.
- Andermann, C., A. Crave, R. Gloaguen, P. Davy, and S. Bonnet (2012), Connecting source and transport: Suspended sediments in the Nepal Himalayas, *Earth and Planetary Science Letters*, 351-352, 158-170, doi:10.1016/j.epsl.2012.06.059.
- Armstrong, J. D., P. S. Kemp, G. J. A. Kennedy, M. Ladle, and N. J. Milner (2003), Habitat requirements of Atlantic salmon and brown trout in rivers and streams, *Fisheries Research*, 62(2), 143-170, doi:10.1016/s0165-7836(02)00160-1.
- Asaeda, T., and M. H. Rashid (2012), The impacts of sediment released from dams on downstream sediment bar vegetation, *Journal of Hydrology*, 430-431, 25-38, doi:10.1016/j.jhydrol.2012.01.040.
- Ashmore, P. (1982), Laboratory Modeling of Gravel Braided-Stream Morphology, *Earth Surface Processes and Landforms*, 7(3), 201-225, doi:10.1016/0197-9337(82)90201-2
- Ashmore, P. (1991), How do gravel-bed rivers braid?, *Canadian Journal of Earth Sciences*, 28(3), 326-341, doi:10.1139/e91-030.

Ashmore, P., W. Bertoldi, and J. T. Gardner (2011), Active width of gravel-bed braided rivers, *Earth Surface Processes and Landforms*, 36(11), 1510-1521, doi:10.1002/esp.2182.

Asselman, N. E. M. (1999), Suspended sediment dynamics in a large drainage basin: the River Rhine, *hydrological Processes*, 13, 1437-1450, doi:10.1002/(SICI)1099-1085(199907)13:10<1437::AID-HYP821>3.0.CO;2-J.

Attal, M., and J. Lavé (2009), Pebble abrasion during fluvial transport: Experimental results and implications for the evolution of the sediment load along rivers, *Journal of Geophysical Research*, 114(F4), doi:10.1029/2009jf001328.

Baca, P. (2010), Hysteresis effect in suspended sediment concentration in the Rybárik basin, Slovakia / Effet d'hystérèse dans la concentration des sédiments en suspension dans le bassin versant de Rybárik (Slovaquie), *Hydrological Sciences Journal*, 53(1), 224-235, doi:10.1623/hysj.53.1.224.

Bagnold (1966), An approach to the Sediment Transport Problem From General Physics *Geological survey professional paper 422 - I*.

Bakker, M., F. Gimbert, T. Geay, C. Misset, S. Zanker, and A. Recking (2019), Field validation and application of a seismic bedload transport model, *Geomorphology*, doi:under review.

Bakker, M., and S. N. Lane (2017), Archival photogrammetric analysis of river-floodplain systems using Structure from Motion (SfM) methods, *Earth Surface Processes and Landforms*, 42(8), 1274-1286, doi:10.1002/esp.4085.

Baranya, S., and J. Józsa (2013), Estimation of Suspended Sediment Concentrations with Adcp in Danube River, *Journal of Hydrology and Hydromechanics*, 61(3), 232-240, doi:10.2478/johh-2013-0030.

Barzilai, R., J. B. Laronne, and I. Reid (2013), Effect of changes in fine-grained matrix on bedload sediment transport in a gravel-bed river, *Earth Surface Processes and Landforms*, 38(5), 441-448, doi:10.1002/esp.3288.

Bel, C., F. Liébault, O. Navratil, N. Eckert, H. Bellot, F. Fontaine, and D. Laigle (2017), Rainfall control of debris-flow triggering in the Réal Torrent, Southern French Prealps, *Geomorphology*, 291, 17-32, doi:10.1016/j.geomorph.2016.04.004.

Belperio, A. P. (1979), The combined use of wash load and bed material load rating curves for the calculation of total load: An example from the Burdekin River, Australia, *Catena*, 6(3-4), 317-329, doi:10.1016/0341-8162(79)90027-4.

Benacchio, V., H. Piegay, T. Buffin-Belanger, and L. Vaudor (2017), A new methodology for monitoring wood fluxes in rivers using a ground camera: Potential and limits, *Geomorphology*, 279, 44-58, doi:10.1016/j.geomorph.2016.07.019.

Bertoldi, W., P. Ashmore, and M. Tubino (2009), A method for estimating the mean bed load flux in braided rivers, *Geomorphology*, 103(3), 330-340, doi:10.1016/j.geomorph.2008.06.014.

Bertoldi, W., A. M. Gurnell, and N. A. Drake (2011), The topographic signature of vegetation development along a braided river: Results of a combined analysis of airborne lidar, color air photographs, and ground measurements, *Water Resources Research*, 47(6), doi:10.1029/2010wr010319.

Bertoldi, W., L. Zanoni, and M. Tubino (2010), Assessment of morphological changes induced by flow and flood pulses in a gravel bed braided river: The Tagliamento River (Italy), *Geomorphology*, 114(3), 348-360, doi:10.1016/j.geomorph.2009.07.017.

Bertrand, M. (2014), PhD thesis : Debris-flow susceptibility assessment at the regional scale of the Southern French Alps, Ecole normale supérieure de lyon, <NNT : 2014ENSL0895>. <tel-01022867>.

Bertrand, M., F. Liébault, and H. Piégay (2017), Regional Scale Mapping of Debris-Flow Susceptibility in the Southern French Alps, *Revue de géographie alpine*(105-4), doi:10.4000/rga.3543.

Bogen, J. (1980), The hysteresis effect of sediment transport systems, *Norsk Geografisk Tidsskrift - Norwegian Journal of Geography*, 34(1), 45-54, doi:10.1080/00291958008545338.

Borselli, L., P. Cassi, and D. Torri (2008), Prolegomena to sediment and flow connectivity in the landscape: A GIS and field numerical assessment, *Catena*, 75(3), 268-277, doi:10.1016/j.catena.2008.07.006.

Bossong, C. R., M. R. Stevens, J. T. Doerfer, and B. R. Glass (2006), Summary and Evaluation of the Quality of Stormwater in Denver, Colorado, Water Years 1998–2001, *U.S. Geological Survey Scientific Investigations, Report 2005–5150*, 90 p.

Boukhrissa, Z. A., K. Khanchoul, Y. Le Bissonnais, and M. Tourki (2013), Prediction of sediment load by sediment rating curve and neural network (ANN) in El Kebir catchment, Algeria, *Journal of Earth System Science*, 122(5), 1303-1312, doi:10.1007/s12040-013-0347-2.

- Brewer, P., G. J. L. Leeks, and J. Lewin (1992), Direct measurement of in-channel abrasion processes, *Erosion and Sediment Transport Monitoring Programmes in River Basins (Proceedings of the Oslo Symposium, August 1992)*. IAHS, 210.
- Brousse, G., F. Liébault, G. Arnaud-Fassetta and D. Tarrío, Experimental bed active-layer survey with active RFID scour chains: Example of two braided rivers (the Drac and the Vénéon) in the French Alps, *E3S Web of Conferences*, doi: 10.1051/e3sconf/20184004016.
- Buendia, C., D. Vericat, R. J. Batalla, and C. N. Gibbins (2016), Temporal Dynamics of Sediment Transport and Transient In-channel Storage in a Highly Erodible Catchment, *Land Degradation & Development*, 27(4), 1045-1063, doi:10.1002/ldr.2348.
- Burtin, A., L. Bollinger, J. Vergne, R. Cattin, and J. L. Nabelek (2008), Spectral analysis of seismic noise induced by rivers: A new tool to monitor spatiotemporal changes in stream hydrodynamics, *J Geophys Res-Sol Ea*, 113(B5), doi:Artn B05301, 10.1029/2007jb005034.
- Burtin, A., R. Cattin, L. Bollinger, J. Vergne, P. Steer, A. Robert, N. Findling, and C. Tiberi (2011), Towards the hydrologic and bed load monitoring from high-frequency seismic noise in a braided river: The “torrent de St Pierre”, French Alps, *Journal of Hydrology*, 408(1-2), 43-53, doi:10.1016/j.jhydrol.2011.07.014.
- Burtin, A., N. Hovius, and J. M. Turowski (2016), Seismic monitoring of torrential and fluvial processes, *Earth Surface Dynamics*, 4(2), 285-307, doi:10.5194/esurf-4-285-2016.
- Camenen, B., A. Herrero, G. Dramais, F. Thollet, C. L. Bescond, E. Perret, and C. Berni (2015), Field experiment on the dynamics of fine and coarse sediments over a gravel bar in an alpine river, *36th IAHR - World congress, Jun 2015, La Haye, Netherlands. 36th IAHR world congress*, 8, doi:<hal-01275256>.
- Camenen, B., M. Jodeau, and M. Jaballah (2013), Estimate of fine sediment deposit dynamics over a gravel bar using photography analysis, *International Journal of Sediment Research*, 28(2), 220-233, doi:10.1016/s1001-6279(13)60033-5.
- Camenen, B., and M. Larson (2008), A General Formula for Noncohesive Suspended Sediment Transport, *Journal of Coastal Research*, 24(3), 615-627, doi:10.2112/06-069.
- Cassel, M., T. Dépret, and H. Piégay (2017a), Assessment of a new solution for tracking pebbles in rivers based on active RFID, *Earth Surf. Process. Landforms*, 42, 1938–1951, doi:10.1002/esp.4152.

- Cassel, M., H. Piégay, and J. Lavé (2017b), Effects of transport and insertion of radio frequency identification (RFID) transponders on resistance and shape of natural and synthetic pebbles: applications for riverine and coastal bedload tracking, *Earth Surface Processes and Landforms*, 42(3), 399-413, doi:10.1002/esp.3989.
- Cavalli, M., S. Trevisani, F. Comiti, and L. Marchi (2013), Geomorphometric assessment of spatial sediment connectivity in small Alpine catchments, *Geomorphology*, 188, 31-41, doi:10.1016/j.geomorph.2012.05.007.
- Celik, I., and W. Rodi (1991), Suspended sediment - Transport capacity for open channel flow, *Journal of Hydraulic Engineering*, 117(2).
- Chapuis, M., S. Dufour, M. Provansal, B. Couvert, and M. de Linares (2015), Coupling channel evolution monitoring and RFID tracking in a large, wandering, gravel-bed river: Insights into sediment routing on geomorphic continuity through a riffle–pool sequence, *Geomorphology*, 231, 258-269, doi:10.1016/j.geomorph.2014.12.013.
- Chen, X. Y., and K. W. Chau (2016), A Hybrid Double Feedforward Neural Network for Suspended Sediment Load Estimation, *Water Resources Management*, 30(7), 2179-2194, doi:10.1007/s11269-016-1281-2.
- Clark, S. E., C. Y. S. Siu, R. Pitt, C. D. Roenning, and D. P. Treese (2009), Peristaltic Pump Autosamplers for Solids Measurement in Stormwater Runoff, *Water Environment Research*, 81(2), 192-200, doi:10.2175/106143008x325737.
- Claude, N., C. Leroux, M. Duclercq, P. Tassi, K. El Kadi Abderrezzak, and N. Rivière (2018), Limiting the development of riparian vegetation in the Isère River: A physical modelling study, *E3S Web of Conferences*, 40, doi:10.1051/e3sconf/20184002015.
- Collins, A. L., and D. E. Walling (2007a), Fine-grained bed sediment storage within the main channel systems of the Frome and Piddle catchments, Dorset, UK, *Hydrological Processes*, 21(11), 1448-1459, doi:10.1002/hyp.6269.
- Collins, A. L., and D. E. Walling (2007b), The storage and provenance of fine sediment on the channel bed of two contrasting lowland permeable catchments, UK, *River Research and Applications*, 23(4), 429-450, doi:10.1002/rra.992.
- Cook, K. L., C. Andermann, F. Gimbert, B. R. Adhikari, and N. Hovius (2018), Glacial lake outburst floods as drivers of fluvial erosion in the Himalaya, *Science*, 362(6410), 53-57, doi:10.1126/science.aat4981.
- Costa, A., P. Molnar, L. Stutenbecker, M. Bakker, T. A. Silva, F. Schlunegger, S. N. Lane, J.-L. Loizeau, and S. Girardclos (2018), Temperature signal in suspended

sediment export from an Alpine catchment, *Hydrology and Earth System Sciences*, 22(1), 509-528, doi:10.5194/hess-22-509-2018.

Davies, J. A. C., and K. Beven (2015), Hysteresis and scale in catchment storage, flow and transport, *Hydrological Processes*, 29(16), 3604-3615, doi:10.1002/hyp.10511.

de Vente, J., J. Poesen, P. Bazzoffi, A. V. Rompaey, and G. Verstraeten (2006), Predicting catchment sediment yield in Mediterranean environments: the importance of sediment sources and connectivity in Italian drainage basins, *Earth Surface Processes and Landforms*, 31(8), 1017-1034, doi:10.1002/esp.1305.

DeVries, P. (2002), Bedload layer thickness and disturbance depth in gravel bed streams, *J Hydraul Eng-Asce*, 128(11), 983-991, doi:10.1061/(Asce)0733-9429(2002)128:11(983).

Di Baldassarre, G., and A. Montanari (2009), Uncertainty in river discharge observations: a quantitative analysis, *Hydrol. Earth Syst. Sci.*, 13(6), 913-921, doi:10.5194/hess-13-913-2009.

Diplas, P. (1994), Modelling of fine and coarse sediment interaction over alternate bars, *Journal of Hydrology*, 159, 335-351.

Doomen, A. M. C., E. Wijma, J. J. G. Zwolsman, and H. Middelkoop (2008), Predicting suspended sediment concentrations in the Meuse river using a supply-based rating curve, *Hydrological Processes*, 22(12), 1846-1856, doi:10.1002/hyp.6767.

Douglas, I. A. N. (1967), Man, Vegetation and the Sediment Yields of Rivers, *Nature*, 215(5104), 925-928, doi:10.1038/215925a0.

Dudill, A., P. Frey, and M. Church (2017), Infiltration of fine sediment into a coarse mobile bed: a phenomenological study, *Earth Surface Processes and Landforms*, 42(8), 1171-1185, doi:10.1002/esp.4080.

Duerdoth, C. P., A. Arnold, J. F. Murphy, P. S. Naden, P. Scarlett, A. L. Collins, D. A. Sear, and J. I. Jones (2015), Assessment of a rapid method for quantitative reach-scale estimates of deposited fine sediment in rivers, *Geomorphology*, 230, 37-50, doi:10.1016/j.geomorph.2014.11.003.

Duvert, C., N. Gratiot, O. Evrard, O. Navratil, J. Nemery, C. Prat, and M. Esteves (2010), Drivers of erosion and suspended sediment transport in three headwater catchments of the Mexican Central Highlands, *Geomorphology*, 123(3-4), 243-256, doi:10.1016/j.geomorph.2010.07.016.

Duvert, C., et al. (2012), Towards prediction of suspended sediment yield from peak discharge in small erodible mountainous catchments (0.45–22km²) of France, Mexico and Spain, *Journal of Hydrology*, 454-455, 42-55, doi:10.1016/j.jhydrol.2012.05.048.

Eaton, B. C., R. G. Millar, and S. Davidson (2010), Channel patterns: Braided, anabranching, and single-thread, *Geomorphology*, 120(3-4), 353-364, doi:10.1016/j.geomorph.2010.04.010.

Edwards, T. K., and G. D. Glysson (1999), Field Methods for Measurement of Fluvial Sediment, *Book 3, Applications of Hydraulics, techniques of Water-Resources Investigations of the U.S. Geological Survey, Chapter C2*.

Einstein, H. A., A. G. Anderson, and J. W. Johnson (1940), A distinction between bed-load and suspended load in natural streams, *Transactions American Geophysical Union*, 21(2), 628–633, doi:10.1029/TR021i002p00628.

Engelund, F., and E. Hansen (1967), A monograph on sediment transport in alluvial streams, *Technical University of Denmark, Hydraulic Laboratory*.

Esteves, M., C. Legout, O. Navartil, and O. Evrard (2018), Medium term high frequency observation of discharge and suspended sediment in a Mediterranean mountainous catchment, *Journal of Hydrology*, *Accepted*.

Estrany, J., C. Garcia, D. E. Walling, and L. Ferrer (2011), Fluxes and storage of fine-grained sediment and associated contaminants in the Na Borges River (Mallorca, Spain), *Catena*, 87(3), 291-305, doi:10.1016/j.catena.2011.06.009.

Ferguson, R. (2007), Flow resistance equations for gravel- and boulder-bed streams, *Water Resources Research*, 43(5), doi:10.1029/2006wr005422.

Ferguson, R. (2010), Time to abandon the Manning equation?, *Earth Surface Processes and Landforms*, 35(15), 1873-1876, doi:10.1002/esp.2091.

Ferguson, R., and M. Church (2004), *A Simple Universal Equation for Grain Settling Velocity*, 933-937 pp., doi:10.1306/051204740933.

Ferguson, R. I. (1986), River Loads Underestimated by Rating Curves, *WATER RESOURCES RESEARCH*, 22(1), 74-76, doi:0043-1397/86/005W-4146505.00.

Fowler, K. K., and J. T. Wilson Characteristics, Transport, and Yield of Sediment in Juday Creek, St. Joseph County, Indiana., *U.S. GEOLOGICAL SURVEY, Water-Resources Investigations Report*, 95-4135

Frostick, L. E., P. M. Lucas, and I. Reid (1984), The infiltration of fine matrices into coarse-grained alluvial sediments and its implications for stratigraphical interpretation *Journal of the Geological Society*, 141(6), 955-965, doi:10.1144/gsjgs.141.6.0955.

Gellis, A. C. (2013), Factors influencing storm-generated suspended-sediment concentrations and loads in four basins of contrasting land use, humid-tropical Puerto Rico, *Catena*, 104, 39-57, doi:10.1016/j.catena.2012.10.018.

Gharari, S., and S. Razavi (2018), A review and synthesis of hysteresis in hydrology and hydrological modeling: Memory, path-dependency, or missing physics?, *Journal of Hydrology*, 566, 500-519, doi:10.1016/j.jhydrol.2018.06.037.

Gibson, S., D. Abraham, R. Heath, and D. Schoellhamer (2009), Vertical gradational variability of fines deposited in a gravel framework, *Sedimentology*, 56(3), 661-676, doi:10.1111/j.1365-3091.2008.00991.x.

Gimbert, F., B. M. Fuller, M. P. Lamb, V. C. Tsai, and J. P. L. Johnson (2019), Particle transport mechanics and induced seismic noise in steep flume experiments with accelerometer-embedded tracers, *Earth Surface Processes and Landforms*, 44(1), 219-241, doi:10.1002/esp.4495.

Gimbert, F., V. C. Tsai, and M. P. Lamb (2014), A physical model for seismic noise generation by turbulent flow in rivers, *Journal of Geophysical Research: Earth Surface*, 119(10), 2209-2238, doi:10.1002/2014jf003201.

Glasbergen, K. (2014), The Effect of Coarse Gravel on Cohesive Sediment Entrapment in an Annular Flume, *Thesis - University of Waterloo, degree of Master of Science in Geography*.

Gomez, B., R. L. Naff, and D. W. Hubbell (1989), Temporal variations in bedload transport rates associated with the migration of bedforms, *Earth Surface Processes and Landforms*, 14(2), 135-156, doi:10.1002/esp.3290140205.

Gran, K., and C. Paola (2001), Riparian vegetation controls on braided stream dynamics, *Water Resources Research*, 37(12), 3275-3283, doi:10.1029/2000wr000203.

Grangeon, T., I. G. Droppo, C. Legout, and M. Esteves (2014), From soil aggregates to riverine flocs: a laboratory experiment assessing the respective effects of soil type and flow shear stress on particles characteristics, *HYDROLOGICAL PROCESSES*, 28(13), 4141-4155.

Guertault, L., B. Camenen, A. Paquier, and C. Peteuil (2018), A one-dimensional process-based approach to study reservoir sediment dynamics during management

operations, *Earth Surface Processes and Landforms*, 43(2), 373-386, doi:10.1002/esp.4249.

Guillon, H., J.-L. Mugnier, and J.-F. Buoncristiani (2018), Proglacial sediment dynamics from daily to seasonal scales in a glaciated Alpine catchment (Bossons glacier, Mont Blanc massif, France), *Earth Surface Processes and Landforms*, 43(7), 1478-1495, doi:10.1002/esp.4333.

Haas, F., T. Heckmann, V. Wichmann, and M. Becht (2011), Quantification and Modeling of Fluvial Bedload Discharge from Hillslope Channels in two Alpine Catchments (Bavarian Alps, Germany), *Zeitschrift für Geomorphologie, Supplementary Issues*, 55(3), 147-168, doi:10.1127/0372-8854/2011/0055s3-0056.

Hamm, N. T., W. B. Dade, and C. E. Renshaw (2009), Fine particle deposition to initially starved, stationary, planar beds, *Sedimentology*, 56(7), 1976-1991, doi:10.1111/j.1365-3091.2009.01065.x.

Hamshaw, S. D., M. M. Dewoolkar, A. W. Schroth, B. C. Wemple, and D. M. Rizzo (2018), A New Machine-Learning Approach for Classifying Hysteresis in Suspended-Sediment Discharge Relationships Using High-Frequency Monitoring Data, *Water Resources Research*, 54(6), 4040-4058, doi:10.1029/2017wr022238.

Harvey, J. W., et al. (2012), Hydrogeomorphology of the hyporheic zone: Stream solute and fine particle interactions with a dynamic streambed, *Journal of Geophysical Research: Biogeosciences*, 117(G4), doi:10.1029/2012jg002043.

Haschenburger, J. K. (1999), A Probability model of scour and fill depths in gravel-bed channels, *Water Resources Research*, 35(9), 2857-2869, doi:10.1029/1999wr900153.

Heckmann, T., M. Cavalli, O. Cerdan, S. Foerster, M. Javaux, E. Lode, A. Smetanová, D. Vericat, and F. Brardinoni (2018), Indices of sediment connectivity: opportunities, challenges and limitations, *Earth-Science Reviews*, 187, 77-108, doi:10.1016/j.earscirev.2018.08.004.

Heckmann, T., and W. Schwanghart (2013), Geomorphic coupling and sediment connectivity in an alpine catchment — Exploring sediment cascades using graph theory, *Geomorphology*, 182, 89-103, doi:10.1016/j.geomorph.2012.10.033.

Helsen, M. M., P. J. M. Koop, and H. Van Steijn (2002), Magnitude-frequency relationship for debris flows on the fan of the Chalance torrent, Valgaudemar (French Alps), *Earth Surface Processes and Landforms*, 27(12), 1299-1307, doi:10.1002/esp.412.

Hill, K. M., J. Gaffney, S. Baumgardner, P. Wilcock, and C. Paola (2017), Experimental study of the effect of grain sizes in a bimodal mixture on bed slope, bed texture, and the transition to washload, *Water Resources Research*, 53(1), 923-941, doi:10.1002/2016wr019172.

Hoey, T. (1992), Temporal Variations in Bedload Transport Rates and Sediment Storage in Gravel-Bed Rivers, *Progress in Physical Geography*, 16(3), 319-338, doi:10.1177/030913339201600303.

Horowitz, A. J. (2008), Determining annual suspended sediment and sediment-associated trace element and nutrient fluxes, *Sci Total Environ*, 400(1-3), 315-343, doi:10.1016/j.scitotenv.2008.04.022.

Horowitz, A. J., K. A. Elrick, and J. J. Smith (2001), Estimating suspended sediment and trace element fluxes in large river basins: methodological considerations as applied to the NASQAN programme, *Hydrological Processes*, 15(7), 1107-1132, doi:10.1002/hyp.206.

Horowitz, A. J., K. A. Elrick, P. B. Von Guerard, N. O. Young, G. R. Buell, and T. L. Miller (1992), The use of automatically collected point samples to estimate suspended sediment and associated trace element concentrations for determining annual mass transport, *Erosion and Sediment Transport Monitoring Programmes in River Basins (Proceedings of the Oslo Symposium, August 1992)*. IAHS, 210.

Jansson, M. B. (2002), Determining sediment source areas in a tropical river basin, Costa Rica, *Catena*, 47(1), 63-84, doi:10.1016/S0341-8162(01)00173-4, Doi 10.1016/S0341-8162(01)00173-4.

Jodeau, M., A. Hauet, J. Le Coz, Y. Bercovitz, and L. F. (2017), Laboratory and field LSPIV measurements of flow velocities using Fudaa-LSPIV, a free user-friendly software, *HydroSenSoft, International Symposium and Exhibition on Hydro-Environment Sensors and Software, 1-3 March 2017, Madrid, Spain*.

Jourdain, C. (2017), Action des crues sur la dynamique sédimentaire et végétale dans un lit de rivière à galets : l'Isère en Combe de Savoie, *Hydrologie. Université Grenoble Alpes, Français. NNT : 2017GREAU002 . tel-01616077v2*.

Karickhoff, S., D. Brown, and T. Scott (1979), Sorption of hydrophobic pollutants on natural sediments, *Water Research*, 13(3), 241-248, doi:10.1016/0043-1354(79)90201-x.

Khosravi, K., L. Mao, O. Kisi, Z. M. Yaseen, and S. Shahid (2018), Quantifying hourly suspended sediment load using data mining models: Case study of a glacierized

Andean catchment in Chile, *Journal of Hydrology*, 567, 165-179, doi:10.1016/j.jhydrol.2018.10.015.

Khullar, N. K. (2007), Transport of fines/wash load through channels - A review, *Hydrology journal*, 30(3-4).

King, J. G., W. W. Emmett, P. J. Whiting, R. P. Kenworthy, and J. J. Barry (2004), Sediment Transport Data and Related Information for Selected Coarse-Bed Streams and Rivers in Idaho, *United States Department of Agriculture - Forest Service - Rocky Mountain Research Station, General Technical Report RMRS-GTR-131*, 26p, doi:10.2737/RMRS-GTR-131.

Klein, M. (1984), Anti clockwise hysteresis in suspended sediment concentration during individual storms: Holbeck Catchment; Yorkshire, England, *Catena*, 11, 251-257, doi:[https://doi.org/10.1016/0341-8162\(84\)90014-6](https://doi.org/10.1016/0341-8162(84)90014-6).

Kondolf, G. M., et al. (2014), Sustainable sediment management in reservoirs and regulated rivers: Experiences from five continents, *Earth's Future*, 2(5), 256-280, doi:10.1002/2013ef000184.

Krishnappan, B. G., and P. Engel (2006), Entrapment of fines in coarse sediment beds, *River Flow 2006 - conference paper – Ferreira, Alves, Leal & Cardoso (eds)*.

Krone, R. B. (1962), Flume studies of the transport in estuarine shoaling processes, hydraulics engineering laboratory, *university of berkeley, california. USA*, , 110.

Lallias-Tacon, S., F. Liebault, and H. Piegay (2014), Step by step error assessment in braided river sediment budget using airborne LiDAR data, *Geomorphology*, 214, 307-323, doi:10.1016/j.geomorph.2014.02.014.

Lamb, M. P. (2008), Is the critical Shields stress for incipient sediment motion dependent on channel-bed slope?, *J. Geophys. Res.* , 113, doi:10.1029/2007JF000831.

Lambert, C. P., and D. E. Walling (1988), Measurement of Channel Storage of Suspended Sediment in a Gravel-Bed River, *Catena*, 15(1), 65-80, doi:10.1016/0341-8162(88)90017-3.

Landers, M. N., and T. W. Sturm (2013), Hysteresis in suspended sediment to turbidity relations due to changing particle size distributions, *Water Resources Research*, 49(9), 5487-5500, doi:10.1002/wrcr.20394.

Lane, S. N., K. S. Richards, and J. H. Chandler (1996), Discharge and sediment supply controls on erosion and deposition in a dynamic alluvial channel, *Geomorphology*, 15(1), 1-15, doi:Doi 10.1016/0169-555x(95)00113-J.

Lane, S. N., R. M. Westaway, and D. M. Hicks (2003), Estimation of erosion and deposition volumes in a large, gravel-bed, braided river using synoptic remote sensing, *Earth Surface Processes and Landforms*, 28(3), 249-271, doi:10.1002/esp.483.

Launay, M., V. Dugué, J. B. Faure, M. Coquery, B. Camenen, and J. Le Coz (2019), Numerical modelling of the suspended particulate matter dynamics in a regulated river network, *Science of The Total Environment*, 665, 591-605, doi:10.1016/j.scitotenv.2019.02.015.

Le Bouteiller, C., F. Naaim-Bouvet, N. Mathys, and J. Lavé (2011), A new framework for modeling sediment fining during transport with fragmentation and abrasion, *Journal of Geophysical Research*, 116(F3), doi:10.1029/2010jf001926.

Le Pape, O., et al. (2013), Sources of organic matter for flatfish juveniles in coastal and estuarine nursery grounds: A meta-analysis for the common sole (*Solea solea*) in contrasted systems of Western Europe, *Journal of Sea Research*, 75, 85-95, doi:10.1016/j.seares.2012.05.003.

Lefrançois, J., C. Grimaldi, C. Gascuel-Oudou, and N. Gilliet (2007), Suspended sediment and discharge relationships to identify bank degradation as a main sediment source on small agricultural catchments, *Hydrological Processes*, 21(21), 2923-2933, doi:10.1002/hyp.6509.

Legout, I. G. Droppo, J. Coutaz, C. Bel, and M. Jodeau (2018), Assessment of erosion and settling properties of fine sediments stored in cobble bed rivers: the Arc and Isère alpine rivers before and after reservoir flushing, *Earth Surface Processes and Landforms*, 43(6), 1295-1309, doi:10.1002/esp.4314.

Legout, C., J. Poulenard, J. Nemery, O. Navratil, T. Grangeon, O. Evrard, and M. Esteves (2013), Quantifying suspended sediment sources during runoff events in headwater catchments using spectroradiometry, *Journal of Soils and Sediments*, 13(8), 1478-1492, doi:10.1007/s11368-013-0728-9.

Lenzi, M. A., V. D'Agostino, and P. Billi (1999), Bedload transport in the instrumented catchment of the Rio Cordon Part I: Analysis of bedload records, conditions and threshold of bedload entrainment, *Catena*, 36(3), 171-190, doi:10.1016/S0341-8162(99)00016-8.

Lewis, J. (1996), Turbidity-controlled suspended sediment sampling for runoff-event load estimation, *Water Resources Research*, 32(7), 2299-2310.

Liébault, F., H. Bellot, M. Chapuis, S. Klotz, and M. Deschâtres (2012), Bedload tracing in a high-sediment-load mountain stream, *Earth Surface Processes and Landforms*, 37(4), 385-399, doi:10.1002/esp.2245.

- Liebault, F., S. Lallias-Tacon, M. Cassel, and N. Talaska (2013), Long Profile Responses of Alpine Braided Rivers in Se France, *River Research and Applications*, 29(10), 1253-1266, doi:10.1002/rra.2615.
- Lisle, T. E., and M. Church (2002), Sediment transport-storage relations for degrading, gravel bed channels, *Water Resources Research*, 38(11), 1-1-1-14, doi:10.1029/2001wr001086.
- Lloyd, C. E., J. E. Freer, P. J. Johnes, and A. L. Collins (2016), Using hysteresis analysis of high-resolution water quality monitoring data, including uncertainty, to infer controls on nutrient and sediment transfer in catchments, *Sci Total Environ*, 543(Pt A), 388-404, doi:10.1016/j.scitotenv.2015.11.028.
- Loire, R., L. Grosprêtre, J.-R. Malavoi, O. Ortiz, and H. Piégay (2019), What Discharge Is Required to Remove Silt and Sand Downstream from a Dam? An Adaptive Approach on the Selves River, France, *Water*, 11(2), doi:10.3390/w11020392.
- Luchi, R., W. Bertoldi, G. Zolezzi, and M. Tubino (2007), Monitoring and predicting channel change in a free-evolving, small Alpine river: Ridanna Creek (North East Italy), *Earth Surface Processes and Landforms*, 32(14), 2104-2119, doi:10.1002/esp.1511.
- Ludwig, W., and J. L. Probst (1998), River sediment discharge to the oceans; present-day controls and global budgets, *American Journal of Science*, 298(4), 265-295, doi:10.2475/ajs.298.4.265.
- Mano, V. (2008), PhD thesis : Processus fondamentaux conditionnant les apports de sédiments fins dans les retenues. Optimisation de méthodes de mesure et modélisation statistique., *Université Joseph-Fourier -Grenoble I*.
- Mano, V., J. Nemery, P. Belleudy, and A. Poirel (2009), Assessment of suspended sediment transport in four alpine watersheds (France): influence of the climatic regime, *Hydrological Processes*, 23(5), 777-792, doi:10.1002/hyp.7178.
- Mao, L., and R. Carrillo (2016), Temporal dynamics of suspended sediment transport in a glacierized Andean basin, *Geomorphology*, doi:10.1016/j.geomorph.2016.02.003.
- Marden, M., G. Arnold, B. Gomez, and D. Rowan (2005), Pre- and post-reforestation gully development in Mangatu Forest, East Coast, North Island, New Zealand, *River Research and Applications*, 21(7), 757-771, doi:10.1002/rra.882.
- Marteau, B., R. J. Batalla, D. Vericat, and C. Gibbins (2018), Asynchronicity of fine sediment supply and its effects on transport and storage in a regulated river, *Journal of Soils and Sediments*, 18(7), 2614-2633, doi:10.1007/s11368-017-1911-1.

Marttila, H., and B. Kløve (2010), Dynamics of erosion and suspended sediment transport from drained peatland forestry, *Journal of Hydrology*, 388(3-4), 414-425, doi:10.1016/j.jhydrol.2010.05.026.

Marttila, H., and B. Kløve (2014), Storage, properties and seasonal variations in fine-grained bed sediment within the main channel and headwaters of the River Sanginjoki, Finland, *Hydrological Processes*, 28(17), 4756-4765, doi:10.1002/hyp.9953.

Mathers, K. L., A. L. Collins, J. England, B. Brierley, and S. P. Rice (2017), The fine sediment conundrum; quantifying, mitigating and managing the issues, *River Research and Applications*, 33(10), 1509-1514, doi:10.1002/rra.3228.

McDonald, D. M., and S. F. Lamoureux (2009), Hydroclimatic and channel snowpack controls over suspended sediment and grain size transport in a High Arctic catchment, *Earth Surface Processes and Landforms*, 34(3), 424-436, doi:10.1002/esp.1751.

Métivier, F., P. Meunier, A. Crave, C. Chaduteau, B. Ye, and G. Liu (2004), *River Flow, Transport dynamics and morphology of a high mountain stream during the peak flow season: the Urümqi River (Chinese Tian Shan)*. (1), 761– 777.

Meunier, P., F. Métivier, E. Lajeunesse, A. S. Mériaux, and J. Faure (2006), Flow pattern and sediment transport in a braided river: The “torrent de St Pierre” (French Alps), *Journal of Hydrology*, 330(3-4), 496-505, doi:10.1016/j.jhydrol.2006.04.009.

Meybeck, M., L. Laroche, H. H. Dürr, and J. P. M. Syvitski (2003), Global variability of daily total suspended solids and their fluxes in rivers, *Global and Planetary Change*, 39(1-2), 65-93, doi:10.1016/s0921-8181(03)00018-3.

Meyer-Peter, E., and R. Mueller (1948), Formulas for bed-load transport, *Proceedings 2nd Meeting IAHR, Stockholm*.

Milan, D. J., G. L. Heritage, and D. Hetherington (2007), Application of a 3D laser scanner in the assessment of erosion and deposition volumes and channel change in a proglacial river, *Earth Surface Processes and Landforms*, 32(11), 1657-1674, doi:10.1002/esp.1592.

Misset, C., A. Recking, O. Navratil, C. Legout, A. Poirel, M. Cazihlac, V. Briguet, and M. Esteves (2019), Quantifying bed-related suspended load in gravel bed rivers through an analysis of the bedload-suspended load relationship, *Earth Surface Processes and Landforms*, doi:10.1002/esp.4606.

Montgomery, D. R., and J. M. Buffington (1997), Channel-reach morphology in mountain drainage basins, *Geological Society of America Bulletin*, 109(5), 596-611.

- Mooneyham, C., and K. Strom (2018), Deposition of Suspended Clay to Open and Sand-Filled Framework Gravel Beds in a Laboratory Flume, *Water Resources Research*, doi:10.1002/2017wr020748.
- Mueller, E. R. (2005), Morphologically based model of bed load transport capacity in a headwater stream, *Journal of Geophysical Research*, 110(F2), doi:10.1029/2003jf000117.
- N. Moriasi, D., J. G. Arnold, M. W. Van Liew, R. L. Bingner, R. D. Harmel, and T. L. Veith (2007), Model Evaluation Guidelines for Systematic Quantification of Accuracy in Watershed Simulations, *Transactions of the ASABE*, 50(3), 885-900, doi:<https://doi.org/10.13031/2013.23153>.
- Naden, P. S., et al. (2016), Understanding the controls on deposited fine sediment in the streams of agricultural catchments, *Sci Total Environ*, 547, 366-381, doi:10.1016/j.scitotenv.2015.12.079.
- Navratil, O., M. Esteves, C. Legout, N. Gratiot, J. Nemery, S. Willmore, and T. Grangeon (2011), Global uncertainty analysis of suspended sediment monitoring using turbidimeter in a small mountainous river catchment, *Journal of Hydrology*, 398(3-4), 246-259, doi:10.1016/j.jhydrol.2010.12.025.
- Navratil, O., et al. (2012), Temporal variability of suspended sediment sources in an alpine catchment combining river/rainfall monitoring and sediment fingerprinting, *Earth Surface Processes and Landforms*, 37(8), 828-846, doi:10.1002/esp.3201.
- Navratil, O., C. Legout, D. Gateuille, M. Esteves, and F. Liebault (2010), Assessment of intermediate fine sediment storage in a braided river reach (southern French Prealps), *Hydrological Processes*, 24(10), 1318-1332, doi:10.1002/hyp.7594.
- Navratil, O., F. Liébault, H. Bellot, E. Travaglini, J. Theule, G. Chambon, and D. Laigle (2013), High-frequency monitoring of debris-flow propagation along the Réal Torrent, Southern French Prealps, 201, 157–171, doi:10.1016/j.geomorph.2013.06.017.
- Nistor, C. J., and M. Church (2005), Suspended sediment transport regime in a debris-flow gully on Vancouver Island, British Columbia, *Hydrological Processes*, 19(4), 861-885, doi:10.1002/hyp.5549.
- Núñez-González, F. (2016), Infiltration of fine sediment mixtures through poorly sorted immobile coarse beds, *Water Resources Research*, 52(12), 9306-9324, doi:10.1002/2016wr019395.

- Orwin, J. F., and C. C. Smart (2004a), The evidence for paraglacial sedimentation and its temporal scale in the deglaciating basin of Small River Glacier, Canada, *Geomorphology*, 58(1-4), 175-202, doi:10.1016/j.geomorph.2003.07.005.
- Orwin, J. F., and C. C. Smart (2004b), Short-term spatial and temporal patterns of suspended sediment transfer in proglacial channels, Small River Glacier, Canada, *Hydrological Processes*, 18(9), 1521-1542, doi:10.1002/hyp.1402.
- Owens, P. N., et al. (2005), Fine-grained sediment in river systems: Environmental significance and management issues, *River Research and Applications*, 21(7), 693-717, doi:10.1002/rra.878.
- Owens, P. N., D. E. Walling, and G. J. L. Leeks (1999), Deposition and storage of fine-grained sediment within the main channel system of the River Tweed, Scotland, *Earth Surface Processes and Landforms*, 24(12), 1061-1076, doi:10.1002/(Sici)1096-9837(199911)24:12<1061::Aid-Esp35>3.0.Co;2-Y.
- Park, Batalla, Birgand, Esteves, Gentile, Harrington, Navratil, T. López, and Vericat (2019), Influences of Catchment and River Channel Characteristics on the Magnitude and Dynamics of Storage and Re-Suspension of Fine Sediments in River Beds, *Water*, 11(5), doi:10.3390/w11050878.
- Park, J., and J. R. Hunt (2017), Coupling fine particle and bedload transport in gravel-bedded streams, *Journal of Hydrology*, 552, 532-543, doi:10.1016/j.jhydrol.2017.07.023.
- Park, J., and J. R. Hunt (2018), Modeling fine particle dynamics in gravel-bedded streams: Storage and re-suspension of fine particles, *Sci Total Environ*, 634, 1042-1053, doi:10.1016/j.scitotenv.2018.04.034.
- Parsons, A. J., L. Bracken, R. E. Poepl, J. Wainwright, and S. D. Keesstra (2015), Introduction to special issue on connectivity in water and sediment dynamics, *Earth Surface Processes and Landforms*, 40(9), 1275-1277, doi:10.1002/esp.3714.
- Partheniades, E. (1977), Unified View of Wash Load and Bed Material Load *Journal of the Hydraulics Division*, 103(9), 1037-1057.
- Peirce, S., P. Ashmore, and P. Leduc (2018), The variability in the morphological active width: Results from physical models of gravel-bed braided rivers, *Earth Surface Processes and Landforms*, 43(11), 2371-2383, doi:10.1002/esp.4400.
- Perret, E., C. Berni, B. Camenen, A. Herrero, and K. El Kadi Abderrezzak (2018), Transport of moderately sorted gravel at low bed shear stresses: The role of fine sediment infiltration, *Earth Surface Processes and Landforms*, 43(7), 1416-1430, doi:10.1002/esp.4322.

- Petticrew, E. L., A. Krein, and D. E. Walling (2007), Evaluating fine sediment mobilization and storage in a gravel-bed river using controlled reservoir releases, *Hydrological Processes*, 21(2), 198-210, doi:10.1002/hyp.6183.
- Picouet, C., B. Hingray, and J. C. Olivry (2009), Modelling the suspended sediment dynamics of a large tropical river: the Upper Niger river basin at Banankoro, *Hydrological Processes*, 23(22), 3193-3200, doi:10.1002/hyp.7398.
- Piégay, H., F. Arnaud, M. Cassel, T. Dépret, A. Alber, K. Michel, A.-J. Rollet, and L. Vaudor (2016), Suivi par RFID de la mobilité des galets : Retour sur 10 ans d'expérience en grandes rivières, *Bulletin de la Societe Royale des Sciences de Liege* 67, 77-91.
- Piqué, G., J. A. López-Tarazón, and R. J. Batalla (2014), Variability of in-channel sediment storage in a river draining highly erodible areas (the Isábena, Ebro Basin), *Journal of Soils and Sediments*, 14(12), 2031-2044, doi:10.1007/s11368-014-0957-6.
- Pitlick, J., E. R. Mueller, C. Segura, R. Cress, and M. Torizzo (2008), Relation between flow, surface-layer armoring and sediment transport in gravel-bed rivers, *Earth Surface Processes and Landforms*, 33(8), 1192-1209, doi:10.1002/esp.1607.
- Piton, G., and A. Recking (2017), The concept of travelling bedload and its consequences for bedload computation in mountain streams, *Earth Surface Processes and Landforms*, 42(10), 1505-1519, doi:10.1002/esp.4105.
- Pryor, B. S., T. Lisle, D. S. Montoya, and S. Hilton (2011), Transport and storage of bed material in a gravel-bed channel during episodes of aggradation and degradation: a field and flume study, *Earth Surface Processes and Landforms*, 36(15), 2028-2041, doi:10.1002/esp.2224.
- Recking, A. (2009), Theoretical development on the effects of changing flow hydraulics on incipient bed load motion, *Water Resources Research*, 45(4), n/a-n/a, doi:10.1029/2008wr006826.
- Recking, A. (2010), A comparison between flume and field bed load transport data and consequences for surface-based bed load transport prediction, *Water Resources Research*, 46(3), n/a-n/a, doi:10.1029/2009wr008007.
- Recking, A. (2013a), An analysis of nonlinearity effects on bed load transport prediction, *Journal of Geophysical Research: Earth Surface*, 118(3), 1264-1281, doi:10.1002/jgrf.20090.
- Recking, A. (2013b), Simple Method for Calculating Reach-Averaged Bed-Load Transport, *Journal of Hydraulic Engineering*, 139, doi:10.1061/(ASCE)HY.1943-7900.0000653.

Recking, A., P. Frey, A. Paquier, and P. Belleudy (2009), An experimental investigation of mechanisms involved in bed load sheet production and migration, *Journal of Geophysical Research*, 114(F3), doi:10.1029/2008jf000990.

Recking, A., G. Piton, D. Vazquez-Tarrio, and G. Parker (2016), Quantifying the Morphological Print of Bedload Transport, *Earth Surface Processes and Landforms*, 41(6), 809-822, doi:10.1002/esp.3869.

Rickenmann, D., and A. Recking (2011), Evaluation of flow resistance in gravel-bed rivers through a large field data set, *Water Resources Research*, 47(7), n/a-n/a, doi:10.1029/2010wr009793.

Rouse (1937), Modern conception of the mechanics of turbulence *Trans ASCE*, 102, 463-543.

Roux, C., A. Alber, M. Bertrand, L. Vaudor, and H. Piégay (2015), "FluvialCorridor": A new ArcGIS toolbox package for multiscale riverscape exploration, *Geomorphology*, 242, 29-37, doi:10.1016/j.geomorph.2014.04.018.

Sadaoui, M., W. Ludwig, F. Bourrin, and P. Raimbault (2016), Controls, budgets and variability of riverine sediment fluxes to the Gulf of Lions (NW Mediterranean Sea), *Journal of Hydrology*, 540, 1002-1015, doi:10.1016/j.jhydrol.2016.07.012.

Schalchli, U. (1992), The clogging of coarse gravel river beds by fine sediment, *Hydrobiologia* 235/236, 189-197.

Schümm, S. A., and M. A. Stevens (1973), Abrasion in Place: A Mechanism for Rounding and Size Reduction of Coarse Sediments in Rivers, *Geology*, 1, 37-40, doi:10.1130/0091-7613(1973)1<37:AIPAMF>2.0.CO;2.

Sear, D. A. (1993), Fine Sediment Infiltration into Gravel Spawning Beds within a Regulated River Experiencing Floods - Ecological Implications for Salmonids, *Regul River*, 8(4), 373-390, doi:DOI 10.1002/rrr.3450080407.

Smalley, M. L., W. W. Emmett, and A. M. Wacker (1994), Annual replenishment of bed material by sediment transport in the Wind river near Riverton, Wyoming, U.S. *Geological survey Water-Resources Investigations Report 94-4007*.

Smith, B. P. G., P. S. Naden, G. J. L. Leeks, and P. D. Wass (2003), The influence of storm events on fine sediment transport, erosion and deposition within a reach of the River Swale, Yorkshire, UK, *Science of the Total Environment*, 314, 451-474, doi:10.1016/S0048-9697(03)00068-8.

Smith, H. G., and D. Dragovich (2009), Interpreting sediment delivery processes using suspended sediment-discharge hysteresis patterns from nested upland catchments,

south-eastern Australia, *Hydrological Processes*, 23(17), 2415-2426, doi:10.1002/hyp.7357.

Soler, M., J. Latron, and F. Gallart (2008), Relationships between suspended sediment concentrations and discharge in two small research basins in a mountainous Mediterranean area (Vallcebre, Eastern Pyrenees), *Geomorphology*, 98(1-2), 143-152, doi:10.1016/j.geomorph.2007.02.032.

Sumi, T., M. Okano, and Y. Takata (2004), Reservoir sedimentation management with bypass tunnels in Japan, *Proceedings of 9th International Symposium on River Sedimentation, Yichang, China*, 1036–1043.

Sun, L., M. Yan, Q. Cai, and H. Fang (2016), Suspended sediment dynamics at different time scales in the Loushui River, south-central China, *Catena*, 136, 152-161, doi:10.1016/j.catena.2015.02.014.

Tananaev, N. I. (2012), Hysteresis effect in the seasonal variations in the relationship between water discharge and suspended load in rivers of permafrost zone in Siberia and Far East, *Water Resources*, 39(6), 648-656, doi:10.1134/s0097807812060073.

Tananaev, N. I. (2015), Hysteresis effects of suspended sediment transport in relation to geomorphic conditions and dominant sediment sources in medium and large rivers of the Russian Arctic, *Hydrology Research*, 46(2), doi:10.2166/nh.2013.199.

Thomas, R. B. (1985), Measuring Suspended Sediment in Small Mountain Streams, *United States Department of Agriculture General Technical Report PSW-83*.

Trustrum, N. A., and P. R. Stephens (1981), Selection of hill-country pasture measurement sites by interpretation of sequential aerial photographs, *New Zealand Journal of Experimental Agriculture*, 9(1), 31-34, doi:10.1080/03015521.1981.10427799.

Tsai, V. C., B. Minchew, M. P. Lamb, and J.-P. Ampuero (2012), A physical model for seismic noise generation from sediment transport in rivers, *Geophysical Research Letters*, 39(2), n/a-n/a, doi:10.1029/2011gl050255.

Turley, M. D., G. S. Bilotta, G. Arbocciute, R. P. Chadd, C. A. Extence, and R. E. Brazier (2017), Quantifying Submerged Deposited Fine Sediments in Rivers and Streams Using Digital Image Analysis, *River Research and Applications*, 33(10), 1585-1595, doi:10.1002/rra.3073.

Turowski, J. M., D. Rickenmann, and S. J. Dadson (2010), The partitioning of the total sediment load of a river into suspended load and bedload: a review of empirical data, *Sedimentology*, 57(4), 1126-1146, doi:10.1111/j.1365-3091.2009.01140.x.

- Van Rijn, L. C. (1984a), Sediment Transport, Part II: Suspended Load Transport, *Journal of Hydraulic Engineering*, 110(11), 1613-1641.
- Van Rijn, L. C. (1984b), Sediment transport, part II: Suspended load transport, *Journal of Hydraulic Engineering*, 110.
- Vanmaercke, M., J. Poesen, G. Verstraeten, J. de Vente, and F. Ocakoglu (2011), Sediment yield in Europe: Spatial patterns and scale dependency, *Geomorphology*, 130(3-4), 142-161, doi:10.1016/j.geomorph.2011.03.010.
- Vaughan, A. A., P. Belmont, C. P. Hawkins, and P. Wilcock (2017), Near-Channel Versus Watershed Controls on Sediment Rating Curves, *Journal of Geophysical Research: Earth Surface*, 122(10), 1901-1923, doi:10.1002/2016jf004180.
- Vercruyssen, K., R. C. Grabowski, and R. J. Rickson (2017), Suspended sediment transport dynamics in rivers: Multi-scale drivers of temporal variation, *Earth-Science Reviews*, 166, 38-52, doi:10.1016/j.earscirev.2016.12.016.
- Vrieling, A. (2006), Satellite remote sensing for water erosion assessment: A review, *Catena*, 65(1), 2-18, doi:10.1016/j.catena.2005.10.005.
- Walling, D., and B. Webb (1988), *The Reliability of Rating Curve Estimates of Suspended Sediment Yield: Some Further Comments*.
- Walling, D. E., and A. L. Collins (2008), The catchment sediment budget as a management tool, *Environmental Science & Policy*, 11(2), 136-143, doi:10.1016/j.envsci.2007.10.004.
- Walling, D. E., P. N. Owens, J. Carter, G. J. L. Leeks, S. Lewis, A. A. Meharg, and J. Wright (2003), Storage of sediment-associated nutrients and contaminants in river channel and floodplain systems, *Applied Geochemistry*, 18(2), 195-220, doi:10.1016/S0883-2927(02)00121-X, Doi 10.1016/S0883-2927(02)00121-X.
- Walling, D. E., P. N. Owens, and G. J. L. Leeks (1998), The role of channel and floodplain storage in the suspended sediment budget of the River Ouse, Yorkshire, UK, *Geomorphology*, 22, 225-242.
- Wang, Z. Y., and A. Dittrich (1992), A study on problems in suspended sediment transportation, *Proceedings, 2nd International Conference on Hydraulics and Environmental Modelling of Coastal, Estuarine and River Waters, Ashgate, Burlington, Vt*, 467-478.
- Wang, Z. Y., Y. T. Li, and Y. P. He (2007), Sediment budget of the Yangtze River, *Water Resources Research*, 43(4), doi:10.1029/2006wr005012, 10.1029/2006wr005012.

Warburton, J. (1992), Observations of Bed Load Transport and Channel Bed Changes in a Proglacial Mountain Stream, *Arctic and Alpine Research*, 24(3), doi:10.2307/1551657.

Warburton, J., and T. Davies (1994), Variability of bedload transport and channel morphology in a braided river hydraulic model, *Earth Surface Processes and Landforms*, 19(5), 403-421, doi:10.1002/esp.3290190503.

Waters, T. F. (1995), *Sediment in streams : sources, biological effects, and control*, American Fisheries Society, Bethesda, Md.

Welch, P. (1967), The use of fast Fourier transform for the estimation of power spectra: A method based on time averaging over short, modified periodograms, *IEEE Transactions on Audio and Electroacoustics*, 15(2), 70-73, doi:10.1109/tau.1967.1161901.

Wendling, V., N. Gratiot, C. Legout, I. G. Droppo, C. Coulaud, and B. Mercier (2015), Using an optical settling column to assess suspension characteristics within the free, flocculation, and hindered settling regimes, *Journal of Soils and Sediments*, 15(9), 1991-2003, doi:10.1007/s11368-015-1135-1.

Wilkinson, S. N., I. P. Prosser, and A. O. Hughes (2006), Predicting the distribution of bed material accumulation using river network sediment budgets, *Water Resources Research*, 42(10), doi:Artn W10419, 10.1029/2006wr004958.

Williams, G. P. (1989), Sediment concentration versus water discharge during single hydrologic events in rivers, *Journal of Hydrology*, 111, 89-106, doi:10.1016/0022-1694(89)90254-0.

Williams, G. P., and D. L. Rosgen (1989), Measured total sediment loads (suspended loads and bedloads) for 93 United States Streams, *U.S. Geological Survey*.

Wischmeier, W. H., and D. D. Smith (1978), *Predicting Rainfall Erosion Losses —A Guide To Conservation Planning*, 62 pp. pp.

Wohl, E. (2017), Connectivity in rivers, *Progress in Physical Geography*, 41(3), 345-362, doi:10.1177/0309133317714972.

Wolman, M. G. (1954), A METHOD OF SAMPLING COARSE RIVER-BED MATERIAL, *Transactions, American Geophysical Union*, 35(6), 6, doi:10.1029/TR035i006p00951.

Zuecco, G., D. Penna, M. Borga, and H. J. van Meerveld (2016), A versatile index to characterize hysteresis between hydrological variables at the runoff event timescale, *Hydrological Processes*, 30(9), 1449-1466, doi:10.1002/hyp.10681.

THESE DE DOCTORAT DE L'UNIVERSITE DE GRENOBLE

THE ROLE OF RIVERBED ON SUSPENDED SEDIMENT TRANSPORT DYNAMICS IN ALPINE CATCHMENTS

Clément Misset

Résumé : Les grandes quantités de sédiments transportés par suspension dans les rivières alpines sont associées à d'importantes problématiques socio-économiques et environnementales telles que le transport de polluants, la dégradation des milieux aquatiques ou l'envasement des retenues hydroélectriques. Pour faire face à ces enjeux, il est nécessaire de mieux comprendre le rôle joué par le lit des rivières alpines sur la dynamique de ce transport. A partir de larges bases de données issues de la littérature et de nouvelles mesures de terrain, la première partie de cette thèse propose une étude à une échelle régionale de i) l'influence de la configuration des sources sédimentaires sur la variabilité du transport solide par suspension, ii) l'estimation de la quantité et de la disponibilité des particules fines dans le lit des rivières alpines et iii) l'analyse de la relation entre transport solide par suspension et mobilité du lit de ces rivières. Ces analyses montrent que la configuration du bassin versant en amont du point d'observation contrôle significativement la dynamique du transport solide par suspension observée en aval. De grandes quantités de sédiments fins sont en effet stockées dans les rivières alpines alluviales et il est ainsi possible de prédire une partie significative de leurs flux en suspension pour les forts débits à partir d'une modélisation de la mobilité de leurs lits. La seconde partie de la thèse teste ces résultats à une échelle locale. Pour cela, une campagne de mesures a été réalisée durant une saison complète de fonte sur un cours d'eau alpin typique, la Séveraisse. Un large panel de mesures directes et indirectes a été mis en œuvre pour mesurer la suspension, le charriage et les évolutions topographiques sur un tronçon de 3.5 km. Ces mesures confirment que les particules fines transportées par suspension interagissent fortement avec le lit dans ce type de tronçon morphodynamiquement actif. Ce dernier peut être perçu comme une zone tampon intermédiaire contrôlée par le forçage amont sédiments-débit liquide ainsi que par la mobilité et la morphologie de son lit.

Abstract: The large quantities of sediments transported as suspension in Alpine rivers are associated with important socio-economic and environmental issues such as pollutant transfer, aquatic habitat degradation or dam siltation. To address these issues, it is required to better understand the role of Alpine river beds on the dynamics of this transport. In the first part of this thesis, we use large datasets from the literature and new field measurements to investigate at a regional scale i) the influence of sediment sources configuration on suspended load variability, ii) the quantity and availability of fine particles in Alpine river beds and iii) the relation between suspended load and river bed mobility. These analyses show that the catchment configuration upstream the observation point can significantly control the suspended load dynamics observed downstream. This first part also shows that large quantities of fine particles can be stored in alluvial Alpine rivers. For these rivers and for high flow rates, it was possible to predict a significant part of suspended load based on riverbed mobility modeling. The second part of the thesis tests these results at a local scale. To do so, an important field campaign was performed during the entire melting season of a typical Alpine river, the Séveraisse. A large panel of direct and indirect measurements was used to measure suspended load, bedload and topographic changes on a 3.5-km reach. These measurements confirm that suspended particles strongly interact with the river bed of that kind of morphodynamically active streams. The latter can be considered as an intermediate buffer controlled by the upstream hydro-sedimentary forcing and by the river bed mobility and morphology.